ELECTROMAGNETIC RADIATION CALORIMETRY OF THERMOPLASTICS, ELASTOMERS AND COMPOSITES SYSTEMS

by

Ming Chen

Dissertation submitted to the Faculty of the
Virginia Polytechnic Institute and State University
in partial fulfillment of the requirements for the degree of

DOCTOR OF PHILOSOPHY

in

Materials Engineering Science

APPROVED:

Thomas C. Ward, Chairman

Larry C. Burton

Jack D. Graybeal

Edmund G. Henneke

Judy S. Riffle

May, 1989

Blacksburg, Virginia

ELECTROMAGNETIC RADIATION CALORIMETRY OF THERMOPLASTICS, ELASTOMERS AND COMPOSITES SYSTEM

by

Ming Chen

Committee Chairman: Dr. Thomas C. Ward
Chemistry

(ABSTRACT)

The application of microwave radiation for processing of glassy and semicrystalline thermoplastics, elastomeric polymers and composites was investigated. The goal of this research was to reveal the relationship between polymer structure and microwave absorptivity, and hence processability. The specimens were subjected to an electric field at 2.45 GHz either inside a rectangular waveguide or in a cylindrical resonant cavity applicator with less than 100 watts applied power. Both travelling wave modes and standing wave modes were examined. Temperatures, powers and times were recorded, leading to the concept of "microwave calorimetry." Low frequency dynamic mechanical and dielectric frequency-temperature spectra were obtained on the materials and combined to conveniently extrapolate structure-property relationships into the GHz region. A correlation was found between the dielectric properties of various polymers and the dipole moments of small molecule analogues. Evaluating heatability was most accurately found to be determined by the magnitude of $(\varepsilon_s - \varepsilon_\infty)$, the oscillator strength. The value of $(\varepsilon_s - \varepsilon_\infty)$ should be used together with the distribution of relaxation times and the activation energies of dipolar dispersion to predict heatability for microwave processing. The critical temperatures, T_c, of dielectric loss were obtained from the intercepts of positive slope tangents of heating rate versus temperature plots at 2.45 GHz for polymers. Microwave processing was rapid above

the critical temperature where the maximum dielectric loss fell in the 2.45 GHz frequency domain for efficient coupling of energy to the polymers. Shifting the dielectric relaxation spectrum into the microwave region by directly or indirectly increasing the temperature of each sample was unique and of key importance to processability. A schematic model was proposed to explain the behavior of two-phase materials subjected to microwave heating. Combining the heatability, $(\varepsilon_s - \varepsilon_\infty)$, and the dielectric relaxation spectral response was found to be helpful in evaluating formulations of two phase materials for electromagnetic radiation processing at high frequencies.

ACKNOWLEDGEMENTS

The author would like to express sincere appreciation to his advisor, Dr. Thomas C. Ward for general guidance and support throughout the pursuit of this research. Thanks to Drs. Larry C. Burton, Jack D. Graybeal, Edmund G. Henneke, Judy S. Riffle and James F. Wolfe for agreeing to serve as my committee members.

This work was supported by DARPA under Air Force contract number F33615-85-C-5153. I would like to acknowledge for providing helpful suggestions in the purchase of the microwave system and for helping set up part of the microwave instrumentation.

A special thanks to the Polymer Physical Chemistry Group for their friendship and research cooperation. To and for their helpful discussion and proofreading of this dissertation.

I need to thank my parents and parents-in-law whose support kept me going. Finally, I thank my wife , for taking care of our two sons and my parents. She sacrificed the best five years of her life. Her love provided stability in my pursuit of this "**P**romoting **h**usband to **D**octor degree."

TABLE OF CONTENTS

LIST OF FIGURES

LIST OF TABLES

CHAPTER 1

INTRODUCTION

1.1 RESEARCH GOALS AND FACTORS AFFECTING MICROWAVE PROCESSING

The application of microwave processing to glassy and semicrystalline thermoplastics, elastomeric polymers and composites has been pursued in these labs for several years. The goal of some of the more fundamental aspects of this research was to reveal the relationship between polymer structure and microwave energy absorptivity. The specimens were subjected to an electric field at 2.45 GHz inside either rectangular waveguides or a cylindrical cavity applicator at low powers (<100 watts). Both travelling wave modes and standing wave modes were examined. Temperatures, powers and times were recorded, leading to the concept of "microwave calorimetry."

The use of microwave energy for processing of polymers has been intensively investigated only in the past two decades. A positive impact has been made in the rubber and food industries where processing with microwaves has special advantages, such as: (a) rapid volumetric heating, (b) no overheating at the surface, (c) addressable heating, (d) energy saving and low operating costs, (e) increased throughput, (f) no direct degradation, and (g) potential for field repair.

Computer searches of chemical abstracts from 1967 until the present were conducted by an on-line search. The key words chosen were: a) microwave or high frequency or dielectric, b) curing or polymerization or crosslink or absorption or preparation or heating or drawing or processing, c) polymer or macromolecule or

composite or adhesive. The response that was obtained was useful but not inclusive. The information on electromagnetic radiation (EMR) in polymer science was distributed over a large number of different journals and reports and was not confined to the polymer literature. The "Journal of Microwave Power" and "IEEE Tran. Microwave Theory Tech." are two major sources outside of the polymer field.

Currently there are several research groups working in the EMR processing area, including: A. Gourdenne et al. in France, K. Nakagawa et al. in Japan, M. C. Hawley, J. Asmussen and coworkers at Michigan State University. Publications from the various groups have been categorized and are listed in appendix A. That appendix also includes references for dielectric and microwave techniques.

All groups depend on the following principles. Dielectric power absorption of a material can be represented by the following equation :

$$P = KfE^2\varepsilon'\tan\delta \qquad [1\text{-}1]$$

where P is the power dissipation in W/cm^3, K is a constant equal to 55.61×10^{-14}, f is the applied frequency in Hz, E is the electric field strength in V/cm, ε' is the dielectric constant and $\tan\delta$ is the dielectric loss tangent. Both ε' and $\tan\delta$ depend, in addition to the frequency, on the sample temperature.

The electromagnetic field energy dissipated as heat per unit volume is seen to be proportional to the dielectric loss factor ($\varepsilon'\tan\delta$), the square of the field strength (E^2) and frequency (f) of the applied field. The ratio of the dielectric loss factor to the dielectric constant is called the loss tangent for a nonionic material. The dielectric loss factor, ε'', determines the rate of conversion of electrical energy into thermal energy in the material before losses. Since the electric field penetrates the material, the heat is generated internally so that dielectric power dissipation is independent of the heat flow through the surface of the material, at least until convection and conduction contact with

the environment becomes important. This is in contrast to conventional thermal heating which is much more time consuming and is dependent upon the thermal conductivity of the material.

If we ignore convection and conduction losses, the heating rate of a material placed in an electromagnetic field depends on several key parameters as described by the relationship:

$$\frac{dT}{dt} = \frac{KfE^2\varepsilon'(T)\tan\delta(T)}{\rho C_v} \qquad [1\text{-}2]$$

where ρ is the density of the material, C_v is the specific heat and other parameters are the same as in Equation [1-1]. Therefore, the heating rate of a material depends directly on the square of the electric field strength and the dielectric loss factor which is usually a function of the temperature (due to the variation of ε'' with temperature).

Because the complexity of the field distribution within a multimode EMR processing cavity and the variation in dielectric properties of materials with temperature, moisture content, density and other parameters, in this research, only single mode applicators are discussed. These devices are relatively simple to analyze and possess well defined field patterns.

1.2 SPECIFIC RESEARCH TOPICS

This particular research is directed towards development and investigation of electromagnetic radiation calorimetry. Five topics were investigated and are discussed in the following chapters.

In chapter 2, the variation of the dielectric constant, ε', and the dielectric loss factor, ε'', with frequency will be discussed. Polymer chain mobility from -150°C to T_g or T_m

was studied by using a Polymer Laboratory's Dynamic Mechanical Thermal Analyzer (DMTA) at frequencies of 0.3, 1, 3, 10 & 30 Hz. Dielectric spectra from -150°C to above T_g or T_m were obtained via a Polymer Laboratory's Dielectric Thermal Analyzer (DETA) at frequencies of 0.1, 1, 10 & 100 kHz. A correlation was found between the dielectric properties of various polymers and the dipole moments of their small molecule analogues. From the mechanism of microwave absorption, heatability was found to be directly proportional to the dielectric loss factor. Experimentally, the dielectric loss factor was more closely related to the materials' heatability than was the loss tangent. Due to the difficulties of measuring the variation of ε'' with temperature directly at 2.45 GHz, a more experimentally convenient DETA measurement, specifically $(\varepsilon_s - \varepsilon_\infty)$, the oscillator strength, was used to evaluate the materials' processability.

In chapter 3, the dielectric behavior of nitrile rubbers was studied in the kHz frequency region via DETA (Dielectric Thermal Analyzer) and at a frequency of 2.45 GHz using a travelling wave applicator. The overall objective of this chapter was to show how convenient low frequency mechanical and dielectric testing (0.33 Hz - 100 kHz) could explain the heatability of nitrile rubbers at microwave frequencies in a travelling wave applicator. The dielectric loss factor ($\varepsilon'\tan\delta$) obtained from the low frequency tests was found to be directly proportional to the heatability of polymers in the microwave environment. A WLF plot was used to predict the shift of the dielectric loss maximum into or out of the microwave region.

Chapter 4 focuses on the dielectric behavior of glassy thermoplastics. For thermoplastics at room temperature, the dielectric loss at microwave frequencies consists of only a very low background loss because the location of the dielectric loss spectrum at 2.45 GHz is well above room temperature. The goal of this fundamental study was to improve the coupling of microwave energy to glassy thermoplastics which

are nearly transparent to microwave frequencies at room temperature and to understand the fundamental mechanisms involved in this optimization. Various starting temperatures for the investigations were induced by external heating of the waveguide. The specimens were subjected to an alternating electric field of 2.45 GHz inside a rectangular waveguide. Two different approaches were used in these experiments: both a travelling wave applicator and a TE_{10n} standing wave applicator were employed. From the plot of heating rate vs. temperature, the critical temperature of dielectric loss, T_c, was estimated for various glassy polymers. T_c gives an approximate indication of the point at which the dielectric loss factor increases significantly with increasing temperature.

In chapter 5, the processing of semicrystalline polymers such as poly(ether ether ketone) (PEEK), nylons, poly(ethylene terephthalate) (PET) via a cylindrical cavity and a rectangular standing wave applicator is described. Since the mechanism and the equations describing rapid microwave heating of thermoplastics are relatively independent of thermal conductivity, microwave heating avoids heat transfer rate problems encountered in conventional thermal heating for low thermal conductivity polymers. Due to the high temperatures needed to process semicrystalline polymers, the avoidance of thermal gradients as a result of microwave processing offers distinct advantages. Microwave heating may greatly reduce operating cost and improve processing speeds. In order to compare thermoplastic heating phenomena between amorphous and semicrystalline PEEK, both DMTA and DETA spectra were investigated to explain the rapid crystallizing rate of PEEK just above its glass transition temperature. The EMR heating phenomena also calorimetrically mapped the melting temperature of PEEK.

In chapter 6, a schematic model is proposed to explain the behavior of two phase materials subjected to microwave heating. Such materials include graphite composites and polymer blends. Field repair application of microwave processing to composite materials is also suggested. This chapter emphasizes how microwave calorimetry can be used to better understand the processing of two phase systems in general.

These findings are summarized in chapter 7. Some suggestions are also listed in that chapter.

CHAPTER 2

STRUCTURE-PROPERTY RELATIONSHIPS

2.1 INTRODUCTION

In the following chapters, microwave energy absorption of several nitrile rubbers, the dielectric properties of amorphous polymers and the microwave processibility of semicrystalline polymers will be investigated. Heatability in general will be found to be a direct function of the variation of the dielectric loss dispersion with temperature and frequency. Evaluating the applicability of microwave power processing requires a detailed knowledge of the material properties at numerous stages in the process. This information can be easily obtained by determining the dielectric properties as a function of frequency, temperature and moisture content, etc. via commercial Dielectric Thermal Analyzers. The variation of the dielectric constant, ε', and the dielectric loss factor, ε'', with frequency will be explained in section 1.2. The potential for selective coupling of microwave radiation into different materials will also be presented in order to utilize the value of the structure-property relationships on microwave processing.

Contour maps (1, 2) of the dielectric constant and the dielectric loss factor (or loss tangent) versus temperature and log frequency reveal different loss mechanisms in different regions of the temperature-log frequency space. Interpretation of these mechanisms usually requires information over a wide frequency range along with other material data such as the melting point and the glass transition temperatures. An optimum frequency for dielectric heating can be selected from the point of maximum dielectric loss as a starting point; but , the process is much more complex overall.

The dielectric behavior of a polymer is determined largely by the charge distribution within bonds, the chain configuration, bulk morphology and also by the statistical thermal motion of the polar groups. The most influential factor is the chemical structure. Thus, a detailed study of dielectric properties will not only permit one a better understanding of the polymer structure but will also allow determination of the optimum chemical structure for maximizing the coupling of microwave energy. Ultimately, this technique allows an assignment to those materials which would be most suitable for microwave processing.

There are numerous measurement techniques for obtaining the dielectric properties of polymers. Figure 2.1 (3) summarizes different measurement methods which are commonly used according to their appropriate frequency regimes. The measurement of the complex dielectric constant requires specialized techniques. For frequencies below 100 MHz, bridge methods are employed. Above this frequency, the measurement is accomplished by either a reentrant cavity, standing wave, or cavity resonator methods. Above 10 GHz, free space methods are used.

Analyses should be performed on various polymer structures to better understand the mechanism for coupling microwave energy into a material. Dielectric properties can be monitored as a function of frequency at a fixed temperature or as a function of temperature at a fixed frequency. The resultant contour surface of loss (temperature, frequency) is highly desirable. The activation energy, ΔE_a, can be determined by following the shift in absorption frequency as a function of temperature. A plot of the logarithm of the frequency versus the reciprocal of the absolute temperature maximum over a narrow frequency range yields a straight line whose slope is used in equation [2-1] for calculating the energy of activation.

$$\Delta E_a = -2.303R \times \text{slope} \qquad [2\text{-}1]$$

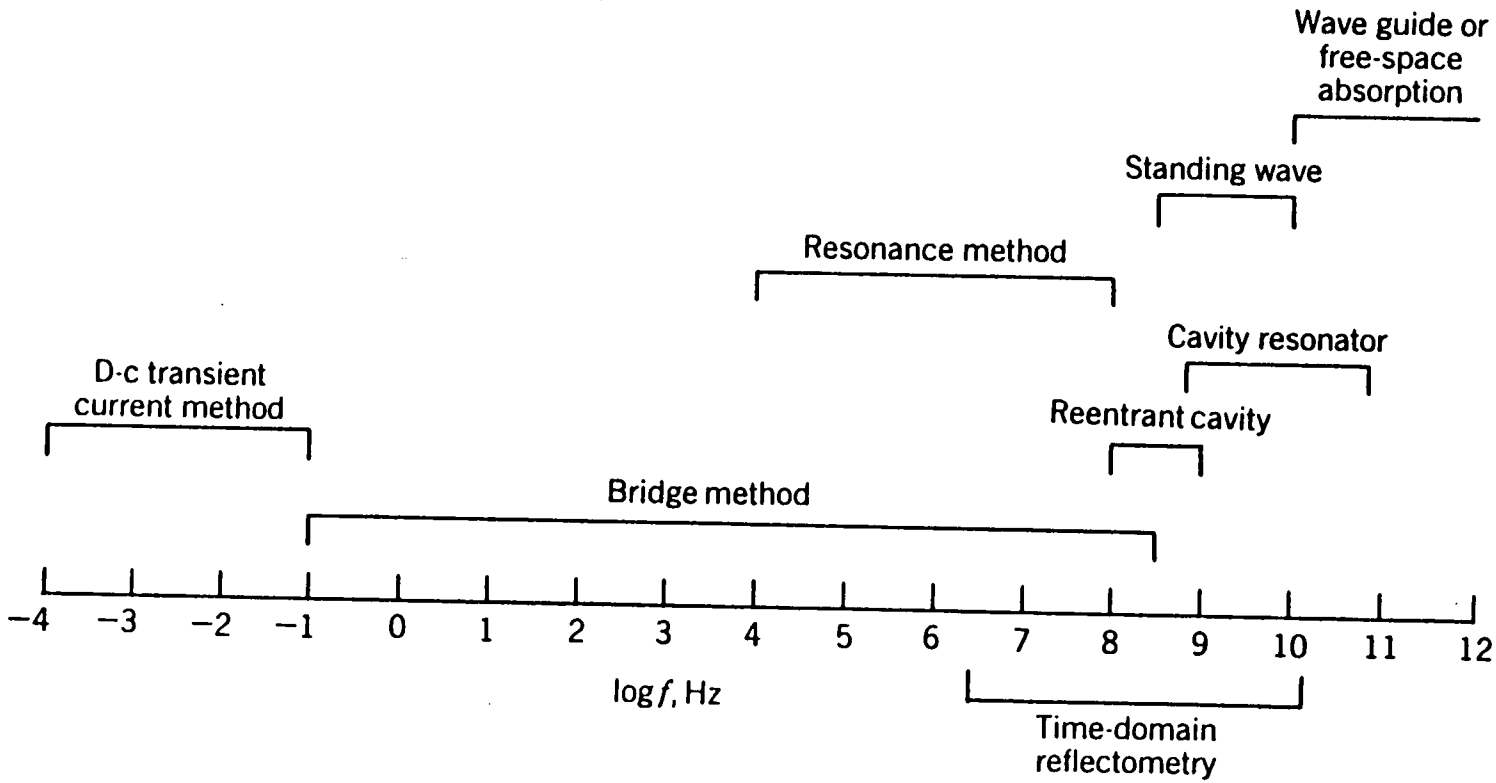

Figure 2.1 Frequency ranges suited for various techniques of dielectric measurement (3).

It is more experimentally convenient, however, to measure dielectric absorption spectra as a function of temperature, at various frequencies. Thus, variations caused by phase transitions can be observed directly. In addition, since the electrical properties of polymers are closely associated with the mechanical properties (polarization and relaxation), they are complementary in characterizing the structure-property relationships described in this chapter.

Every polymer has a spectrum of relaxation times which is determined by a set of structural units of differing mobility and which fix its dielectric loss dispersion. Polymer chain mobility from -150°C to T_g or T_m was studied by using a Polymer Laboratory's Dynamic Mechanical Thermal Analyzer (DMTA) at frequencies of 0.3, 1, 3, 10 & 30 Hz. Dielectric spectra from -150°C to above T_g or T_m were obtained via a Polymer Laboratory's Dielectric Thermal Analyzer (DETA) at frequencies of 0.1, 1, 10 & 100 kHz. A correlation was found between the dielectric properties of various polymers and the dipole moments of their small molecule counterparts. The mechanism of microwave heating was found to be related to the dielectric loss factor. Experimentally, the dielectric loss factor was more closely related to the materials' heatability than was the loss tangent. Due to the difficulties of measuring the variation of ε'' with temperature directly at 2.45 GHz, the more experimentally convenient DETA measurements, specifically the oscillator strength ($\varepsilon_s - \varepsilon_\infty$), were used to evaluate the materials' heatability. But, as will emerge, other considerations are equally important.

2.2 THEORY OF STRUCTURE-PROPERTY RELATIONSHIPS

Figure 2.2 depicts the general relationship of the dielectric constant and the dielectric loss factor to the applied frequency for a polar molecule. At high frequencies, electronic polarization is observed as a result of the displacement of the electrons in the atoms relative to the positive nuclei. Typically, the time required for electronic polarization is around 10^{-15} s which corresponds approximately to the frequency of ultraviolet radiation. Electronic polarization occurs in all materials and produces a dielectric constant of about 2.

Atomic polarization arises from the displacement of atoms relative to one another in the molecule. The movement of heavy nuclei is more sluggish than that of electrons; therefore, the time required for atomic polarization is around 10^{-13} s which corresponds to the frequency of infrared radiation. Electronic and atomic polarizations may also be called displacement deformations or distortion polarizations, in which case, the dipole moment so produced is called an induced dipole moment. Both of the above discussed rapid events are referred to as "optical polarizations."

If the polar molecules intrinsically possess a permanent dipole moment, the moment will tend to be aligned by the applied field to give a net polarization in that direction. Within the frequency range of dielectric relaxation, the polarizability of the electronic and atomic polarization remain unchanged. This is because the distortion polarization of a molecule reaches an equilibrium with the applied field in a much shorter time than does the orientation polarization. At lower frequencies, the contribution of the induced dipole moments becomes negligible compared to the permanent dipole moments of the system.

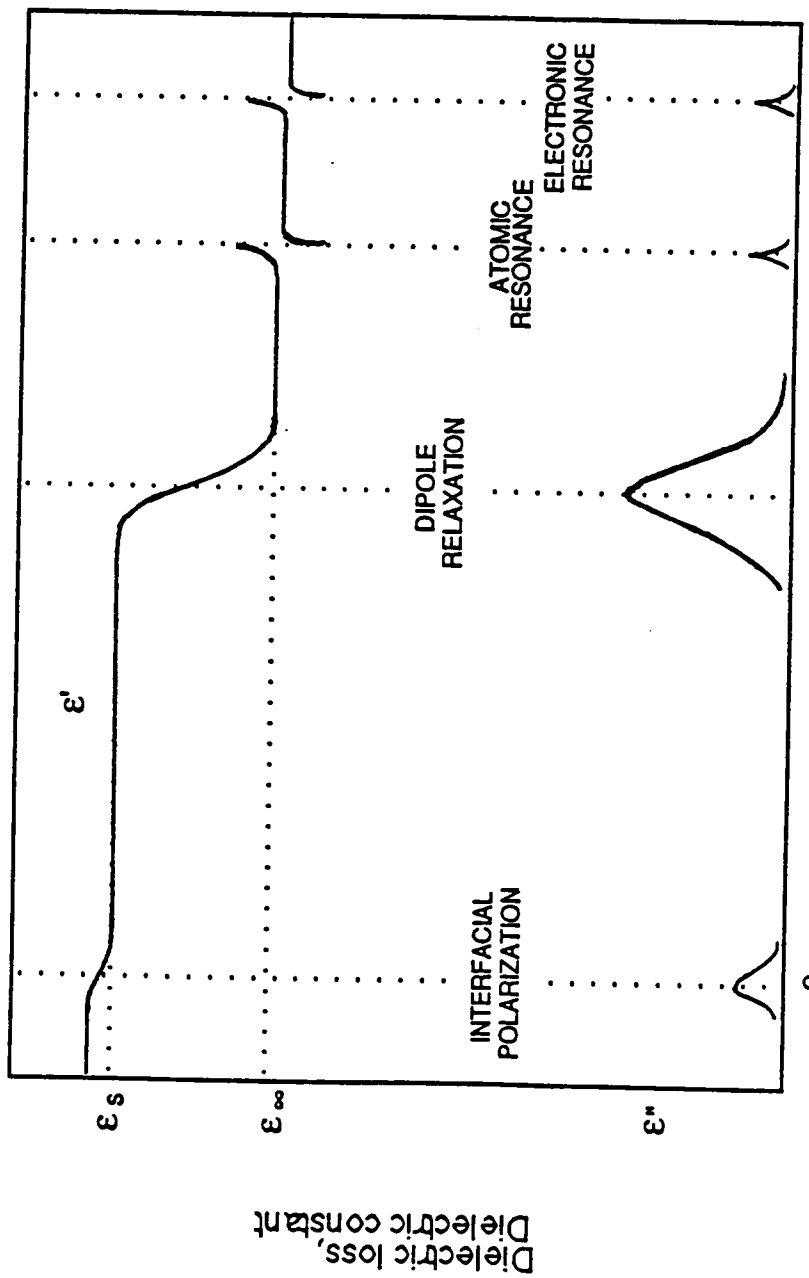

Figure 2.2 Schematic diagram of the dielectric spectra for a polar molecule.

Electronic, atomic, and orientation polarization are all due to changes that are locally bound in atoms, molecules, or the structures of solids and liquids. Interfacial polarization occurs as a result of their differences in the conductivities and dielectric constants of the materials at the interfaces. This accumulation of space charge is responsible for field distortions and dielectric loss.

Since the atomic and electronic polarization for polar molecules and polymers are often small compared with orientation polarization, they will not be considered further in this chapter. Dipole relaxation is commonly in the frequency range of 10^{-6} to 10^{10} Hz. The static (relaxed) dielectric constant, ε_s, and the high frequency (unrelaxed, or optical) dielectric constant, ε_∞, are defined in Figure 2.2 as the maximum and minimum dielectric constant in the dipole relaxation region. Dielectric relaxation is the exponential decay of the polarization with time in a dielectric material when an externally applied field is removed. The time required for the polarization to decay to 1/e of the original equilibrium value is identified as the relaxation time. Dielectric relaxation is the cause of anomalous dispersion in which the dielectric constant decreases with increasing frequency, as depicted in Figure 2.2. The decay function can be described in the following relationship:

$$\text{fun}(t) \approx e^{-t/\tau}, \qquad [2\text{-}2]$$

where τ is the relaxation time, which is time independent but highly temperature dependent. From a structural point view, the dipole relaxation depends on the internal structures of the molecules and on the molecular arrangement or structure of the dielectric material. In polymeric systems, this relationship is highly simplified.

The relaxation time depends on the viscosity of the medium, which in turn depends on the temperature. In gases where the molecular motion is vigorous and rapid, the time required for dipole relaxation is about 10^{-12} s. For small molecules in the liquid

state of low viscosity, the time required is about 10^{-11} - 10^{-10} s, which corresponds directly to the microwave frequency region. For large molecules or viscous liquids, the time required is about 10^{-6} s, ie., radio frequencies. The phase lag between the polarization and the applied field reveals an absorption of energy. The energy change (loss) involved will, therefore, be temperature dependent. Increasing temperature, and thus mobility of the molecules, allows for rapid orientation of polar molecules in the direction of the external electric field. In the case of alternating field, the polarization will be related to frequency.

As indicated diagrammatically in Figure 2.2, at high frequencies the viscosity of polymer molecules is too great so that the dipoles cannot orient in the rapidly reversing field. Consequently, the dipoles do not influence the a-c characteristics (ε'_∞ and ε''_∞) at high frequencies. As the frequency decreases, the dipoles respond more freely with an associated loss of energy. The loss peaks ultimately decrease when the oscillations of individual units no longer couple. As the frequency is reduced still further, the applied power is no longer converted to heat by viscous transfer. At this point, the dielectric constant possesses its highest static value, ε_S, in relation to the dipole contribution, and the dielectric loss factor and loss tangent reach a minimum. As the frequency approaches zero, ε'' approaches zero and ε' approaches the static dielectric constant, ε_S. As the frequency approaches infinity, ε' approaches ε_∞, the optical dielectric constant. The optical dielectric constant is defined as the product of the permittivity in free space and the square of the refractive index.

Separating the real and the imaginary parts of Debye equations.

$$\varepsilon' = \varepsilon_\infty + \frac{\varepsilon_S - \varepsilon_\infty}{1 + \omega^2 \tau^2} \qquad [2\text{-}3]$$

$$\varepsilon'' = \frac{(\varepsilon_s - \varepsilon_\infty)\,\omega\tau}{1 + \omega^2\tau^2} \qquad [2\text{-}4]$$

ε' is the dielectric constant at angular frequency, ω. ε_S is the static (low frequency) dielectric constant. ε_∞ is the the high-frequency dielectric constant. τ is the dielectric relaxation time. ω is the angular frequency of $2\pi f$. As the frequency or the relaxation time is increased or decreased via a temperature differential, ε'' reveals a maximum value at $(\varepsilon_S - \varepsilon_\infty)/2$ where $\omega\tau = 1$ in the simplified model where one τ is sufficient. At the same time, ε' decreases from ε_S to ε_∞ with increasing frequency.

For polar liquids this decrease may occur within a 100-fold frequency range. For polymers, however, the dispersion commonly occurs over a much wider frequency range. Also, the maximum value of ε'' is typically lower than that predicted by Equation [2-4]. Polar polymers realistically never follow the simple Debye equations. The real situation can be represented by the superposition of several Debye curves representing a set or distribution of relaxation times. To obtain the needed information, measurements should be made over a frequency range of 10^{-3} to 10^{10} Hz. The high-frequency value of the dielectric constant, ε_∞, is 2.2 to 2.5 for polymers. The static quantity, ε_S, may have a wide range of values depending on the polymer structure.

In simple liquids, the relationship of dielectric constant and dipole moment has been successfully expressed by the Onsager equation (4). At ordinary temperatures a polymer molecule in the liquid phase will undergo continuous Brownian motion and the moment of the chain will vary continuously in time. The Onsager theory is still not sufficient to describe the dielectric properties of polymer molecules.

In the condensed phase or not-too-dilute solutions, the dipole moments of the molecules or groups interact strongly resulting in a decrease of the total dipole moment. This reduction factor, g_r, was first defined by Kirkwood (5).

$$g_r = \frac{\mu_{eff}^2 (condensed)}{\mu_0^2 (gas)} \qquad [2\text{-}5]$$

where μ_0 is the total dipole moment of the group or molecule and μ_{eff} is the effective dipole moment measured in the condensed state. The value of the reduction factor is determined by the number and distance of the nearest polar neighbors to the group considered. Typically, the Kirkwood reduction factor is significantly different from unity, even for dilute solutions, due to the intramolecular interactions of the polar units of the macromolecule. The Kirkwood coefficient is highly temperature dependent because it is a measure of the intra- and inter-molecular interactions.

Intramolecular interactions are very important in bulk polymers in the solid and in the viscoelastic fluid states, however, their corresponding reduction factors have yet to be determined. Since the conformational motions of polymer molecules in bulk is not yet completely understood, it is difficult to determine which specific part of the molecule behaves rigidly during thermal motion in a given temperature range.

Fröhlich (6) modified the Onsager theory by incorporating the Kirkwood reduction factor into the Onsager equation which resulted in the Fröhlich-Kirkwood equation:

$$\varepsilon_s - \varepsilon_\infty = \frac{3\varepsilon_s}{(2\varepsilon_s + \varepsilon_\infty)} \frac{4\pi N}{3kT} \left(\frac{\varepsilon_\infty + 2}{3} \right)^2 g_r \mu_0^2 \qquad [2\text{-}6]$$

The quantity (ε_S - ε_∞) is an important quantity in the analysis of dielectric data in terms of molecular structure. It is a measure of the intensity or the strength of the relaxation process and is proportional to the number of dipoles involved in the relaxation process, but inversely proportional to the temperature.

If the dipole moment, μ_0, and the intra- and intermolecular interactions, g_r, are not changed in the working temperature range, then the dielectric constant should

decrease with increasing temperature. This is the case for dilute solutions and for some polymers in the molten state. However, the dielectric constant of practically all polar polymers increases with increasing temperature, indicating that the dependence is mainly governed by the change in the intra- and intermolecular interactions.

The area beneath the dielectric loss factor versus frequency curve, pictured in Figure 2.2, is proportional to (ε_s - ε_∞). In addition, the maximum dielectric loss factor varies with the distribution of relaxation times, as governed in the following equation:

$$\varepsilon_s - \varepsilon_\infty = \frac{2}{\pi}\int_{-\infty}^{\infty} \varepsilon'' d\ln f \qquad [2\text{-}7]$$

These general remarks apply to all dispersions, and are useful in checking the internal consistency of data; but are particularly important for the polymer dipolar relaxation region.

Polymers usually exhibit more than one dipolar dispersion as shown in Figure 2.3. A prominent feature of polymers' dipolar motions involves complex movement of multiple chain sections consisting of a large number of monomeric units (segments). This occurs at the T_g. Besides segments, smaller and more mobile kinetic units are also moving in polymers at appropriate temperatures. Such kinetically independent units may be side chains, chain ends, or individual atomic groups, e.g., polar substituents. The relaxation time of the orientation moment of such groups is smaller than the relaxation time of main-chain segments. For this reason, they can retain their mobility at lower temperatures where the segments of the main chain are practically immobile.

In order to identify and compare the locations of loss peaks in different polymers, the nomenclature first suggested by Deutsch, et al. (7) is used. The relaxation observed at the highest temperature (constant frequency) or lowest frequency (constant

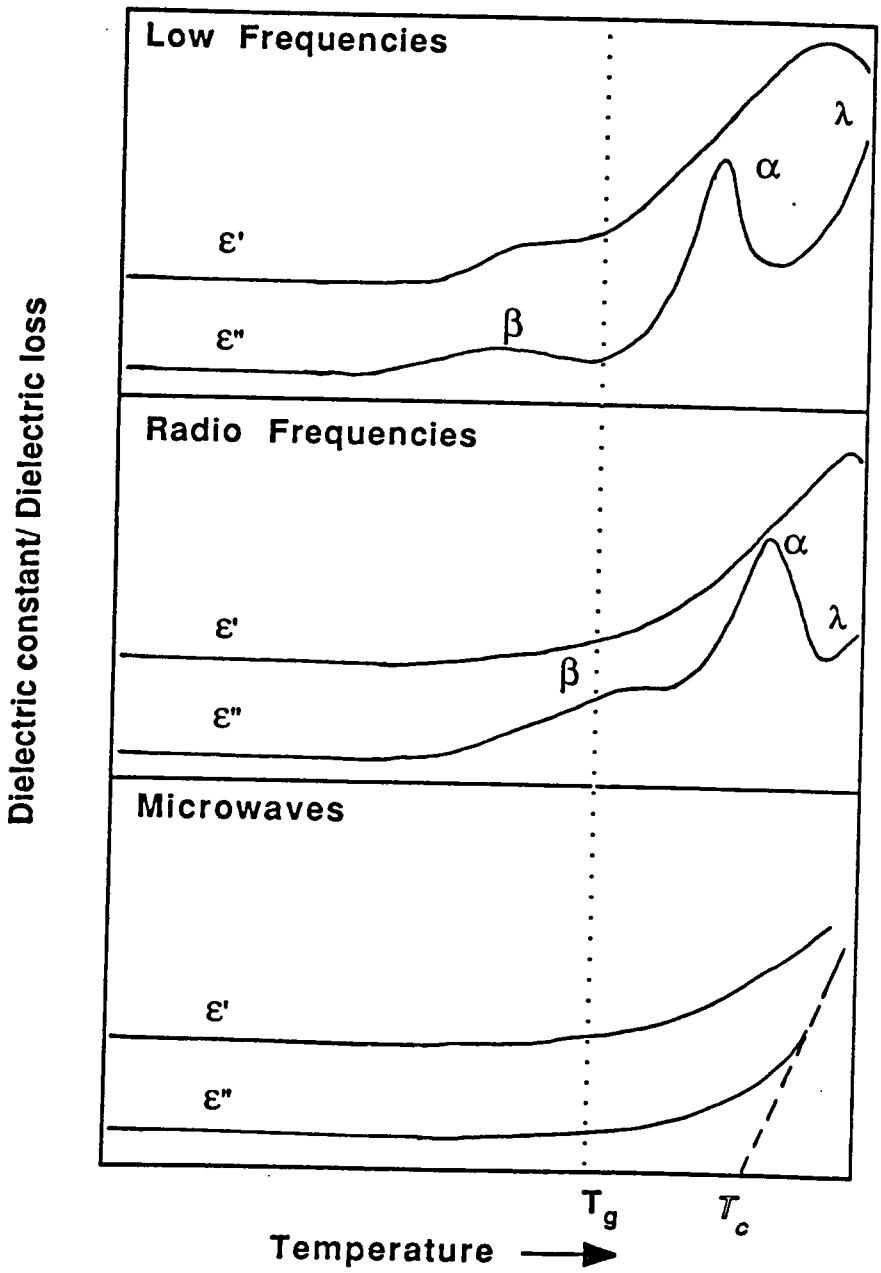

Figure 2.3 Schematic representation of the dielectric behavior of polar polymers at various frequencies.

temperature) is called the α loss. Subsequent losses: β, γ, etc., are identified with the remaining relaxation regions in order of decreasing temperature (or increasing frequency).

In amorphous polymers a loss region associated with the glass-rubber transition is observed at or above the "equilibrium", or "zero heating-rate", glass-transition temperature, T_g, and is usually labelled the α relaxation. The glass to rubber transition in polymers is associated with orientation rotation of multiple main chain units of the macromolecule under conditions where segmental movement is possible as the fluid condition is achieved. If there are polar groups in the polymer's side chains which are capable of orientation in an electric field independent of one another and which have different relaxation times, two dipole-group loss maxima will appear on the ε'' vs. temperature or ε'' vs. frequency curves. Losses of this kind may also occur below the T_g of the polymer (in the glassy state).

This chapter focuses on the variation of ε' and ε'' with frequency, as shown schematically in Figure 2.4. This figure reveals that there is a relationship to the data in Figure 2.3. The peak values will be identical. The relaxation time of each process can be described by the following equation:

$$\tau = \tau_0 exp(\frac{\Delta E_a}{RT}) \qquad [2\text{-}8]$$

where τ_0 is the period of vibration of atoms which is equal to 10^{-13} sec. The higher the temperature is, or the smaller the activation energy, the shorter the relaxation time will be. In Figure 2.3, the activation energy of the local chain motion (β process) is less than that of the main chain motion (α process) at a given temperature. Therefore, for a given increase in temperature, the β relaxation will shift faster than that of α relaxation. As a result, both relaxations tend to merge together as frequency is increased. In the

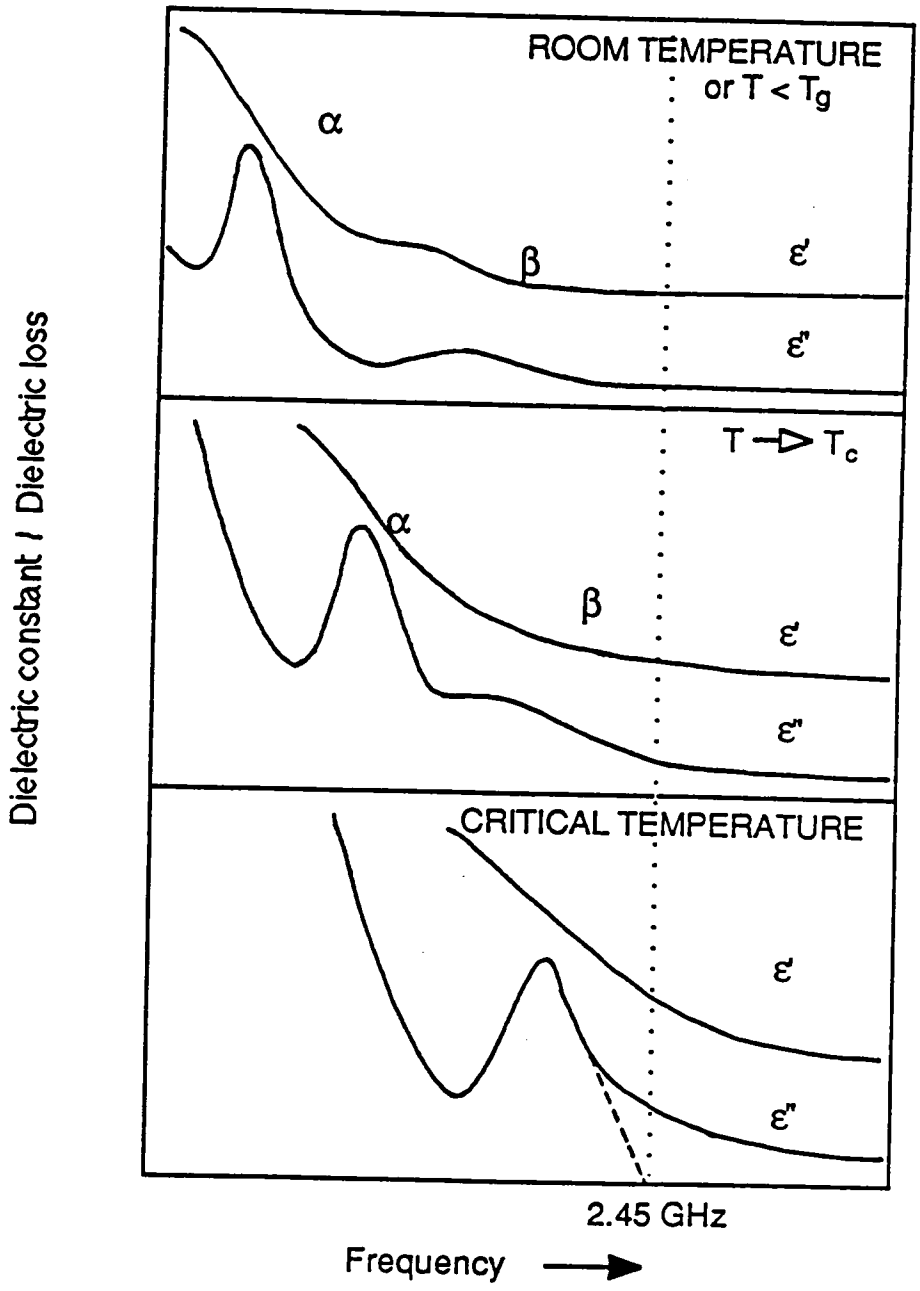

Figure 2.4 Schematic representation of the dielectric behavior of polar polymers at various temperatures.

frequency domain (see Figure 2.4), the shift of the α relaxation is faster than that of β relaxation. Therefore, both relaxations eventually merge together as frequency is increased.

There is no single method available for characterizing the dielectric behavior over a very wide frequency range; however, it is easy to monitor the dielectric properties via a thermal scan at a given fixed frequency up to the 100 kHz range. According to the principle of time-temperature superposition (8-10), the dielectric spectra in Figure 2.2 will shift to a higher frequency region by increasing the temperature. Merging α and β relaxations (see Figure 2.4) at higher frequencies will change the shape of the ε'' distribution, but will not affect the values of the oscillator strength, $(\varepsilon_S - \varepsilon_\infty)$, over the frequency domain of dipole relaxation . Evaluating the heatability by ascertaining the values of $(\varepsilon_S - \varepsilon_\infty)$ for various polymers is thus a rather simple task, under the proper conditions.

To evaluate the influence that structure-property relationships will have on microwave processability, it is imperative that the dielectric properties be thoroughly investigated and be correlated with chemical and morphological conformation. One must first examine the relationships between the dielectric constants of polymers and the effective dipole moments, as described in Equation [2-6]. In considering effective dipole moments, it is helpful to use group moments instead of bond moments. Group moments are the dipole moments of such chemical groups which are known to have a stable configuration even during thermal motion. For polymers containing dipolar groups, dielectric relaxation effects are observed owing to the time required for the orientation of the permanent dipoles subsequent to the application of the electric field.

It is important to examine the dipole moment of a molecule in some detail; orientation polarization due to the presence of permanent dipoles in a molecule is the

major energy coupling mechanism available for heating. The distance between charges is approximately 10^{-8} cm. The charges are about 10^{-10} electrostatic units each. Hence, dipole moments of molecules are typically of the order of 10^{-18} esu cm (1 Debye). One can calculate for all polymer structures a "static" dipole per repeat structure.

A. L. McClellan collected all experimentally determined dipole moments reported prior to 1962 and published them in a book for simple comparison (11). Dipole moments were usually determined in the gas phase or in a solution of a polar substance in a nonpolar solvent where, at infinite dilution, the interaction of the polar molecules with each other can be neglected. The tabulated dipole moments are arranged in the order of decreasing dipole moments (see Tables 2.1 and 2.2). The nomenclature used in these Tables is as follows. Column 1 indicates the chemical formula. The arrangement indicates decreasing dipole moments. Column 2 gives the compound name. Columns 3 and 5 show the respective dipole moments. The values of dipole moment given in column 3 are for samples in the gaseous state as indicated by column 4. The values of dipole moment in various solvents are given in column 5. The solvent types are indicated by symbols in column 6. The symbols, B and D, correspond to benzene and dioxane, respectively.

From the dipole moments of these model molecules, the order of polarity of group moments in polymer structure units is shown in Figure 2.5. In general, urea and sulfone groups have the highest dipole moments, with their Debye values over 4. These are followed by the lactone, amide and nitrile groups with values between 3 and 4 Debyes. Next, the isocyanate and ketone groups have values between 2 and 3 Debyes. The ether and carbonate groups have the lowest dipole moments at around 1 Debye. Other

Table 2.1 Dipole moments of small model molecules (I).

Formula	Compound Name	μ, D	State	μ, D	S
CH_4N_2O	Urea			4.56	D
$C_2H_6O_2S$	Dimethyl sulfone	4.47	gas	4.25	B
$C_3H_4O_2$	ß-Propiolactone	4.18	gas	3.85	B
C_2H_5NO	Acetamide			3.44~3.90	B
				3.60~3.92	D
C_2H_3N	Acetonitrile	3.92~4.01	gas	3.14~3.54	B
C_3H_3N	Acrylonitrile	3.89~3.91	gas	3.54	B
C_3H_5NO	Ethyl isocyanate			2.84	B
C_3H_6O	Acetone	2.80~2.97	gas	2.40~2.83	B
C_4H_6O	Cyclobutanone			2.76	B
$C_3H_8O_3$	Glycerol			2.56,2.68	D
$C_2H_6O_2$	Ethylene glycol	2.27	gas	1.5~2.30	B
				2.28~2.40	D
$C_3H_{10}N_2$	1,3-Diaminopropane			1.96	B
$C_2H_4Cl_2$	1,1-Dichloroethane	2.07~2.63	gas	1.8~2.0	B
CH_3Cl	Chloromethane	1.66~2.02	gas	1.69,1.88	B
CH_4O	Methanol	1.61~1.71	gas	1.60~1.78	B
				1.86~1.93	D
$C_3H_6O_2$	Methyl acetate	1.68~1.71	gas	1.45~1.75	B
$C_2H_4O_2$	Acetic acid	1.4~1.75	gas	0.74~1.64	B
				1.76	D
CH_5N	Methyl amine	1.00~1.34	gas	1.47	B
C_2H_6O	Methyl ether	1.29~1.33	gas	1.25	B
$C_3H_6O_3$	Dimethyl carbonate	0.87~1.01	gas	0.82~1.07	B

S: Solvent, B: Benzene, D: Dioxane

Table 2.2 Dipole moments of small model molecules (II).

Formula	Compound Name	μ, D	State	μ, D	S
$C_3H_8N_2O$	1,3-Dimethyl urea			5.1	B
				4.6,4.8	D
$C_4H_{10}O_2S$	Diethyl sulfone			4.44,4.50	B
$C_4H_6O_2$	g-Butyrolactone			3.82~4.15	B
C_3H_7NO	Propionamide			3.30,3.47	B
				3.85	D
C_3H_5N	Propionitrile	4.02~4.06	gas	3.37~3.69	B
C_4H_8O	2-Butanone			2.5~2.82	B
C_5H_8O	Cyclopentanone	3.30	gas	2.86~3.03	B
$C_4H_{10}O_3$	Diethylene glycol			2.69	D
$C_3H_8O_2$	1,3-Propanediol			2.37~2.52	D
$C_4H_{12}N_2$	1,4-Butanediamine			1.95,2.35	B
$C_3H_6Cl_2$	1,2-Dichloropropane	1.46~1.68	gas	1.87	B
	1,3-Dichloropropane	2.09	gas	2.09,2.10	B
C_2H_5Cl	Chloroethane	1.76~2.09	gas	2.0	B
C_2H_6O	Ethanol	1.1~1.7	gas	1.67~1.80	B
$C_4H_8O_2$	Ethyl acetate	1.78	gas	1.50~1.88	B
	Methyl propionate			1.70	B
$C_3H_6O_2$	Propionic acid	1.76	gas	0.63~1.69	B
				1.51~1.77	D
C_2H_7N	Ethyl amine	1.00~1.22	gas	1.28~1.40	B
C_3H_8O	Methyl ethyl ether	1.22	gas		
$C_4H_{10}O$	Ethyl ether	1.0~1.19	gas	0.74~1.53	B
$C_5H_{10}O_3$	Diethyl carbonate	1.07	gas	0.91~1.05	B

S: Solvent, B: Benzene, D: Dioxane

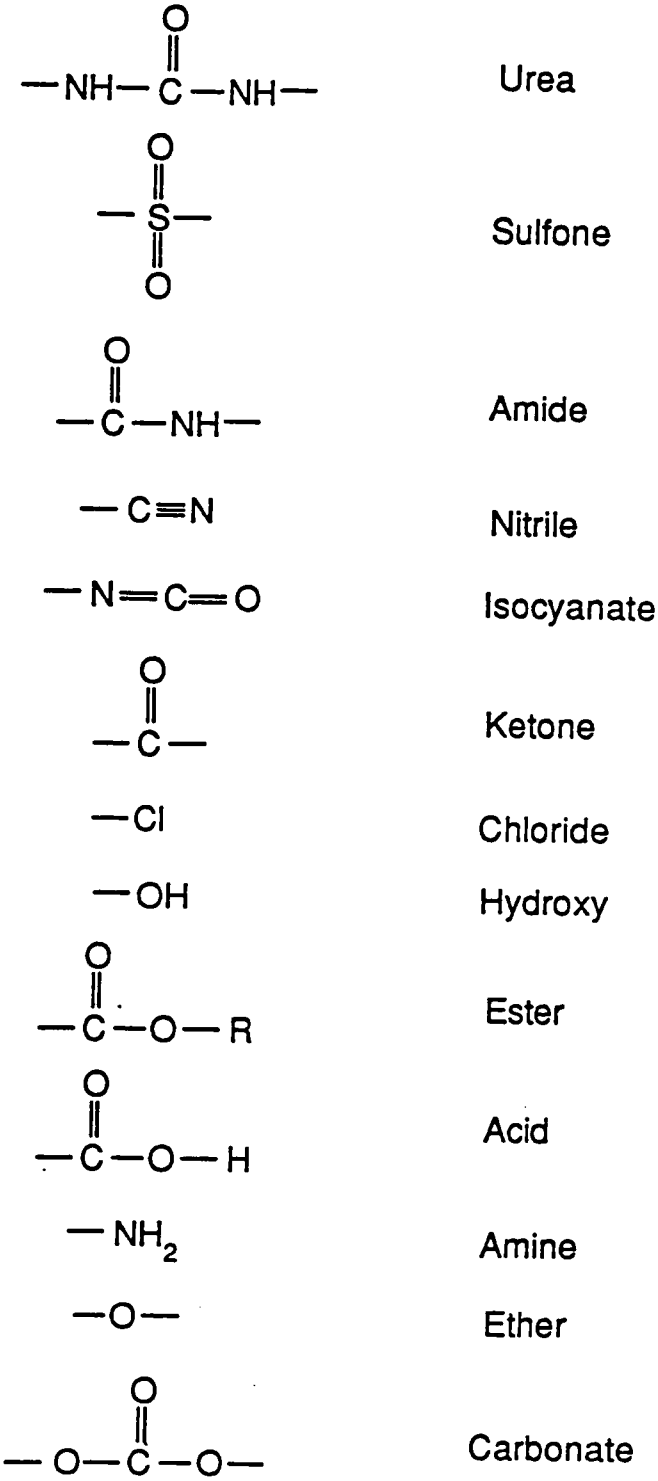

Figure 2.5 The polarity of group dipole moments.

mono-substituted molecules such as -Cl, -OH, -COOR, -COOH, $-NH_2$, have values between 1 Debye and 2 Debyes.

2.3 EXPERIMENTAL

2.3.1 Materials

Table 2.3 summarizes the glass transition temperatures, melting temperatures and the suppliers of the polymers used in this study. Specimen preparation methods are summarized in Table 2.4. For the semicrystalline polymers, some samples were quenched from the melt state into an ice water bath, while others of higher crystallinity were prepared by quenching in the platten press (Pasadena Hydraulics, Inc. model number P210C-X3-5-7-20).

2.3.2 Relaxation Spectrometer System

Polymer Laboratory's DETA (Dielectric Thermal Analyzer) and DMTA (Dynamic Mechanical Thermal Analyzer) were used to provide relaxation information covering the broad frequency range of 0.3 Hz to 100 kHz. Dielectric spectra from -150°C to above T_g or T_m were obtained via DETA at fixed frequencies of 0.1, 1, 10 & 100 kHz. Thermal mechanical spectra from -150°C to T_g or T_m were studied by using the DMTA at frequencies of 0.3, 1, 3, 10 and/or 30 Hz. All samples, except the nitrile rubbers, were tested in the bending mode.

2.3.3 Microwave Instrumentation

The details of the experimental instrumentation will be described in the following chapters. A travelling wave applicator was used to process the nitrile rubbers with three different percentages of acrylonitrile content. A cylindrical cavity applicator was used

Table 2.3 Thermal properties and sources of polymers.

Polymer	T_g, °C	T_m, °C	Sources	Catalog #
Polysulfone	190		SP[2]	046
Nylon6	63	229	Polysciences	18180
Nylon612	46		SP[2]	313
Nylon12	37	178	SP[2]	044
Nylon66	45	254	SP[2]	033
NBR455(40%ACN)	-19		BF Goodrich	
NBR355(30%ACN)	-31		BF Goodrich	
NBR210(19%ACN)	-50		BF Goodrich	
SAN	101		Union Carbide	RMD4400
PVC	85		Polysciences	9709
Polychloroprene	-48		SP[2]	502
PVAc	30		Aldrich	18949-9
PMMA	105		Inland Leidy	Elvacite
PEMA	66		Inland Leidy	Elvacite
PBMA	20		Aldrich	18152-8
Polycaprolactone	-60	60	Polysciences	7039
PET	81	260	SP[2]	138
PEEK	150	334	ICI	380G
Polyacetal	-30	180	Aldrich	18126-9
PPO	210	268	SP[2]	126
PC	150	267	SP[2]	035
SBR			Polysciences	7073

* SP[2]: Scientific Polymer Products

Table 2.4 Sample preparation condition in a platten press [a].

Polymer	T_g °C	T_m °C	Press Temp. °C	°F	Pressure x 10^{-3} lb	Teflon[b] #	Thick[c] mm
Polysulfone	190		245	473	10	0	0.36
Nylon6	63	229	230	446	3	2	0.30
Nylon612	46		210	410	3	2	0.30
Nylon12	37	178	185	365	3	2	0.30
SAN	101		155	311	10	0	0.28
PVC	85		145	293	12	0	0.83
Polychloroprene	-48	115	115	239	4	0	0.46
PVAc	30		71	160	10	0	0.40
PMMA	105		180	356	8	0	0.46
PEMA	66		115	239	10	0	0.46
PBMA	20		85	185	10	0	0.46
PET	81	260	265	509	3	2	0.27
PEEK	150	334	340	644	10	*[d]	0.32
Polyacetal	-30	180	180	356	3	1	0.29
PPO	210	268	275	527	4	1	0.42
PC	150	267	270	518	3	2	0.23
SBR			110	230	10	0	0.45

a) Pasadena Hydraulics, Inc. model number P210C

b) Number of teflon sheets (0.01 in. thick) as space bar

c) Sample thickness

d) *Use aluminum foil as space bar

to process the ethylene/vinyl acetate copolymers. The TE_{111} mode was chosen to process these polymers. The specimens for microwave processing (1 cm x 1 cm x 0.5 cm) were put in the trough of a flexible silicone mold. The size of the silicone mold was about 2 cm x 2 cm x 1.2 cm. Two more pieces of silicone mold were stacked to support the specimen and to raise the specimen to the center of the TE_{111} mode. An additional silicone mold was placed on the top of the specimen in order to secure the fiber optical temperature probe in place. The other function of the top mold was to insulate the sample so as to prevent heat convection losses from the specimen.

2.4 RESULTS AND DISCUSSION

2.4.1 Thermal Spectra from DETA and DMTA

Figure 2.6 depicts the temperature dependence of the log storage modulus and the loss tangent for bisphenol A based polysulfone at 1, 3, 10 and 30 Hz using the DMTA instrument. The glass transition temperature of bisphenol-A polysulfone was observed at around 195°C as identified by the peak in the loss tangent. At T_g, the storage modulus dropped 1.5 decades, as shown in Figure 2.6. Molecular chain stiffness resulting from the bulky phenyl groups in the main chain was responsible for the high T_g. Another mechanical transition was found near to -70°C, which is the well-known β-transition.

Figure 2.7 illustrates the temperature dependence of the dielectric loss tangent of polysulfone in two linear scales for 0.1, 1, 10 and 100 kHz. The loss tangent scale between -60°C and 40°C was enlarged 50 times in order to amplify the β relaxation. The peak intensity of the α relaxation was about 100 times larger than that of the β

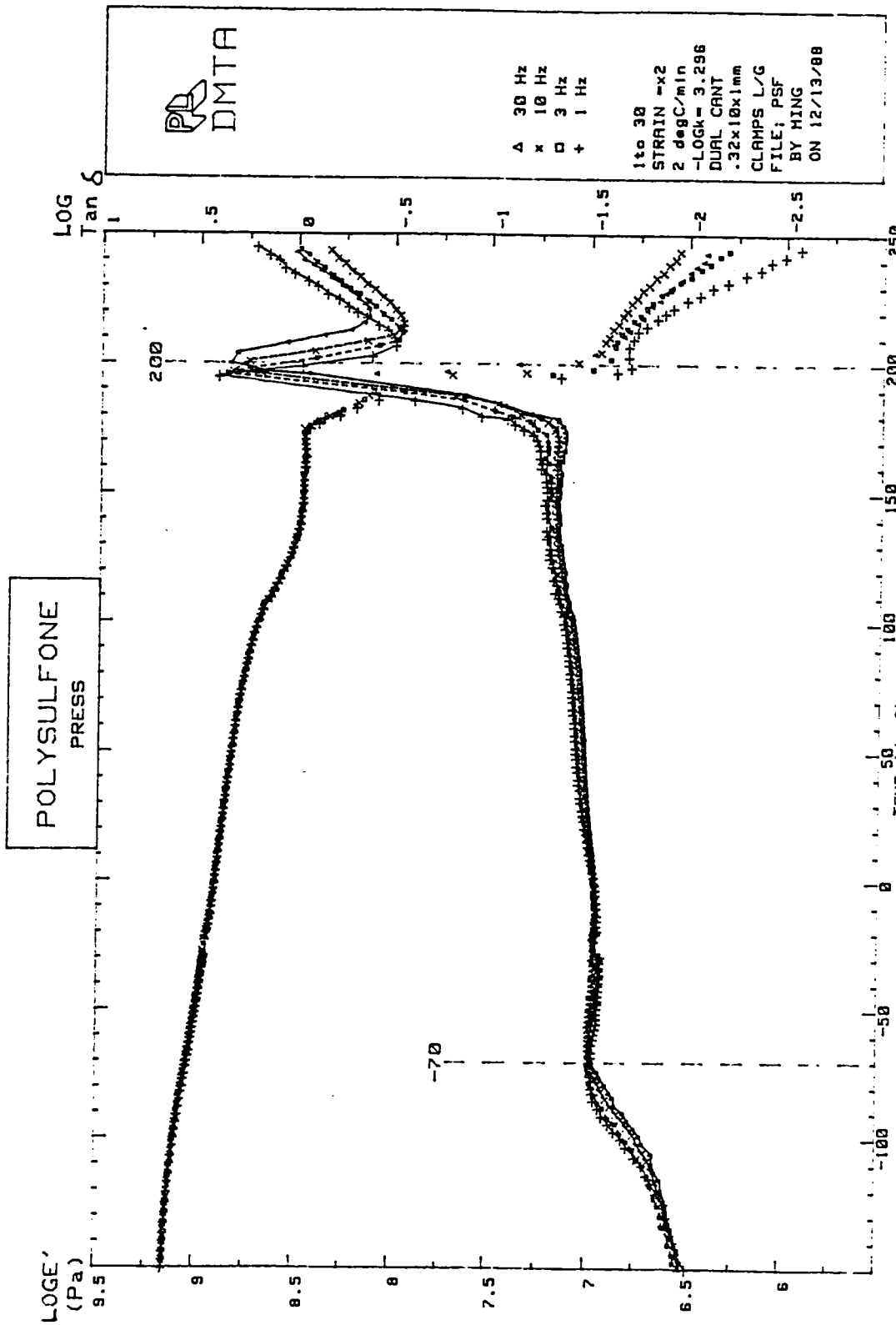

Figure 2.6 Temperature dependence of the storage modulus and loss tangent of polysulfone at various frequencies.

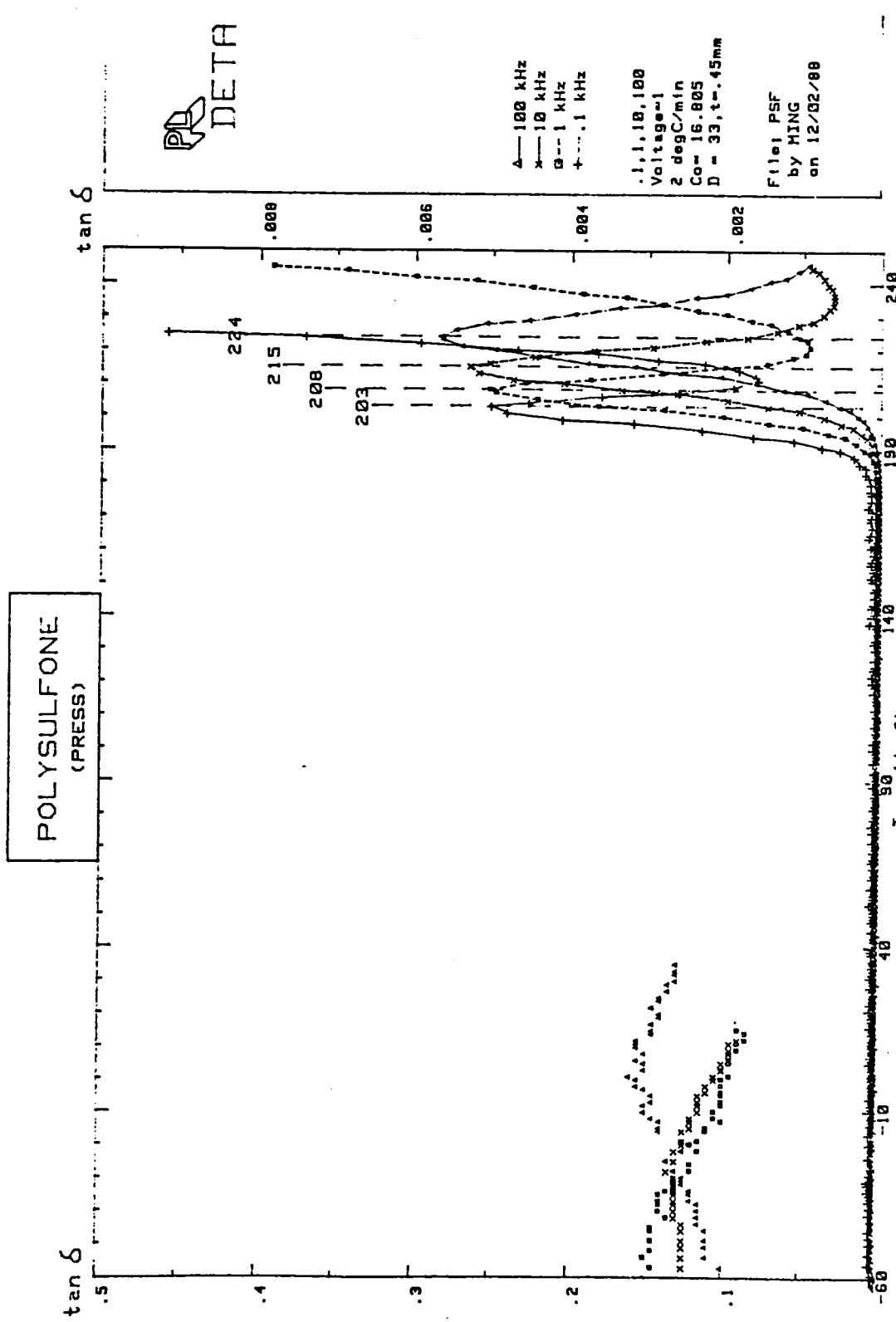

Figure 2.7 Temperature dependence of the dielectric loss tangent of polysulfone at various frequencies.

relaxation. The intensity of the dielectric absorption depended on the position of the polar bonds in the polymer chain with respect to the specific units involved in the thermal motion. In the case of polysulfone, the very polar sulfone groups, as shown in Tables 2.1, 2.2 and Figure 2.5, were integral to the main chain. This polarity, only exhibited in the glass transition region, resulting in a large dielectric relaxation. The low dielectric intensity of the β relaxation for polysulfone indicated that the corresponding mechanical β relaxation didn't involve the motion of polar sulfone groups. The change in main chain and local chain dielectric losses in polymers with temperature and frequency are associated with the mobility of the kinetic units of the polymer chain. For this reason, it would seem logical that mechanical and dielectric properties would be complementary.

Table 2.5 summarizes the T_g's determined from the plot of tanδ versus temperature at 0.1, 1, 10 and 100 kHz for various polymers via a DETA. The outline letters in the case of the methacrylates indicate that a and β relaxations merged. The outline italic letters indicate those transitions which were difficult to get from the T_g. For the semicrystalline polymers, the T_g's for both the quenched and the slow cooled materials were also determined.

T_g, T_m, and the apparent activation energies calculated from the frequency range of 0.1 kHz to 100 KHz are summarized in Table 2.6. As frequency increased, the T_g's determined from the peaks of tanδ were shifted to higher temperatures. A plot of the dependence of log(frequency) on the reciprocal of absolute temperature maximum (T_g) for the α relaxation fell on a smooth curve, indicating a continuously changing activation energy with temperature. Placement of a straight line through the data over a narrow frequency range yielded a slope proportional to the activation energy, ΔE_a, as depicted in Equation [2-1]. These calculated values are summarized in the 4th and 5th columns

Table 2.5 T_g's from 0.1 kHz to 100 KHz for several polymers.

Polymer	10^2Hz	10^3Hz	10^4Hz	10^5Hz	Remark
Polysulfone	203	208	215	224	
Nylon6	75	80	85	93	Q in ice water
	72	77	83	91	Q in press
Nylon612	66	70	76	87	Q in ice water
Nylon12	58	62	70	82	Q in ice water
Nylon66	79	84	87	96	Q in ice water
NBR455(40%ACN)	-9	-2	5	14	
NBR355(30%ACN)	-14	-10	-4	6	
NBR210(19%ACN)	-26	-22	-15	-5	
SAN	123	131	141	153	
PVC	100	105	111	120	
Polychloroprene	-18	-14	-7	0	
PVAc	59	67	77	90	
PMMA		90	129	145	Partially merge
PEMA	88	95	110	129	α & β merge
PBMA	52	66	81	102	α & β merge
PET	92	98	105	111	Q in ice water
	96	105	112	121	Q in press
PEEK	152	156	161	165	Q in ice water
	166	168	174	182	Cooled in DETA
BTDA/APB		225	235	246	Nondoped imide
		219	229	241	Doped Polyimide
Polyacetal	-55	-44	-35	-27	Q in press
PPO	219	228	238	251	Q in ice water
	220	232	239	251	Q in press
PC	163	168	174	182	Q in ice water
	163	168	174	182	Q in press
SBR		78	88	99	

Table 2.6 Thermal properties and the apparent activation energies for several polymers

Polymer	T_g,°C	T_m,°C	E_a*	E_a#	Remark
Polysulfone	190		570	640	
Nylon6	63	229	370	410	Q in ice water
			350	380	Q in press
Nylon612	46		270	320	Q in ice water
Nylon12	37	178	230	270	Q in ice water
Nylon66	45	254	390	440	Q in ice water
NBR455(40%ACN)	-19		185	190	
NBR355(30%ACN)	-31		170	200	
NBR210(19%ACN)	-50		150	175	
SAN	101		300	320	
PVC	85		380	420	
Polychloroprene	-48		190	220	
PVAc	30		210	220	
PMMA	105		100		Partially merge
PEMA	66		170	200	α & β merge
PBMA	20		130	140	α & β merge
PET	81	260	420	420	Q in ice water
			350	340	Q in press
PEEK	150	334	790	810	Q in ice water
			550		Cooled in DETA
BTDA/APB			470		Nondoped imide
			440		Doped Polyimide
Polyacetal	-30	180	130	110	Q in press
PPO	210	268	430	460	Q in ice water
			520	490	Q in press
PC	150	267	550	600	Q in ice water
			550	600	Q in press
SBR			240		

Activation energy in kJ/mole calculated from a)*1,10 & 100 kHz b)#0.1,1,10 & 100 kHz

in Table 2.6. In general, the activation energies in the 4th columns, calculated from the T_g's at 1, 10 and 100 kHz, are smaller than those in the 5th column, calculated from the T_g's at 0.1, 1, 10 and 100 kHz. Although four decades of frequency were not enough to show a Williams-Landel-Ferry (WLF) relationship, these calculated activation energies fit the trend of the WLF relationship. These Arrhenius activation energies were useful in predicting the shift of the dielectric loss factor spectra into or out of the 2.45 GHz frequency region. Generally, the stiffer the polymer chain, the higher the T_g and the larger the apparent activation energy. This resulted in a slower shift of the dielectric loss spectra and a narrower span between T_g and T_c, the critical temperature of dielectric loss.

Figure 2.8 shows the variation of the dielectric constant and the dielectric loss of polysulfone with temperature. The relative dielectric constant increased by only 0.2 in the β relaxation region, but it increased from 2.9 to 7.65 in the glass transition zone which was evidence for a strong dielectric relaxation. As discussed before, we can consider the inverse of the temperature axis as equivalent to a frequency axis so that the static and high frequency dielectric constants can be identified, as in Figure 2.8. The static (relaxed) dielectric constant, ε_s, was assigned as the maximum dielectric constant, 7.65 for polysulfone. The high frequency (unrelaxed) dielectric constant, ε_∞, was assigned as the minimum dielectric constant, 2.7. The difference, $(\varepsilon_s - \varepsilon_\infty)$, for polysulfone is tabulated in Table 2.7. The maximum value of the dielectric loss factor from Figure 2.8 and the loss tangent from Figure 2.7 at 100 kHz are 1.68 and 0.282, respectively, which are also listed in Table 2.7.

Merging of α and β relaxations has a large influence on the dielectric loss factor. The maximum in dielectric loss as well as the shape of the dielectric loss dispersion depends on the distribution of the relaxation times. The area below the dielectric loss

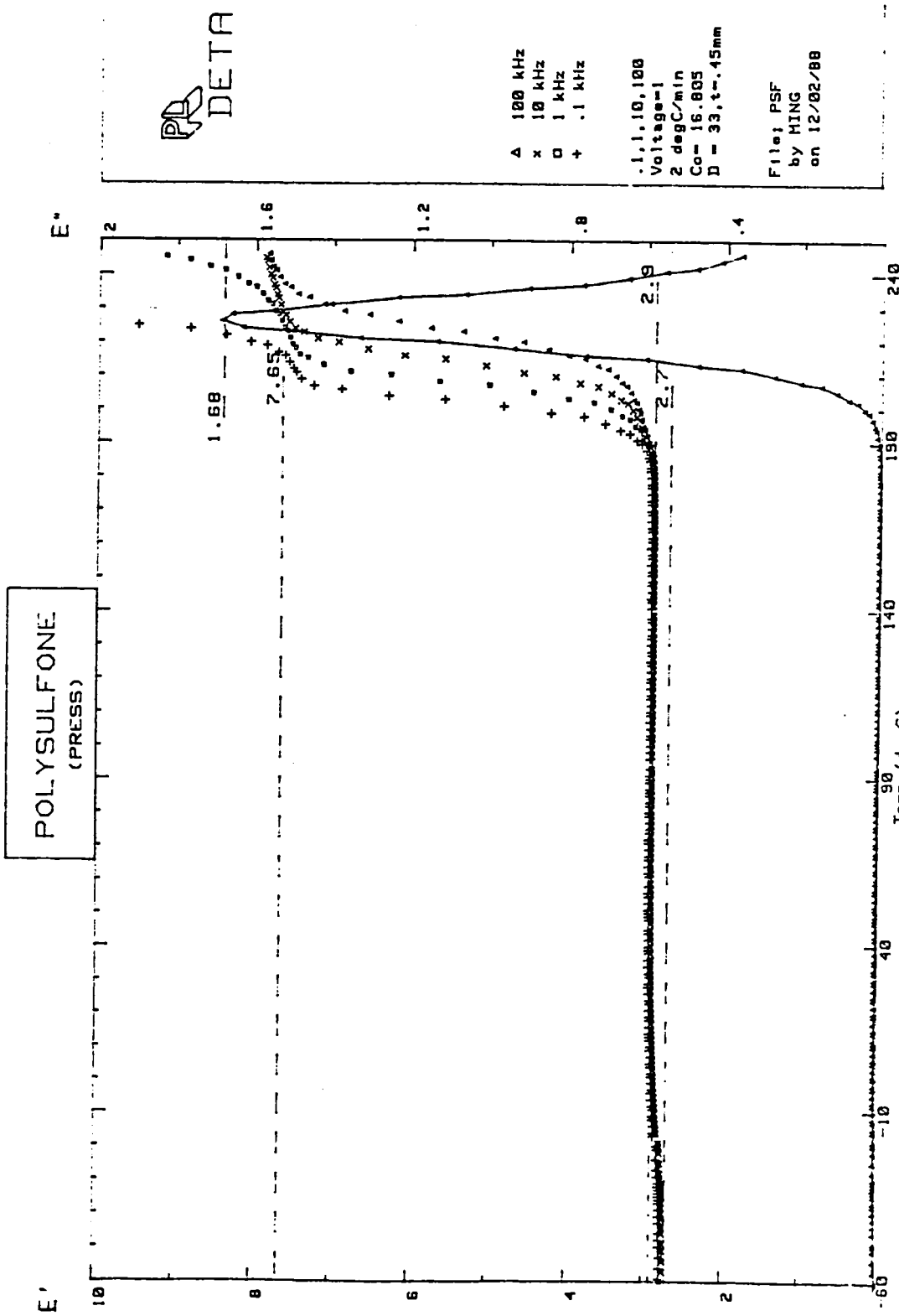

Figure 2.8 Temperature dependence of the dielectric constant and the dielectric loss factor of polysulfone at various frequencies.

Table 2.7 Dielectric properties at 100 kHz for several polymers.

Polymer	ε_s-ε_∞	ε''_{max}	$\tan\delta_{max}$	Remark
Polysulfone	4.80	1.69	0.282	
Nylon6	9.60	1.41	0.184	Q in ice water
	7.38	1.31	0.198	Q in press
Nylon612	6.72	0.75	0.147	Q in ice water
Nylon12	6.72	0.86	0.177	Q in ice water
Nylon66	4.80	0.60	0.120	Q in ice water
NBR455(40%ACN)	14.60	5.56	0.425	
NBR355(30%ACN)	10.40	3.52	0.346	
NBR210(19%ACN)	5.60	1.68	0.269	
SAN	5.25	1.59	0.269	
PVC	5.60	1.20	0.186	
Polychloroprene	3.45	0.99	0.185	
PVAc	5.00	1.60	0.261	
PMMA	2.25	0.52	0.128	α & β merge
PEMA	1.60	0.51	0.137	α & β merge
PBMA	1.50	0.49	0.127	α & β merge
PET	2.60	0.27	0.066	Q in ice water
	1.40	0.08	0.024	Q in press
PEEK	0.85	0.22	0.064	Q in ice water
	0.85	0.06	0.022	Cooled in DETA
BTDA/APB	1.55	0.17	0.058	Nondoped imide
	0.75	0.10	0.034	Doped Polyimide
Polyacetal	0.65	0.07	0.029	Q in press
PPO	0.50	0.01	0.005	Q in ice water
	0.20	0.01	0.004	Q in press
PC	1.15	0.08	0.027	Q in ice water
	1.10	0.07	0.027	Q in press
SBR	0.20	0.01	0.005	

factor curve changes as relaxations merge; however, the value of (ε_s - ε_∞) will remain unchanged in the transition region. The square of the dipole moment is closely related to (ε_s - ε_∞), as shown in Equation [2-6], rather than to the distribution of the dielectric loss peak. Evaluating the heatability of polymers using the difference of (ε_s - ε_∞) was found to be an easy task by using a DETA.

Table 2.7 summarizes the dielectric properties of various polymers according to the polarity of their group moments shown separately in Figure 2.5 and Tables 2.3 and 2.4. The values of (ε_s - ε_∞) are summarized in the 2nd column. In order to predict the heatability at 2.45 GHz, the peak values of ε'' and tanδ at the highest frequency, 100 kHz, obtained via DETA, are listed in the 3rd and 4th columns. In general, the variation of tanδ is relatively small compared to the variations of (ε_s - ε_∞) or ε''. Highly polar polymers in the upper half of Table 2.7 had dielectric properties that were a stronger function of temperature than the lower polarity polymers in the bottom half of the Table. In the majority of cases, the α peak dielectric loss was higher than the β dielectric loss, although the reverse was true for poly(methyl methacrylate) and a few other examples. Thus, the investigation of the low frequency response of dielectric properties is one of the most methods of studying polymer microwave behavior.

In summary, dielectric properties in polymers - (ε_s - ε_∞), ε'', tanδ - and their coupling with EMR are related to the various most probable relaxation times which depend highly on the chemical constitution of the repeating unit in the chain, the nature and number of the polar groups, substituent size, steric as well as some other factors. From Table 2.7, it was proposed that the value of (ε_s - ε_∞) for polymer depended on several factors that can be used for advanced processing methods:

(A) Group dipole moments: Dielectric loss depends on the chemical constitution of polymers. It mimics the trend of polarity of small model molecules, but other factors matter.

(B) Mole percentage of polar groups: The dielectric properties of a copolymer chain composed of different randomly alternating monomeric units depended on the constitution of the monomeric units and on their ratio. The value of $(\varepsilon_s - \varepsilon_\infty)$ and ε'' were found to rise monotonically with increasing content of the polar component. Dilution of the polar components in a acrylonitrile-butadiene copolymer caused the maximum ε'' to decrease with increasing butadiene content, as shown in Figures 2.9-2.11. The maximum ε'' at 100 kHz are listed in the 3rd column of Table 2.7. Figures 2.12-2.14 show the variation of dielectric constant with temperature at 100 kHz. The T_g's from DSC are also shown in the figures. On the cool side of the maximum dielectric constant, the effect of increasing temperature on the value of $(\varepsilon_s - \varepsilon_\infty)$ is less important. Beyond the transition region, $(\varepsilon_s - \varepsilon_\infty)$ decreased with increasing temperature. This phenomena can be explained by Equation [2-6] in that the dielectric constant decreased with increasing temperature. The differences between the maximum and minimum dielectric constants, $(\varepsilon_s - \varepsilon_\infty)$ are listed in the 2nd column of Table 2.7. These DETA spectra will be used to investigate the heating behavior in the microwave field.

The oscillator strength of the dielectric transition $(\varepsilon_s - \varepsilon_\infty)$ or the area under the dielectric loss factor versus frequency curves are related to the concentrations of the various polar groups involved. The effect of mole percentage of polar groups can also be seen as a function of (a) % of -CONH (amide) group in different nylons; (b) % of -Cl (chloride) group in poly(vinyl chloride) and polychloroprene; (c) % of -COOR (ester) group in poly(methacrylates).

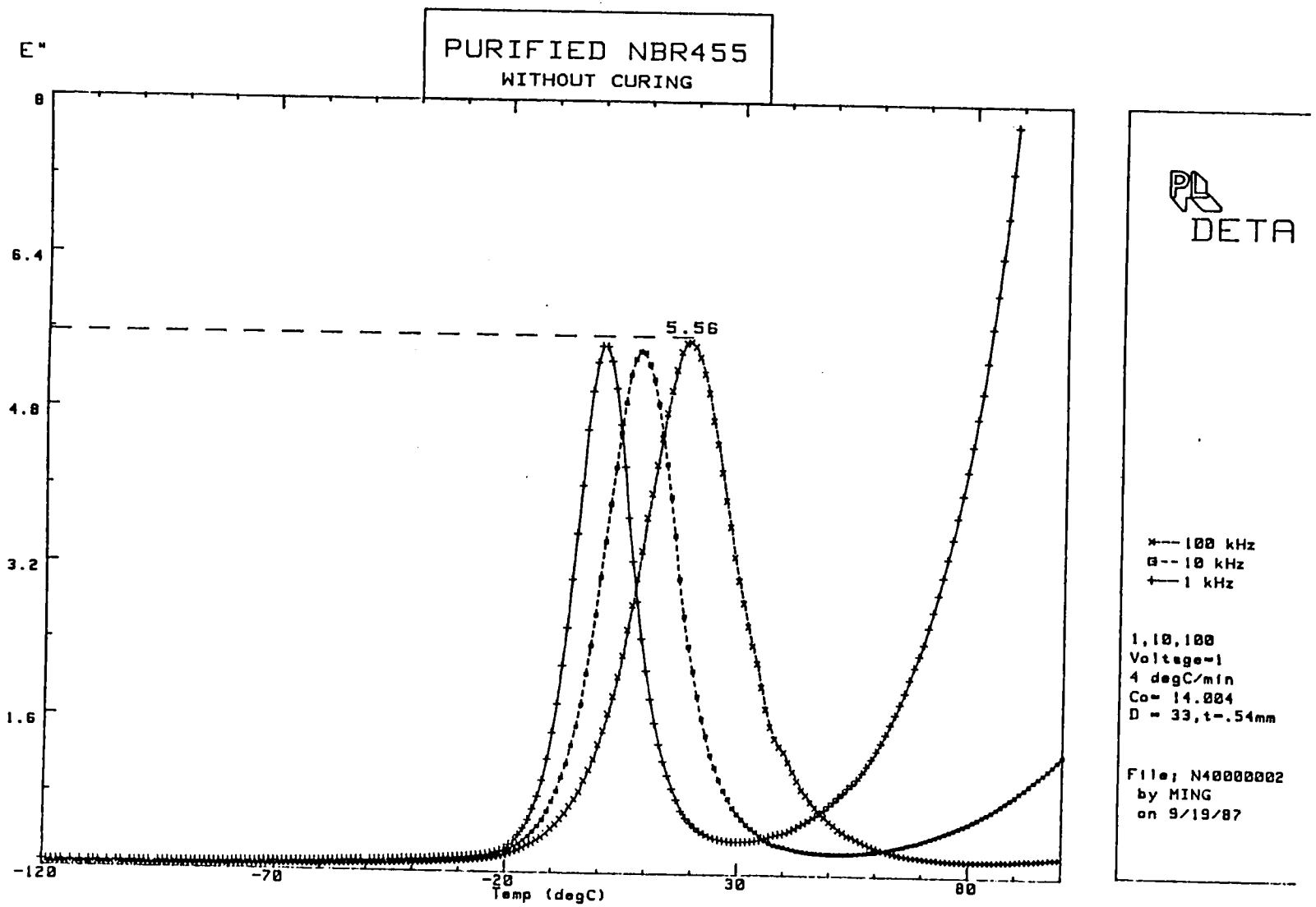

Figure 2.9 Temperature dependence of the dielectric loss factor of 40% acrylonitrile nitrile rubber at various frequencies.

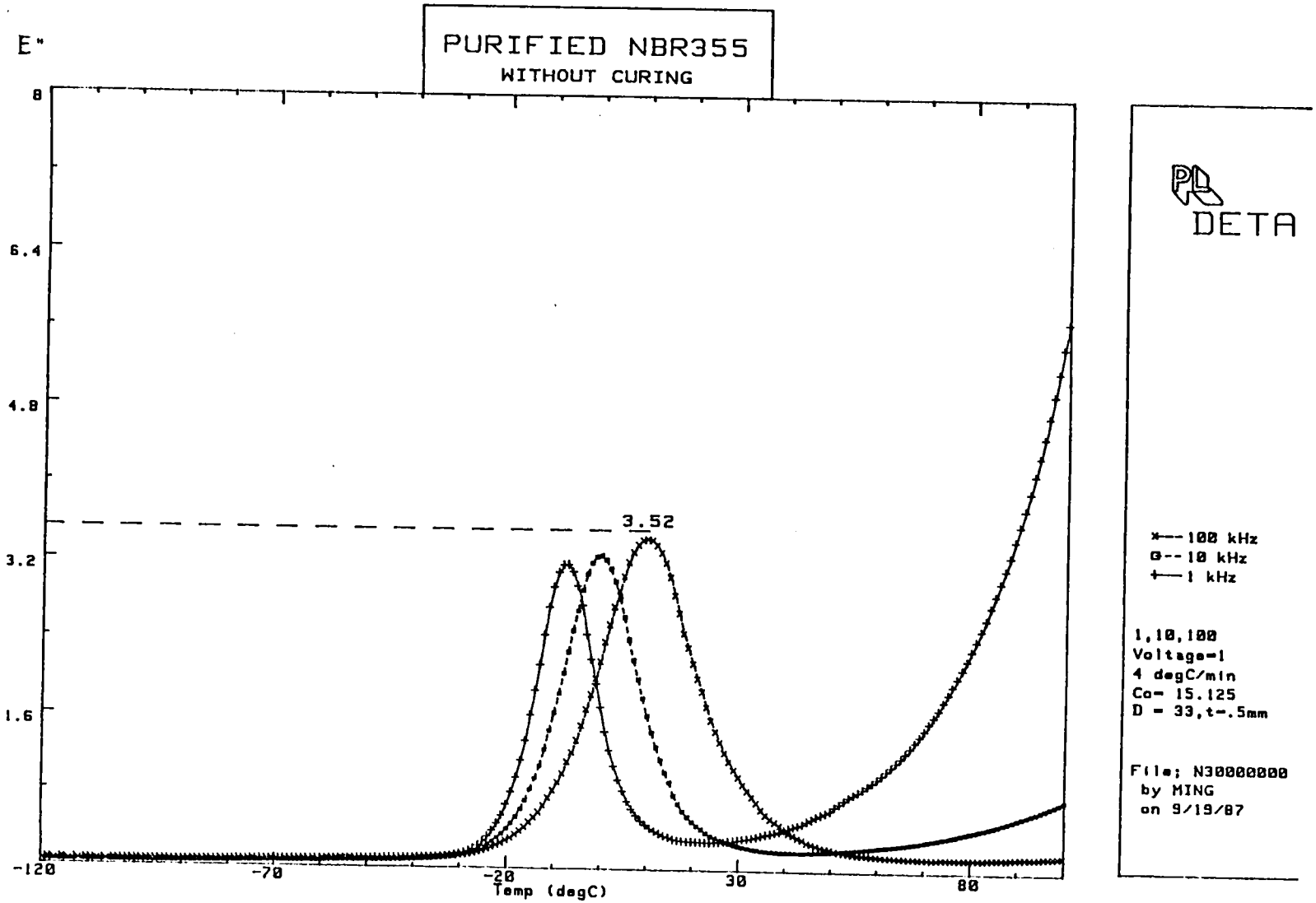

Figure 2.10 Temperature dependence of the dielectric loss factor of 30% acrylonitrile nitrile rubber at various frequencies.

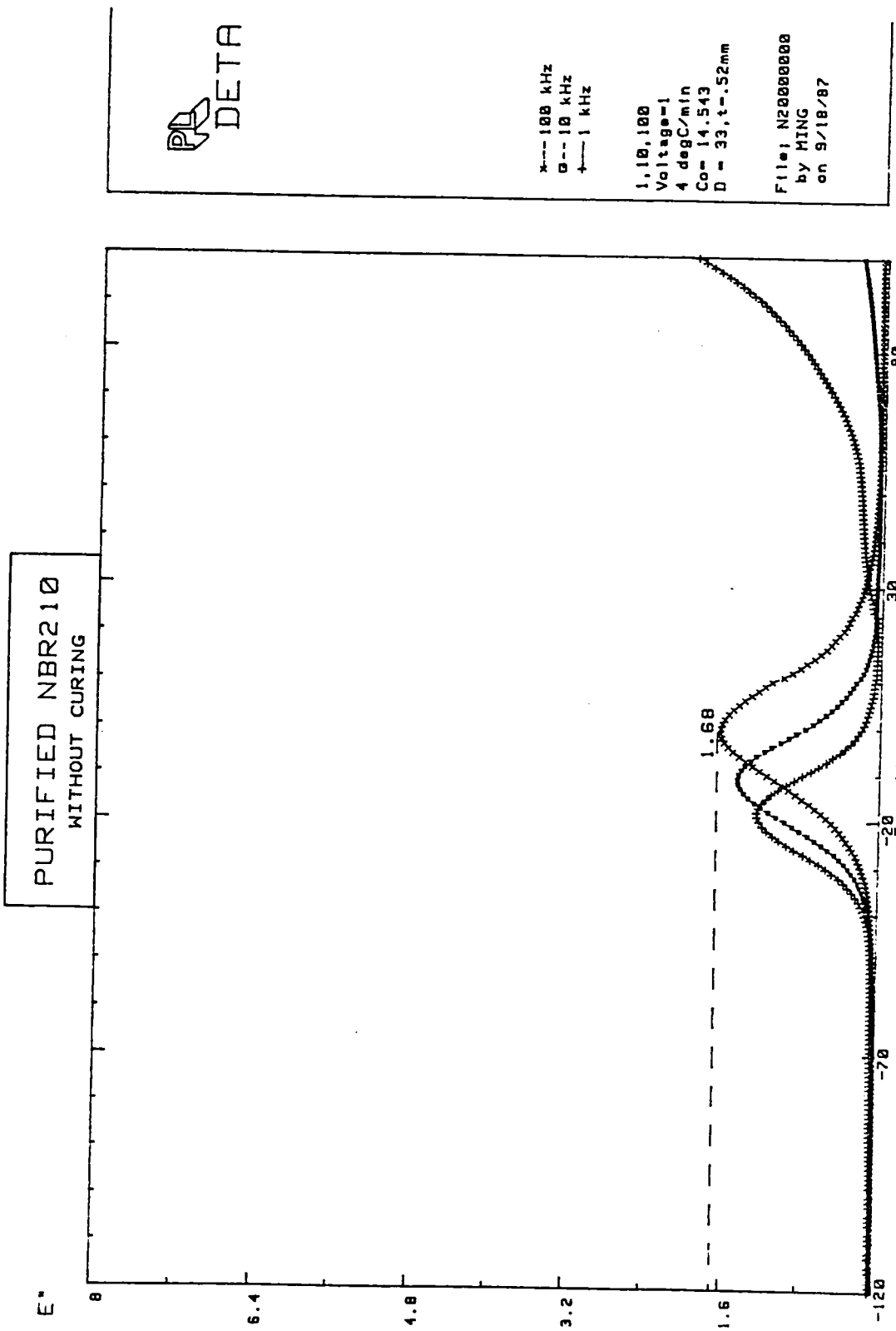

Figure 2.11 Temperature dependence of the dielectric loss factor of 19% acrylonitrile nitrile rubber at various frequencies.

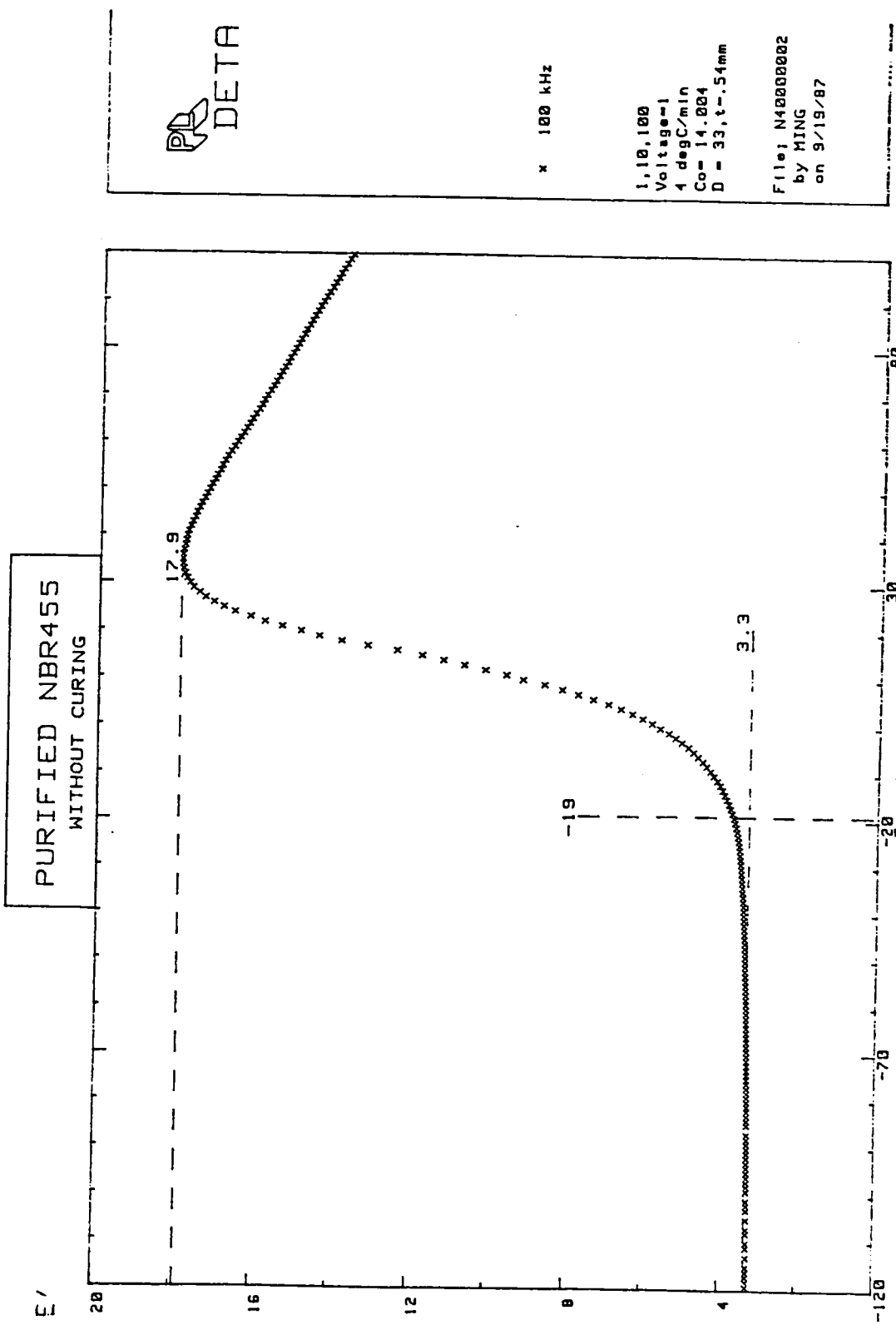

Figure 2.12 Temperature dependence of the dielectric constant of 40% acrylonitrile nitrile rubber at various frequencies.

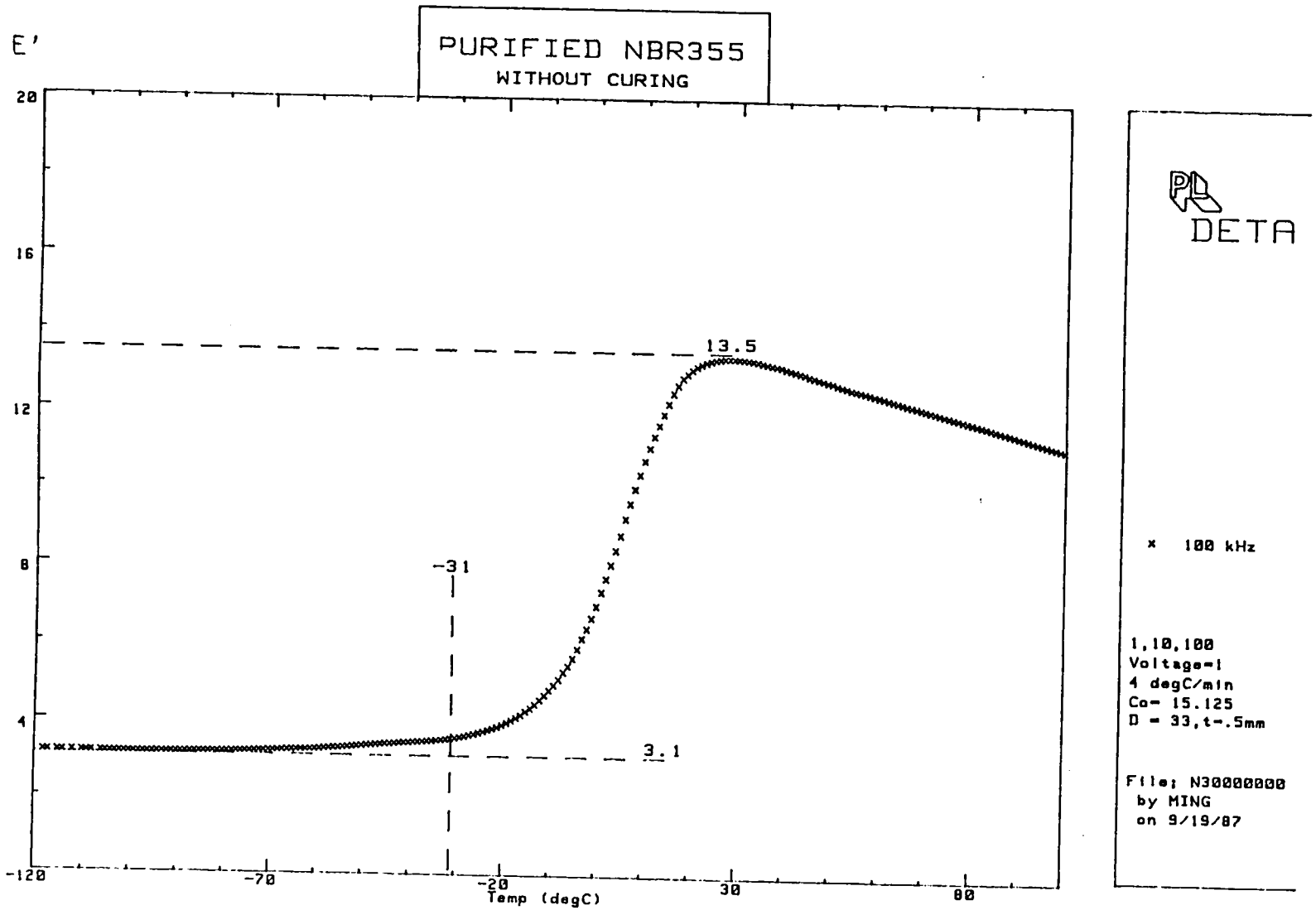

Figure 2.13 Temperature dependence of the dielectric constant of 30% acrylonitrile nitrile rubber at various frequencies.

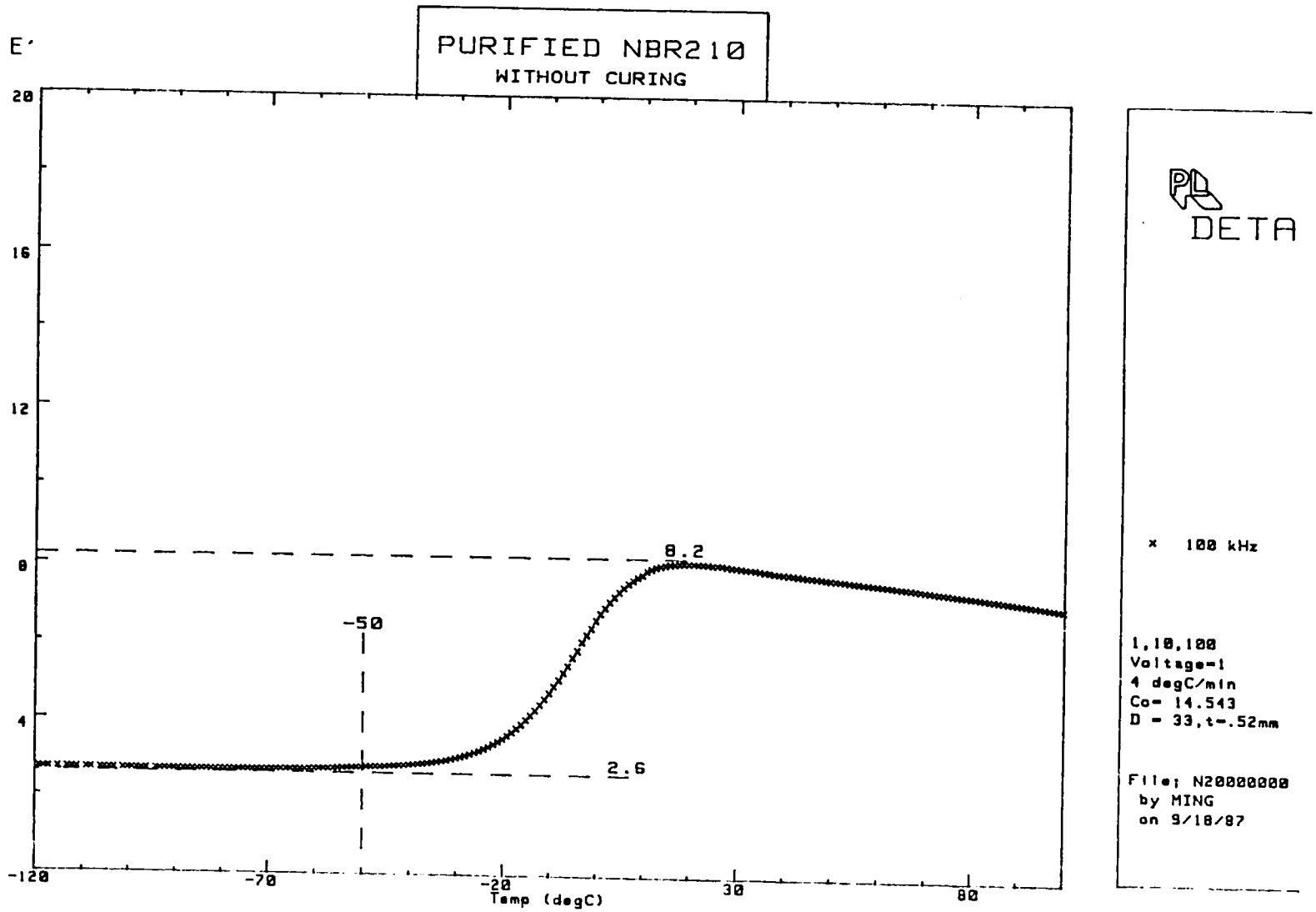

Figure 2.14 Temperature dependence of the dielectric constant of 19% acrylonitrile nitrile rubber at various frequencies.

(C) Hydrogen bonding: In nylons, the dielectric properties are mainly determined by inter-molecular and intra-molecular hydrogen bonding. At the glass transition temperature, especially, hydrogen bonds must be broken to allow for large-scale motions of the chains. This results in larger values of $(\varepsilon_s - \varepsilon_\infty)$.

(D) Chemical structure: The nature of the dielectric properties is dependent to a great extent not only on the mole percentage of polar groups, but also on their position in the polymer chain. For example, polar groups in the main chain are far less mobile than those in side chains. Hence, the effective dipole moment as contributing to loss in the first case is smaller than that considered secondly. In PVAc, the ester group is on the side chain, whereas in PET, the ester group is in the backbone polymer chain.

In polyvinyl esters the side group is linked to the main backbone chain by polar C-O bonds which makes the dielectric glass transition more intense than as observed for the case of acrylates and methacrylates, where the linkage is an apolar C-C bond.

(E) Steric effects: Steric hindrance provided by the α methyl group was essential for the occurrence of the β dielectric loss maximum in PMMA, for example. The α-methyl groups maintain the chain backbone as essentially rigid while the $-COCH_3$ group undergoes hindered rotation, so that the α and β peaks were resolved for PMMA at frequencies below 1 kHz. Steric effects can also affect percentage crystallinity and chain mobility.

(F) Percentage of crystallinity: Increased crystallinity tends to decrease the magnitude of the dielectric loss as well as increase the temperature of maximum dielectric loss at a given frequency.

(G) Crosslinking density: Any crosslinking of polymers decreases segmental mobility and increases the relaxation times of the dipole-segmental loss. The

temperature and magnitude dependence of the dielectric loss is determined by the density of the crosslinking.

(H) Physical state: The effect of physical state of polymers can be illustrated by the values of dielectric constant. For example, although the percentage of -Cl group in polyvinyl chloride is greater than that of polychloroprene, at room temperature the dielectric constant of polychloroprene is higher than that of PVC. The reason lies in the fact that at room temperature, polychloroprene is in its rubbery state. The chain segments can move freely, so that the high value of ε' is related to the dipole orientation polarization of the chain segments. PVC at room temperature is in the glassy state, its chain segment mobility is limited, and the dipole orientation polarization comes only from the movement of the polar group itself. At sufficiently high temperatures, PVC will transform to the rubbery state, and its dielectric constant will eventually be larger than polychloroprene's.

Other factors such as stereochemical structure, branching, and orientation also influence the effective dipole moment.

2.4.2 Microwave Experimental Results

Experiments were first conducted on ethylene/vinyl acetate copolymers. Due to the nonpolarity of PE, the cylindrical cavity applicator was used to process PE/PVAc copolymers of four different percentages of PVAc (0, 18, 28 and 33%). Figure 2.15 is a typical time-temperature profile for the PE/PVAc copolymers, PE and the silicone flexible mold. The input power was fixed at 20 watts. In the first 1.5 min., the temperature rose almost the same for all polymers. Beyond 1.5 min., the temperature increments became greater for the copolymers having a higher percentage of PVAc. From the microwave experiment in chapter 4, the critical temperature of dielectric loss for PVAc was estimated to be 65°C. PE with carbon-carbon linkages had a very low

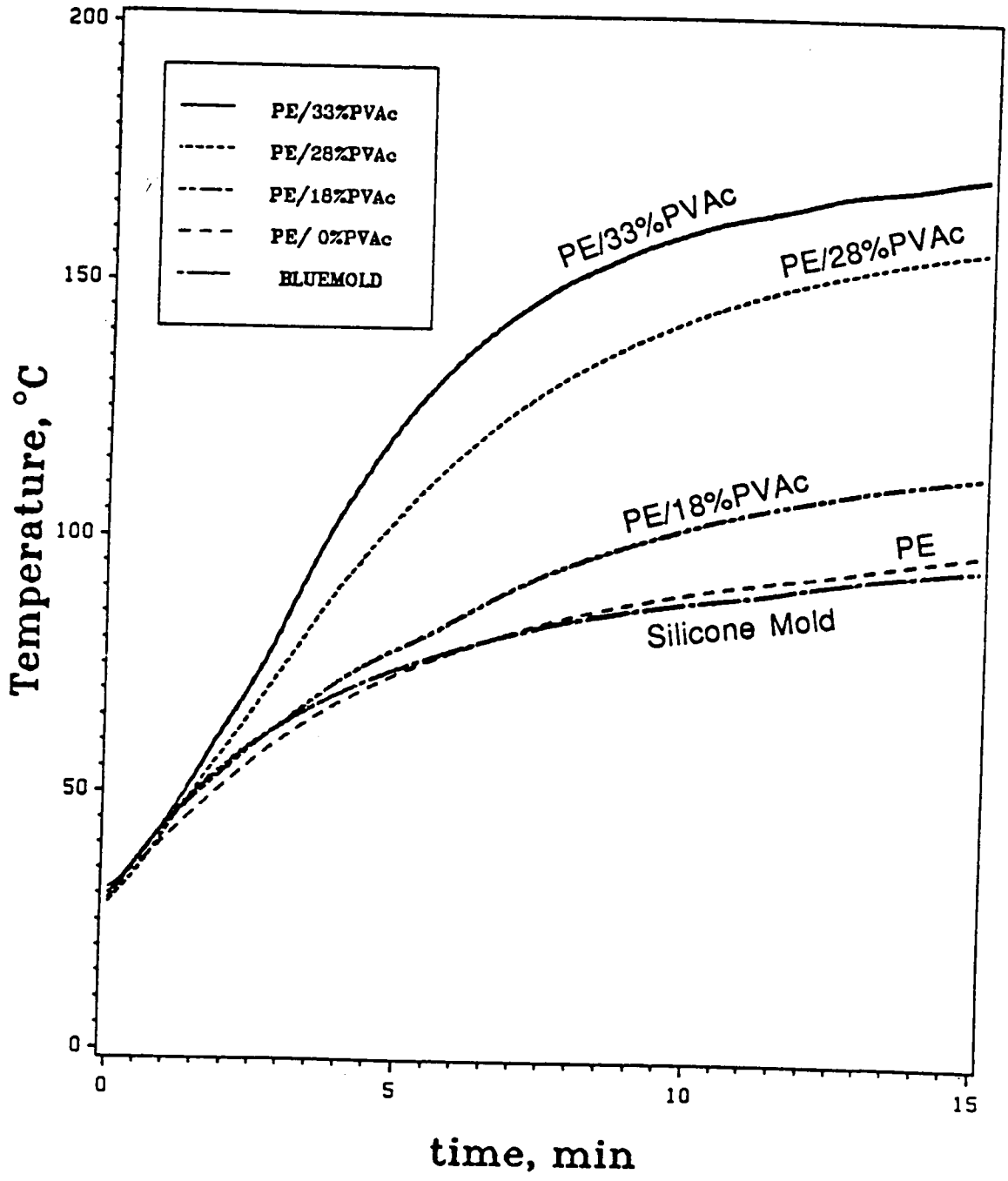

Figure 2.15 Variation of the temperature of ethylene/vinyl acetate copolymers and silicone mold with time in the center of TE_{111} mode of a cylindrical cavity applicator. Input power was 20 watts.

dielectric loss factor. Thus, in the first 1.5 min., the temperature increment was due to the heating of the silicone mold. As will be discussed in chapter 5, the microwave energy coupled first with the silicone mold, then to the polymer, once T_c was encountered. The heat flowed from silicone mold to the PE/PVAc copolymer specimen via thermal conduction at temperatures below the T_c of PVAc. Above the T_c of PVAc, PVAc absorbed microwave energy by itself because the dielectric loss factor of PVAc was higher than that of the silicone mold. The temperature variation of PE in the silicone mold was almost the same as the empty silicone mold indicating the low dielectric loss of PE. Thus the final leveling of temperature depended on the mole percentage of the polar PVAc. The microwave energy absorption of PE/PVAc copolymers was improved by the silicone mold as it was for the semicrystalline polymers discussed in chapter 5.

The second case investigated was for nitrile rubbers with different percentage of acrylonitrile (19, 30 and 40%). Due to the high polarity of the -CN triple bond, a travelling wave applicator was used to process the nitrile rubbers. The microwave curing reactions of nitrile rubbers with 2% dicumyl peroxide were carried out at an input power of 50 watts, as shown in Figures 2.16-2.19. Accurate input, reflected and transmitted powers were obtained by completely calibrating each set of attenuators and cables. The percentage of loss on the wall and system was based on the experiments with empty loading, teflon rod and empty sample holder. These values were averaged to get a factor of about 93% (7% loss in the applicator).

$$P_a = (P_i - P_r - P_t) \times 0.93 \qquad [2\text{-}9]$$

In Figure 2.16, these three power readings are plotted vs. time for nitrile rubbers. The input powers, P_i, of 50 watts remained unchanged with time. The transmitted powers , P_t , were constant only until the sample began to heat rapidly where P_t

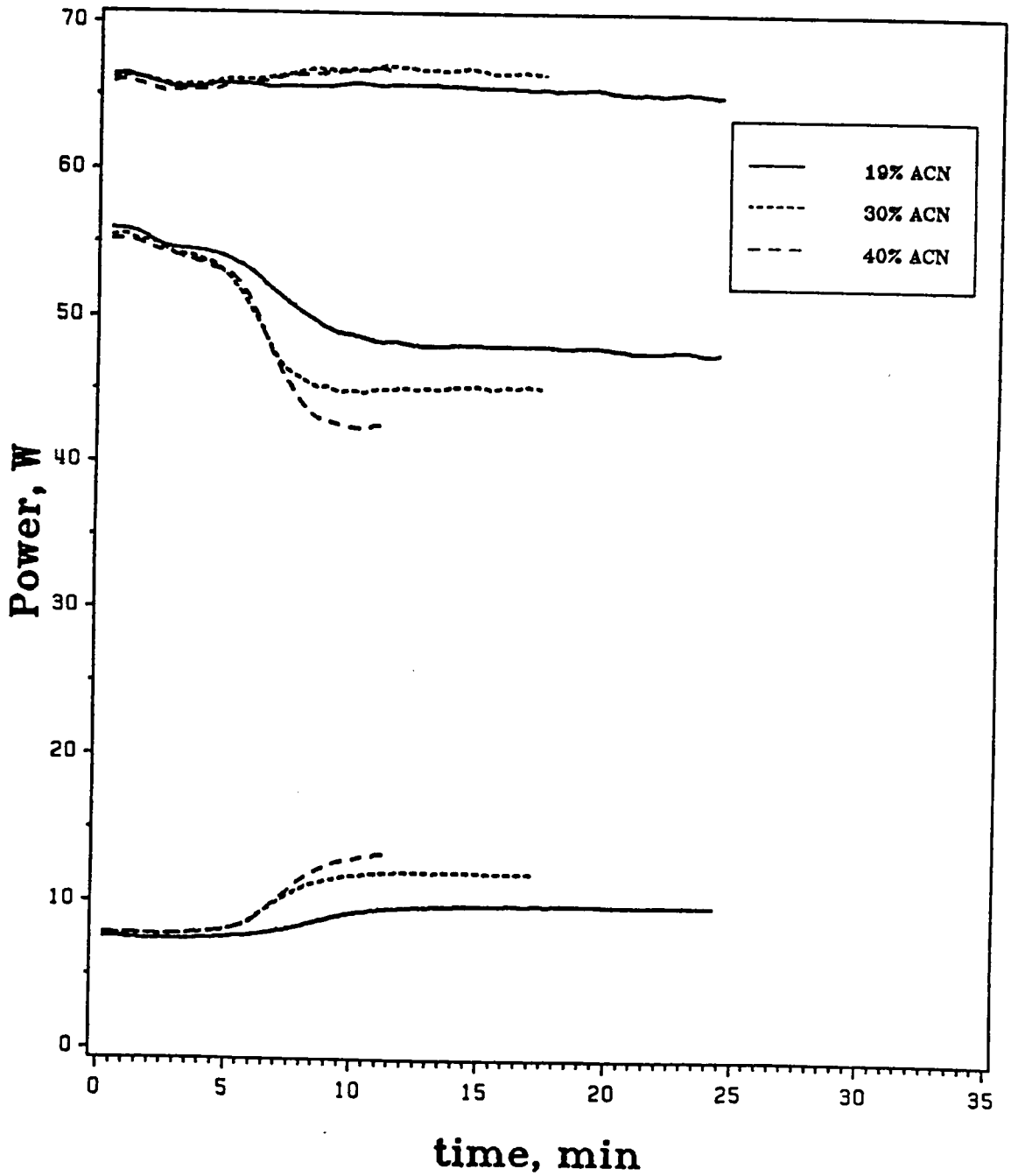

TOP :INPUT POWER
CENTER :TRANSMITTED POWER
BOTTOM :REFLECTED POWER

Figure 2.16 Variation of the input powers, reflected powers and transmitted powers with time for (19, 30, 40% acrylonitrile) nitrile rubbers with 2% w/w dicumyl peroxide in the travelling wave applicator.

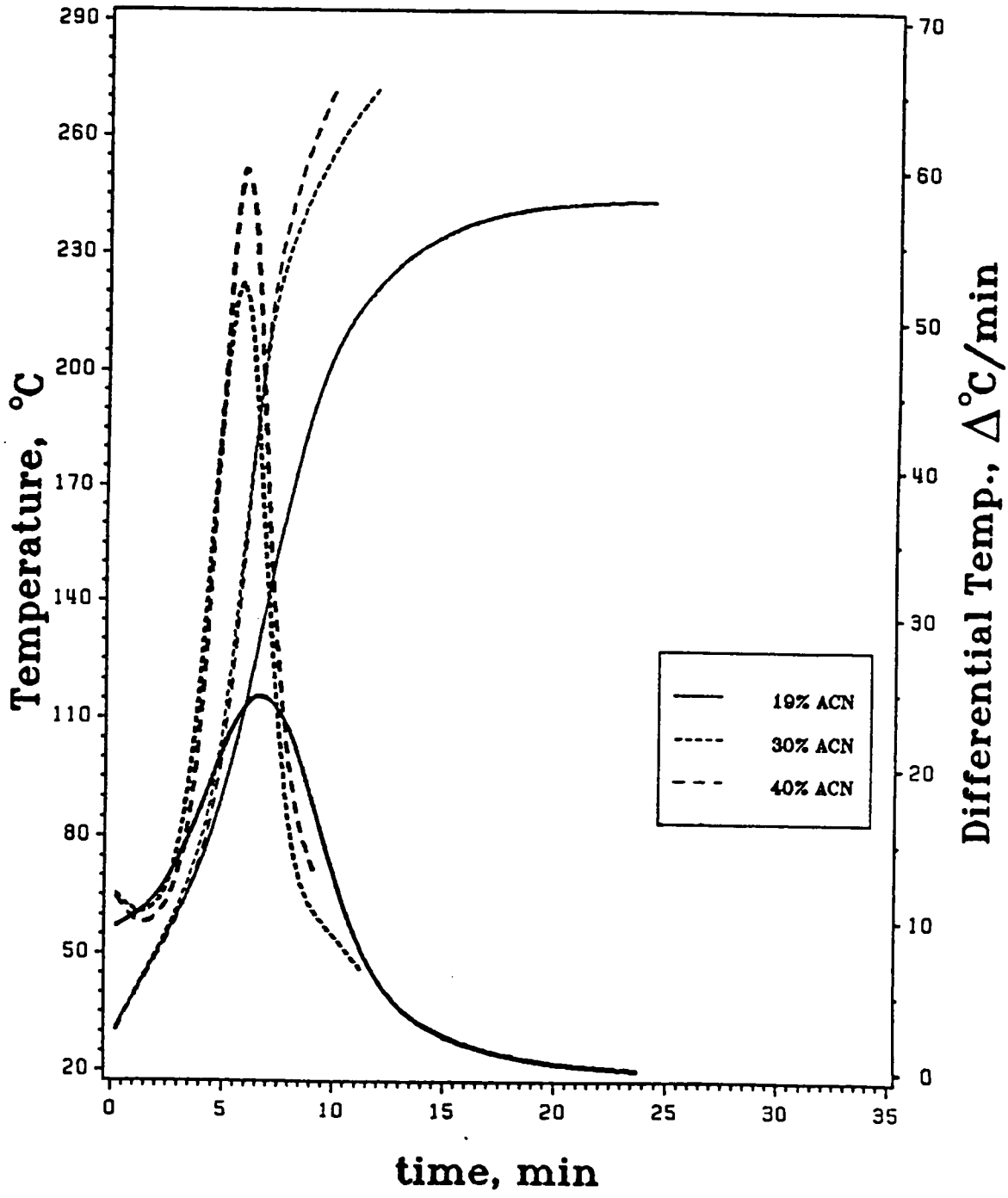

THICKER LINE: DIFFERENTIAL

Figure 2.17 Variation of the temperatures and heating rates with time for (19, 30, 40% acrylonitrile) nitrile rubbers with 2% w/w dicumyl peroxide in the travelling wave applicator.

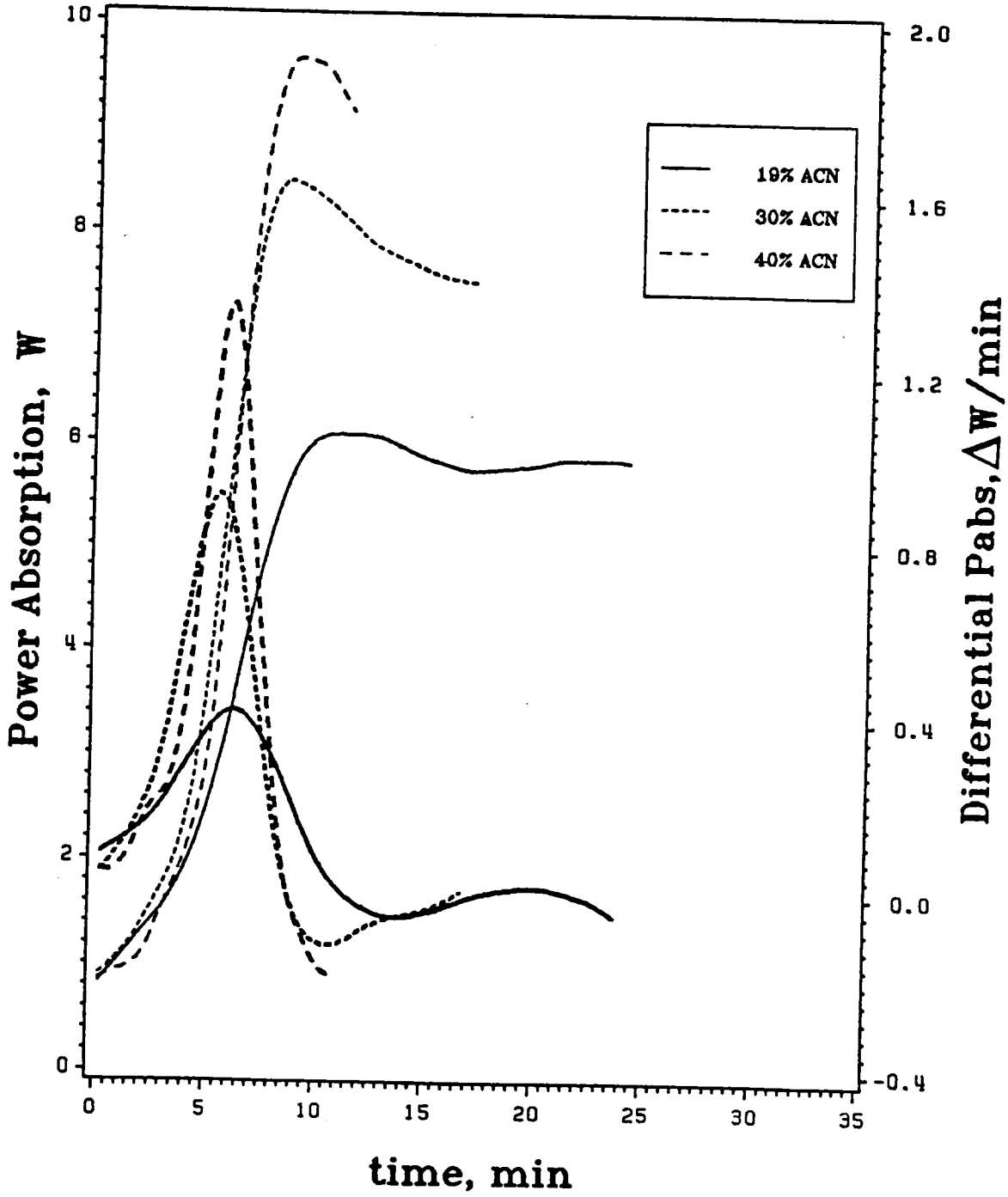

THICKER LINE : DIFFERENTIAL

Figure 2.18 Variation of the power absorptions and power absorption rates with time for (19, 30, 40% acrylonitrile) nitrile rubbers with 2% w/w dicumyl peroxide in the travelling wave applicator.

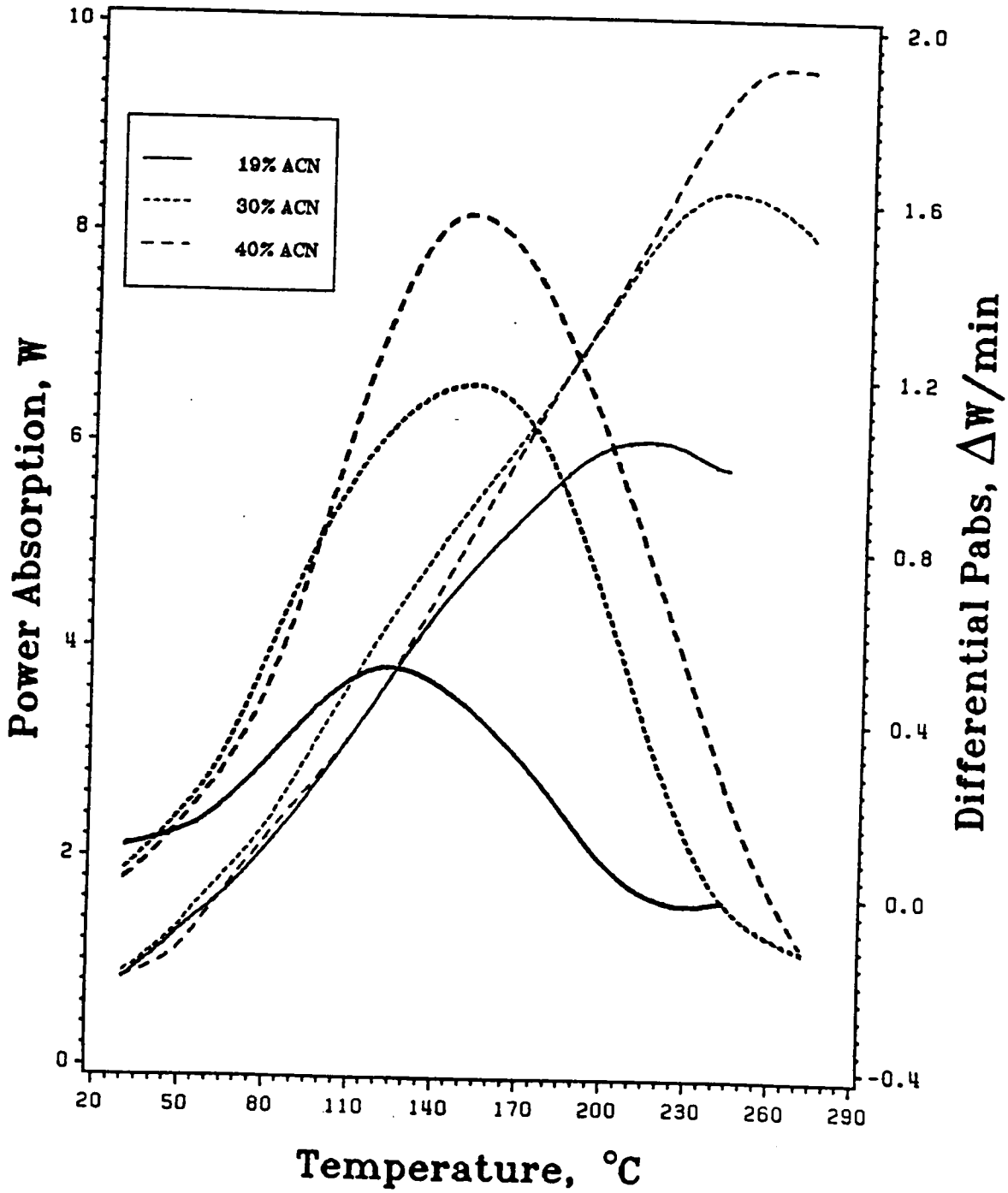

THICKER LINE: DIFFERENTIAL

Figure 2.19 Variation of the power absorptions and power absorption rates with temperature for (19, 30, 40% acrylonitrile) nitrile rubbers with 2% w/w dicumyl peroxide in the travelling wave applicator.

decreased and leveled off. The reflected powers, P_r, were also constant initially, but increased and then leveled off once the sample began heating rapidly. Increasing the acrylonitrile content from 19% to 40% resulted in the overall decrease in transmitted power and an increase in reflected power. This indicated that the energy absorbed by the nitrile rubber increased with the acrylonitrile content. Both variations of transmitted and reflected powers with increasing acrylonitrile content were shifted toward shorter times. Due to the increasing temperature, the dielectric loss factor increased and the impedance of nitrile rubber changed. At the same time, reflected powers, P_r, increased to higher values. Figure 2.17 represents temperature and heating rate versus time curves for these materials. This plot reveals how receptive the nitrile rubbers were to the microwave radiation. The steeper the slope, the shorter the processing time. Figure 2.18 represents the power absorption and the power absorption rate versus time. The plateau of temperature and power absorption, P_a, in Figures 2.17 or 2.18, increased when the acrylonitrile content was stepped from 19% to 40%. In addition, the maximum rate of power absorption, or rate of heating, was shifted to shorter times. The loss tangent value in cured rubber was found to be less than the loss tangent value of the uncured rubber. This can be explained by examining the loss tangent DETA spectra, as will be discussed in chapter 3. Since heating rate is proportional to the magnitude of the dielectric loss, as shown in Equation [1-2], it was expected that the uncured nitrile rubber would heat faster. The effective dipole moment motion associated with energy loss caused by thermal motion of polar groups decreases with crosslinking. Because the polar -CN group was not involved in curing, the dipolar relaxation of the cured rubber did not disappear completely so that the sample could be heated and maintained at a high temperature by the appropriate input power. Indeed the power absorption curve increased to a maximum and then decreased to a plateau. This

This suggested that the microwave energy absorbed by the sample was in equilibrium with the loss energy conducted away from the sample. Thus, the dielectric loss factor became fixed by thermal equilibrium processes.

Figure 2.19 projects the variation of power absorption and power absorption rate with temperature for the three different nitrile rubbers. Power absorption increased continuously with increasing temperature, but then decreased due to the chemical crosslinking which induced a strong viscosity effect which consequently hindered dipolar relaxation. The polar acrylonitrile group absorbed energy by interacting with the microwave field which then heated up the whole of the mass to be crosslinked. As a result of the increasing temperature, the crosslinking peroxide decomposed thereby generating a network so that the heating rate decreased due to restricted mobility eventually.

2.5 CONCLUSION

The area beneath the dielectric loss factor-frequency plot was proportional to (ε_s - ε_∞) as shown by Equation [2-7], and remained unchanged during the merging of the α and β relaxations. Evaluating the heatability by the magnitude of (ε_s - ε_∞) was an easy task using a DETA. The value of (ε_s - ε_∞) should be used together with the distribution of relaxation times and activation energies to predict the heatability for microwave power processing. In order to relate the structure-property relationships to the values of (ε_s - ε_∞) and chemical and morphological structures, it was necessary to examine the relationship between the dielectric constants of polymers and the effective dipole moments. In considering effective dipole moments it was useful to use group moments

instead of bond moments. The polarity follows the sequence of group dipole moment as

$$SO_2 > CONH > CN > C{=}O > Cl > CO_2R > O > CO_3 > C\text{-}C.$$

Since the electrical properties of polymers are closely associated with the mechanical properties of polymers, DETA and DMTA were combined to conveniently characterize structure-property relationships. A correlation was found between the dielectric properties of various polymers and the dipole moments of their small molecule counterparts. In summary, it was found that the value of $(\varepsilon_s - \varepsilon_\infty)$ depended on several factors: (A) group dipole moments, (B) mole percentage of polar groups, (C) hydrogen bonding, (D) chemical structure, (E) steric effects, (F) percentage of crystallinity, (G) crosslinking density, and (H) physical state.

As a general rule of thumb, the magnitude of the oscillator strength, $(\varepsilon_s - \varepsilon_\infty)$, predicts the heatability assuming the dielectric loss spectra is in the microwave region. The actual heating rate at 2.45 GHz was determined by the dielectric loss factor as a function of temperature at 2.45 GHz. Knowledge of the magnitude of $(\varepsilon_s - \varepsilon_\infty)$ as well as the distribution of dielectric relaxation times is important in the design of a microwave heating system in order to take advantage of the rapid heating in the positive side of $d\varepsilon''/dT$ and to avoid the risk of the thermal runaway effect.

2.6 REFERENCES

1. J. I. Kroschwitz, ***Electrical and Electronic Properties of Polymers: A State-of-the-Art Compendium***, John Wiley & Sons, New York, 1988.

2. A. D. Jenkins, ***Polymer Science: A materials science handbook, Vol. 2***, North-Holland Publishing Co., London, 1972.

3. H. F. Mark, N. M. Bikales, C. G. Overberger and G. Menges, ***Encyclopedia of Polymer Science and Engineering***, Vol. 5: Dielectric Heating to Embedding, 2nd ed., John Wiley & Sons, New York, 1986.

4. L. Onsager, *J. Am. Chem. Soc.*, **58**, 1486 (1936).

5. J. G. Kirkwood, *J. Chem. Phys.*, **7**, 911 (1939).

6. H. Fröhlich, ***Theory of Dielectrics***, Oxford University Press, Oxford, 1949.

7. K. Deutsch, E. A. W. Hoff and W. Reddish, *J. Polym. Sci.*, **13**, 565 (1954).

8. F. Bueche, *J. Chem. Phys.*, **22**, 603 (1954).

9. J. D. Ferry and E. R. Fitzgerald, *J. Colloid Sci.*, **8**, 224 (1953).

10. J. D. Ferry and S. Strella, *J. Colloid Sci.*, **13**, 459 (1958).

11. A. L. McClellan, ***Tables of Experimental Dipole Moments***, W. H. Freeman and Co., San Francisco, 1963.

CHAPTER 3

MICROWAVE ENERGY ABSORPTION OF NITRILE RUBBER

3.1 INTRODUCTION

Microwave vulcanization is one of the most rapidly growing areas in the rubber industry today. The technique originated in Europe in 1967 and was adopted in the U.S.A. in 1969. The microwave method of curing by volumetric heating offers numerous advantages including shortened processing times, reduced power consumption, selective heating etc. For example, microwave radiation can process rubber up to a hundred times faster over conventional thermal heating methods alone. These advantages will be discussed further in chapter 5.

Rubber compounds, such as polyurethanes (1-4) and nitrile rubbers (5-7) which are based on polymers having highly polar groups, are known to heat very rapidly in a microwave field. Compounds in general may be classified by their heatability according to the time required for processing (7). The heatability of low polarity polymers can be enhanced by adding various fillers including: carbon black (5-11), diethylene glycol, polyethylene glycol or triethanolamine (6-9). By modifying the structure of the silicone polymers with such bulky polar substituents as p-NO_2-C_6H_4-, C. L. Lee (12) observed that heatability with microwave radiation was directly dependent upon the dielectric loss factor of the polymer. Such concepts are crucial for optimizing microwave vulcanization processes.

In this chapter, the dielectric behavior of nitrile rubber is described as investigated by kHz frequency radiation measured via DETA (Dielectric Thermal Analyzer) and at a

frequency of 2.45 GHz via a travelling wave applicator. The subambient dielectric relaxation spectra of nitrile rubbers in the kHz region were found to shift to higher temperatures at the microwave frequency. As a result, the highly polar nitrile rubber exhibited excellent heatability even at room temperature in the travelling wave applicator.

The most common applicator today is designed around multimode cavities. Unfortunately, such cavities are very difficult to analyze with great accuracy. This is due to several factors including: the complexity of the field distribution within the cavity, variation in dielectric properties of materials with temperature, moisture content, density and other parameters. In contrast, in this chapter, travelling wave applicators are discussed since they are relatively simple to analyze and possess well defined field patterns. The microwave equipment used for these experiments is listed in section 3.3.5 of this chapter. Experimental methods are discussed for the case of several types of nitrile rubber at three different power levels. Various powers were necessary for quantifying the microwave energy absorption.

This chapter describes the use of low frequency mechanical and dielectric testing (0.33 Hz - 100 kHz) to explain the heatability of nitrile rubbers at a microwave frequency of 2.45 GHz. The dielectric loss factor ($\varepsilon'\tan\delta$) obtained from the low frequency tests was found to be directly proportional to the heatability of the polymers in the microwave environment. A Williams-Landel-Ferry (WLF) plot was used to help the prediction of the shift of the dielectric loss factor into or out of the microwave region.

3.2 THEORY

As shown in Figure 3.1 (13), an alternating field of high frequency radiation is applied to the sample and the molecular dipoles subsequently try to displace rotationally to follow the direction of the alternating electric field. The phase lag between the polarization and the applied field leads to an absorption of energy. Some of this energy manifests itself as heat.

The dielectric heating of a material can be represented by the following equation (14):

$$P = KfE^2\varepsilon'\tan\delta \qquad [3\text{-}1]$$

if we ignore convection, conduction and heats of reaction, where P is the power dissipation in W/cm^3, K is a constant of 55.61×10^{-14}, f is the applied frequency in Hz, E is the electric field strength in V/cm, ε' is the dielectric constant and $\tan\delta$ is the loss tangent. Both ε' and $\tan\delta$ depend, via the frequency, on the sample temperature.

The electromagnetic field energy dissipated as heat per unit volume is seen to be proportional to the dielectric loss factor ($\varepsilon'\tan\delta$), the square of the field strength (E^2) and frequency (f) of the applied field. The ratio of the dielectric loss factor to the dielectric constant is called the loss tangent for a nonionic material. The dielectric loss factor, ε'', determines the rate of conversion of electrical energy into thermal energy in the material. Since the electric field penetrates the material, heat is generated within the sample interior; thus, dielectric heating is independent of the heat entering through the surface of the material. This is in contrast to conventional thermal heating which is much more time consuming and is dependent upon the thermal conductivity of the material.

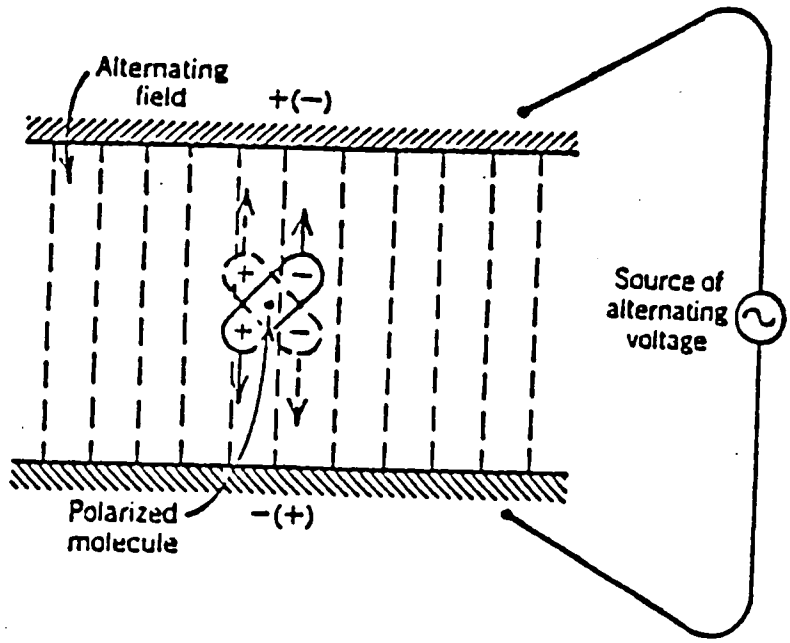

Figure 3.1 A molecular dipole subjected to a high frequency electrical field. (13)

The heating rate of a material placed in an electromagnetic field depends on several key parameters as described by the relationship:

$$\frac{dT}{dt} = \frac{KfE^2\varepsilon'(T)\tan\delta(T)}{\rho C_v} \qquad [3\text{-}2]$$

where ρ is the density of the material, C_v is the specific heat and other parameters are the same as Equation [3-1]. This equation ignores convection and conduction losses as well as heat of reaction. Therefore, the heating rate of a material depends directly on the square of the electric field strength and the dielectric loss factor which is usually a function of the temperature (due to the variation of ε'' with temperature).

3.3 EXPERIMENTAL

3.3.1 Materials

Nitrile rubbers with 19%, 30% and 40% by weight acrylonitrile were supplied courtesy of the BF Goodrich Corporation. Dicumyl peroxide with a minimum of 99% purity was supplied by the Lucidol Division of the Pennwalt Corporation and was used without further purification. These nitrile rubbers were dissolved in chloroform (3% wt. of solid), filtered through a Whatman No. 1 filter paper, coagulated by dropwise addition of chloroform solution to methanol, and dried in a vacuum oven at room temperature for 12 hours. This purification procedure was repeated again to ensure high purity. Purified nitrile rubber containing 2% by weight of dicumyl peroxide was dissolved in chloroform (6% wt. of solid). Films were prepared by casting the solution into a teflon mold. Upon evaporation of the solvent, the films were dried in a vacuum oven at room temperature for 24 hours. These films were kept in the desiccator until they were used for DMTA (Dynamic Mechanical Thermal Analyzer), DETA, and the microwave

experiments. Thermally cured films were prepared in a convection oven at 150°C for 2.5 hours.

3.3.2 Thermal Analysis

The calorimetric responses of samples were measured with a differential scanning calorimeter (Perkin-Elmer model DSC-2) in order to ascertain the glass transition temperature. For subambient work, liquid nitrogen was used as the cooling medium with helium as the purge gas. Tetrahydrofuran (THF) was used as a calibration standard for temperature and energy. The scanning rate was 10°C/min. The thermogravimetric analyses were recorded from 50°C to 750°C at a heating rate of 10°C/min by a Perkin-Elmer model TGS-2. Nitrogen was used as a purge gas at a flow rate of 10 cc/min.

3.3.3 Gel Permeation Chromatography (GPC)

GPC was performed on a Waters 150C GPC having a refractive index detector in parallel with a Viscotek model 100 differential viscometer. HPLC grade THF was used as the mobile phase at a flow rate of 1.0 ml/min with four UltraStyragel columns (10^5Å, 10^4Å, 10^3Å and 500Å) in series. Twelve polystyrene standards were used to calibrate the molecular weight via the universal calibration method (15,16).

3.3.4 Relaxation Spectrometer Systems

Polymer Laboratory's DETA (Dielectric Thermal Analyzer) and DMTA (Dynamic Mechanical Thermal Analyzer) were used to obtain comprehensive relaxation spectra covering the frequency range of 0.33 Hz to 100 kHz. Dielectric spectra from -120°C to 100°C were obtained using DETA at frequencies of 0.1, 1, 10 & 100 kHz. Thermal spectra from -150°C to T_g were collected by using DMTA at frequencies of 0.33, 1, 3, 10 & 30 Hz. The mechanical analyzer was equipped with shear clamps for testing the soft

uncured nitrile rubber. A single cantilever bending mode was chosen for the microwave cured nitrile rubber.

3.3.5 Microwave Instrumentation

Figures 3.2 & 3.3 schematically depict the travelling wave applicators. The individual components of the microwave system are shown below. A more detailed list of equipment including model numbers is included in Appendix B.

(i) A Raytheon model PGM-10X1 variable (0-120 watts) power generator operating at 2.45 GHz which was used as the microwave source.

(ii) A circulator to protect the microwave generator from reflected waves, as well as a matched termination.

(iii) Coaxial directional couplers, attenuators and power meters which measure the incident power, P_i, reflected power, P_r, and transmitted power, P_t.

(iv) Adapter that connects the coaxial cable to the WR284 waveguide.

(v) Samples were separated by teflon sheets of 0.005 in. thick and placed into a 3.3 cm high by 1.27cm inside diameter cylindrical teflon sample holder. See Figure 3.4 for details. The sample holder was put at the maximum electric field region of the TE_{10} mode in the waveguide.

(vi) An adapter fastened at the other end to couple the coaxial cable to the waveguide for the travelling mode.

(vii) A Luxtron fluoroptic thermometry system model 750 was used for temperature measurements. The fiber-optic temperature measuring probe was inserted into the center of the sample to measure the sample temperature.

(viii) An IBM personal computer was used to record powers and temperature versus time, simultaneously.

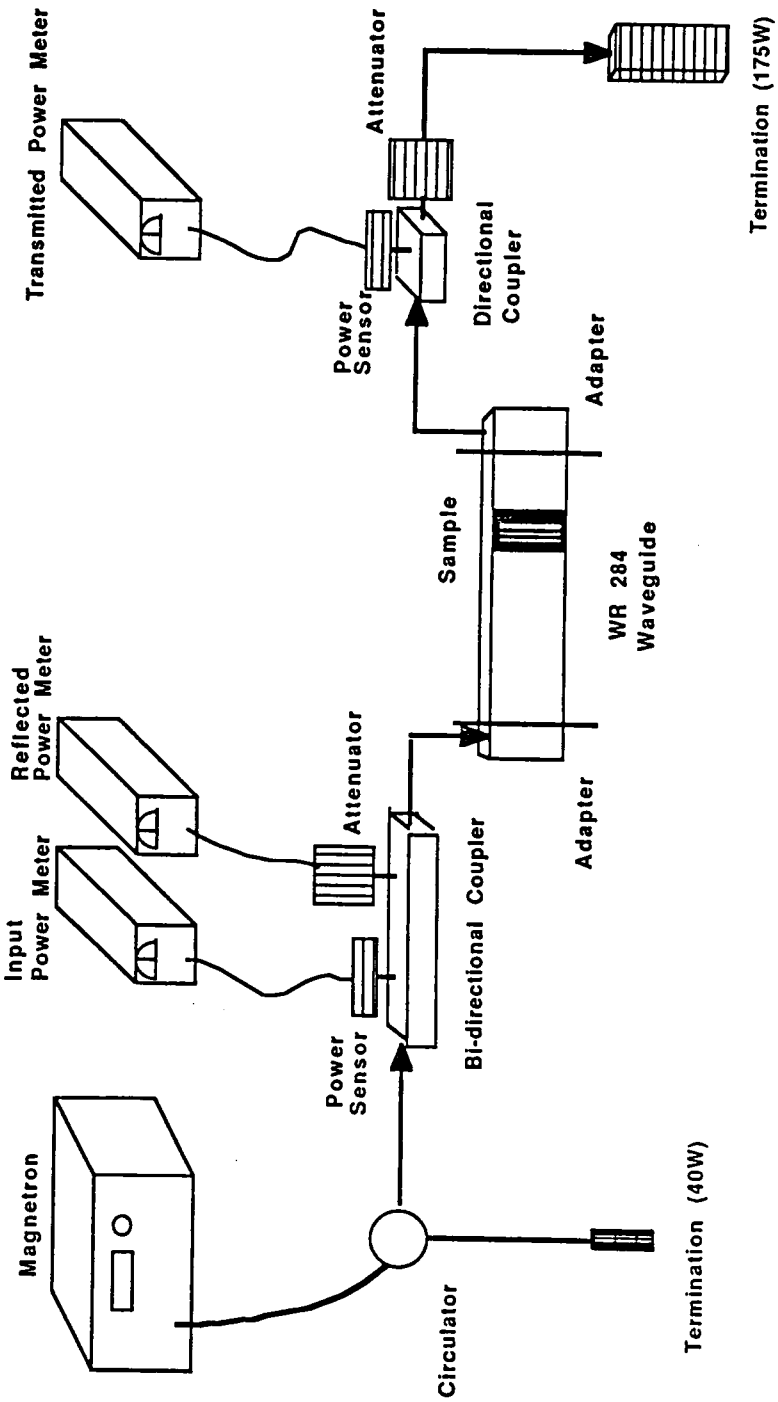

Figure 3.2 Schematic of the experimental set-up for the travelling wave applicator.

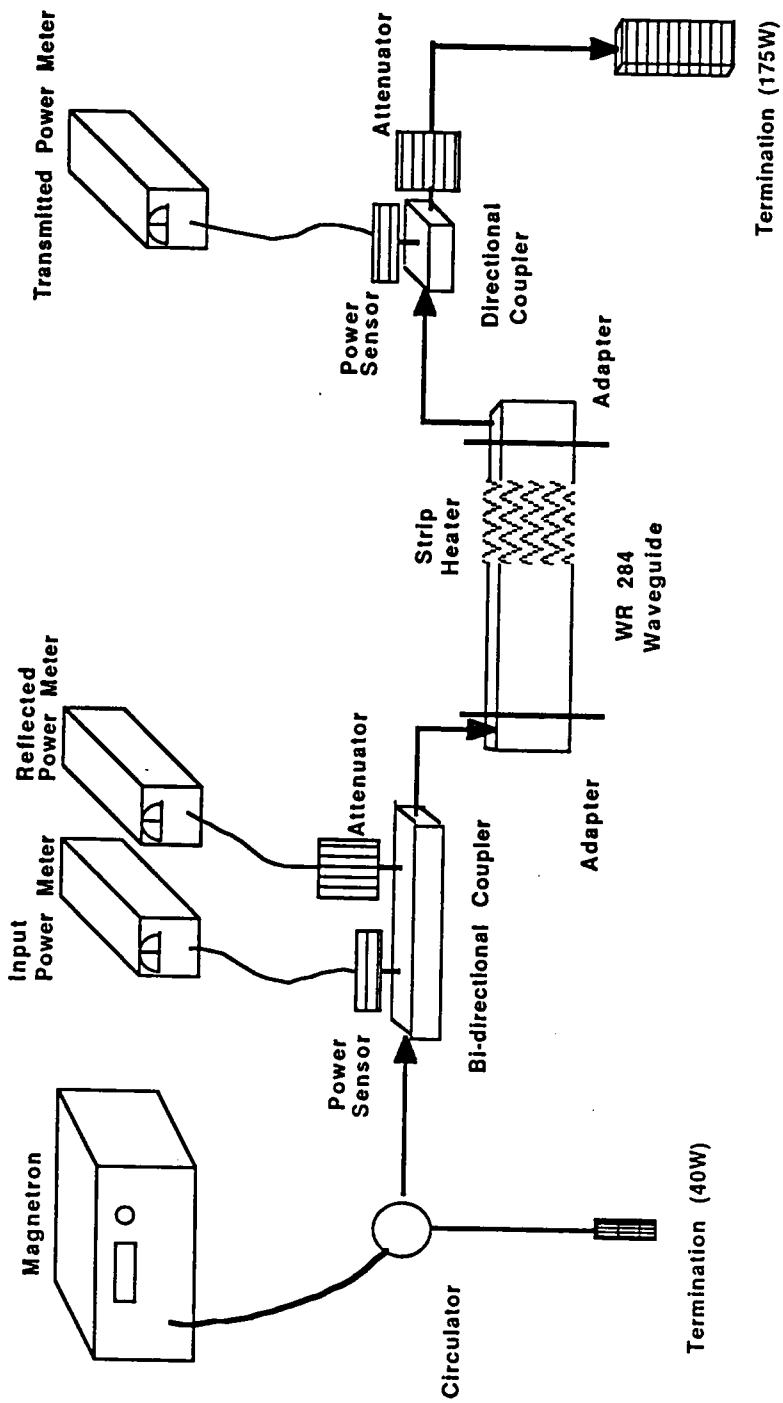

Figure 3.3 Schematic of the experimental set-up for the travelling wave applicator with a stub tuner.

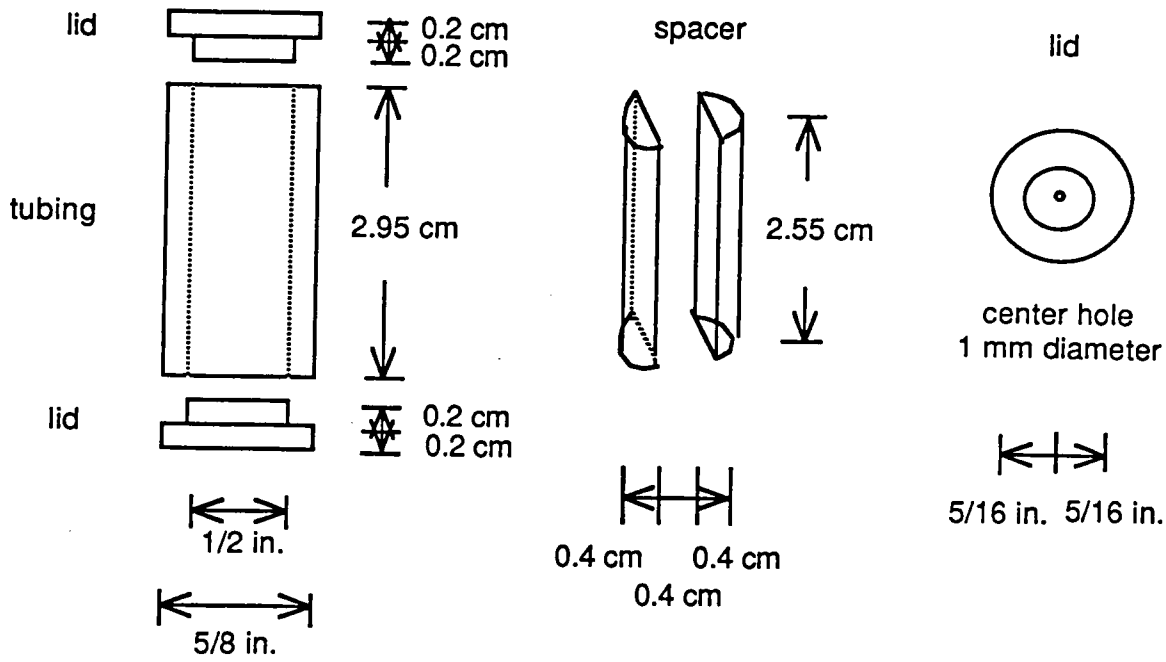

Figure 3.4 Schematic drawing of the teflon sample holder.

(ix) Various starting temperatures for the investigation were induced by external heating of the waveguide with a strip heater.

There is only one mode, TE_{10} (17), which can propagate freely in the rectangular WR284 waveguide. This mode is characterized by an electric field vector (E) which has one component only, linearly polarized parallel to the narrow faces of the waveguide with a half sinusoidal variation between them, having a maximum value at the midpoint.

Travelling wave applicators are those which apply power from the generator into the waveguide allowing absorption of the energy by one pass of the waves through the sample before being absorbed by the terminator. This particular waveguide was characterized by a low VSWR (Voltage Standing Wave Ratio) of less than 1.17 in this experiment. Travelling wave applicators can be operated empty without risk to the generator. Ideally, the waves cannot be reflected back and forth in a travelling mode; therefore, the electric field strength is relatively low.

3.4 RESULTS AND DISCUSSION

3.4.1 Thermal Analysis

The glass transition temperatures of nitrile rubbers with 19%, 30% and 40% acrylonitrile were determined to be -50°C, -31°C and -19°C, respectively, from DSC at a scanning rate of 10°C/min. Less than 1% and 3% weight loss were observed at 280°C and 370°C, respectively, from TGS for these nitrile rubbers.

3.4.2 Molecular Weight Determination

The number average molecular weights, $\overline{M_n}$, and the polydispersities of these polymers were found to be 1.09×10^5, 8.50×10^4, 8.39×10^4 and 3.75, 3.15, 2.87,

respectively, for 19%, 30% and 40% acrylonitrile nitrile rubber. The chromatography results revealed that the materials possessed bimodal molecular weight distributions as well as fractions beyond the exclusion limit of high molecular weight for the described set of columns.

3.4.3 Thermal Spectra from DETA and DMTA

As expected, the dielectric relaxation spectra for nitrile rubber revealed a large magnitude of loss tangent, as shown in Figures 3.5 and 3.6. Transition temperatures were defined as the temperature at which the dielectric loss tangent went through a maximum. Temperature affects the dielectric relaxation time, τ, according to the approximate equation for an activated process:

$$\tau = A\exp(\Delta E_a/RT) \qquad [3\text{-}3]$$

where ΔE_a is the activation energy involved in dipole rotation, R is the ideal gas constant, T is the absolute temperature, and A is a constant. Consequently, the dielectric relaxation time decreases as the temperature increases. Since in this idealized case the dielectric loss is at a maximum when $\omega\tau = 1$, the loss peaks must always shift toward higher frequencies as the temperature increases.

The α relaxations of nitrile rubber, with and without dicumyl peroxide, were obtained via DETA at 1, 10 and 100 kHz and are shown in Figures 3.5, 3.6 and are summarized in Table 3.1. β relaxations due to local motions were small and difficult to detect from the linear plot of $\tan\delta$ versus temperature. Above the glass-transition temperature, ionic conductivity increased due to the increased mobility of the free charges. As seen in Figures 3.5 and 3.6, the maximum values of $\tan\delta$ were almost the same regardless of the addition of 2% by weight of dicumyl peroxide. This was attributed to the fact that dicumyl peroxide is not a polar peroxide (18).

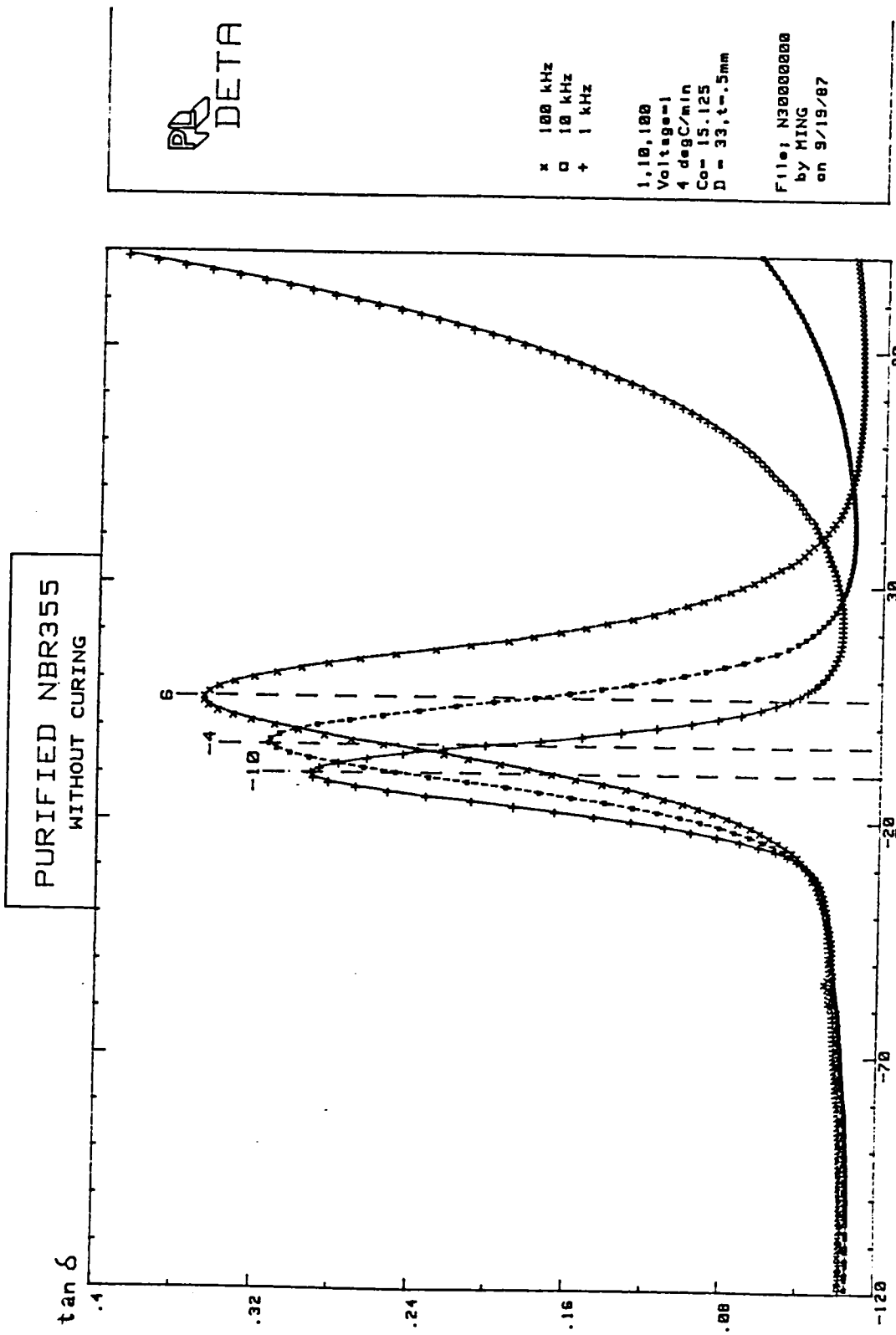

Figure 3.5 Temperature dependence of the loss tangent of 30% acrylonitrile nitrile rubber at various frequencies.

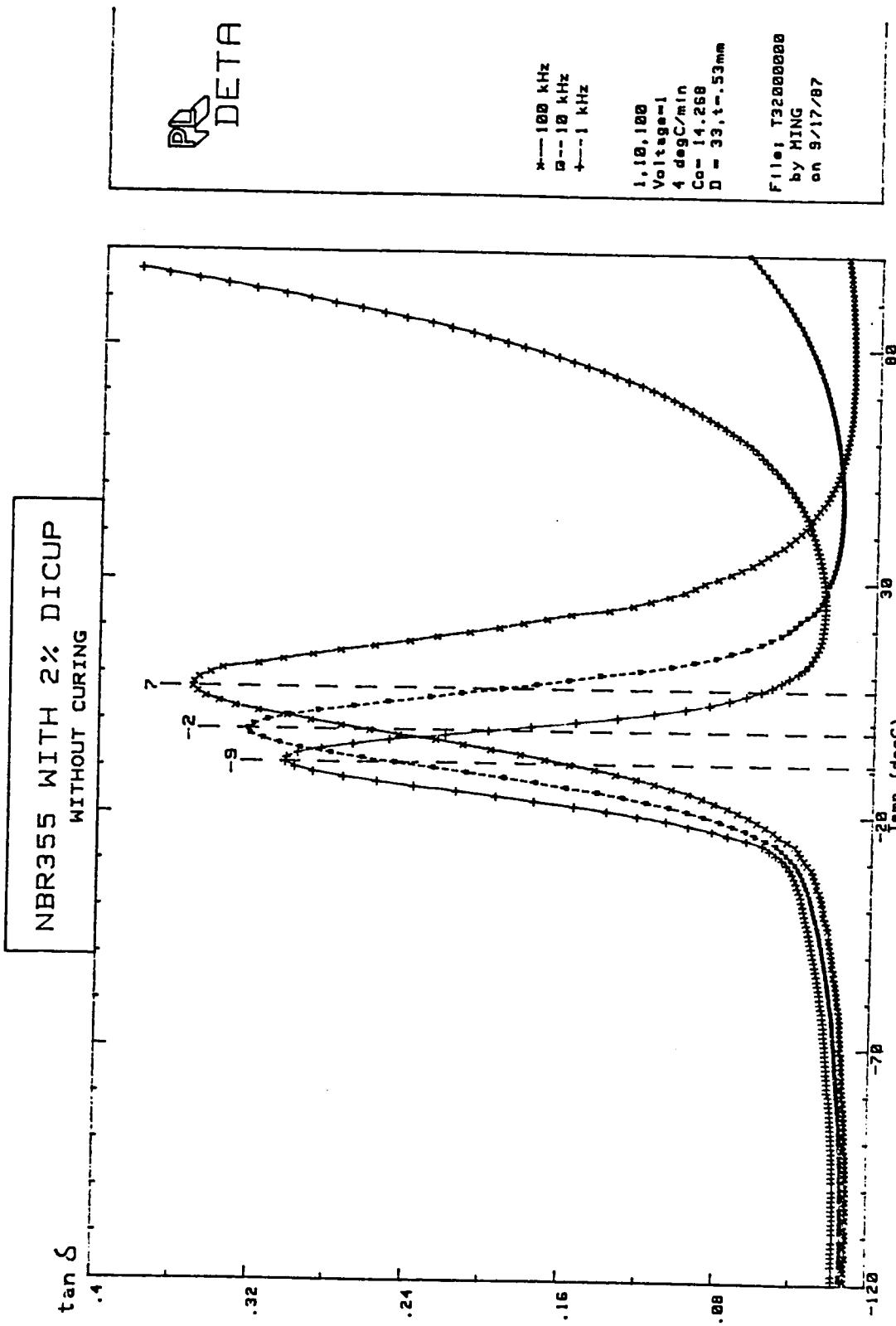

Figure 3.6 Temperature dependence of the loss tangent of 30% acrylonitrile nitrile rubber with 2% w/w dicumyl peroxide at various frequencies.

Table 3.1 Temperatures at the maximum peaks of the loss tangent of nitrile rubber at various frequencies from DETA spectra.

	.1kHz	1kHz	10kHz	100kHz
Purified nitrile rubber (40% acrylonitrile)				
Without curing	-9	-2	5	14
Purified nitrile rubber (30% acrylonitrile)				
Without curing	-14	-10	-4	6
w/2% DICUP w/o curing	-13	-9	-2	7
Thermal cured w/2% DICUP*	-1	3	10	18
Purified nitrile rubber (19% acrylonitrile)				
Without curing	-26	-22	-15	-5
w/2% DICUP w/o curing	-26	-21	-14	-4
Thermal cured w/2% DICUP*	-7	-4	2	10

* Thermally cured at 150°C for 2.5hr

Crosslinking tends to lower energy absorption associated with thermal motion of polar -CN groups. Crosslinking of polymers results in decreased segmental mobility which increases the relaxation time of dipole-segmental loss, so that the dielectric loss maximum temperature is shifted to a higher temperature. This can be clearly seen by contrasting Figures 3.6 and 3.7 for the uncured and cured nitrile rubbers. The maximum loss tangent value of thermally cured nitrile rubber was reduced to one third of that of uncured nitrile rubber. Nonetheless, even at a loss tangent value of 0.1, the cured nitrile rubber was receptive enough to show good heatability.

The maximum value of tanδ increased with increasing percentage of polar acrylonitrile in nitrile rubber. In addition, the corresponding transition temperature shifted to a higher temperature as shown in Table 3.1.

The molecular relaxation process in polymers which gives rise to dielectric relaxation, in general, can also be seen in the mechanical spectroscopy analogue. Because tanδ peaks in DMTA are biased by a fundamental weighting of different molecular motion processes to give approximately a decade mismatch, this frequency region is overlapped by establishing correlations of loss peaks of loss moduli (G" or E") in DMTA, as shown in Table 3.2, and loss peaks of tanδ in DETA.

Taking the case of nitrile rubber with 2% added dicumyl peroxide without curing, as an example, it was seen that the T_{max} from the DMTA spectra were shifted +9°C within two decades of increasing frequency. This is summarized in Table 3.2. In Table 3.1, T_{max} from the corresponding DETA spectra were shifted +20°C within three decades of frequency. In addition, Figures 3.5 and 3.6 reveal that the width of the tanδ spectra tends to broaden with increasing frequency. This indicates a broad distribution of relaxation times. As expected, the maximum value of tanδ also increases with increasing frequency. Overall, the base width in these spectra is larger than 40°C.

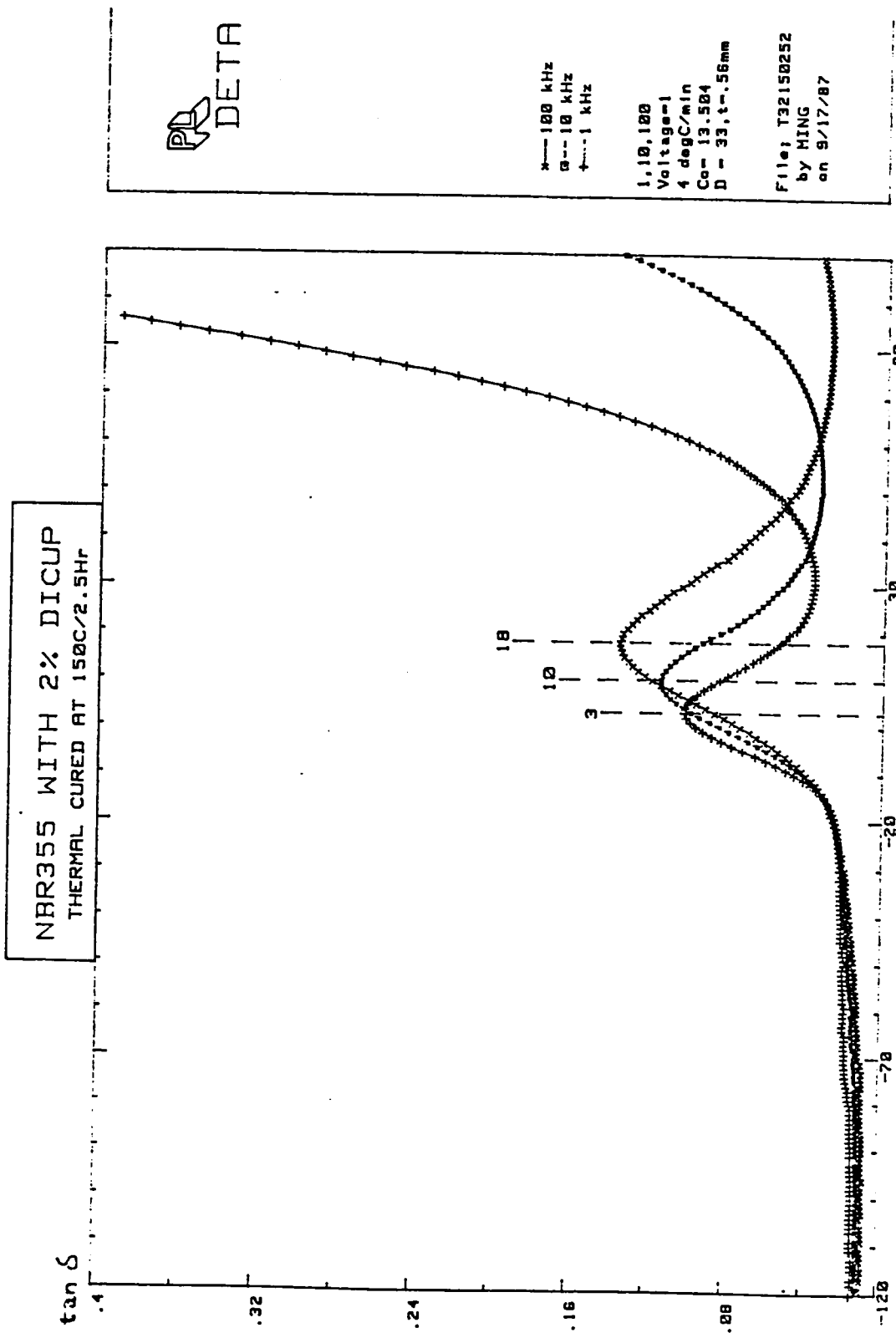

Figure 3.7 Temperature dependence of the loss tangent of thermally cured 30% acrylonitrile nitrile rubber with 2% w/w dicumyl peroxide at various frequencies.

Table 3.2 Temperatures at the maximum peaks of the loss moduli of 30% acrylonitrile nitrile rubber* at various frequencies from DMTA spectra.

		.33Hz	1Hz	3Hz	10Hz	30Hz
Without curing						
(G") (Shear)	-24	-22	-20	-17	-15	
Microwave cured at 38 watts						
for 30min (tanδ) (bending)	-21	-19	-17	-15	-12	

* Purified nitrile rubber (30% acrylonitrile) with 2% dicumyl peroxide

Increasing frequency from 0.33 Hz to 100 kHz, increased T_{max} 31°C within five decades of frequency, while T_{max} at 100 kHz (10^5 Hz) was 7°C - still below room temperature. As a result, the tail of the dielectric loss spectra would be extended to near room temperature when the applied frequency approached the microwave region (2.45×10^9 Hz).

3.4.4 Microwave Experimental Results

The microwave curing reactions of 30% acrylonitrile nitrile rubber with 2% dicumyl peroxide were carried out at three different input power levels (40, 50 & 60 watts). In Figures 3.8-3.12, accurate input, reflected and transmitted powers were obtained by completely calibrating each set of attenuators and cables. The percentage of loss on the wall and system was based on the experiments with empty loading, teflon rods and the empty sample holder. These values were averaged to get a factor of about 93% (7% loss in the applicator); thus,

$$P_a = (P_i - P_r - P_t) \times 0.93 \qquad [3\text{-}4]$$

In Figure 3.8, three power readings are plotted vs. time for a typical sample. The input power source, P_i, of 40, 50 and 60 watts, remained unchanged with time. The transmitted powers, P_t, however were constant only until the sample began to heat rapidly where P_t decreased and then levelled off. The reflected powers, P_r, also were constant initially, but increased and then levelled off once the sample began heating rapidly. Increasing the input powers from 40 to 60 watts resulted in overall increases in transmitted power as well as reflected power. This indicated that the energy absorbed by the nitrile rubber increased with the input power. Both variations of transmitted and reflected powers with increasing input power were shifted toward shorter times. Due to the increasing temperature, the dielectric loss factor increased and the impedance of

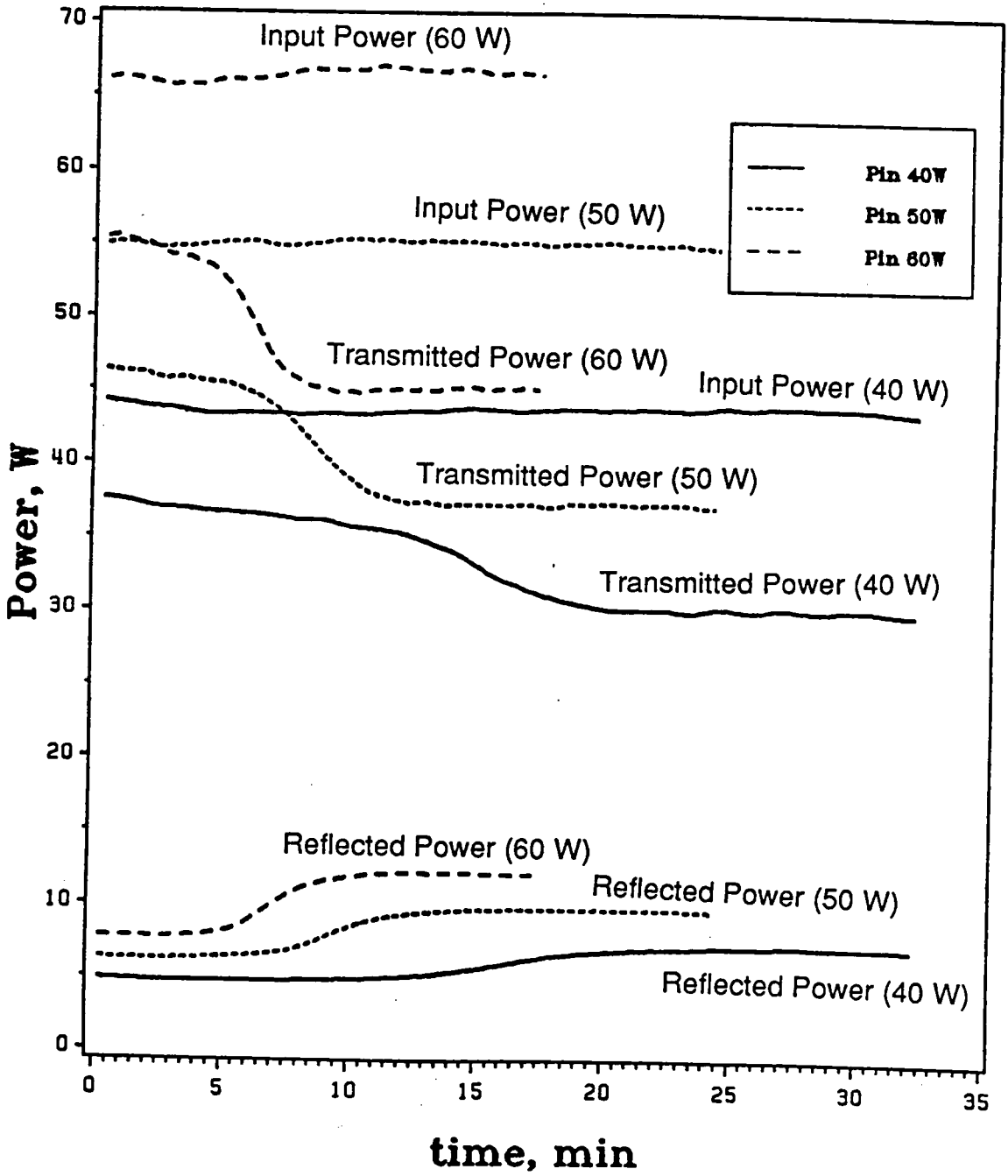

TOP :INPUT POWER
CENTER :TRANSMITTED POWER
BOTTOM :REFLECTED POWER

Figure 3.8 Variation of the input power, reflected power and transmitted power with time for 30% acrylonitrile nitrile rubber with 2% w/w dicumyl peroxide in the travelling wave applicator.

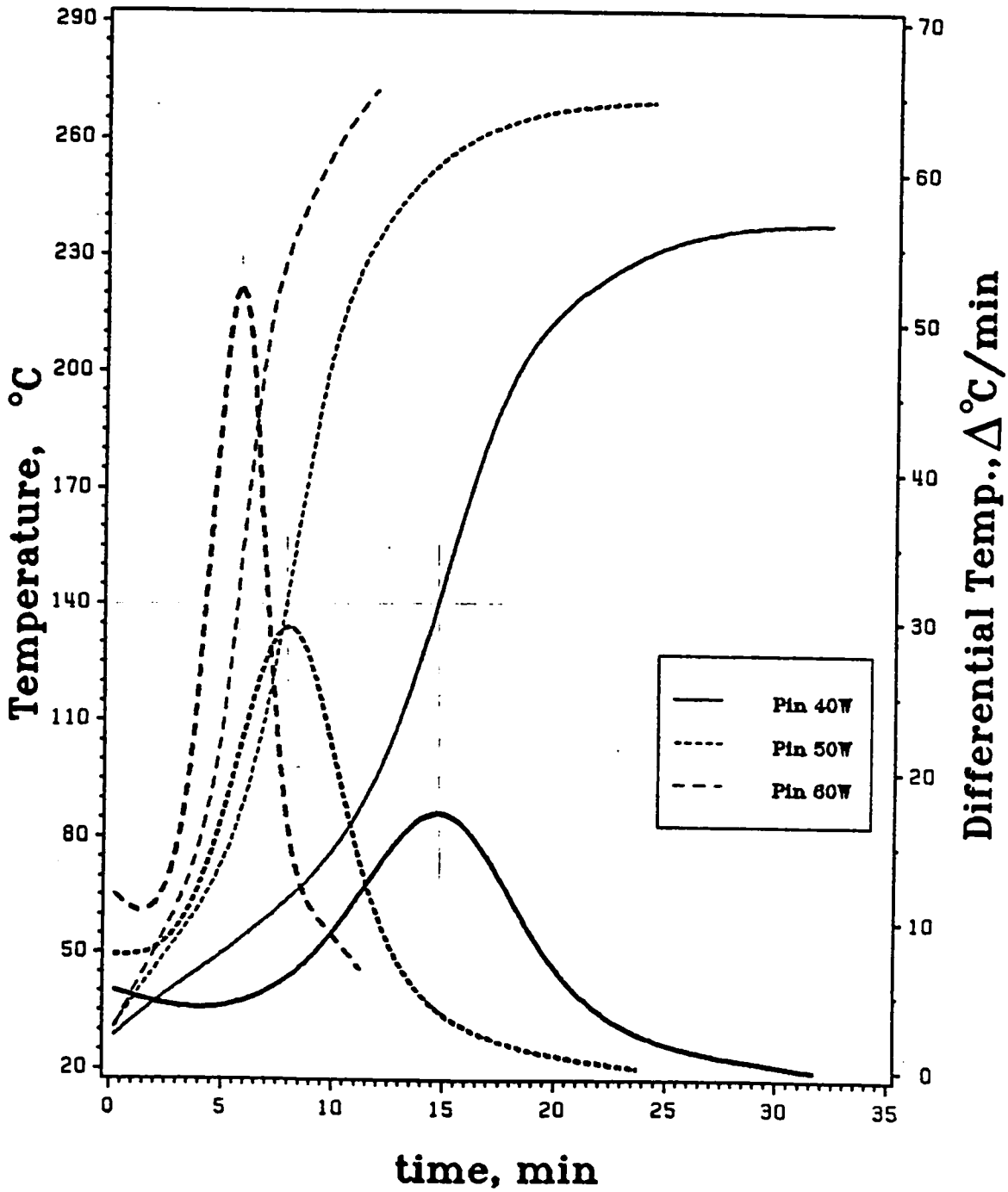

THICKER LINE: DIFFERENTIAL

Figure 3.9 Variation of the temperature and heating rate with time for 30% acrylonitrile nitrile rubber with 2% w/w dicumyl peroxide in the travelling wave applicator.

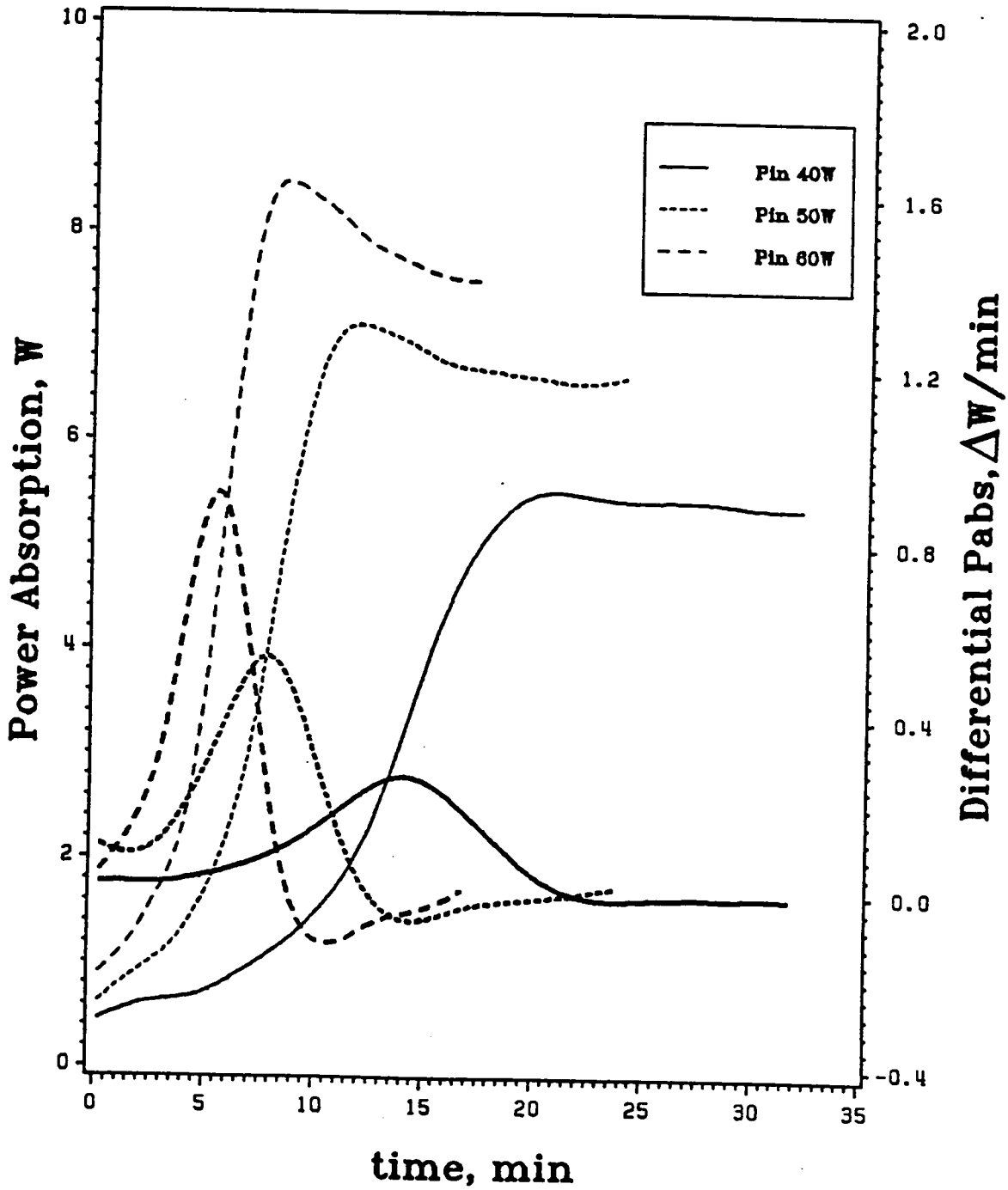

THICKER LINE: DIFFERENTIAL

Figure 3.10 Variation of the power absorption and power absorption rate with time for 30% acrylonitrile nitrile rubber with 2% w/w dicumyl peroxide in the travelling wave applicator.

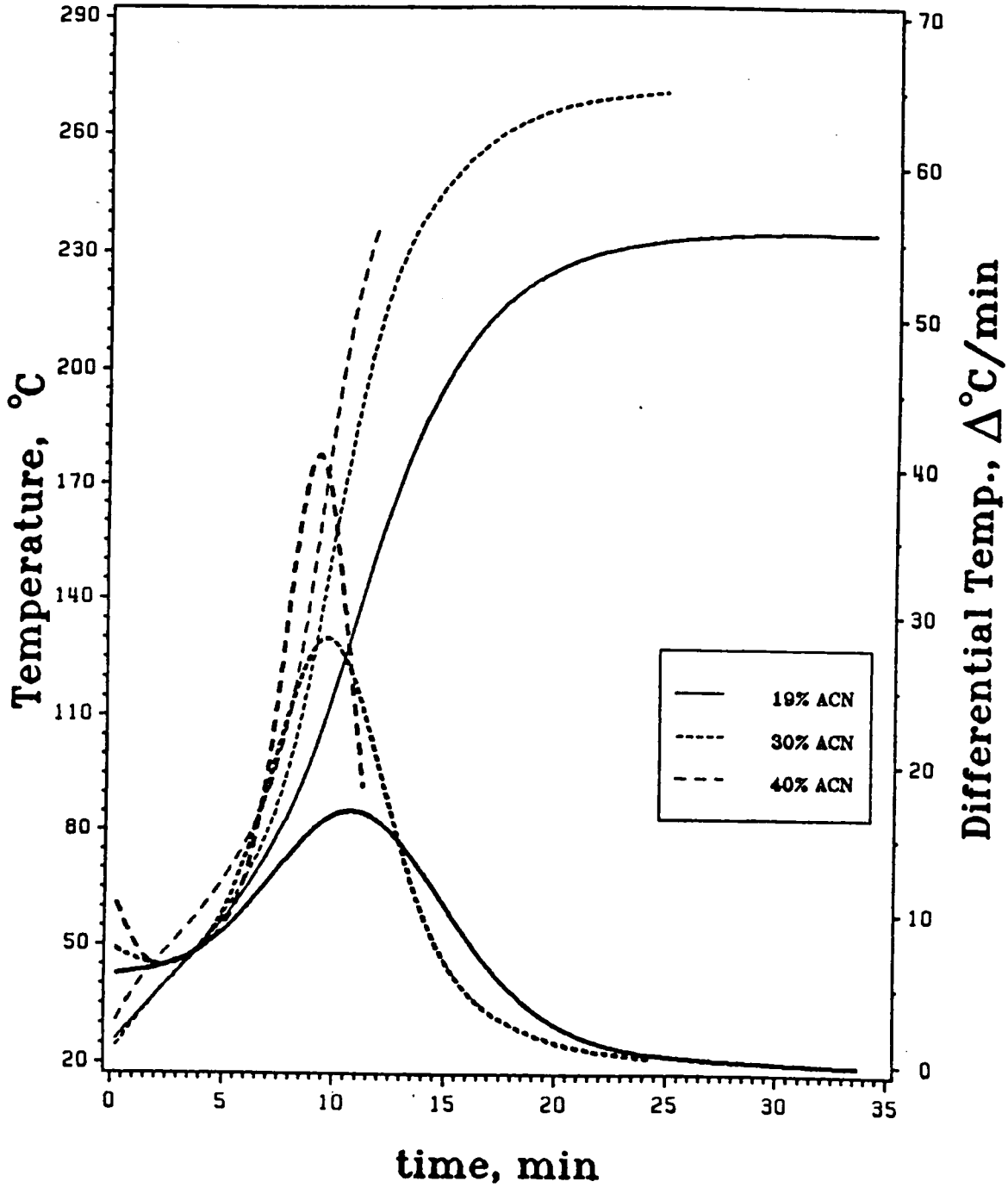

THICKER LINE: DIFFERENTIAL

Figure 3.11 Variation of the temperature and heating rate with time for 19%, 30% and 40% acrylonitrile nitrile rubber without dicumyl peroxide in the travelling wave applicator. Input power was 50 watts.

nitrile rubber changed. At the same time, reflected power, P_r, increased to higher values.

Figure 3.9 represents temperature and heating rate versus time for the same material. This plot reveals how receptive the nitrile rubber was to the microwave radiation. The steeper the slope, the shorter the processing time. Figure 3.10 represents the power absorption and the power absorption rate versus time. The plateau of temperature and power absorption, P_a, in Figures 3.9 or 3.10, increased when power was stepped up from 40 watts to 60 watts. In addition, the maximum rate of power absorption or rate of heating was shifted to shorter times. The loss tangent value in cured rubber was found to be less than the loss tangent value of the uncured rubber. This can be explained by examining the loss tangent DETA spectra. Since heating rate is proportional to the magnitude of the dielectric loss, as shown in Equation [3-2], it is expected that the uncured nitrile rubber would heat faster. The crosslinking of polymers decreases segmental mobility. Thus, the effective loss caused by thermal motion of polar groups decreases. Because the polar -CN group was not involved in curing, the dipolar relaxation of the cured rubber did not disappear completely so that the sample could be heated and maintained at a high temperature by the appropriate input power. Indeed the power absorption curve increased to a maximum and then decreased to a plateau. This suggested that the microwave energy absorbed by the sample was in equilibrium with the loss energy conducted away from the sample. Thus, the dielectric loss factor was fixed by the leveling off of temperature. In Figure 3.9, there was an interesting phenomenon: all three maximum points of heating rate vs. time plots intersected at about 140°C on their respective temperature curves. One possible reason for this is the exothermic curing reaction of dicumyl peroxide. Even without peroxide, though, the same phenomenon occurred, as shown in Figure 3.11. Another

hypothesis for this behavior involves a transition temperature in the 2.45 GHz region. At the maximum value of ε", the heating rate is at a maximum and subsequently decreases with the decreasing value of ε".

Figure 3.12 represents the variation of power absorption and power absorption rate with temperature for three constant input powers. Power absorption increased continuously with increasing temperature, but then decreased due to the chemical crosslinking which induced a strong viscosity effect and consequently hindered dipolar relaxation. The polar acrylonitrile group absorbed energy by interacting with the microwave field which then heated up the whole of the mass to be crosslinked. As a result of the increasing temperature, the peroxide decomposed thereby generating crosslinks. Again, the maximum power absorption rate was at approximately 140°C.

Figure 3.13 is a plot of heating rate vs. temperature for nitrile rubber containing 2% dicumyl peroxide. As discussed on the previous page, the heating rate was proportional to the dielectric loss factor, as shown from Equation [3-2] where k and frequency were constant, ρ and C_v were assumed to remain unchanged, and the electric field strength was considered to be constant by keeping the input power fixed. The plot of heating rate vs. temperature at 2.45 GHz looked remarkably similar to a typical DETA spectra. By drawing tangents to the "cool sides" of the heating rate vs. temperature curves in Figure 3.13, three intercept temperatures were obtained. The intercept temperature for any curve was given a special name coined the "critical temperature of dielectric loss". The critical temperatures for these 3 curves were determined to be between 40 and 45°C. The critical temperature gives a good indication of the point at which the dielectric loss factor, ε", increases significantly. In other words, the tailing of the dielectric relaxation spectra occurred near room temperature. In order to prove this point, various starting temperatures for the

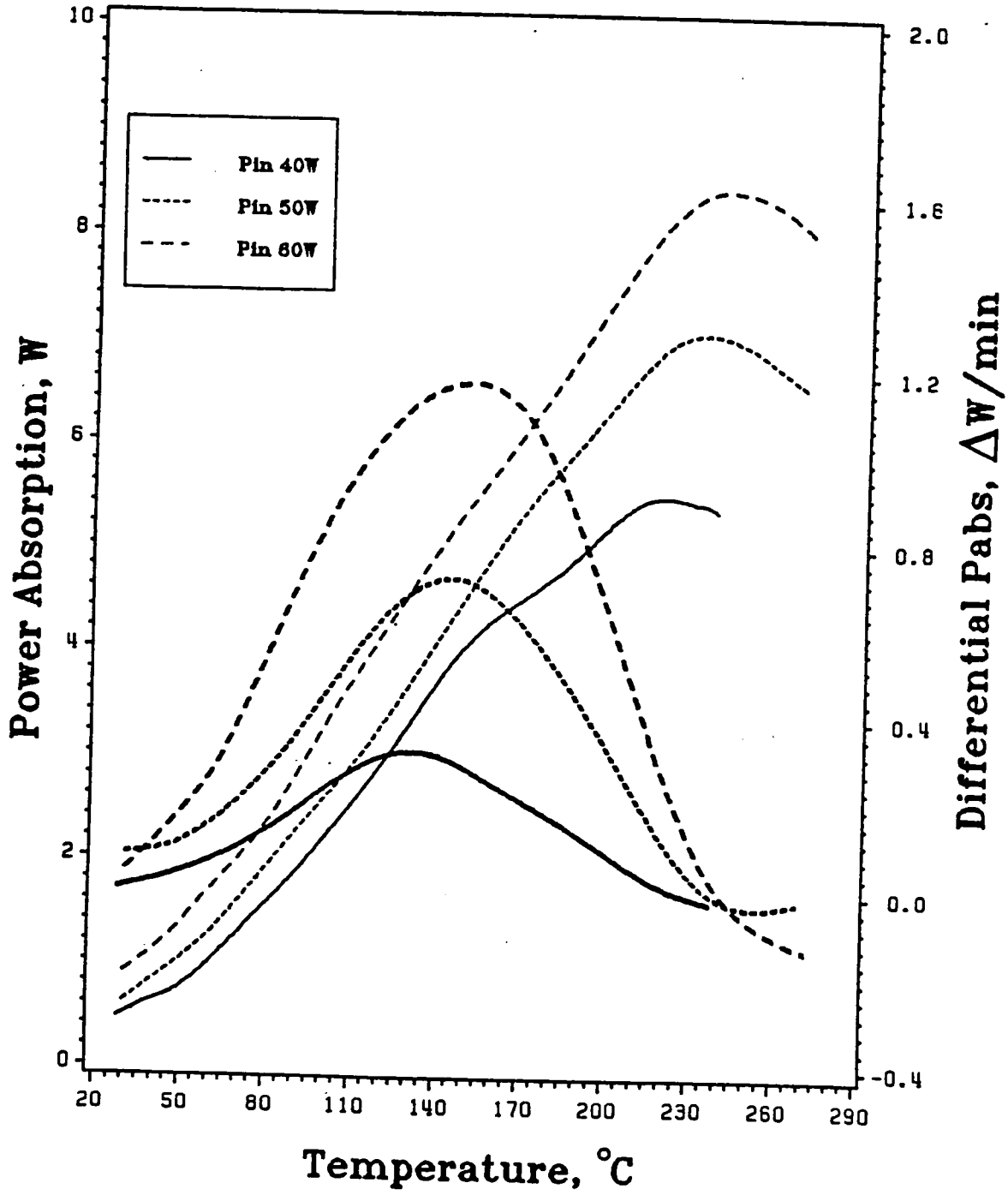

THICKER LINE: DIFFERENTIAL

Figure 3.12 Variation of the power absorption and power absorption rate with temperature for 30% acrylonitrile nitrile rubber with 2% w/w dicumyl peroxide in the travelling wave applicator.

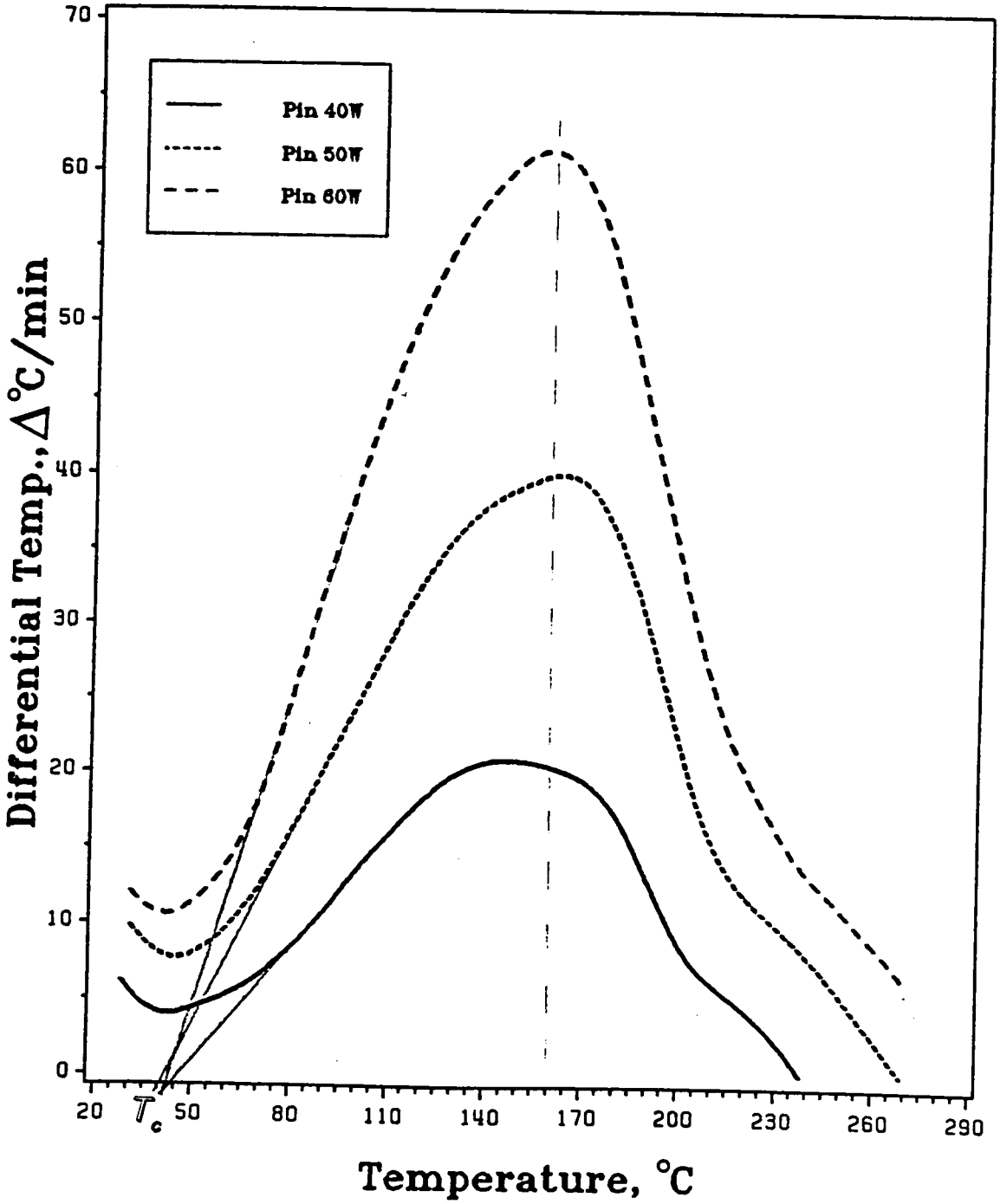

Figure 3.13 Variation of the heating rate with temperature for 30% acrylonitrile nitrile rubber with 2% w/w dicumyl peroxide in the travelling wave applicator.

investigation of 19% acrylonitrile nitrile rubber were induced by externally heating on the waveguide via a strip heater, as shown in Figure 3.3. Figure 3.14 shows the sample temperature vs. time for three different starting temperatures: 26°C, 42°C and 51°C. The input power was fixed at 20.5 watts. The heating rate and the final plateau temperatures increased significantly at the higher starting temperatures. This indicated that the dielectric loss dipole dispersion had increased with increasing temperature into the dielectric loss region between room temperature and 51°C.

In order to avoid trial-and-error experiments in microwave processing, it is necessary to obtain direct and meaningful information about dielectric constant, dielectric loss factor and/or loss tangent as a function of temperature and the degree of curing for crosslinking systems at 2.45 GHz. Interpretation of these dielectric properties usually requires information from a wide frequency and/or temperature range. Therefore, in these experiments, where a large window of frequencies was examined, a WLF plot was used to predict the shift of dielectric loss factor into or out of the microwave region.

The temperature dependence of loss peaks in general follows the well known WLF equation for viscosity and viscoelasticity in polymeric and some nonpolymeric liquids. The applicability of this viscoelastic function to dielectric relaxation data suggests that the temperature dependence of the molecular friction coefficient is common to mechanical and dielectric-relaxation processes. The glass transition temperatures at lower frequencies were obtained from DMTA and DETA spectra and are summarized in Tables 3.1 and 3.2. The glass transition temperature at 2.45 GHz was obtained from the temperature at the maximum heating rate in Figure 3.12. In a typical WLF treatment, Figure 3.15 shows the plot of the logarithm of the frequency versus the reciprocal of

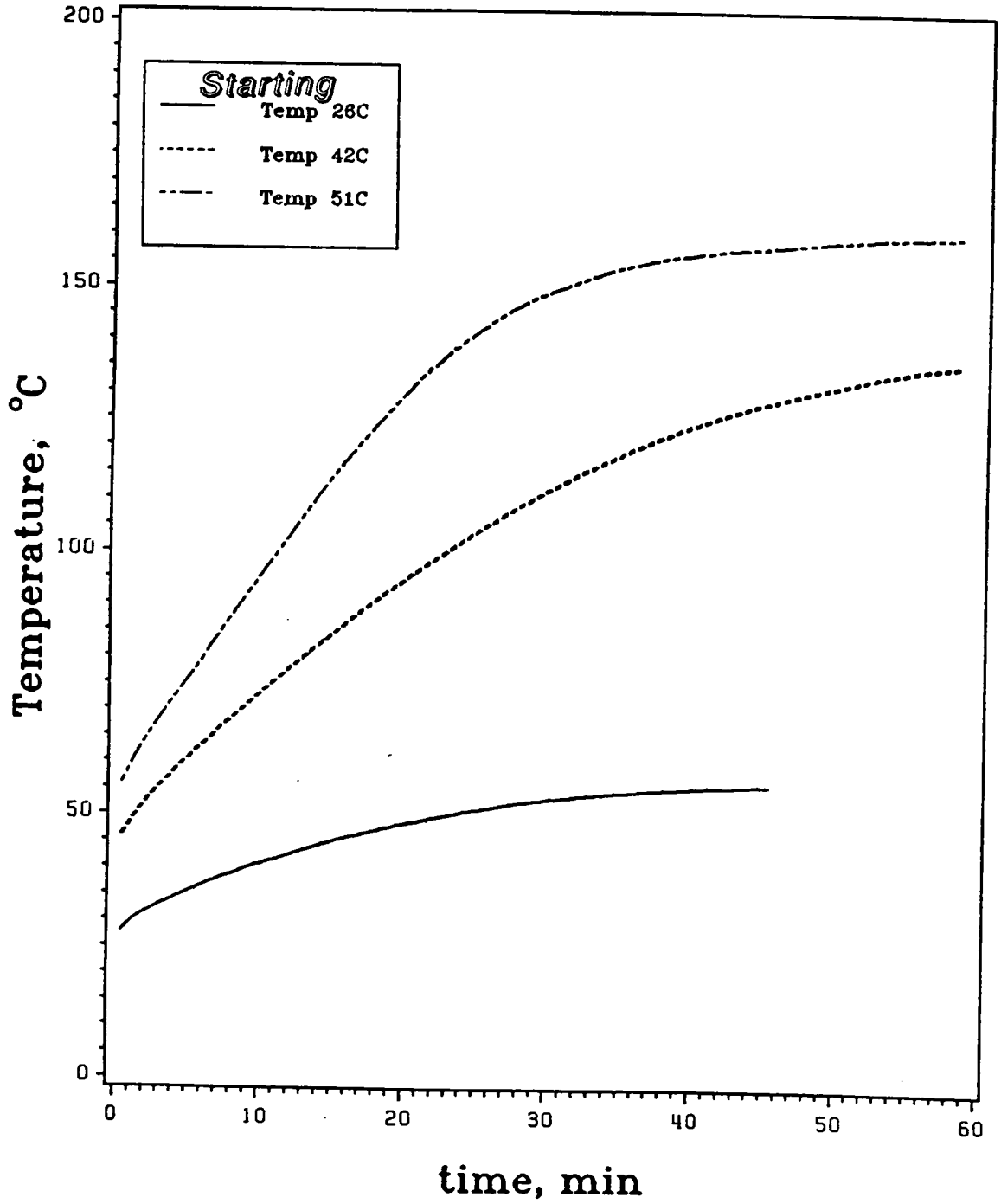

T_g of NBR 210 = −50°C

Figure 3.14 Variation of the temperature with time for 19% acrylonitrile nitrile rubber with 2% w/w dicumyl peroxide in the travelling wave applicator. Input power was 20.5 watts.

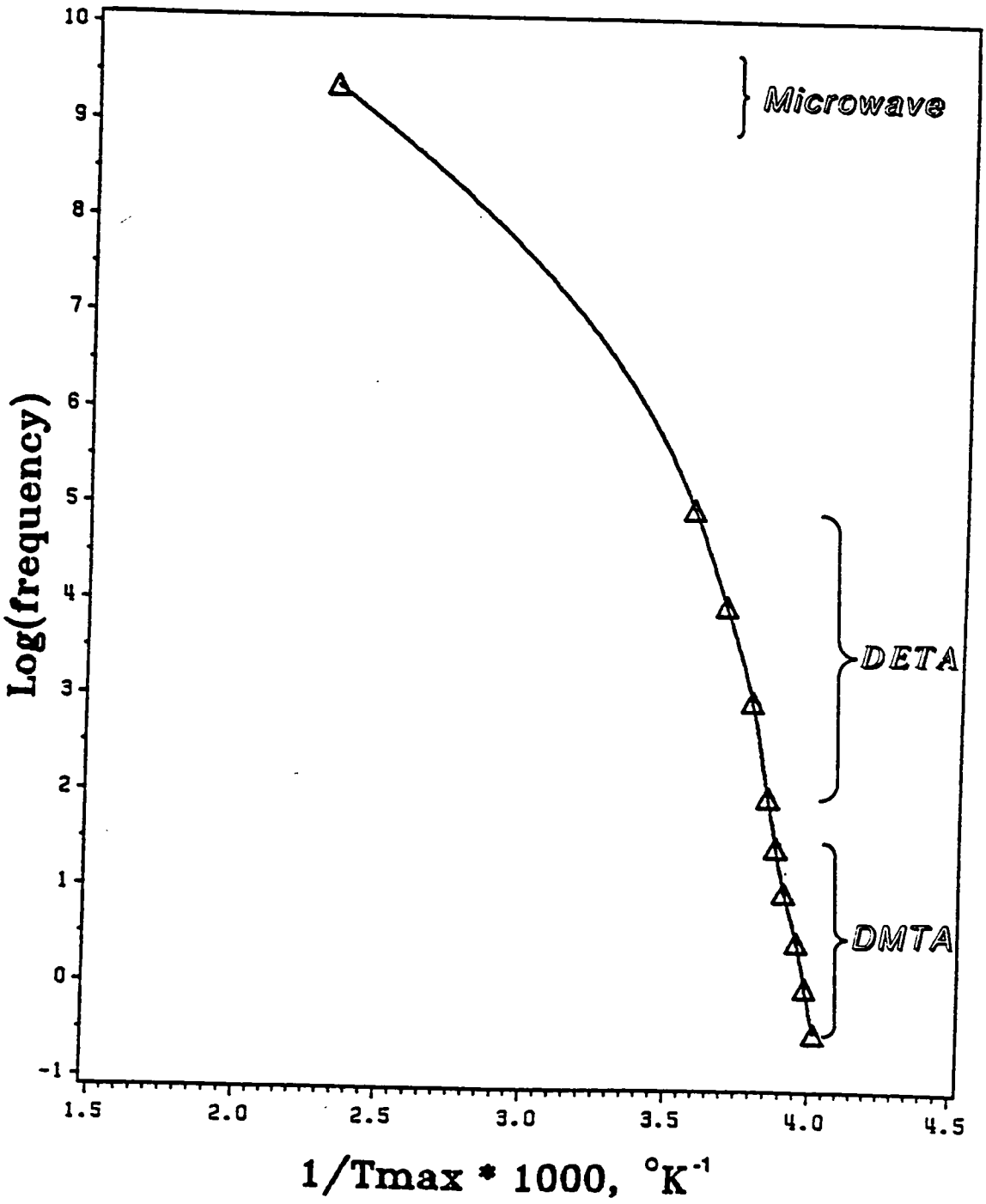

(dT/dt)max=160°C at 2.45 GHz

Figure 3.15 WLF relationship for 30% acrylonitrile nitrile rubber with 2% w/w dicumyl peroxide in the travelling wave applicator.

absolute temperature. All α transitions fell on the curve, indicating a continuously changing activation energy with temperature, as is expected for polymeric materials.

3.5 CONCLUSION

The highly polar -CN group in nitrile rubbers induced a large dipolar relaxation of main chain motions at the glass transition region. From the value of glass transition temperature obtained by DSC, DMTA, DETA, and microwave calorimetry, the 'cool side' tail of the dielectric loss spectra was found to extend into the room temperature regime at 2.45 GHz. Nitrile rubbers can, therefore, be easily heated starting at room temperature. After an initial absorption of microwave energy, the temperature rise caused the dielectric loss factor to increase which, in turn, resulted in a further temperature increase, and so on. Charring of the materials was avoided by turning off the microwave energy source. The heating rate was found to depend on several factors: (1) the glass transition temperature of nitrile rubber, (2) the percentage of acrylonitrile and (3) the extent of curing. The higher the content of acrylonitrile, the better will be the heatability of the nitrile rubber. However, the glass transition of the nitrile rubber would be higher, too. These two effects therefore lead to the heating rate being essentially independent of the acrylonitrile content which is between 19% to 40%.

The dielectric loss factor, ε'', along with the electric field strength, were found to be key parameters in controlling the heatability of a given material. At a fixed electric field strength, the dielectric loss factor controlled the rate of rise of temperature. The larger the dielectric loss factor, the easier the material absorbed the incident microwave

energy. In the case of nitrile rubber, an input power of 60 watts could easily char the material if the microwave source was not turned off. Knowledge of the dependence of dielectric behavior on temperature at 2.45 GHz is important in the design of a microwave heating system to take advantage of the rapid heating on the low temperature side of $d\varepsilon''/dT$ and to avoid the risk of the thermal runaway effect. The WLF plot was used to find the temperature of the maximum heating rate at 2.45 GHz. It is important to summarize that the critical temperature for maximum microwave heating was exceeded by room temperature in these experiments.

An unique advantage of microwave curing that was taken advantage of in this research was that microwaves penetrate the whole mass instantaneously so that thermal peroxide decomposition starts in every point of the polymer simultaneously, avoiding thermal gradients from conduction. The heating process can be turned on or off instantaneously and therefore curing was controlled more accurately than in conventional thermal methods. Tremendous energy savings can be realized by heating only selected regions of the material with microwave radiation.

Due to the small electric field strength in travelling wave applicators, materials of low loss could not be processed in such waveguides. Non-uniformity across the width of material processed in an axial travelling wave applicator continues to be a problem. A practical solution to this is to pass the material through a number of waveguides called a meander type travelling wave applicator which is illustrated in Figure 3.16 (14). Several travelling wave applicator types are used in practice and have been described in the literature (19-21).

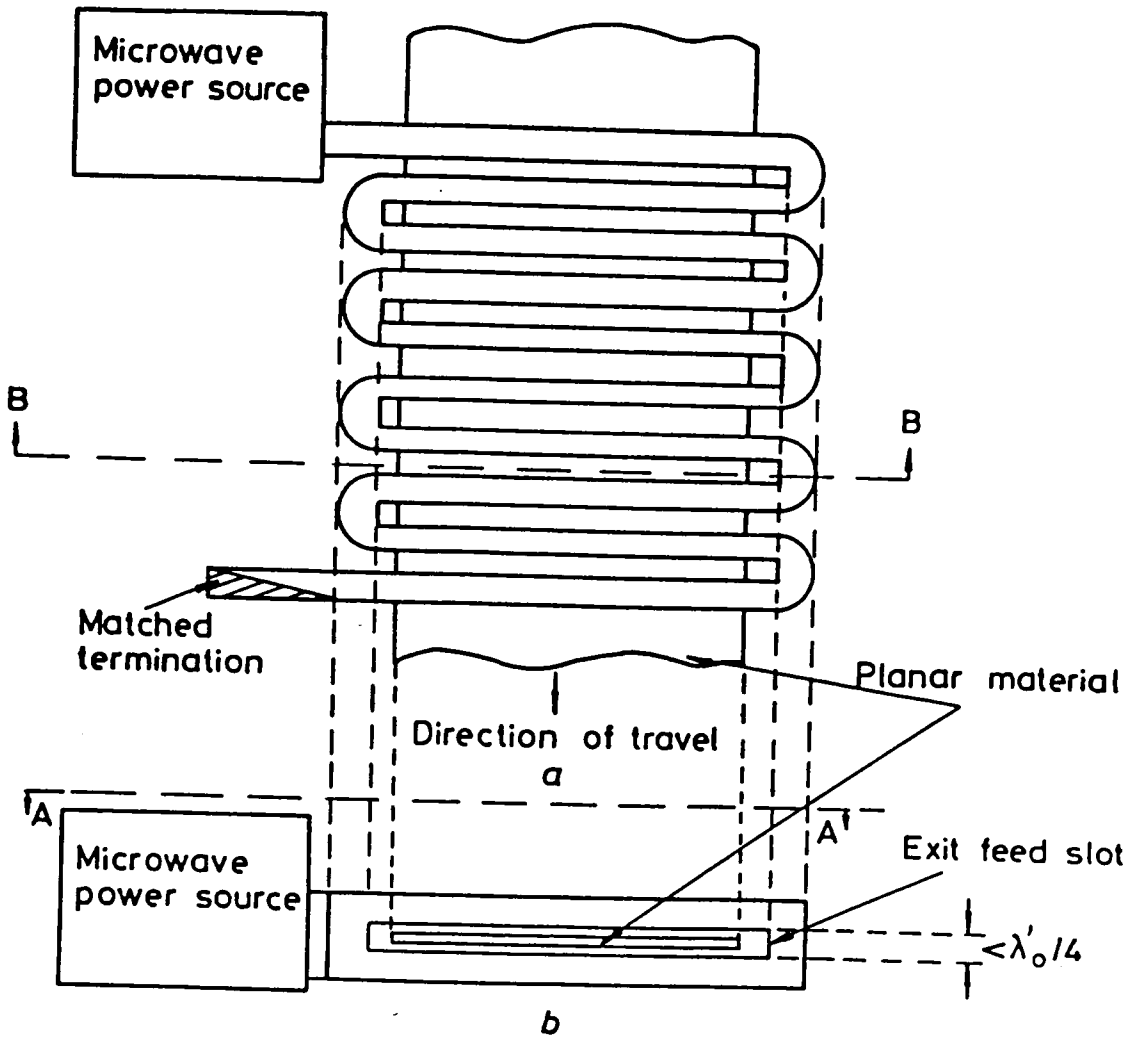

Figure 3.16 Meander applicator

a Plan view A-A
b Cross-sectional view B-B (14)

ACKNOWLEDGMENT

This work was supported by DARPA under Air Force contract number F33615-85-C-5153. We also thank that BF Goodrich Company for supplying us with nitrile rubber and Lucidol Division of Pennwatt Corporation for supplying dicumyl peroxide.

3.6 REFERENCES

1. R. Rajan, *J. Cell. Plast.*, **4**, 304 (1968).
2. H. Jullien and H. Valot, *Polymer*, **26**, 506 (1985).
3. B. Silinski, C. Kuzmycz and A. Gourdenne, *Eur. Polym. J.*, **23**, 273 (1987).
4. N. S. Strand, *Modern Plastics*, **57(10)**, 64 (1980).
5. I. J. Chabinsky, *Rubber World*, **188**, 34, April (1983).
6. J. Ippen, *Rubber Chem. Technol.*, **44**, 294 (1971).
7. I. J. Chabinsky, *Elastomerics*, **115**, 17, January (1983).
8. H. F. Schwarz, R. G. Bosisio, M. R. Wertheimer and D. Couderc, *J. Microwave Power*, **8**, 303 (1973).
9. H. F. Schwarz, R. G. Bosisio, M. R. Wertheimer and D. Couderc, *Rubber Age*, **107(11)**, 27 (1975).
10. N. Probst and J. Iker, *Kautsch. Gummi, Kunstst.*, **37**, 385 (1984).
11. C. H. J. Avons and H. Roebuck, *SGF Publ.*, **46**, **XII**, 19pp. (1975).
12. C. L. Lee, in *ACS Symp. Ser.*, **107**, T. L. Vigo and L. J. Nowack (eds), American Chemical Society, Washington D. C., 1979, p. 45.
13. H. F. Mark, N. M. Bikales, C. G. Overberger and G. Menges, ***Encyclopedia of Polymer Science and Engineering, Vol. 5***: Dielectric Heating to Embedding, 2nd ed., John Wiley & Sons, New York, 1986.

14. A. C. Metaxas and R. J. Meredith, ***Industrial Microwave Heating***, Peter Peregrinus, London, 1983.

15. Z. Grubisic, P. Rempp and H. Benoit, *J. Polym. Sci. Polym. Lett. Ed.*, **5**, 753 (1967).

16. E. J. Siochi, Ph.D. Dissertation, Virginia Polytechnic Institute and State University, Blacksburg, VA, 1989.

17. D. K. Cheng, ***Field and Wave Electromagnetics***, Addison-Wesley Publishing Co., Pennsylvania, 1983.

18. K. Beiss and G. Menges, *Proc. - Eur. Reg. Tech. Conf.: Plast. Process., 2nd*, 19-1-19-9. Edited by: C. Klason and H. R. Skov, Soc. Plast. Eng. Scand. Sect.: Copenhagen, Den. (1980).

19. D. A. Dunn, *J. Microwave Power*, **2**, 7 (1967).

20. N. I. Heenan, in ***Microwave Power Engineering*** , E. C. Okress, (ed.), pp. 126-144. Academic Press, New York, 1968.

21. N. H. Williams and H. C. Warner, in ***Microwave Power Engineering*** , E. C. Okress, (ed.), pp. 175-188. Academic Press, New York, 1968.

CHAPTER 4

THE DIELECTRIC BEHAVIOR OF GLASSY AMORPHOUS POLYMERS AT 2.45 GHz

4.1 INTRODUCTION

The dielectric behavior of glassy polymers at 2.45 GHz is intrinsically different from that of rubbery polymers. For example in chapter 3, nitrile rubbers showed a critical temperature of dielectric loss, T_c, very close to room temperature. Thus, nitrile rubber could be heated very easily at room temperature. Another example of materials which have dielectric loss behavior that are very different from glassy polymers are foodstuffs [1-5]. The predominant material in food is water (60-99% by weight). Since water has a very high dielectric loss factor at around room temperature, as shown in Figure 4.1 (4), foodstuffs can be heated very rapidly. Above the peak temperature the slope of the curve of dielectric loss factor versus temperature becomes negative, thereby affording very good control of microwave heating.

This present investigation focuses on the dielectric behavior of glassy thermoplastics. For thermoplastics at room temperature, the dielectric loss at microwave frequencies consists of background loss because the location of the dielectric loss spectrum at 2.45 GHz is well above room temperature. The dielectric losses observed at 2.45 GHz have their origins outside the microwave region at room temperature (6); it is not possible to isolate attention to a few decades of microwave frequencies. Numerous dielectric loss spectra in the low frequency region can be found

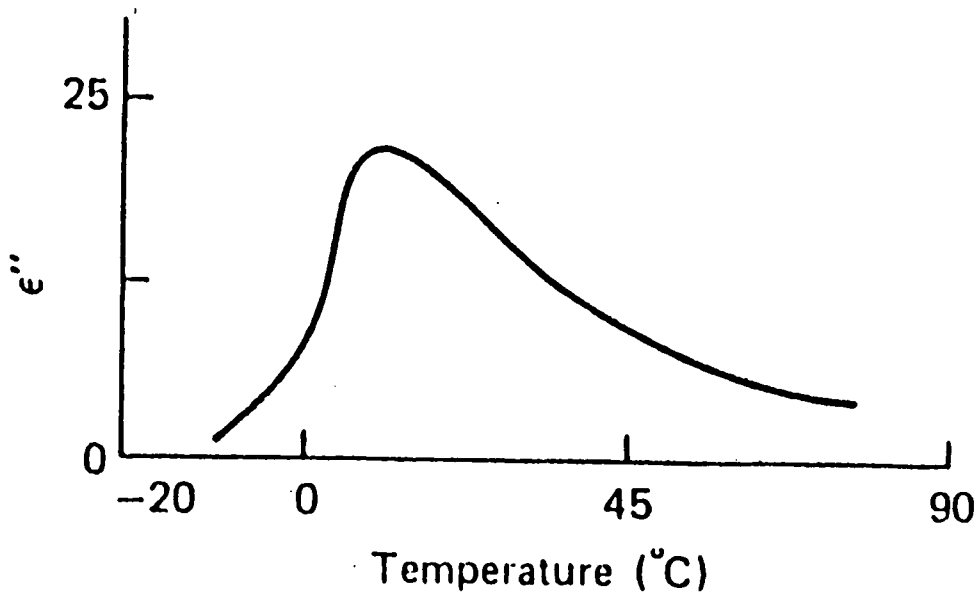

Figure 4.1 Variation in dielectric loss factor of water and ice. (4)

in the literature (7-14). Since little information exists on dielectric behavior in the microwave region (6, 15,16), it is essential that an orderly study of the process be conducted. The effects of sample temperature must not be neglected because the dielectric loss spectra change in shape and position on the frequency scale with a change in temperature. In other words, dielectric loss spectra can be displaced into or out the 2.45 GHz region with appropriate change in temperature. These effects are discussed in detail in the following section.

The goal of this fundamental study was to improve the coupling of microwave energy to glassy thermoplastics which are nearly transparent to microwave frequencies at room temperature and to understand the fundamental mechanisms involved. The specimens were subjected to an alternating electric field of 2.45 GHz inside a rectangular waveguide. Two different applicators were used in these experiments: the travelling wave applicator (discussed in chapter 3) and the TE_{10n} standing wave applicator. From plots of heating rate vs. temperature, the critical temperature of dielectric loss, T_c, was estimated for various glassy polymers. As discussed in chapter 3, T_c gives an approximate indication of the point at which the dielectric loss factor increases significantly with increasing temperature.

Dielectric spectra of polymers were obtained from -150°C to above their glass transition temperatures via a Polymer Laboratory's Dielectric Thermal Analyzer (DETA) at frequencies of 0.1, 1, 10 & 100 kHz. The shifts of the loss tangent peaks with frequency were used to derive the apparent activation energy in each case. A correlation was drawn between: a) the apparent activation energy and the critical temperature, b) the shape of the dielectric spectra at 2.45 GHz and the shape in kHz region. Finally, WLF relationships were examined for glassy thermoplastics to show the difference in changing activation energy with temperature.

4.2 THEORY

As discussed in the preceding chapter, there are two key equations that describe the heatability of polymers in an applied electric field. The total power absorbed is given by:

$$P = KfE^2\varepsilon'\tan\delta \qquad [4\text{-}1]$$

The heating rate is given by:

$$\frac{dT}{dt} = \frac{KfE^2\varepsilon'(T)\tan\delta(T)}{\rho C_v} \qquad [4\text{-}2]$$

if we ignore convection, conduction and heats of reaction.

Both equations are a function of the dielectric properties of the material. The dielectric behavior of polar polymers at various frequencies are depicted schematically in Figure 4.2 (15). Polymers having high molecular weights cannot be described with a single relaxation time spectrum. The α-relaxation peak which is located above the nominal T_g obtained by DSC is associated with the cooperative motions of the main chain. One or more secondary relaxation effects (β, γ etc.) are associated with the motion of side groups or local groups which may participate in dielectric loss. Ionic conduction, λ, is only observed at low frequency and high temperature. The DC conductance, which varies with σ/ω (where σ is the conductivity and ω is the angular frequency), becomes negligible at microwave frequencies. The activation energy of the local chain motion (β process) is smaller than that of main chain cooperative motions (α process). In other words, as Figure 4.2 depicts, when frequency is increased from low to radio frequencies, the β process shifts to higher frequencies faster than the α process. Therefore, both loss processes eventually merge together at high frequencies.

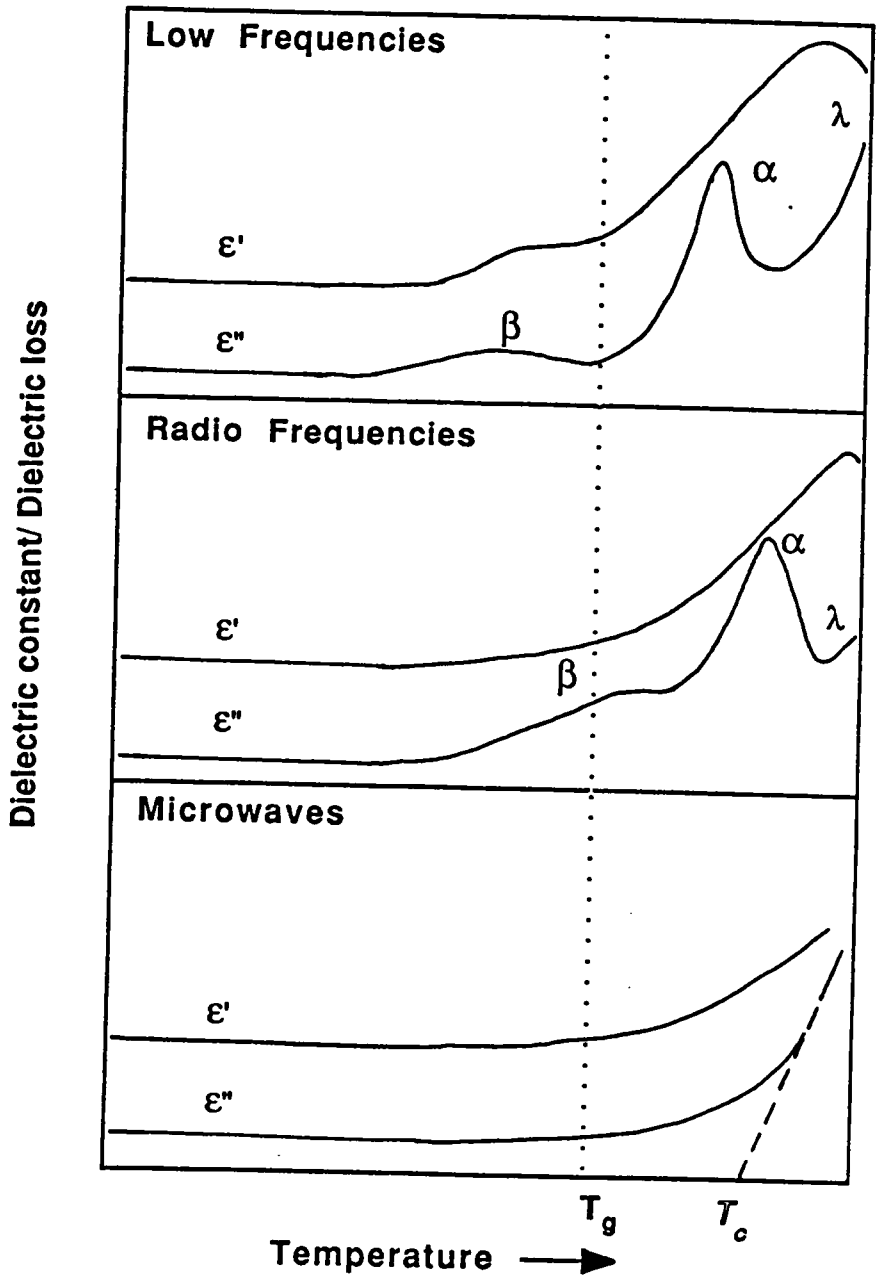

Figure 4.2 Schematic representation of the dielectric behavior of polar polymers at various frequencies.

At microwave frequencies, both processes may be completely merged together. This may be explained on the basis of the fact that, above the glass transition, the α process, corresponding to orientation of segments of the main chain, involves shorter and shorter segments as the temperature increases due to greater chain mobility. Finally, at a high temperature, a small number of monomer repeat units constitute the orienting groups of the main chain and the α and β relaxation processes then become indistinguishable.

4.3 EXPERIMENTAL

4.3.1 Materials

Table 4.1 lists the sources for and T_g's of: poly(n-butyl methacrylate) (PBMA), poly(vinyl acetate) (PVAc), poly(ethyl methacrylate) (PEMA), poly(vinyl chloride) (PVC), styrene acrylonitrile copolymer (SAN) and poly(methyl methacrylate) (PMMA). These polymers were used without further purification, but were vacuum dried just below their respective T_g's for 24 hours before using. Films were prepared by using a platten press (Pasadena Hydraulics, Inc., model number P210C-X3-5-7-20) in the temperature range of 40-50°C above their respective T_g's. These films were kept in the desiccator until they were used for DETA, DMTA and microwave experiments.

4.3.2 Thermal Analysis

The calorimetric responses of samples were measured with a differential scanning calorimeter, DSC (Du Pont model 912), in order to ascertain the glass transition temperature, T_g. For ambient work, nitrogen was used as the purge gas and Indium

Table 4.1 The glass transition temperatures and sources of thermoplastics

Polymer	Tg, °C	Sources	Catalog #
PBMA	20	Aldrich	18152-8
PVAc	30	Aldrich	18949-9
PEMA	66	Inland Leidy	Elvacite
PVC	85	Polysciences	9709
SAN	101	Union Carbide	RMD4400
PMMA	105	Inland Leidy	Elvacite

and lead were used as a calibration standard for temperature and energy. The scanning rate was 10°C/min. Thermogravimetric analyses (TGA) were recorded from 50°C to 750°C at a heating rate 10°C/min by a Du Pont model 951. Air was used as a purge gas at a flow rate of 30 cc/min.

4.3.3 Gel Permeation Chromatography (GPC)

GPC was performed on a Waters 150C GPC having the refractive index detector in parallel with the Viscotek model 100 differential viscometer for obtaining absolute molecular weights. HPLC grade THF was used as the mobile phase at a flow rate of 1.0 ml/min with six UltraStyragel columns (500Å, 10^3Å, 10^4Å, 10^5Å, 10^6Å and 100Å) in series. Twelve polystyrene standards were used to calibrate the molecular weights via the universal calibration method which was referenced in chapter 2.

4.3.4 Relaxation Spectrometer Systems

Polymer Laboratory's DETA (Dielectric Thermal Analyzer) and DMTA (Dynamic Mechanical Thermal Analyzer) were used to provide relaxation information covering the broad frequency range of 0.3 Hz to 100 kHz. Dielectric spectra from -150°C to above T_g were obtained via DETA at fixed frequencies of 0.1, 1, 10 & 100 kHz. Thermal mechanical spectra from -150°C to T_g were studied by using the DMTA at frequencies of 0.3, 1, 3, 10 and/or 30 Hz. All samples were tested in the bending mode.

4.3.5 Microwave Instrumentation

The details of the experimental instrumentation were described in the preceding chapter for the travelling wave applicator. A standing wave applicator was also used for processing glassy thermoplastics. As shown in Figures 4.3 and 4.4, the travelling wave applicator was made into a standing wave applicator for some experiments, by replacing the adapter, directional coupler and termination load with an adjustable

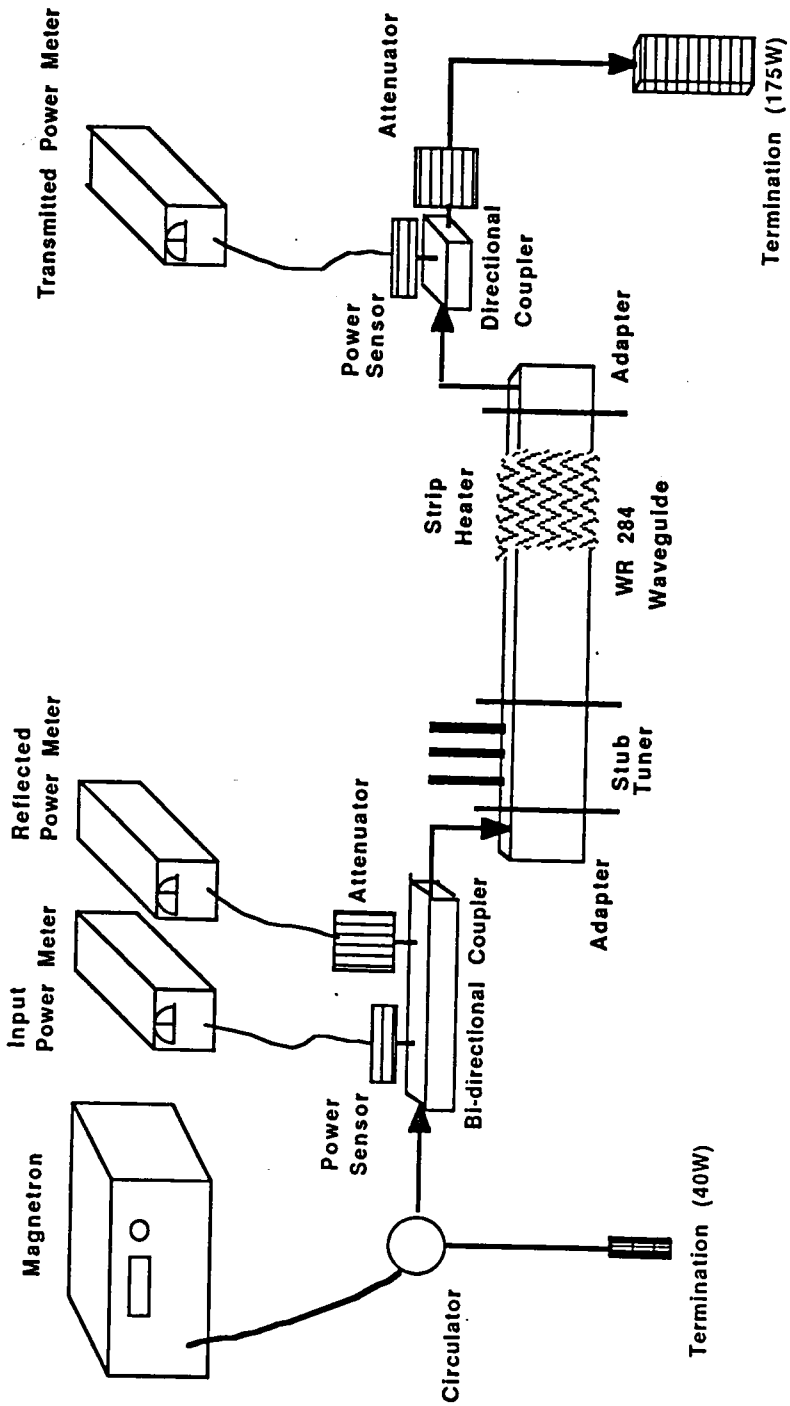

Figure 4.3 Schematic of the experimental set-up for the travelling wave applicator.

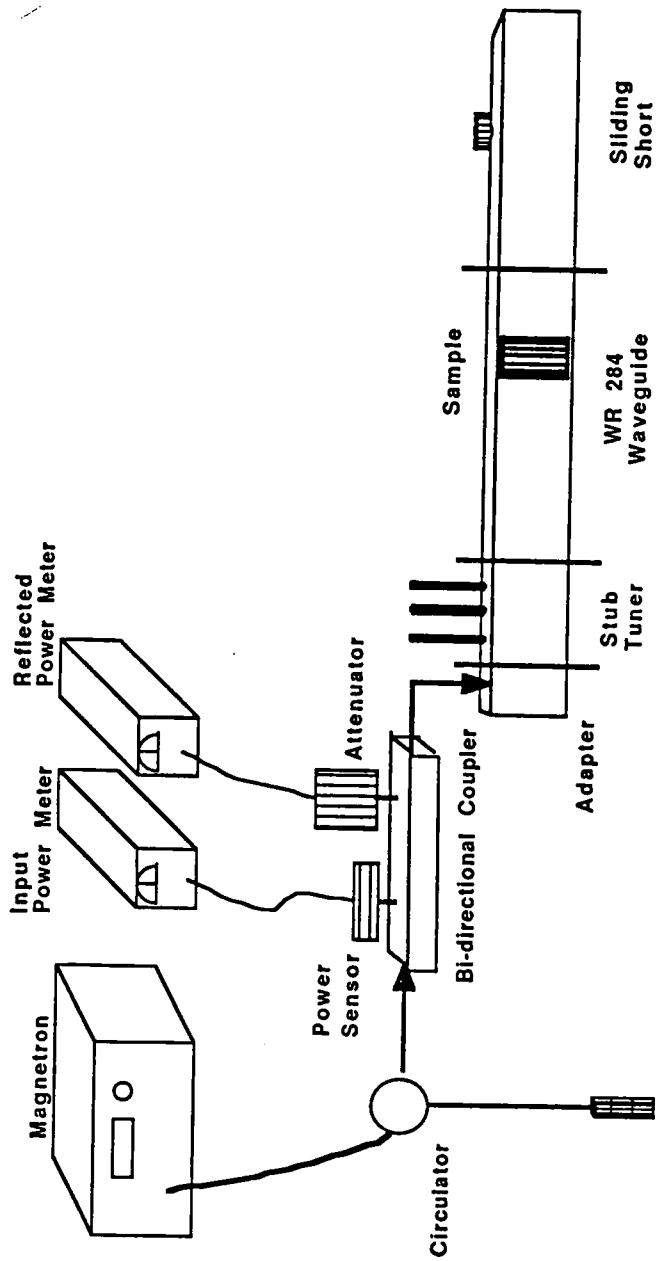

Figure 4.4 Schematic of the experimental set-up for the standing wave applicator.

sliding short fastened to the end of the rectangular waveguide. A stub tuner with six probes was mounted between the adapter and the waveguide. Samples in sheet form were packed in the center section of the 1/2 inch inside diameter cylindrical teflon sample holder.

In an ideal travelling wave applicator, the wave only passes through the specimen once. Thus, the electric field strength is relatively low in the travelling mode. Since heating by microwave energy is essentially an interaction between the permanent dipolar molecules of the material to be heated and the electric field component of the microwave energy, travelling wave applicators are not suitable for materials of low loss. For this reason the electric field component is discussed in detail in this chapter.

There is only one mode, TE_{10}, which can propagate freely in the rectangular waveguide, WR284. The distribution of electric field strength, as shown schematically in Figure 4.5 (17), is related to the peak of the sinusoidal space variation across the width of the waveguide and is therefore at the center-plane through the broad faces. By placing a sliding short at the end of the waveguide, a standing wave is obtained. It is, therefore, the superposition of the incident and reflected waves which gives rise to a standing wave pattern. The peaks (voltage maxima) of the standing wave readily couple power to the specimen because the electric field strength is very high at the maximum. Indeed, this is sometimes the only way to develop adequate coupling to low loss materials. Conversely, the troughs (voltage minima) couple no appreciable power to the material.

The impedance mismatch from the generator to the workload can be indicated by the amount of reflected waves. The presence of any reflected waves indicates a loss of efficiency in energy transfer. The stub tuner was used to adjust the impedance of the work load to a value which the generator could handle. The stub tuner was often

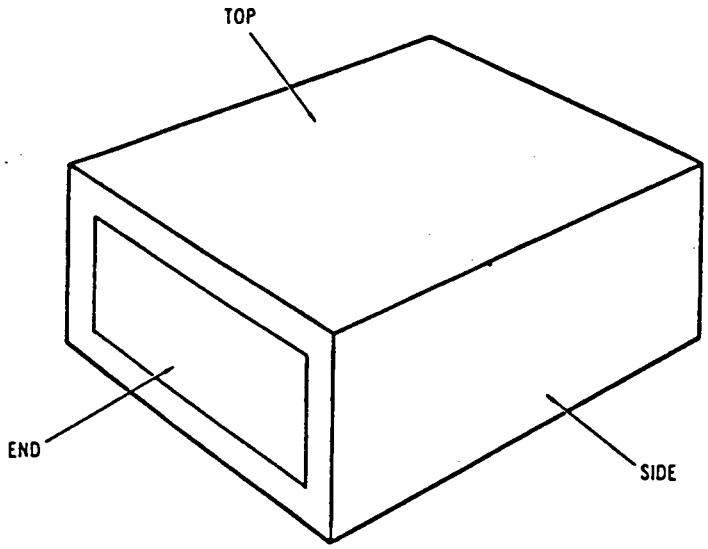

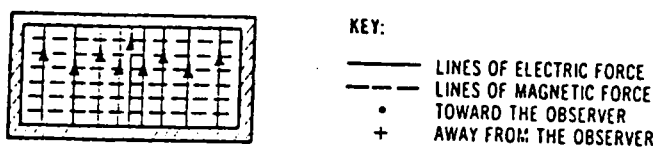

(A) End view of waveguide.

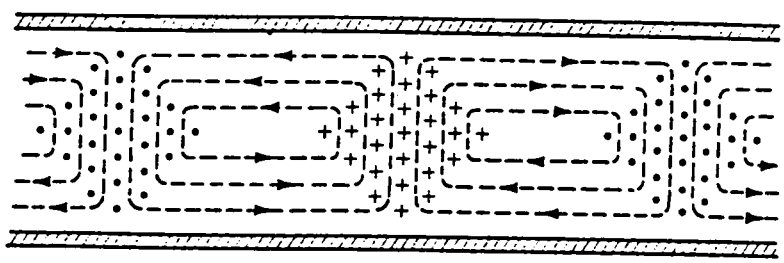

(B) Top view of waveguide.

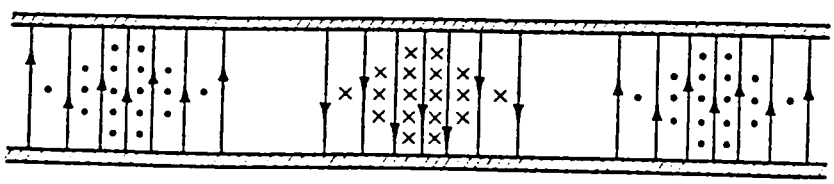

(C) Side view of waveguide.

Figure 4.5 Field lines for TE_{10} mode in a rectangular waveguide.

adjusted by trial and error. An optimum matching with minimum loss can result in an energy efficient heating system. This system works as a tuned cavity. Tuned cavity systems most efficiently use the microwave energy because the radiation from the feed system is continuously reflected from the walls of the cavity, passing through the material many times. The standing wave pattern along the direction of wave propagation is very well defined inside the waveguide and can be monitored via the voltage minima. The precise knowledge of electromagnetic field configurations enables the dielectric material under treatment to be placed in the position of maximum electric field for optimum transfer of the electromagnetic energy to it. In the case of standing waves, the points of maximum field are also the points of maximum heating. If adequate power is available at the correct frequency, the process is characterized by a very dramatic rate of heating throughout its volume.

4.4 RESULTS AND DISCUSSION

4.4.1 Thermal Analysis and Molecular Weight Determination

The glass transition temperatures of these polymers are shown in Table 4.1. In Table 4.2, the 2nd, 3rd and 4th columns show the number average molecular weight, $\overline{M_n}$, the weight average molecular weight, $\overline{M_w}$, and the polydispersity, respectively, as determined by the universal calibration method. All of these polymers had a weight average molecular weight in the order of 10^5 g/mole. Column 5 shows the onset temperature for decomposition as measured by thermogravimetric analysis (TGA). Microwave heating of these polymers was carried out below the onset of the decomposition temperature.

Table 4.2 Molecular weights and the onset of decomposition temperatures of various thermoplastics

Polymer	$\overline{M_n} \times 10^{-5}$	$\overline{M_w} \times 10^{-5}$	Polydispersity	T_{decomp}(°C)*
PBMA	2.37	5.41	2.28	217
PVAc	1.72	7.26	4.21	311
PEMA	0.858	1.78	2.08	225
PVC	0.665	1.36	2.05	274
SAN	2.72	8.80	3.23	349
PMMA	1.39	3.21	2.30	263

* The onset of decomposition temperature from TGA in °C.

4.4.2 Microwave Experimental Results and Thermal Spectra from DETA

Figure 4.6 represents the variations of sample temperature with time for PVAc in the travelling wave applicator shown in Figure 4.3. The various starting temperatures were approximately 0, 15, 30 or 45 °C above T_g (30°C). After the temperature had equilibrated, 50 watts of input power was applied to the system. The temperature rise produced after 20 minutes of processing was minute even at 45°C above the T_g of PVAc. This was due to the fact that the dielectric loss factor, at these temperatures, was still low at the frequency of 2.45 GHz. Similar results are shown in Figure 4.7 for PBMA processed at 60°C above its T_g (20°C) and Figure 4.8 for PEMA processed at 30°C above its T_g (66°C). Under these conditions, all three polymers were still in the background dielectric loss region at 2.45 GHz. Hence, little dielectric coupling occurred. Figure 4.9 represents the variation of sample temperature vs. time for PVC processed at 50 watts in the travelling mode. The temperature rise at 20 minutes was significant when processed at 28°C above the T_g of PVC. This particular observation was important. Indeed, the "cool side" tail of the dielectric relaxation spectra of PVC must have shifted into the 2.45 GHz region at 116°C (28°C above T_g).

In section 4.2, it was mentioned that the dielectric relaxation spectra shifted to higher temperature with increasing frequency. One needs to know how far the ε'' spectra will shift at 2.45 GHz in order to find the critical temperature for dielectric loss factor, T_c, as well as the T_g at 2.45 GHz. T_c gives an approximate indication of the temperature at which the dielectric loss factor, ε'', increases significantly and rapid heating will occur. From equation [4-1], it is known that power absorption can be increased by increasing the electric field strength. Thus, the travelling wave applicator was replaced by the standing wave applicator, as shown in Figure 4.4, to increase the electric field strength. This change of applicators increased the amount of coupling

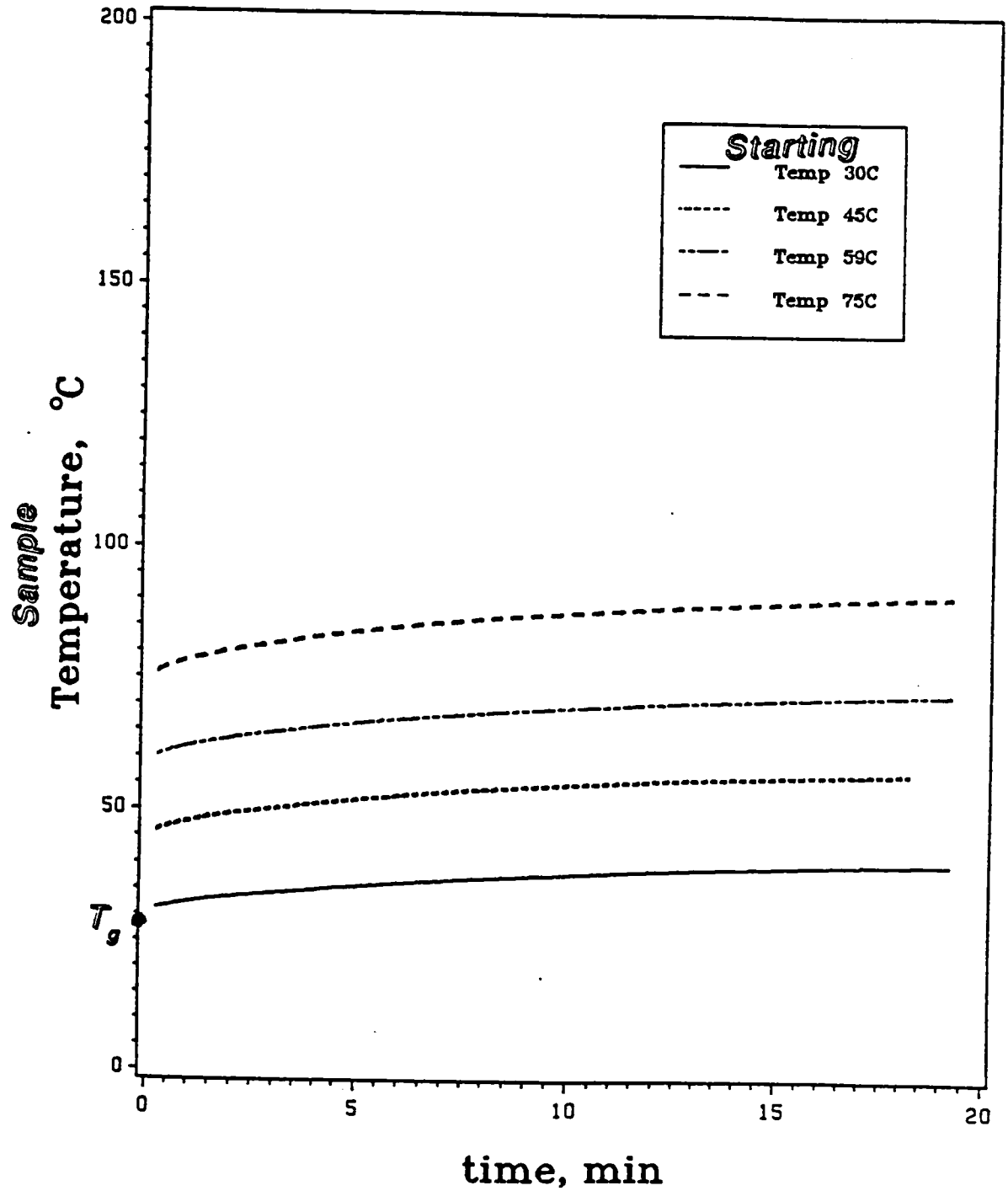

T_g of PVAc = 28°C

Figure 4.6 Variation of the temperature of poly(vinyl acetate) with time in the travelling wave applicator. Input power was 50 watts.

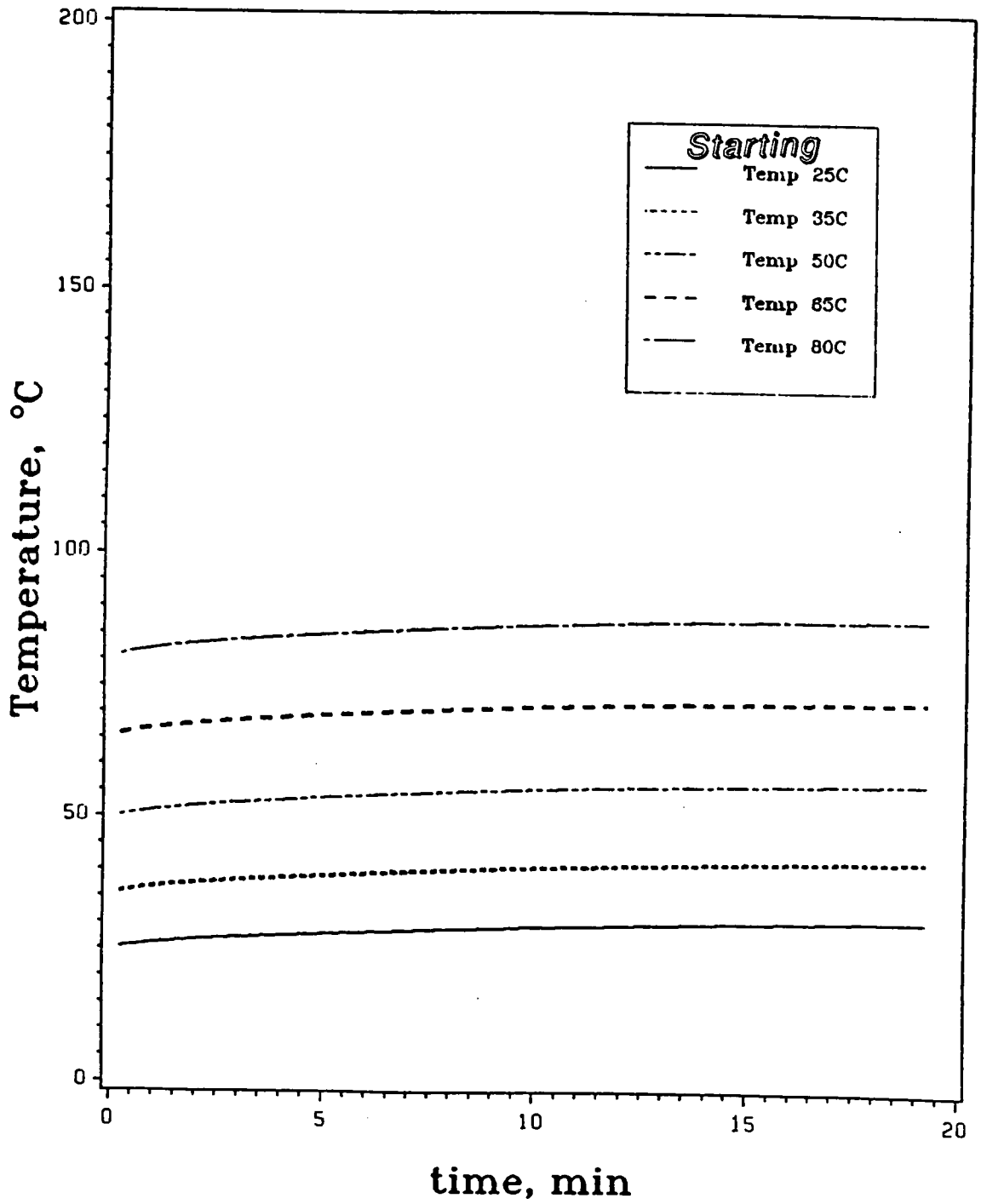

T_g of PBMA = 20°C

Figure 4.7 Variation of the temperature of poly(n-butyl methacrylate) with time in the travelling wave applicator. Input power was 50 watts.

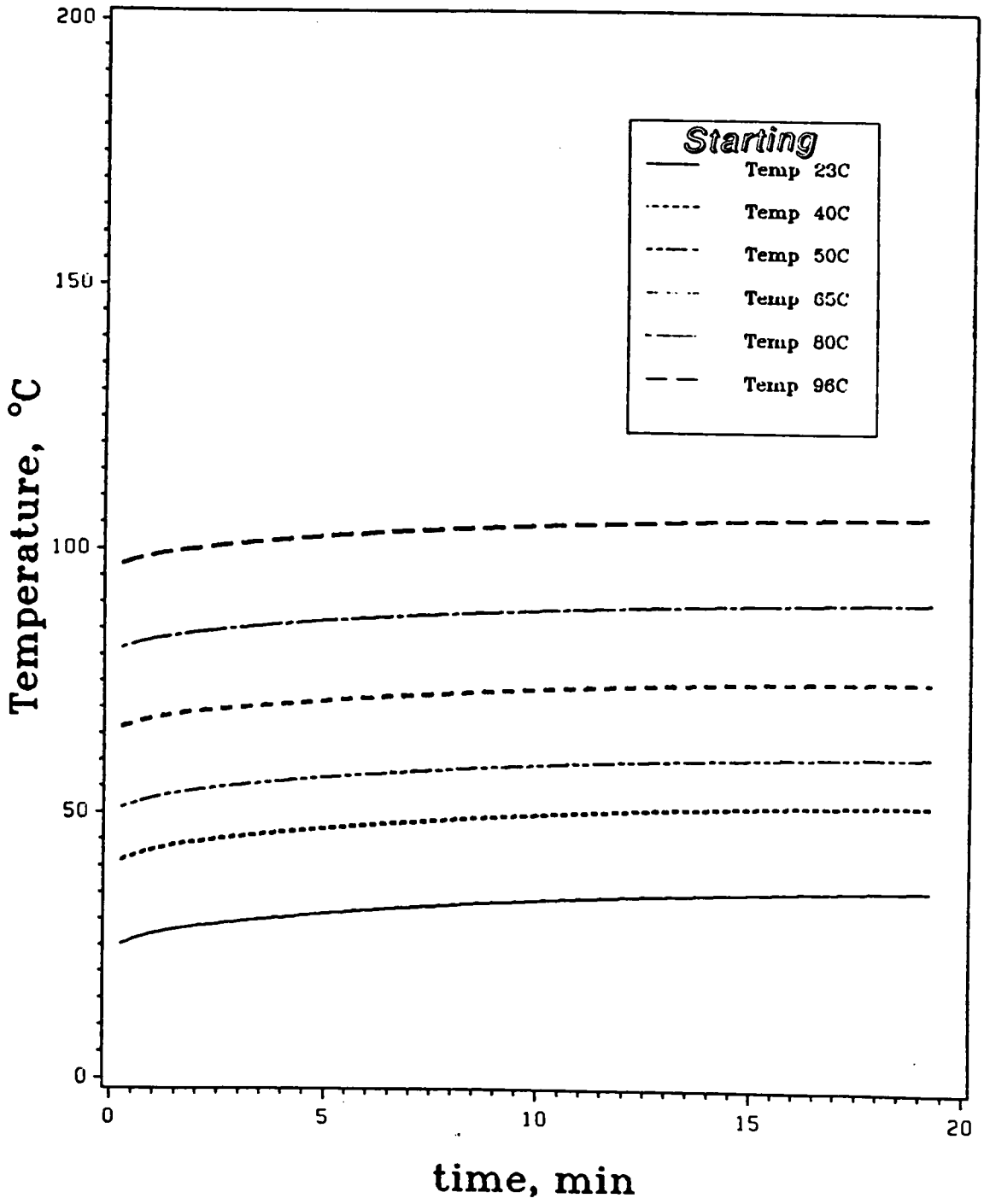

T_g of PEMA = 65°C

Figure 4.8 Variation of the temperature of poly(ethyl methacrylate) with time in the travelling wave applicator. Input power was 50 watts.

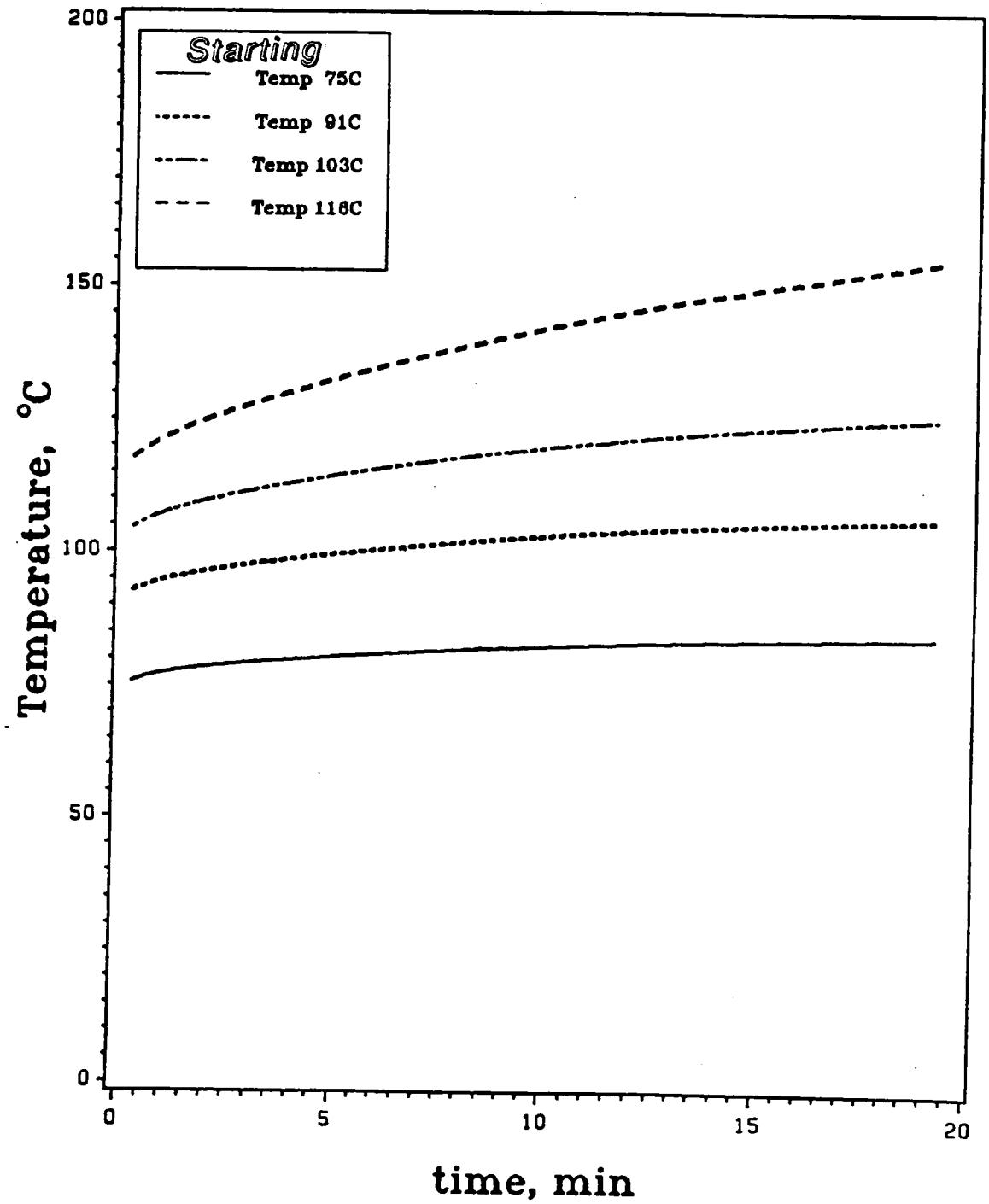

T_g of PVC = 87°C

Figure 4.9 Variation of the temperature of poly(vinyl chloride) with time in the travelling wave applicator. Input power was 50 watts.

between the microwave radiation and the sample. As shown in Figure 4.2, the sample was put at the location of maximum electric field in the TE_{10n} mode in the waveguide at ambient temperature. Figure 4.10 represents the variations of input power, reflected power and sample temperature as a function of time for PVAc in the standing wave applicator. Input power was kept constant at 16 watts. Reflected power was adjusted to zero at the onset of the experiment by using the stub tuner. The sample temperature rose rapidly for the first 10 minutes. From equation [4-2], assuming E, ρ, C_v are constant, the heating rate is proportional to the dielectric loss, ε'', given other qualifications. In Figure 4.11, the heating rate is plotted versus temperature to produce a thermal scan of PVAc at a frequency of 2.45 GHz. This procedure is called microwave calorimetry. As a result, the T_c and T_g of PVAc at 2.45 GHz was qualitatively determined to be 65°C and 150°C, respectively, from Figure 4.11. The thermal conductivity effect was not considered in this short time experiment. For the case of PVAc, shown in Figure 4.12, the temperature was seen to rise significantly at the starting temperature of 92°C (27°C higher than T_c) in the travelling wave applicator indicating that the "cool side" tail of the dielectric loss spectra of PVAc was in the 2.45 GHz region.

Similar results for PMMA in the standing wave applicator are shown in the Figures 4.13 and 4.14. The input power was kept at 21 watts. The rise of temperature was slow in the first 32 minutes; after which time the temperature rose rapidly, as shown in Figure 4.13. In Figure 4.14, there is an induction period below 150°C in the plot of heating rate vs. temperature. The T_c of PMMA is about 185°C which is 80°C above its T_g (measured by DSC). The shape of the dielectric behavior at 2.45 GHz for PMMA is different from that for PVAc. One needs to examine the lower frequency loss responses to explain these differences. Figure 4.15 depicts the dielectric spectra of PMMA obtained by

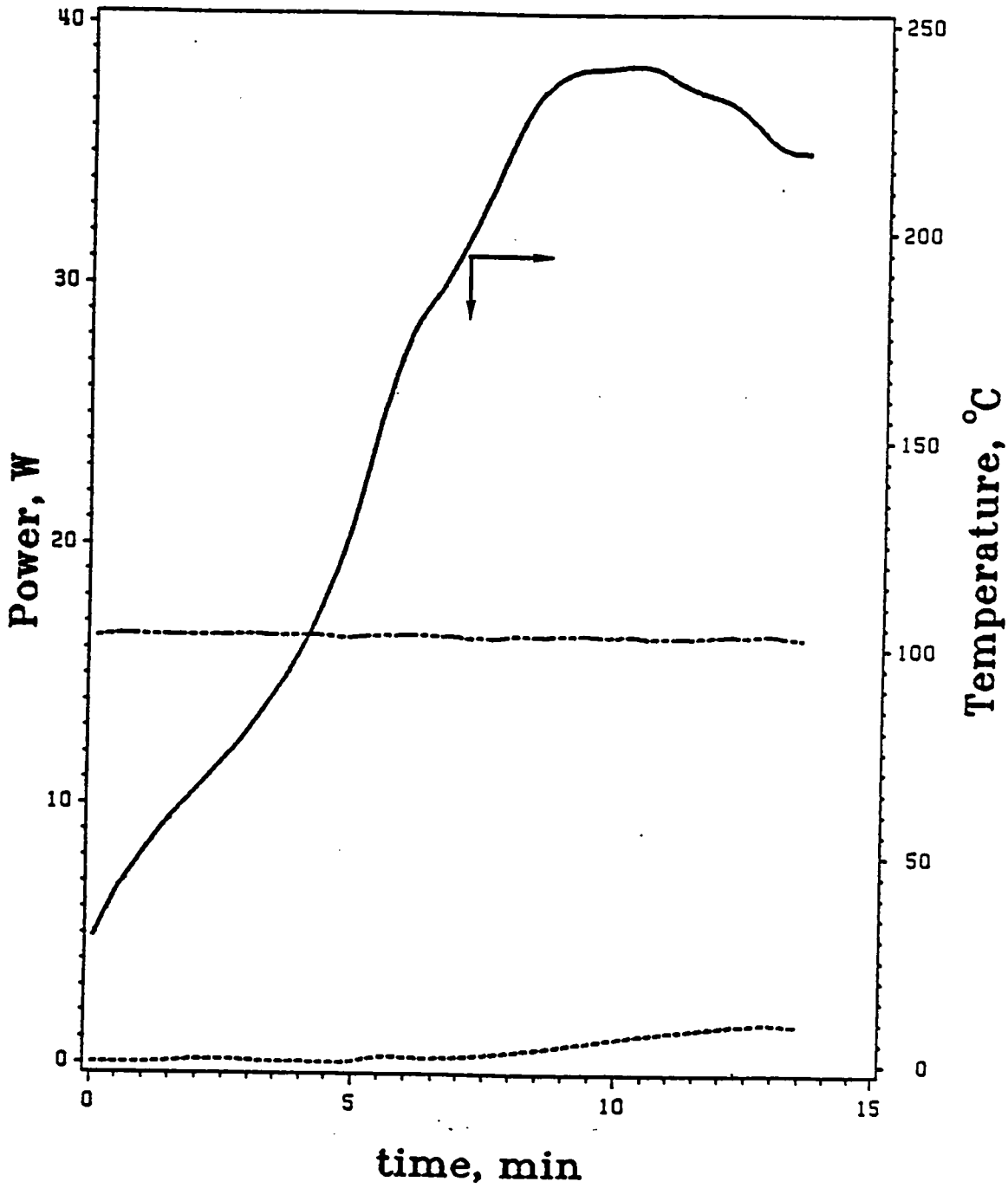

TOP :INPUT POWER
BOTTOM :REFLECTED POWER
SOLID LINE :TEMPERATURE

Figure 4.10 Variation of the temperature, input power and reflected power with time for poly(vinyl acetate) in the standing wave applicator with a stub tuner.

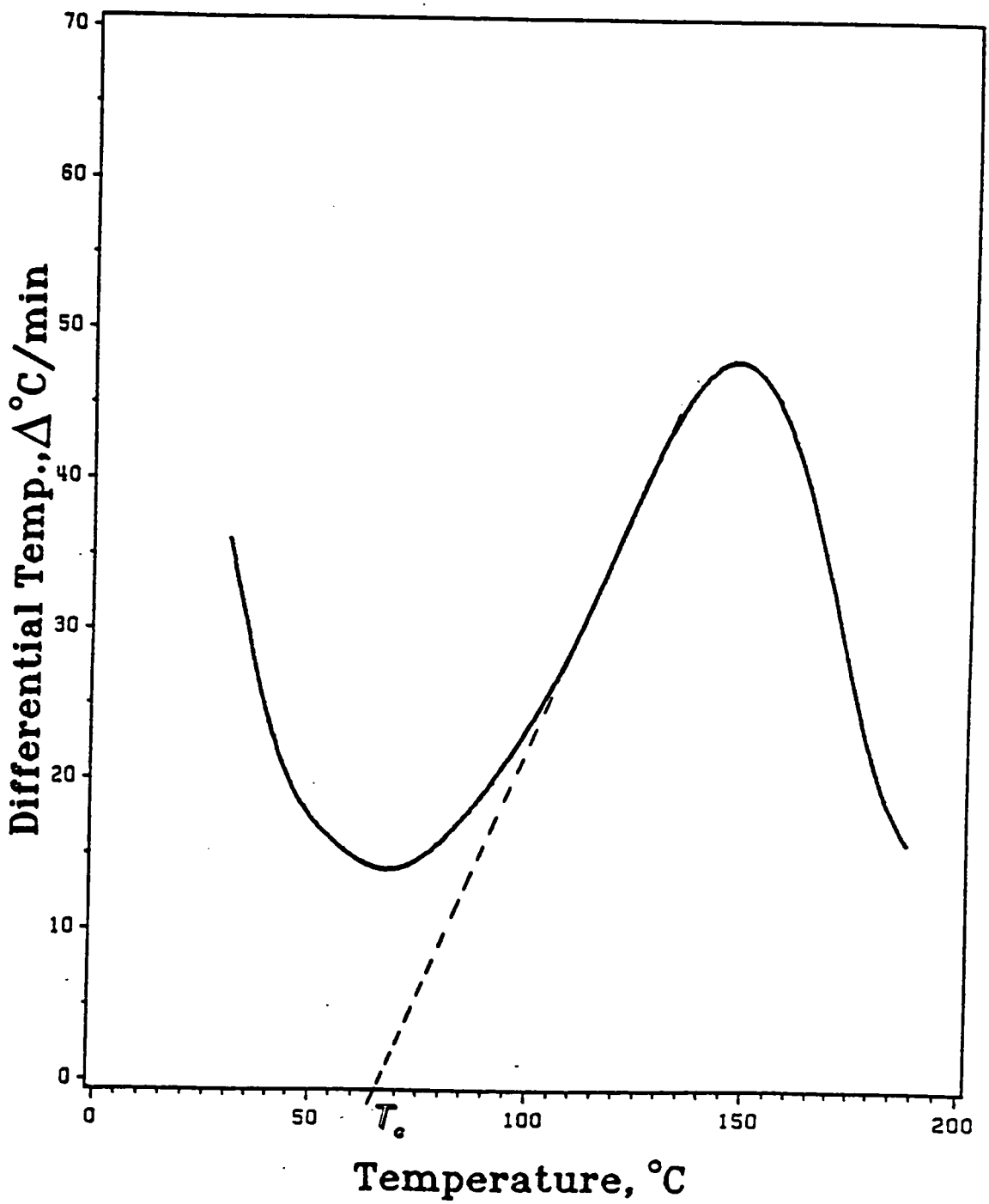

Figure 4.11 Heating rate of poly(vinyl acetate) versus temperature in the standing wave applicator with a stub tuner.

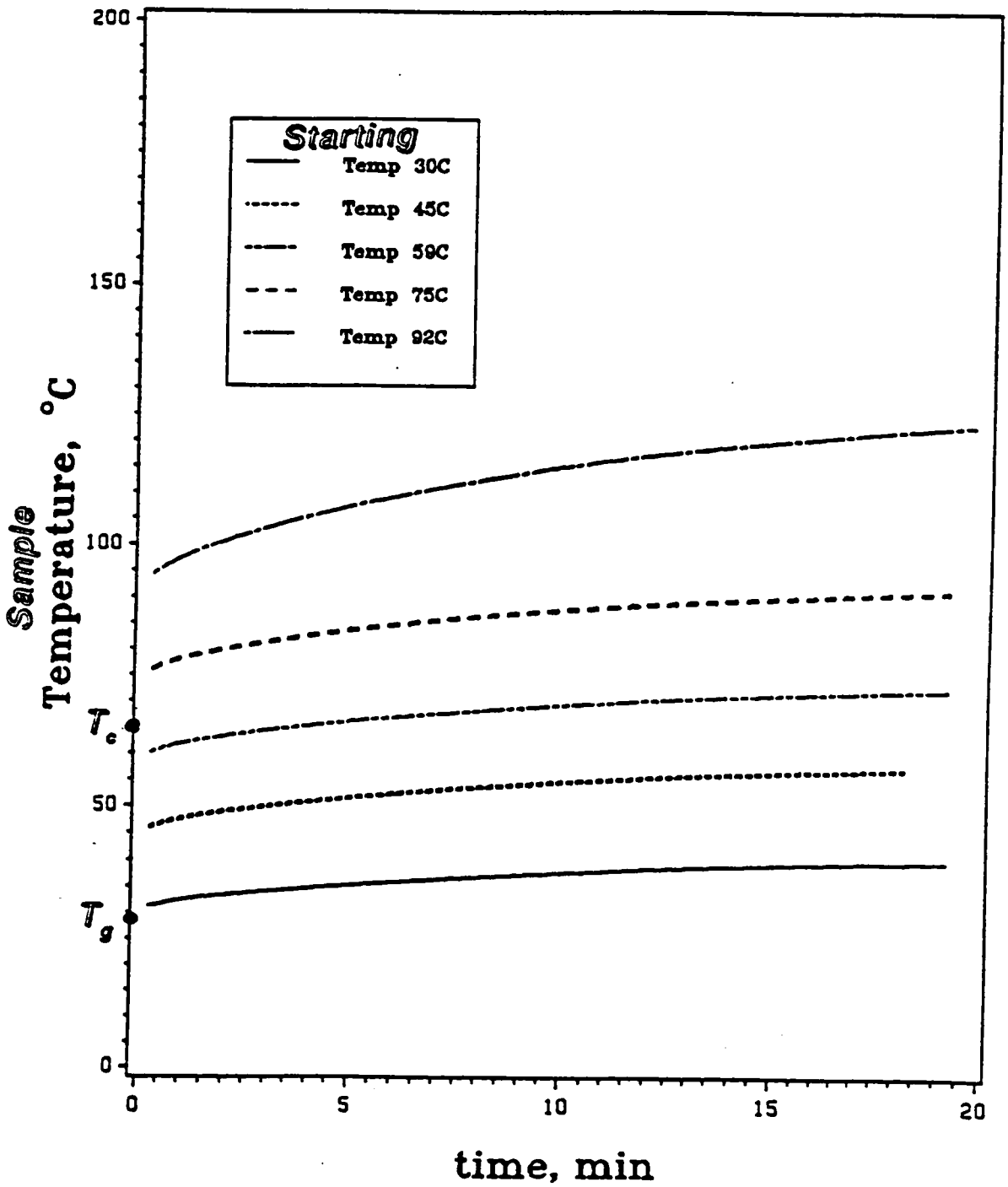

T_g of PVAc = 28°C

Figure 4.12 Variation of the temperature of poly(vinyl acetate) with time in the travelling wave applicator. Input power was 50 watts.

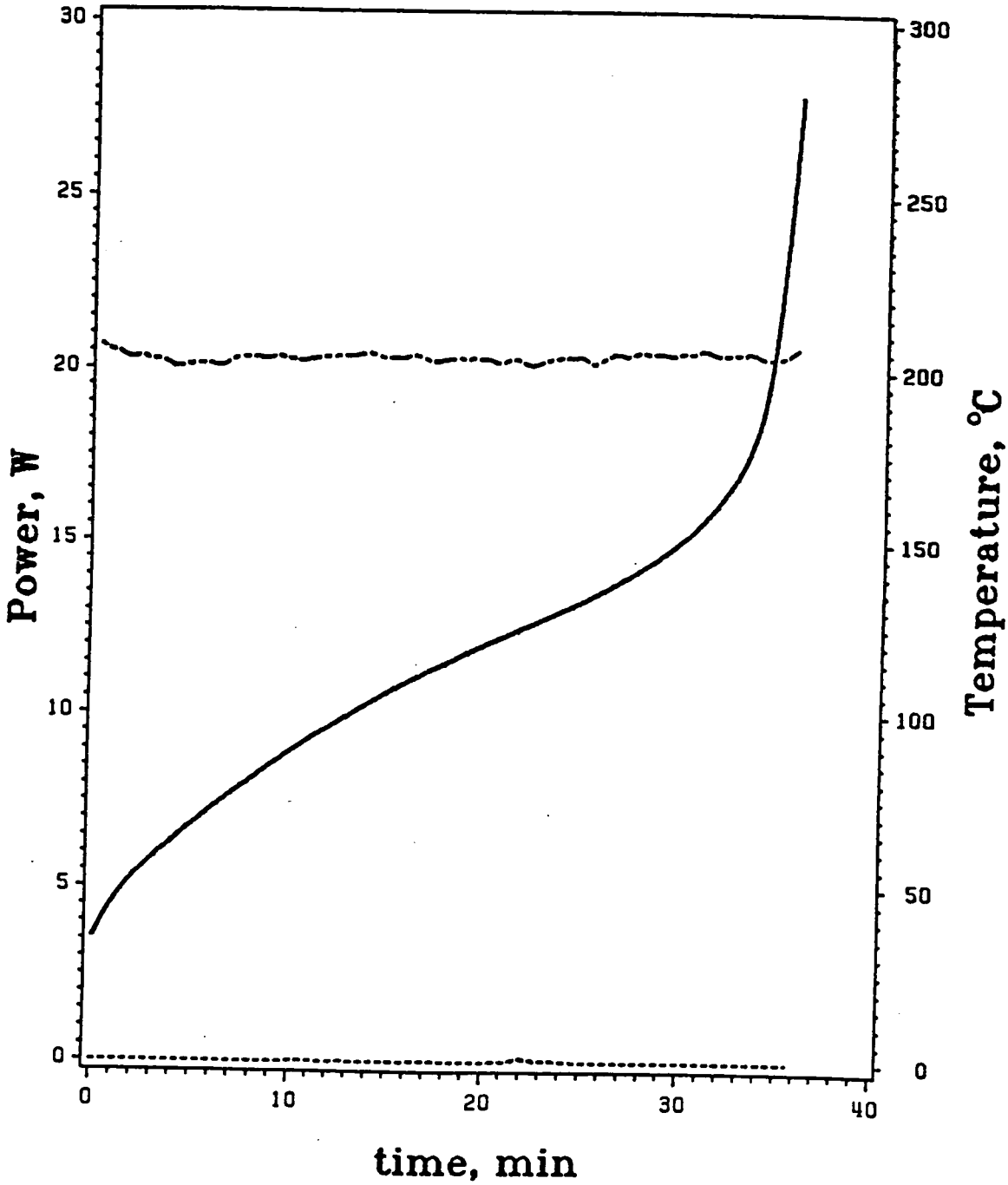

TOP :INPUT POWER
BOTTOM :REFLECTED POWER
SOLID LINE :TEMPERATURE

Figure 4.13 Variation of the temperature, input power and reflected power with time for poly(methyl methacrylate) in the standing wave applicator with a stub tuner.

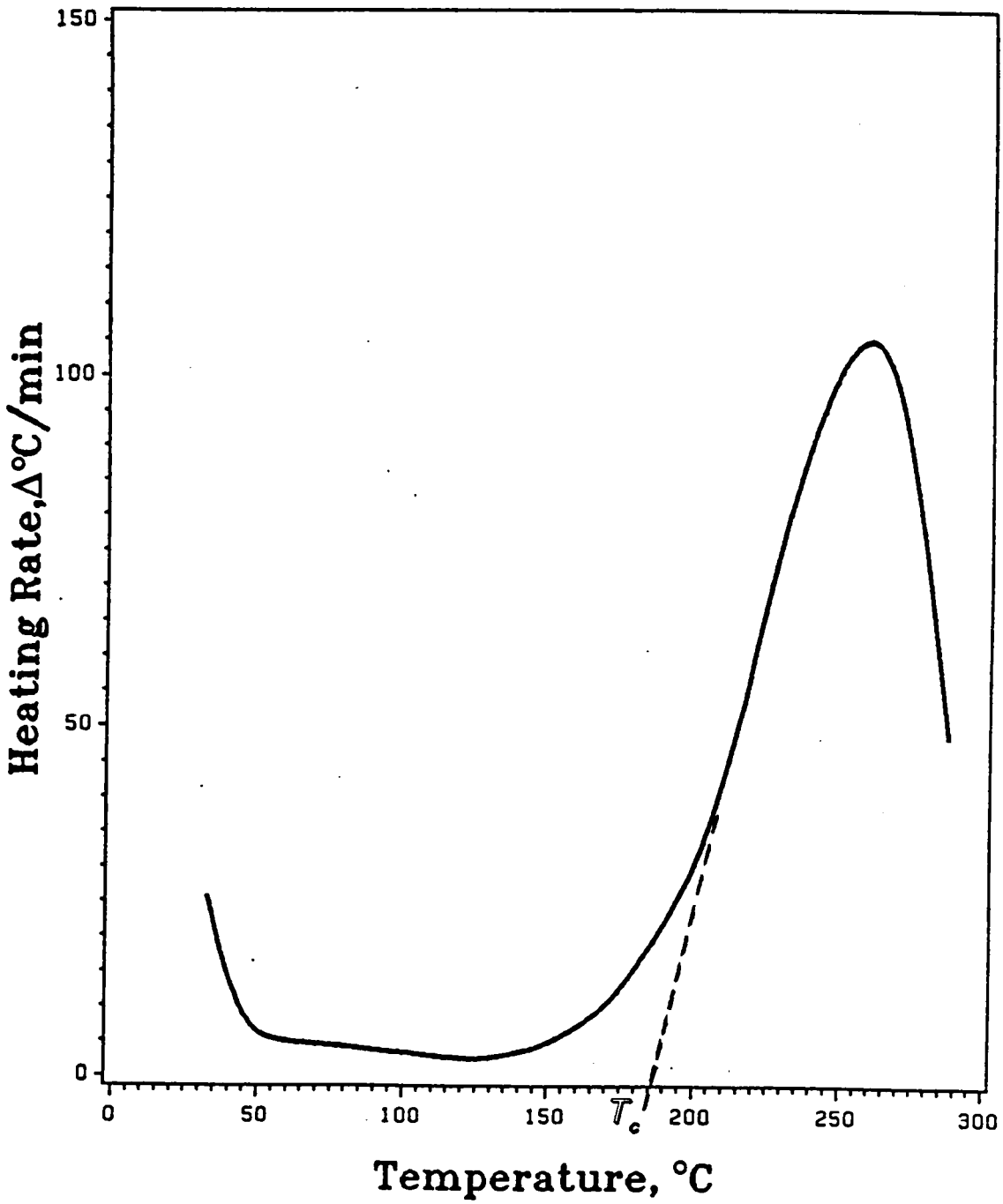

Figure 4.14 Heating rate of poly(methyl methacrylate) versus temperature in the standing wave applicator with a stub tuner.

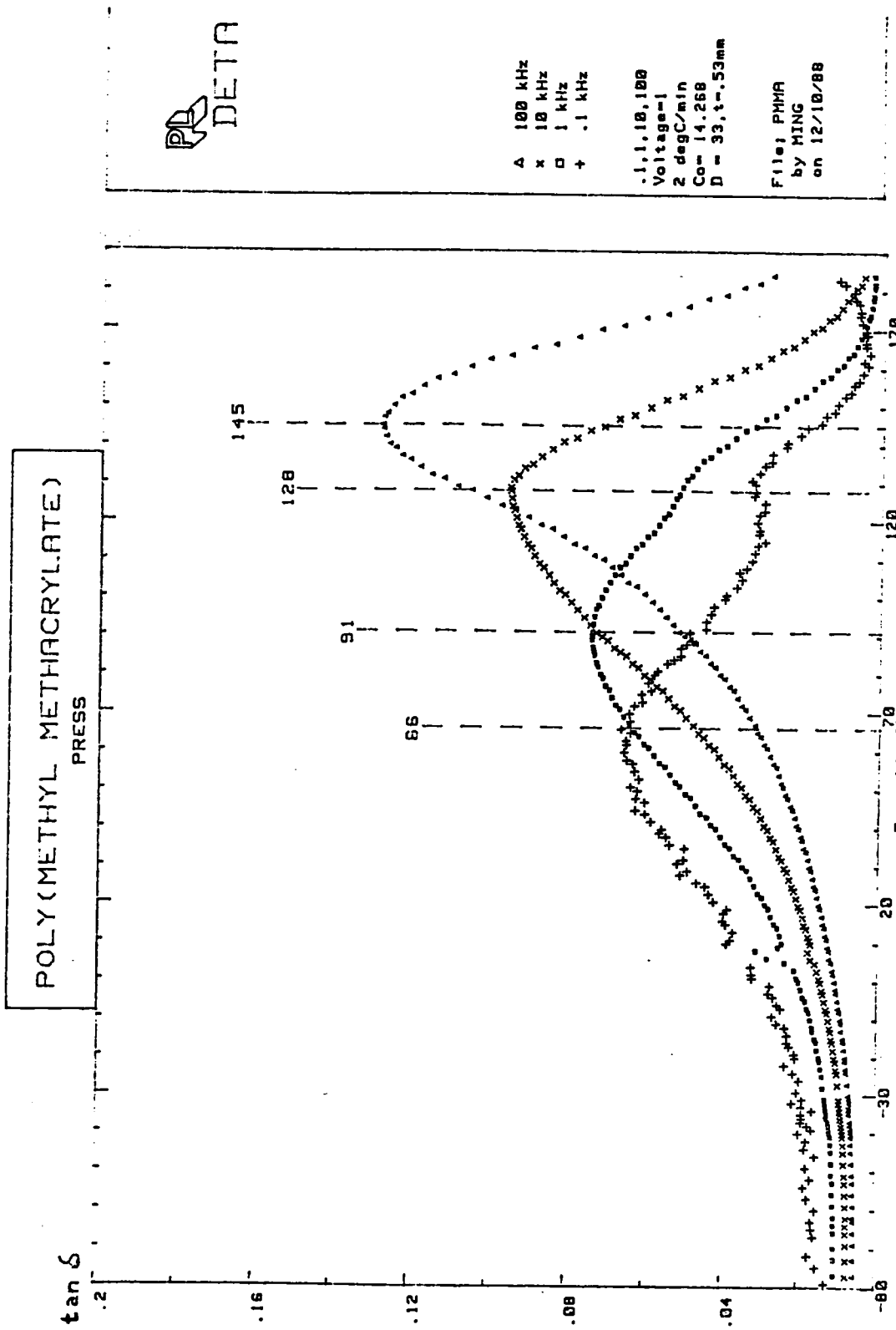

Figure 4.15 Temperature dependence of the loss tangent of poly(methyl methacrylate) at various frequencies.

DETA covering the temperature range from -80°C to 190°C at 0.1, 1, 10 & 100 kHz. The shape of the spectrum at 100 kHz was similar to that at 2.45 GHz for PMMA. However, moving from 100 kHz to 0.1 kHz, the dielectric spectra gradually separated into two peaks. The peak at the higher temperature was associated with the motion of the main chain-α relaxation. The peak at lower temperature was due to the relaxation of the strong electric dipole in the ester ($-COOCH_3$) side group, β relaxation. This is a quite polar group and the dispersion is strong. The β peak shifted more rapidly than the α peak as temperature was increased. The merging of the α and β relaxations in PMMA at a frequency of about 10 kHz can be clearly seen. In contrast, Figure 4.16 shows the dielectric spectra of PVAc obtained by the DETA. In PVAc, the side group is linked to the main chain by polar C-O bonds. The polar C-O bonds were expected to move along the main chain to produce a more intense dielectric glass transition than for the case of PMMA where this link is an apolar C-C bond. A closer inspection of Figures 4.15 and 4.16 reveals how different the dielectric behavior are. This difference can be clearly seen at 2.45 GHz for PMMA and PVAc, as shown in Figures 4.14 and 4.11, since PMMA possess a large β dielectric loss relaxation.

To describe the temperature sensitivity of the relaxation process, Arrhenius plots were made from DETA data. The calculation of the apparent activation energy, ΔE_a, was performed in the following way: the maximum temperature for several frequencies was determined from the plot of $\tan\delta$ vs. temperature, as shown in Figure 4.16. A graph of the applied log(frequency) versus the inverse absolute temperature maximum was made. Placement of a straight line through the data over a narrow temperature range, as shown in Figure 4.17, yielded a slope proportional to the activation energy, ΔE_a:

$$\Delta E_a = -2.303R \times \text{slope} \qquad [4\text{-}3]$$

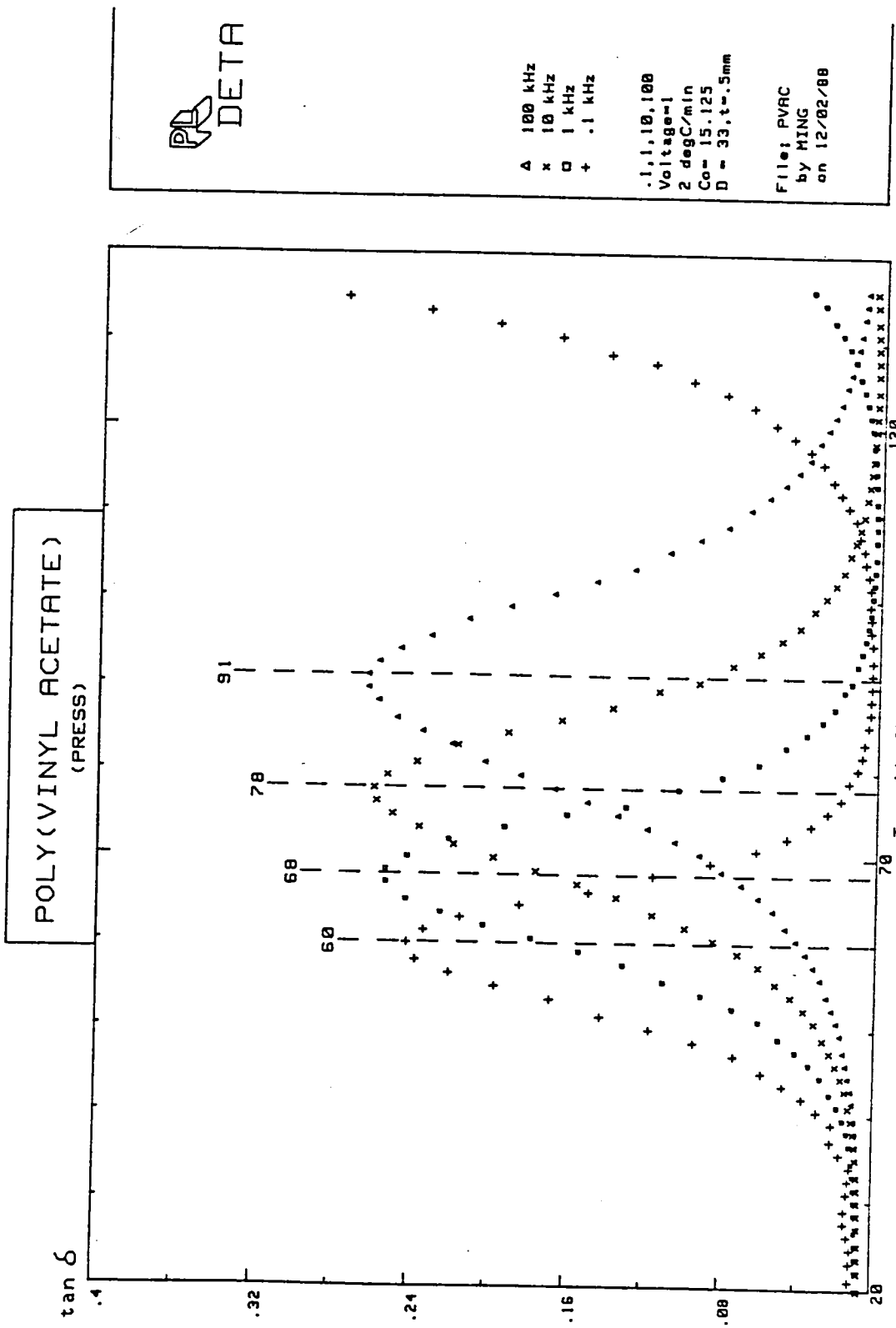

Figure 4.16 Temperature dependence of the loss tangent of poly(vinyl acetate) at various frequencies.

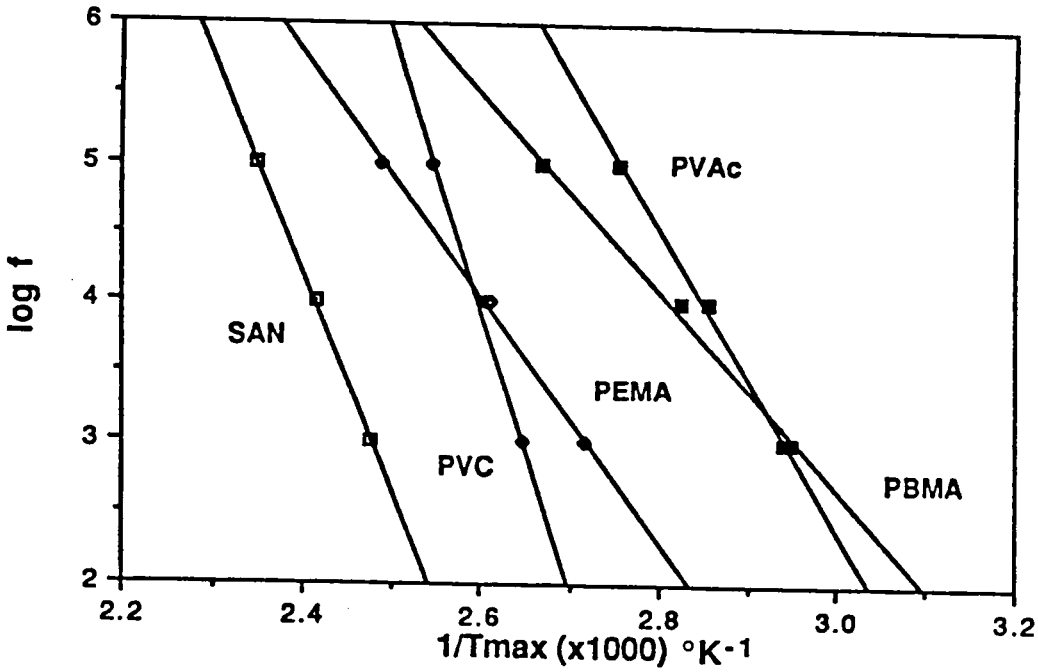

Comparison of the slopes: PVC>SAN>PVAc>PEMA>PBMA

ΔE_a = -2.303R x slope

Figure 4.17 The linear dependence of log(frequency) on the inverse absolute temperature over the kHz region for thermoplastics.

This value, referred to as the "apparent " activation energy is summarized in the third column of Table 4.3.

The smaller the value of ΔE_a, the slower the shift of the relaxation with frequency, and the closer the temperature distance between T_c and T_g. For PVAc, the ΔE_a was 210 kJ/mole and the T_c was 35°C above its T_g. For PMMA, the ΔE_a was 100 kJ/mole and the T_c was 80°C above its T_g. PVC, having the highest ΔE_a of 380 kJ/mole was easily heated at 28°C above its T_g. PBMA, having a ΔE_a of 130 kJ/mole was still in the background dielectric loss region at 2.45 GHz even at 60°C above its T_g. The low activation energy for PEMA and PBMA was attributed to the merging of the α and β relaxations as shown in Figures 4.18 and 4.19.

T_c is very important for microwave processing of polymers. Above T_c, a positive slope, $(+d\varepsilon''/dT)$, of the ε'' vs. temperature plot results. This is the region of rapid volumetric heating. In the extreme case, $d\varepsilon''/dT$ can be so large that the sample can even be charred. This phenomenon is termed the "runaway effect". After the material absorbs microwave energy, the temperature rise causes the ε'' to increase which, in turn, results in a further increase of temperature, and so on. Either decreasing the microwave energy or removing the sample is necessary to avoid damage to the sample. Knowledge of the dependence of dielectric behavior on temperature at 2.45 GHz is important in the design of a microwave heating system to take advantage of the rapid heating in the positive side of $d\varepsilon''/dT$ and to avoid the risk of the thermal runaway effect.

The Williams-Landel-Ferry (WLF) relationships covering a wide frequency range were investigated. The temperature at the maximum heating rate was chosen as the glass transition temperature at 2.45 GHz. The glass transition temperatures at 10 kHz and 100 kHz were obtained from DETA spectra, shown in Figure 4.15. Finally the glass

Table 4.3 T_g's and the apparent activation energies in the kHz region for several thermoplastics

Polymer	Tg, °C	ΔE_a, *kJ/mole	Relaxation Phenomena
PMMA	105	100	α & β partially merge
PBMA	20	130	α & β merge
PEMA	66	170	α & β merge
PVAc	30	210	
SAN	101	300	
PVC	85	380	

* Activation energy, ΔE_a, calculated from the peak temperatures of DETA spectra at 1, 10 & 100 kHz

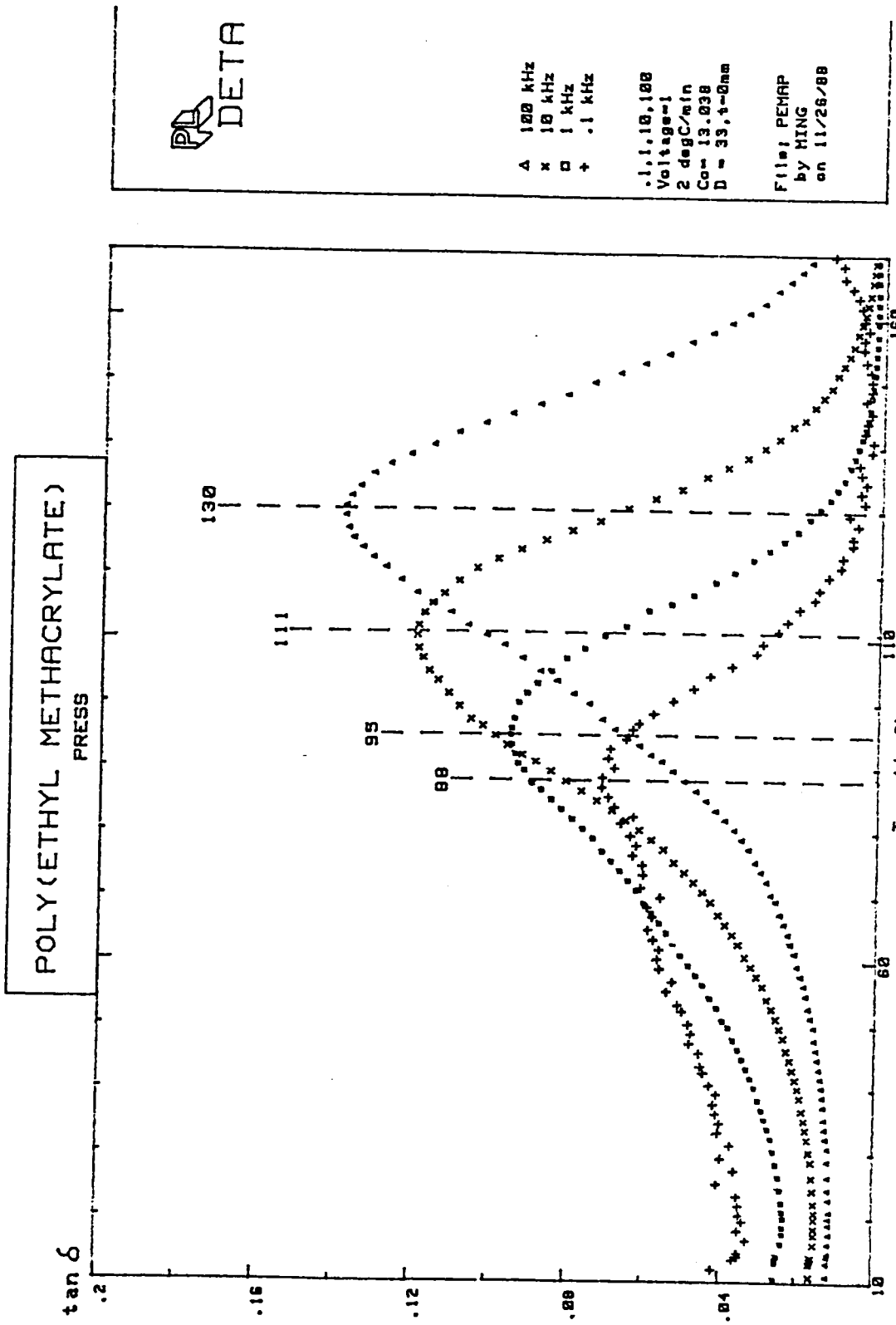

Figure 4.18 Temperature dependence of the loss tangent of poly(ethyl methacrylate) at various frequencies.

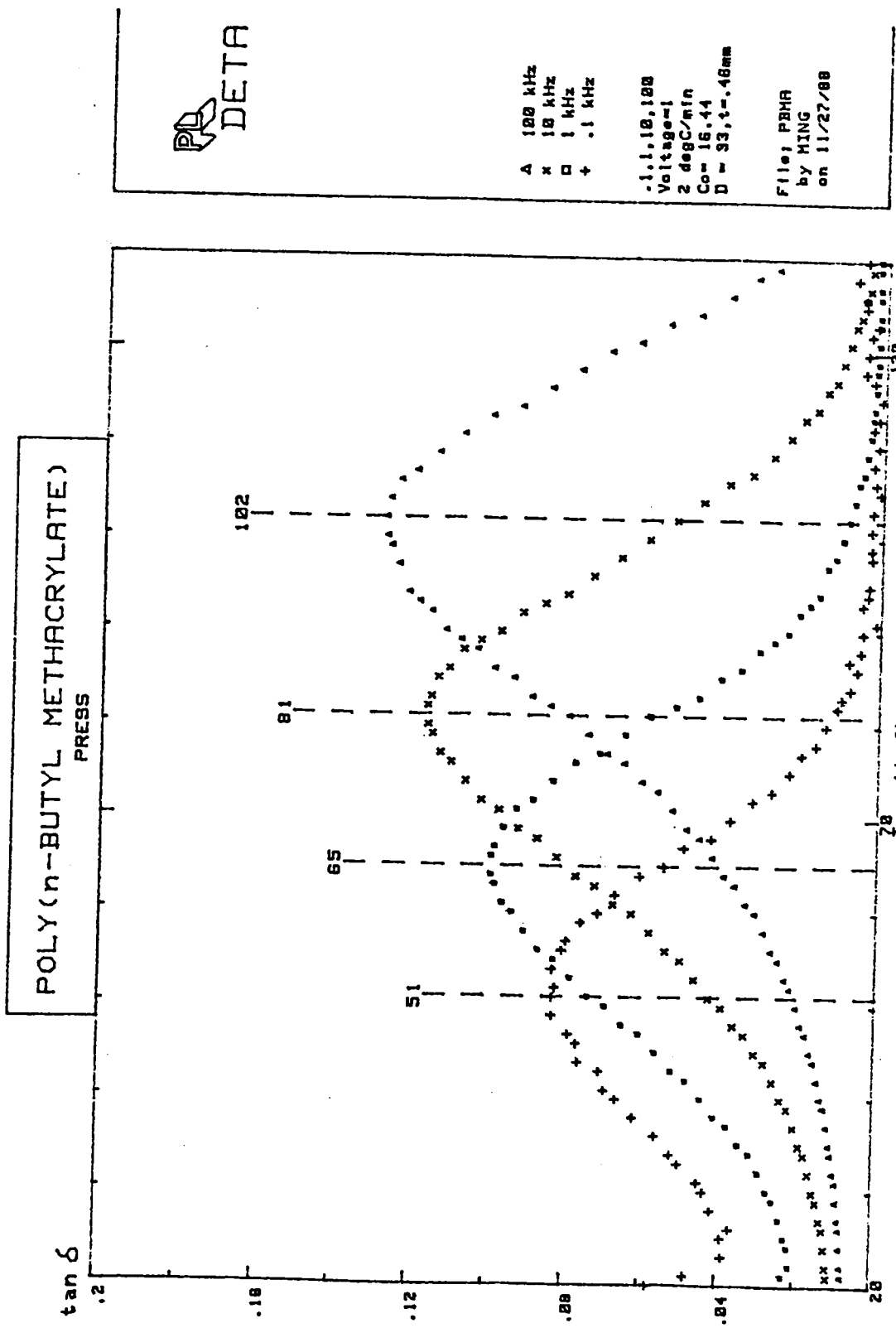

Figure 4.19 Temperature dependence of the loss tangent of poly(n-butyl methacrylate) at various frequencies.

transition temperatures at 0.3, 1, 3, 10 and 30 Hz from the maximum loss moduli E" were obtained from the DMTA spectra. A graph of the dependence of the logarithm of the frequency against the reciprocal of absolute temperature for PMMA is shown in Figure 4.20. The three points at high temperature obeyed Arrhenius behavior with a constant activation energy. The merging of the α and β relaxation at 10 kHz was clearly observed in both Figure 4.15 and 4.20, which produced the kink in the WLF curve at approximate 130°C.

The results for SAN in the standing wave applicator are shown in Figures 4.21 and 4.22. The input power was kept at 32 watts, the temperature rise was slow in the first 6.5 minutes, after which time, the temperature rose rapidly, as shown in Figure 4.21. In Figure 4.22, T_c of SAN was found to be about 145°C which is 40°C above its T_g. Figure 4.23 depicts the dielectric spectra of SAN via DETA covering the temperature range from 40°C to 190°C at 0.1, 1, 10 & 100 kHz. For SAN, ΔE_a was 300 kJ/mole as shown in Table 4.3. The graph of the dependence of the logarithm of the frequency against the reciprocal of absolute temperature for SAN is shown in Figure 4.24. The plot exhibits the curvature which is typical for glass-rubber relaxations of amorphous polymers and is consistent with the WLF relationship. By examining the log(frequency) vs. $1/T_g$ plot, one can find either that (1) the dielectric loss at the microwave region was low, or that (2) the frequency location plots did not extrapolate dielectric loss dispersions to the 2.45 GHz frequency at room temperature for glassy thermoplastics.

A general phenomenon in all these experiments was an initial decrease in heating rate vs. temperature curves. One possible reason for this was related to changes in basic dielectric properties causing an impedance change as temperature increased. This mismatch may have caused more energy to be dissipated in the source rather than in the load. The second possible reason was that the position of the maximum electric

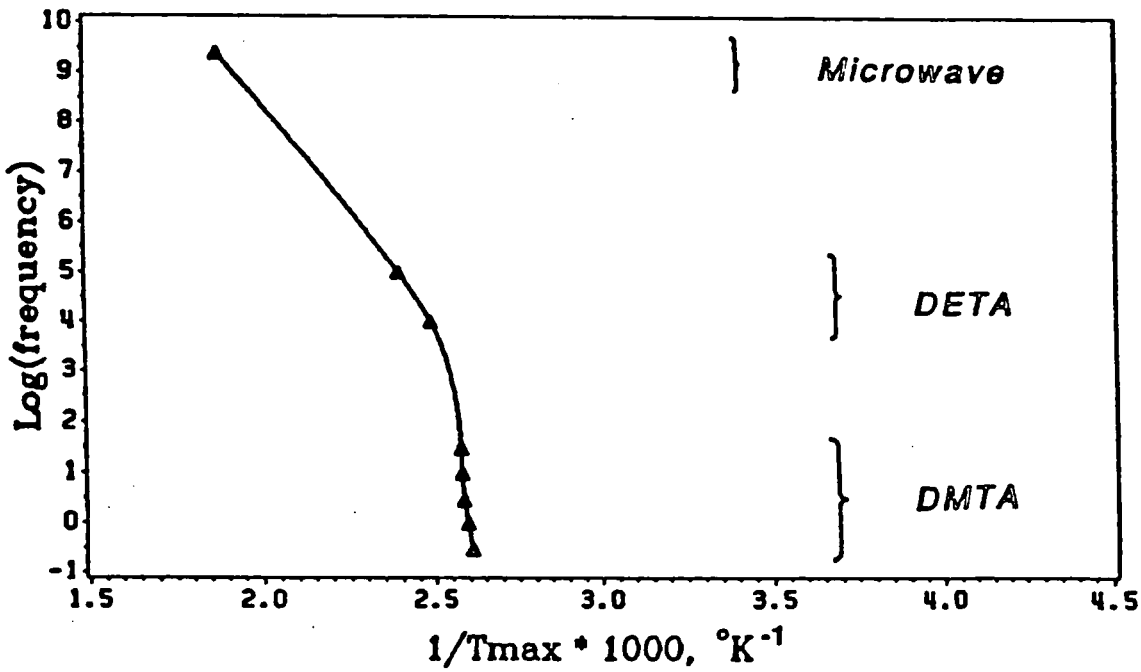

Figure 4.20 WLF relationship for poly(methyl methacrylate).

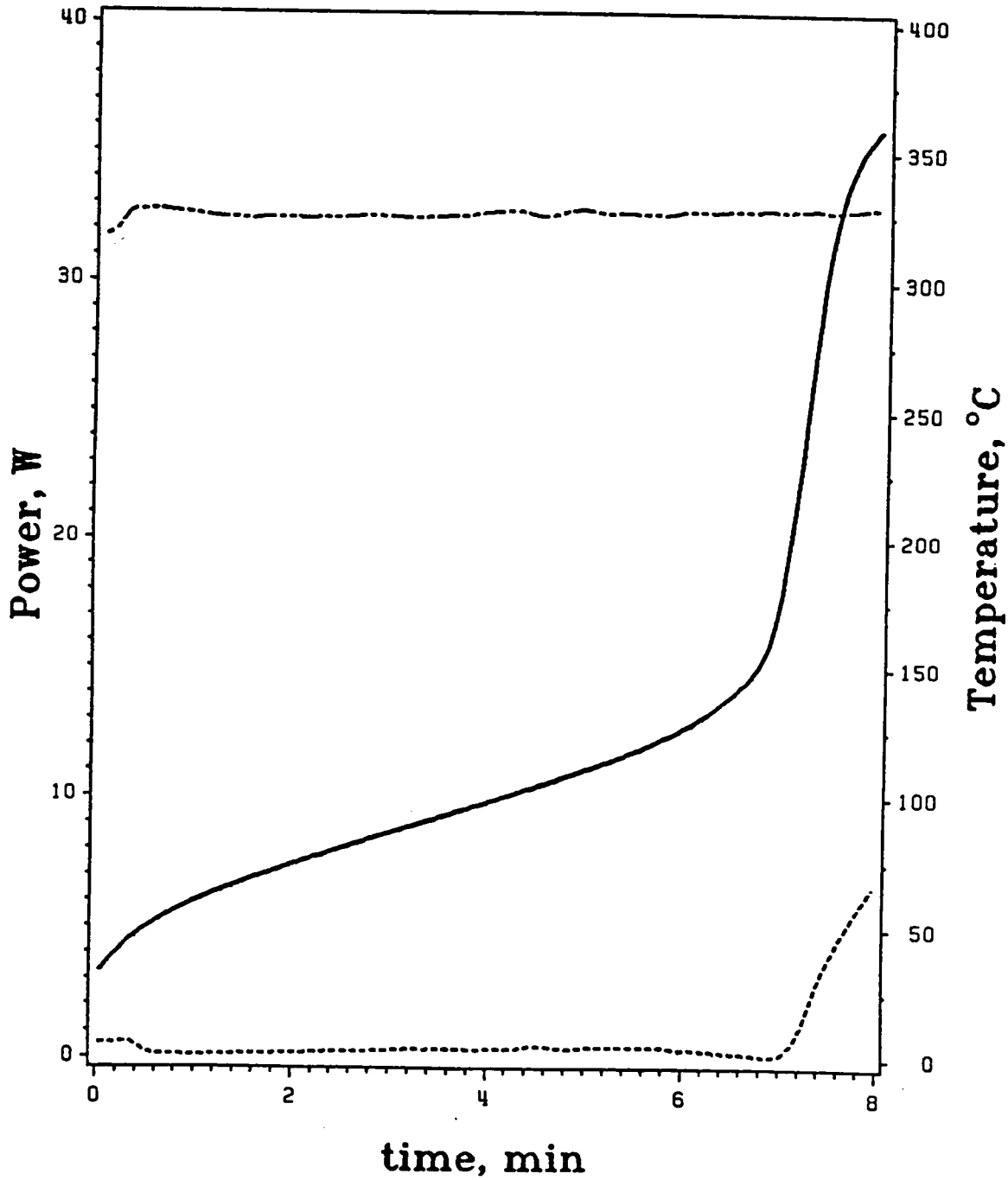

TOP :INPUT POWER
BOTTOM :REFLECTED POWER
SOLID LINE :TEMPERATURE

Figure 4.21 Variation of the temperature, input power and reflected power with time for styrene acrylonitrile copolymer in the standing wave applicator with a stub tuner.

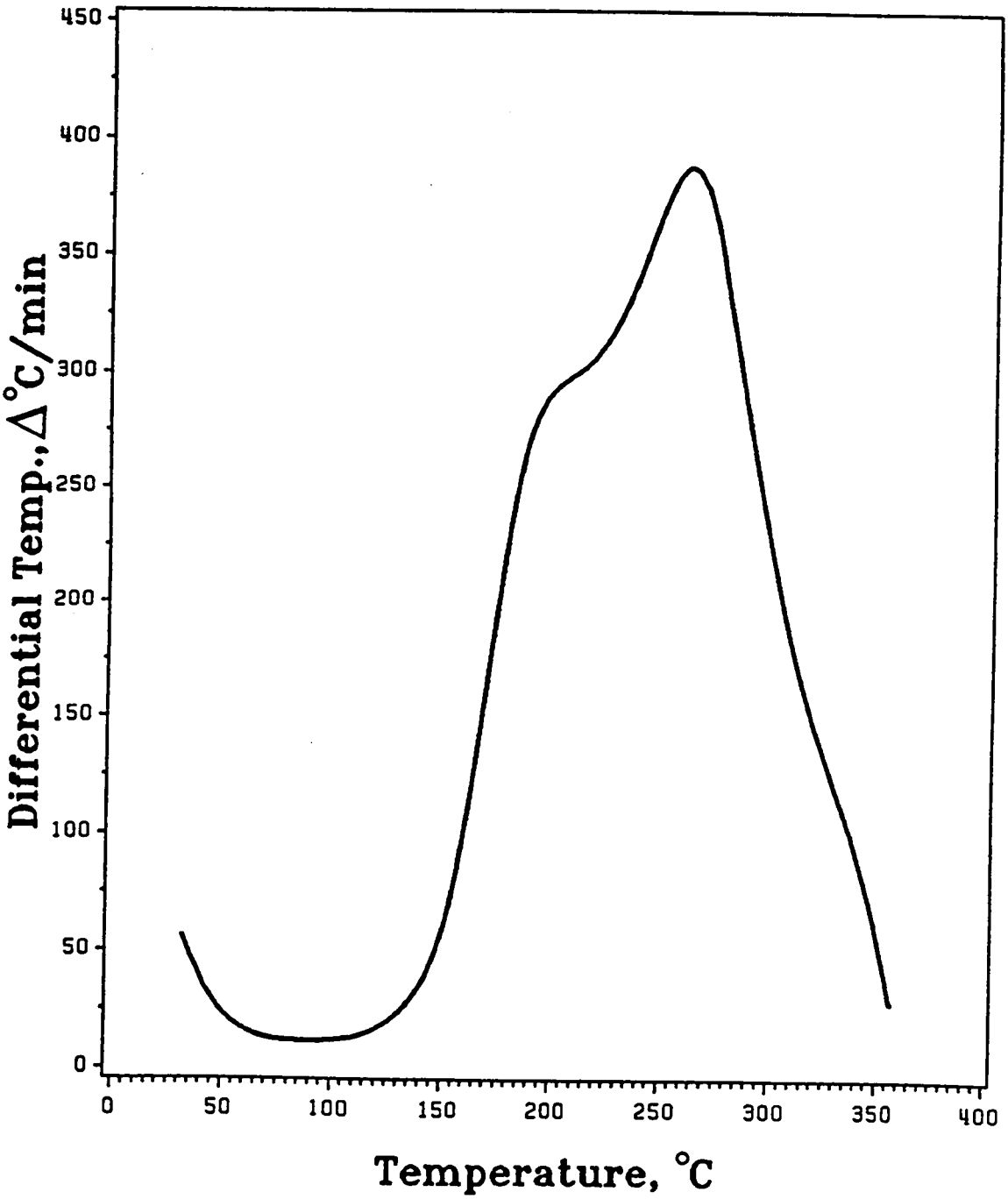

Figure 4.22 Heating rate of styrene acrylonitrile copolymer versus temperature in the standing wave applicator with a stub tuner.

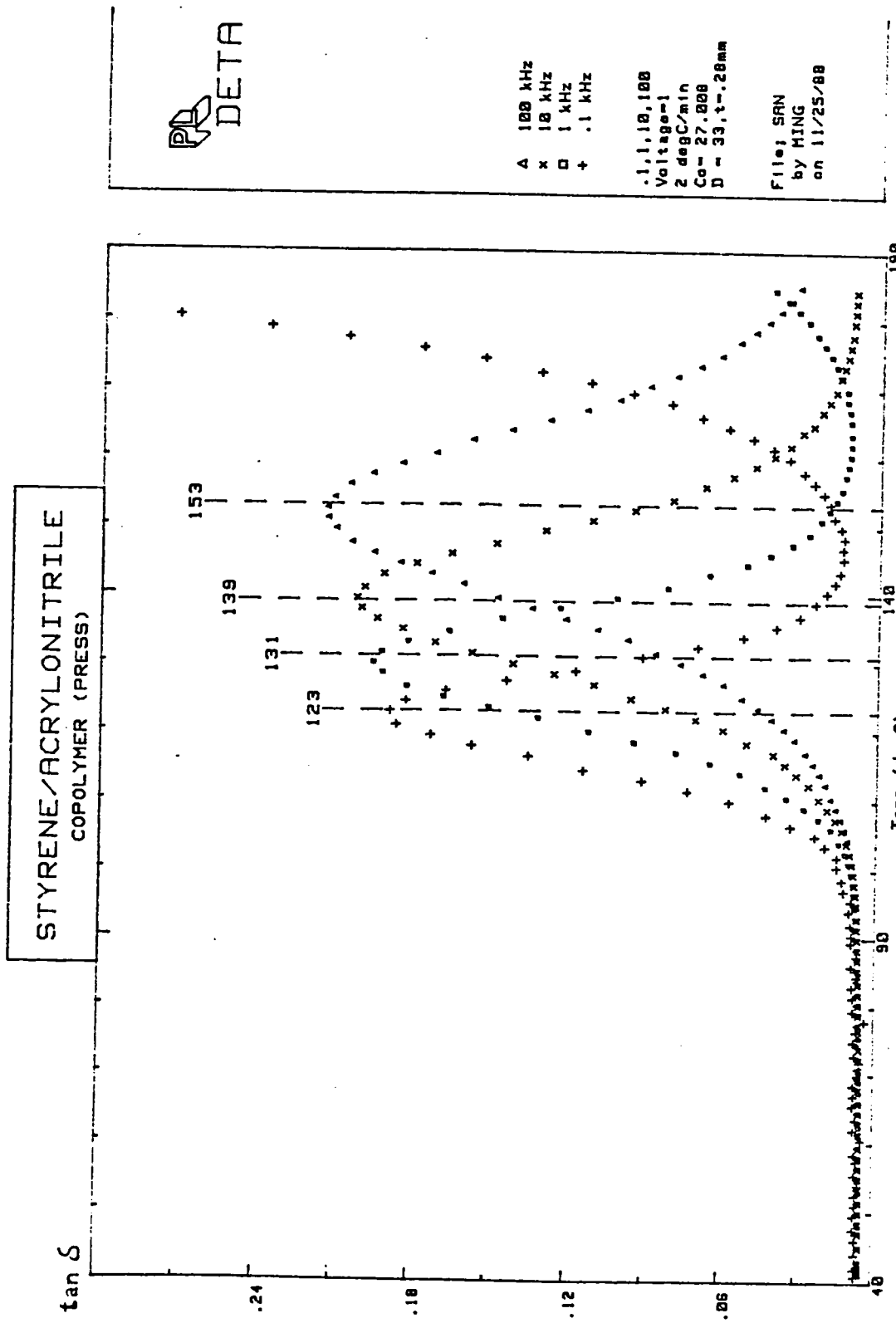

Figure 4.23 Temperature dependence of the loss tangent of styrene acrylonitrile copolymer at various frequencies.

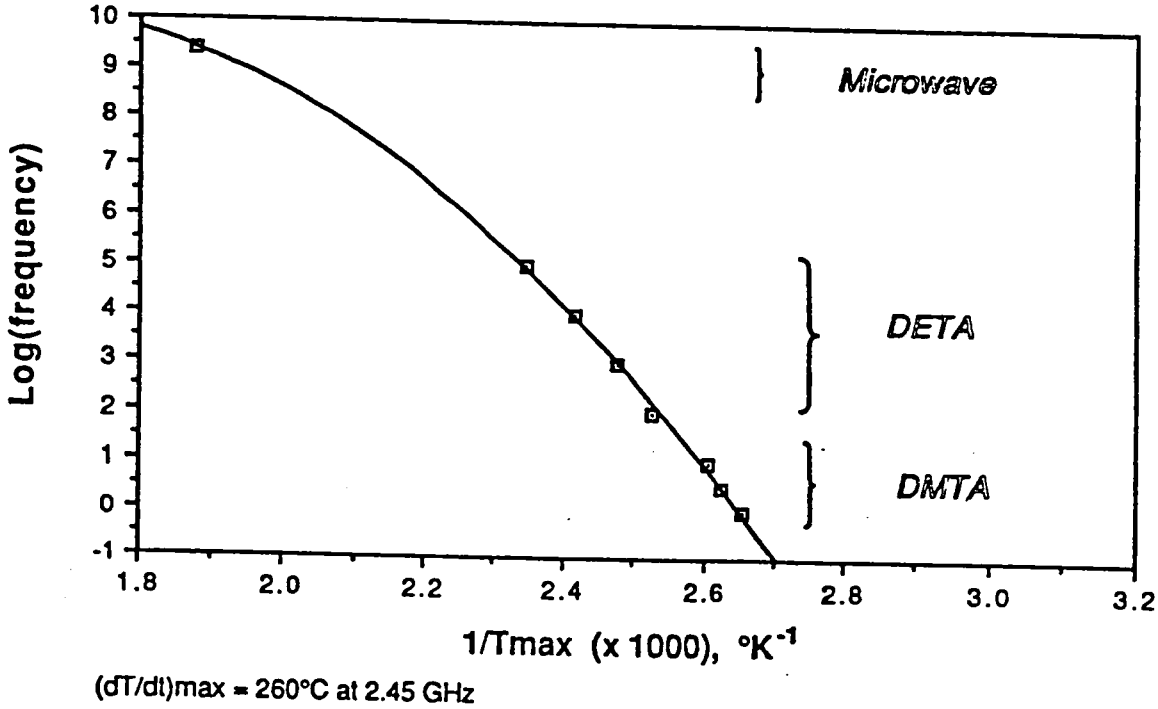

Figure 4.24 WLF relationship for styrene acrylonitrile copolymer.

field was shifted toward the microwave source in the first few minutes. In any case, the initial decrease in heating rate was an artifact of the experiment, not a secondary transition.

4.5 CONCLUSION

Microwave processing of glassy polymers requires detailed knowledge of how temperature affects the location of the dielectric loss peak in the frequency/temperature domain. As a result, several key terms were defined. The critical temperatures, T_c, were obtained from the intercept of the 'cool side' tangent curve of the heating rate versus temperature plots at 2.45 GHz. Microwave processing was rapid above the critical temperature because the dielectric loss spectra had entered the 2.45 GHz domain for efficient coupling of energy to the polymer. The glass transition temperatures at 2.45 GHz were obtained from heating rate, (dT/dt) or (dε"/dt), versus temperature curves. Arrhenius plots of log(frequency) versus the inverse absolute temperature maximum were made from DETA spectra; these experiments showed how sensitive the dielectric loss spectra were to changes in temperature. Finally, WLF plots over a broad range of applied frequencies were made for PMMA and SAN to show the phenomena of merging α and β relaxation of PMMA at 10 kHz.

Outside the region of dispersion, the dependence of dielectric loss factor on temperature for polar molecules was like that for nonpolar molecules (i.e. dε"/dT is small). Within a dispersion region however, dε"/dT was large and positive in that temperature range on the 'cool side' of a dispersion. This was the region of rapid heating. In other words, the dielectric loss factor depended on the relaxation times as

well as the dipole moment. The dipole moment values should only be used in conjunction with the corresponding data for the relaxation times in order to compare the dielectric loss factors. Owing to their high molecular weights, polymer chains possess low mobility and their relaxation times are relatively long. For this reason, increased temperatures were necessary to move the dielectric relaxation spectra of glassy thermoplastics into the microwave region. Plots of dielectric properties as functions of frequency at a single temperature or of temperature at a single frequency, although useful, did not give a complete picture of dielectric behavior. The dielectric spectra of DETA were used to reveal the shift of dielectric relaxation spectra to the microwave region. The plot of heating rate versus temperature via the microwave experiment was used to estimate the T_c and T_g at 2.45 GHz for various glassy thermoplastics. By combining microwave and conventional thermal heating, improved absorption of microwave energy by polymers was obtained.

At room temperature, dielectric loss factors of the studied thermoplastics was very low, therefore, a very high electric field strength was required in order to ensure a reasonable rate of rise of temperature in the material. In general, for the same power applied, the standing wave applicator established much higher electric field strengths than the travelling wave or multimode applicators. From an industrial point of view, low loss thermoplastics at room temperature require standing wave applicators as distinct from travelling wave or multimode applicators for rapid processing.

In the standing mode applicators, the field distribution along the z-direction is a cosine distribution which would result in highly non-uniform energy absorption in the material. To obtain a uniform field across the width, two such cavities need to be used side by side, as shown in Figure 4.25 (18). The dual waveguide would be powered by a single source, splitting the power equally between the two cavities. In addition, a

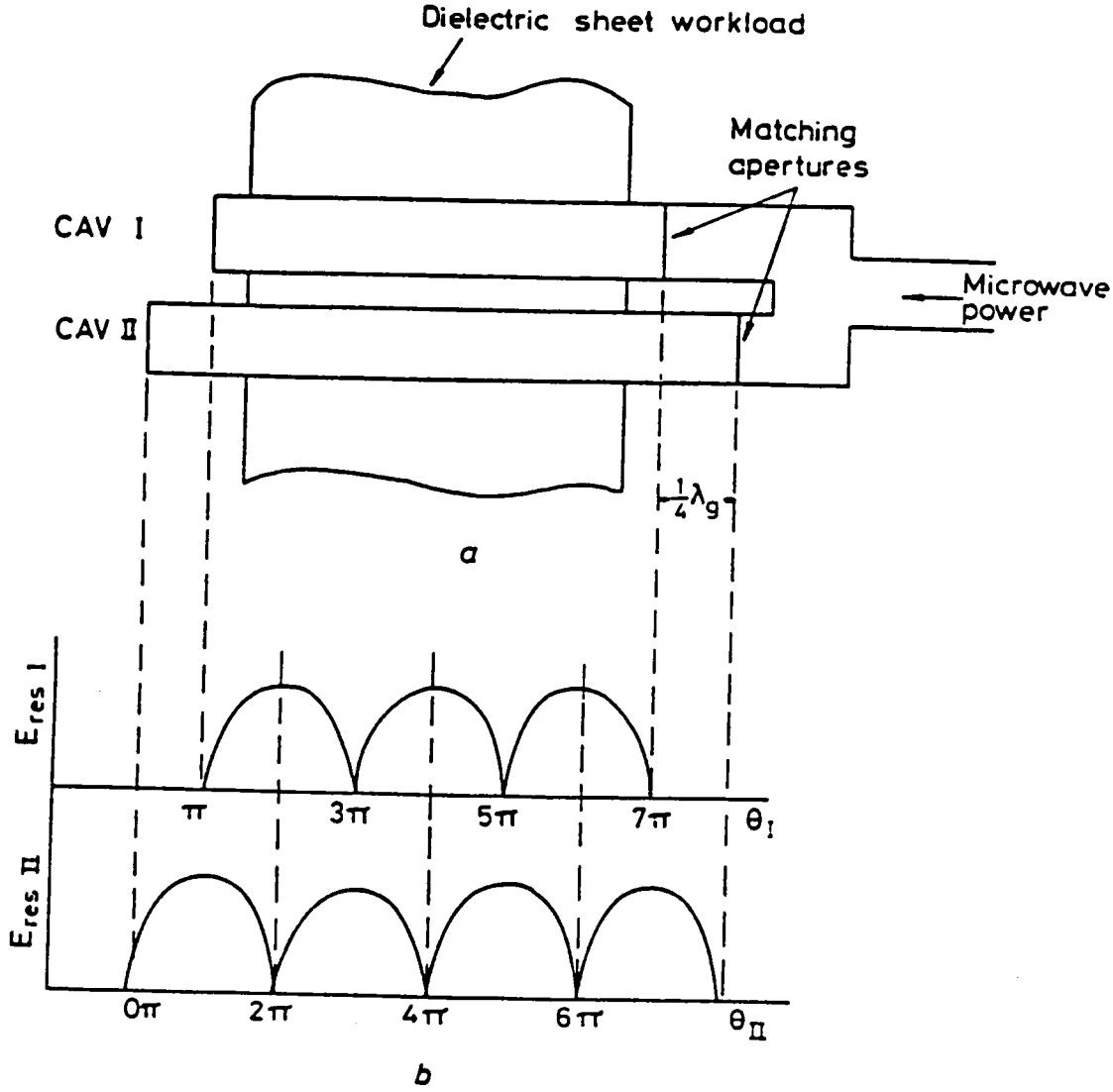

Figure 4.25 Development of a uniform electric field TE_{10n} twin cavity heater (18)
a. Twin TE_{10n} resonant cavity heater (Plan view)
b. Electric field distribution in the plane of the dielectric sheet in each cavity

quarterwave displacement between the electric fields in the two cavities need to be ensured to make a uniform processing. This set-up is only good for processing materials in the form of sheets.

4.6 REFERENCES

1. D. A. Copson, ***Microwave Heating***, 2nd ed., The Avi Publishing Co., Connecticut, 1975.

2. E. C. Okress, ***Microwave Power Engineering***, Vol. 2: Applications, Academic Press, New York, 1968.

3. R. V. Decareau, ***Microwaves in the Food Processing Industry***, Academic Press, Florida, 1985.

4. P. Fellows, ***Food Processing Technology: Principles and Practice***, E. Horwood Ltd., New York, 1988.

5. M. Le Maguer and P. Jelen, ***Food Engineering and Process Applications***, Vol. 1: Transport Phenomena, Elsevier Applied Science Publishers, New York, 1986.

6. A. J. Bur, *Polymer*, **26**, 963 (1985).

7. N. G. McCrum, B. E. Read and G. Williams, ***Anelastic and Dielectric Effects in Polymeric Solids***, John Wiley & Sons, New York, 1967.

8. P. Hedvig, ***Dielectric Spectroscopy of Polymers***, John Wiley & Sons, New York, 1977.

9. Chen C. Ku and R. Liepins, ***Electrical Properties of Polymers: Chemical Principles***, Hanser Publishers, New York, 1987.

10. A. Tager, ***Physical Chemistry of Polymers***, 2nd ed., English translation, Mir Publishers, Moscow, 1978.

11. J. I. Kroschwitz, ***Electrical and Electronic Properties of Polymers: A State-of-the-Art Compendium***, John Wiley & Sons, New York, 1988.

12. R. Bartnikas and R. M. Eichhorn, ***Engineering Dielectrics Volume IIA Electrical Properties of Solid Insulating Materials: Molecular Structure and Electrical Behavior***, ASTM Special Technical Publication 783, Pennsylvania, 1983.

13. A. D. Jenkins, ***Polymer Science: A materials science handbook,*** *Vol. 2*, North-Holland Publishing Co., London, 1972.

14. J. B. Birks and J. H. Schulman, ***Progress in Dielectrics, Vol. 2,*** John Wiley & Sons, New York, 1960.

15. V. Frosini and E. Butta, *J. Appl. Polym. Sci.*, **11**, 527 (1967).

16. P. C. Bandyopadhyay and T. K. Chaki, *Proc. IUPAC, I. U. P. A. C., Macromol. Symp.*, **28th**, 421. Int. Union Pure Appl. Chem.: Oxford, UK (1982).

17. D. K. Cheng, ***Field and Wave Electromagnetics,*** Addison-Wesley Publishing Co., Pennsylvania, 1983.

18. A. C. Metaxas and R. J. Meredith, ***Industrial Microwave Heating,*** Peter Peregrinus, London, 1983.

CHAPTER 5

THE MICROWAVE PROCESSIBILITY OF SEMICRYSTALLINE POLYMER

5.1 INTRODUCTION

In the preceding chapters, microwave energy absorption of nitrile rubbers and the dielectric behavior of amorphous thermoplastics were examined in detail. A combination of microwave and conventional thermal heating was found to improve the absorption of microwave energy by glassy amorphous polymers. By externally heating the sample above the critical temperature of dielectric loss, T_c, the dielectric relaxation spectra observed at low frequency was moved into the microwave region. Within the dispersion region, $d\varepsilon''/dT$ was large and positive on the cool side of the dielectric relaxation temperature spectra at 2.45 GHz so that rapid heating occurred.

Since the mechanism and the equations describing microwave heating are independent of thermal conductivity, microwave heating avoids heat transfer rate problems encountered in conventional thermal heating for low thermal conductivity polymers. Due to the high temperatures needed to process semicrystalline polymers, the avoidance of thermal gradients as a result of microwave processing offers distinct advantages. Microwave energy, with its long wavelength, offers a deeper penetration than ultraviolet (UV) or electron beam irradiation but does not possess sufficient energy to cause bond cleavage. Only accelerated frictional heating occurs in microwave processing. In this way, energy may be dissipated rapidly throughout the volume of the material. Surface overheating or uneven catalyst decomposition is thus avoided. When two materials are simultaneously subjected to microwave irradiation, the higher

loss material will be heated sooner than the lower loss material provided that the dispersion as a whole is properly located near T_c. In general this effect is more sequential than simultaneous, and is related to the dimensions and size of the load. This volumetric, selective absorption of microwave energy can, under suitable conditions, save energy, reduce operating costs, increase the processing speed and improve performance. In addition, the microwave heating process can be switched at high rates in response to a control signal; and therefore, processing can be controlled more accurately than in conventional methods.

In summary, microwave energy absorption offers the following advantages over conventional heating methods: (a) rapid volumetric heating, (b) no overheating at the surface, (c) addressable heating, (d) energy saving and low operating costs, (e) increased throughput, (f) no direct degradation, (g) potential for field repair applications as well as many other advantages which can be found in the literature (1-6).

Several articles have recently appeared in the literature on the microwave processing and diagnosis of epoxy/amine resins as well as nylon66 (7-13). These same researchers described a field pattern study for a single-mode cylindrical cavity applicator. One particular single mode was found to be especially useful for heating monofilament fibers (14). Other researchers found that ultradrawing under microwave heating through a circular or rectangular waveguide was quite effective for obtaining high modulus polymers (15-22).

In this chapter, the processing of semicrystalline polymers such as poly(ether ether ketone) (PEEK), nylons, poly(ethylene terephthalate) (PET) via a cylindrical cavity and a rectangular standing wave applicator is described. Rapid heating rates were observed between the glass transition temperature, T_g, and the melting temperature, T_m, for all these polymers. By conventional methods, the processing temperature

should be greater than the melting temperature of the polymer. The high operating costs of processing high melting temperature materials, such as PEEK, contribute significantly to their overall costs. Microwave heating may greatly reduce such operating cost and improve processing speeds. In order to compare the heating phenomena between amorphous and semicrystalline PEEK, both DMTA and DETA spectra were investigated to explain the rapid crystallizing rate of PEEK just above its glass transition temperature.

5.2 EXPERIMENTAL

5.2.1 Materials

Table 5.1 summarizes the glass transition temperatures, melting temperatures and suppliers, for nylon6, nylon612, nylon12, poly(ether ether ketone) (PEEK), poly(ethylene terephthalate) (PET) and the silicone flexible mold used to support the sample. The T_g and T_m of a semicrystalline polymer is a function of the percentage crystallinity and the processing history. Films were prepared by using a platten press to heat and mold the polymers just above (0-10°C) their respective T_m's. The amorphous counterparts of the crystalline polymers were prepared by quenching from their melt state into an ice water bath. Samples were then dried in a vacuum oven just below their respective T_g's for 24 hours. These films were kept in the desiccator until they were used for the DETA, DMTA and microwave experiments. Semicrystalline PEEK was prepared by annealing at 293°C for 50 minutes before dropping into the bath of ice water. The two parts of silicone flexible mold were made by mixing and vacuum

Table 5.1 Thermal properties and sources of semicrystalline polymer

Polymer	T_g, °C	T_m, °C	Source	Catalog #
PEEK	150	334	ICI	380G
Nylon 6	63	229	Polysciences	18180
Nylon 612	46		SP^2	313
Nylon 12	37	178	SP^2	044
Silicone mold			GE	RTV664
PET	81	~260	SP^2	138

SP^2 (Scientific Polymer Products)

degassing several times. The mixture was cured at room temperature for 24 hours, then further cured under vacuum at 200°C for 24 hours.

5.2.2 Relaxation Spectrometer Systems

Polymer Laboratory's DETA (Dielectric Thermal Analyzer) and DMTA (Dynamic Mechanical Thermal Analyzer) were used to provide comprehensive relaxation spectra covering the broad frequency range of 1 Hz to 100 kHz. Dielectric spectra from -150°C to T_m were obtained via DETA at frequencies of 0.1, 1, 10 & 100 kHz. DMTA thermal spectra from -150°C to T_m were obtained by using the DMTA at frequencies of 1, 3 and 10 Hz. Bending mode was used for DMTA testing.

5.2.3 Microwave Instrumentation

A cylindrical cavity applicator, shown schematically in Figures 5.1 and 5.2 (12-13), was used to study the processing of nylon and PEEK. The seven inch cylindrical cavity was designed and constructed by Michigan State University. Several defined modes can exist in this cavity by adjusting the cavity length (23-25). The TE_{111} mode was chosen to process the polymers described in this chapter. The field distributions of the two-dimensional TE_{11} mode and the three-dimensional TE_{111} mode are shown schematically in Figure 5.3. The lowest mode, TE_{111}, exists in this empty cylindrical cavity with a theoretical cavity length of 6.69 cm. The specimens (1 cm x 1 cm x 0.5 cm) were put in the trough of a silicone flexible mold for microwave processing. The size of the silicone mold was about 2 cm x 2 cm x 1.2 cm. Two more pieces of silicone mold were stacked to support the specimen and to raise the specimen to the center of the TE_{111} mode. An additional silicone mold was placed on the top of the specimen in order to secure the fiber optic temperature probe. The other function of the top mold was to insulate the sample to prevent heat convection losses from the specimen to the air. The cylindrical cavity applicator is quite efficient in design because the radiation

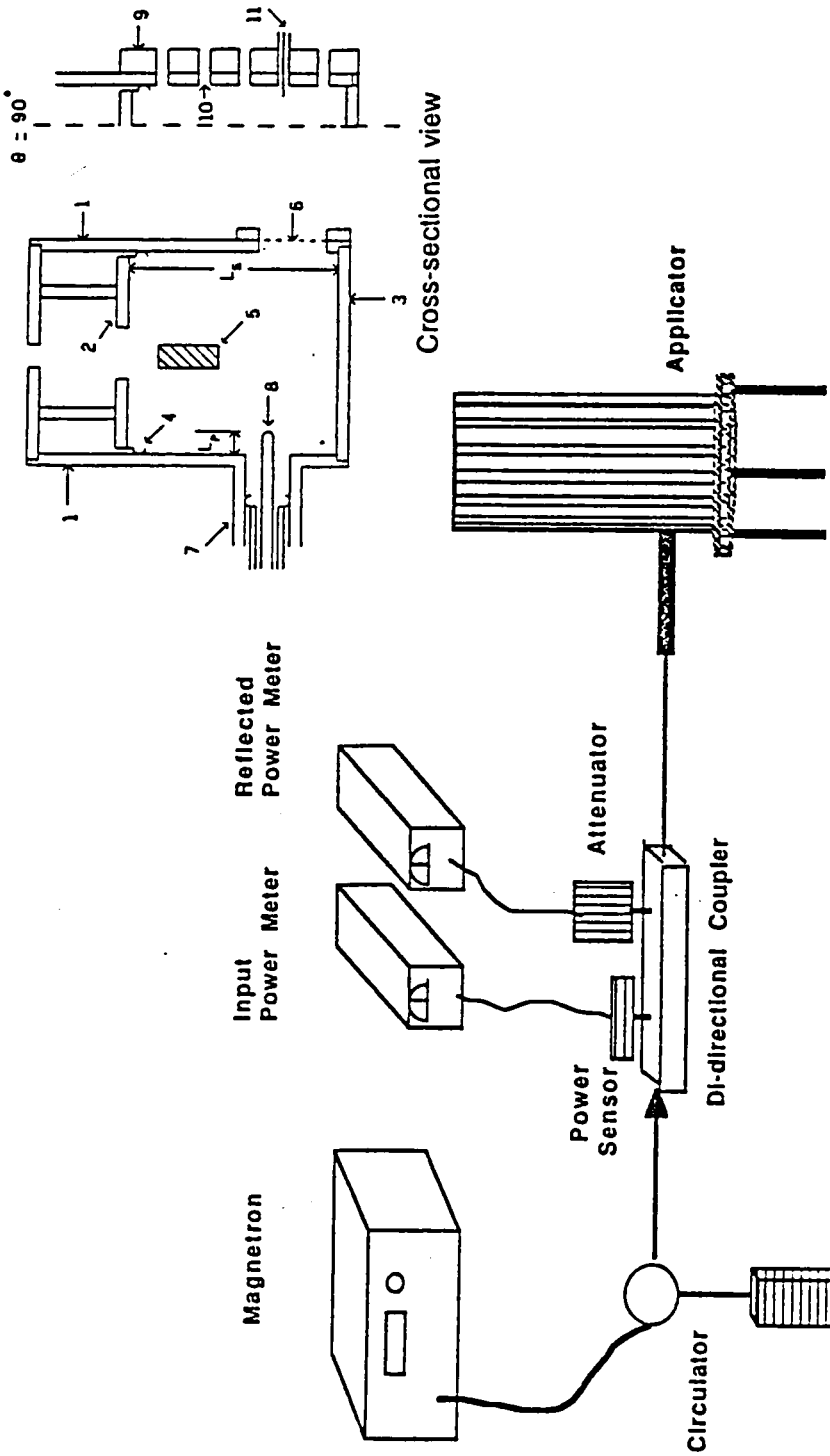

Figure 5.1 Schematic of the experimental set-up for the cylindrical cavity applicator.

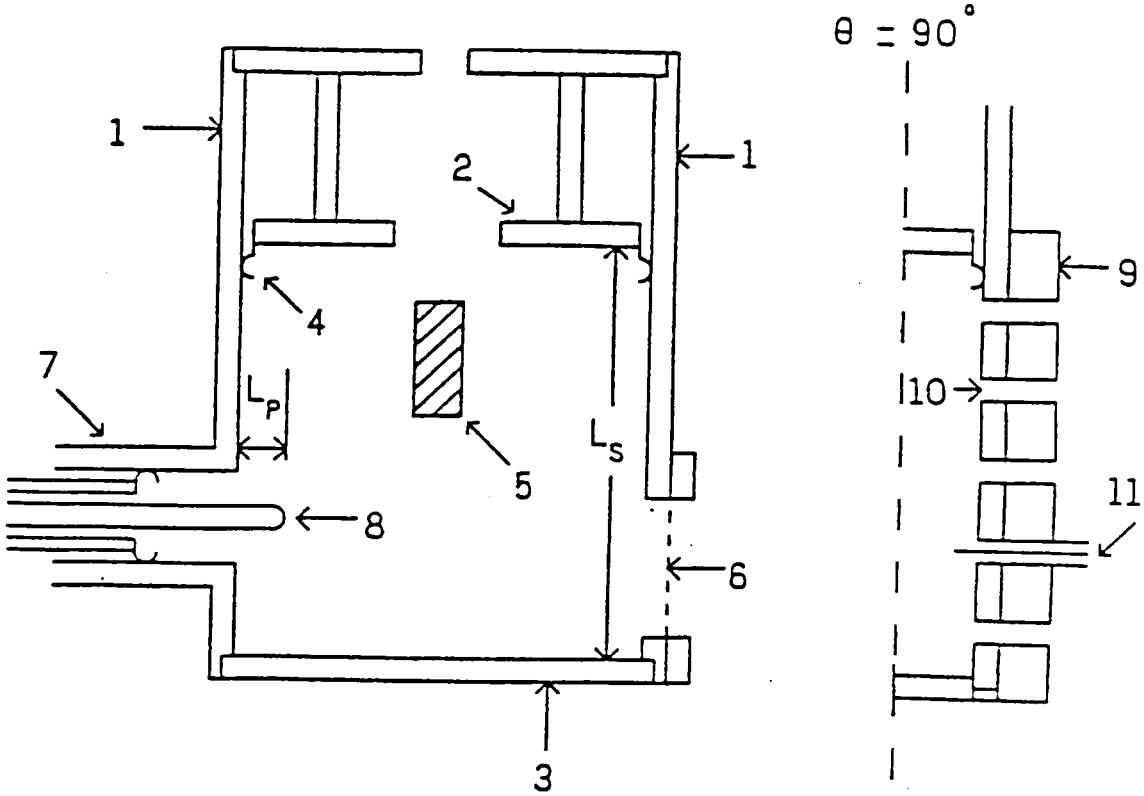

Figure 5.2 Cross-sectional view of a cylindrical cavity applicator. Full cross section is the $\theta = 0°$ plane passing through the input probe. Partial cross section $\theta = 90°$ displays the microcoax inputs. The numbered pieces are: (1) conducting cylindrical shell, (2) sliding short, (3) end plate, (4) silver finger stock, (5) process material, (6) screened viewing port, (7) coaxial input port, (8) adjustable coupling probe, (9) brass microcoax probe holder, (10) diagnostic holes, and (11) microcoax electric field probe. [Reference 12]

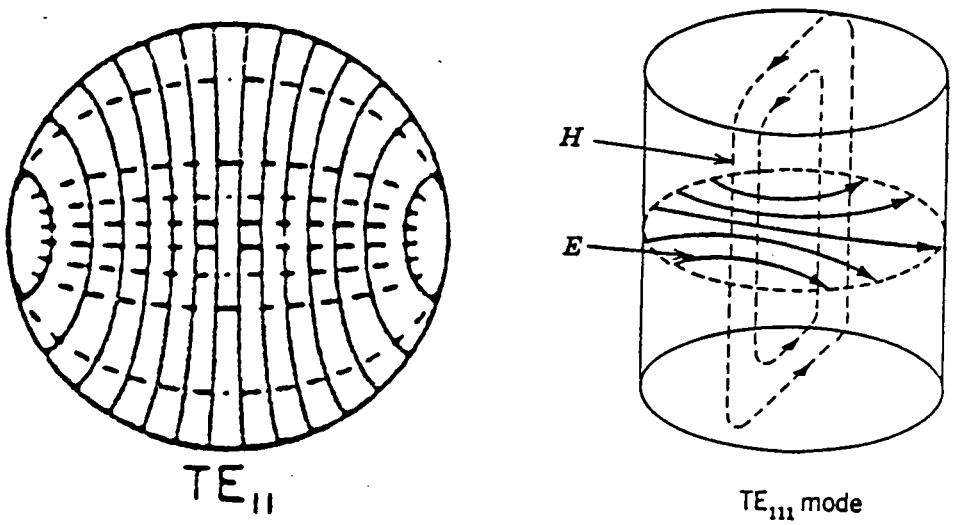

TE_{11} field distribution for a circular waveguide.

TE_{111} field distribution for a cylindrical cavity.

Figure 5.3 Field lines for two-dimensional TE_{11} mode and three-dimensional TE_{111} mode.

from the source is continuously reflected from the walls of the cavity, passing through the specimen many times until it is effectively fully absorbed.

Due to the size of the specimen in the form of films, a standing wave applicator, described in the preceding chapter, was used to process PET. Samples were stacked contiguously and placed into the center section of the 1/2 in. i.d. teflon sample holder.

5.3 RESULTS AND DISCUSSION

5.3.1 Thermal Spectra of DETA and DMTA

Figures 5.4-5.6 show the dielectric transition spectra (tanδ vs. temperature) of nylon6, nylon612 and nylon12 at 0.1, 1, 10 and 100 kHz. By increasing the number of amide groups in the main chain of nylons, the transitions could be shifted to slightly higher temperatures. The dielectric properties of nylons are mainly determined by inter-molecular and intra-molecular hydrogen bonds of the amide groups. The electrical conductivity is very high due to proton transfer along the hydrogen bonding chains. The height of the tanδ peak was hard to compare from sample to sample; variations may be due to differences in percent crystallinity among the different nylon specimens. The other reason may be due to the relatively small variation of tanδ as was discussed in chapter 2. Table 5.2 represents the apparent activation energies calculated from the logarithm of frequency vs. the reciprocal of absolute temperature in the kHz region. Nylon6 had the highest activation energy; the temperature window between T_c and T_g was smaller than that of nylon612 and nylon12 even though nylon6 had the higher T_g.

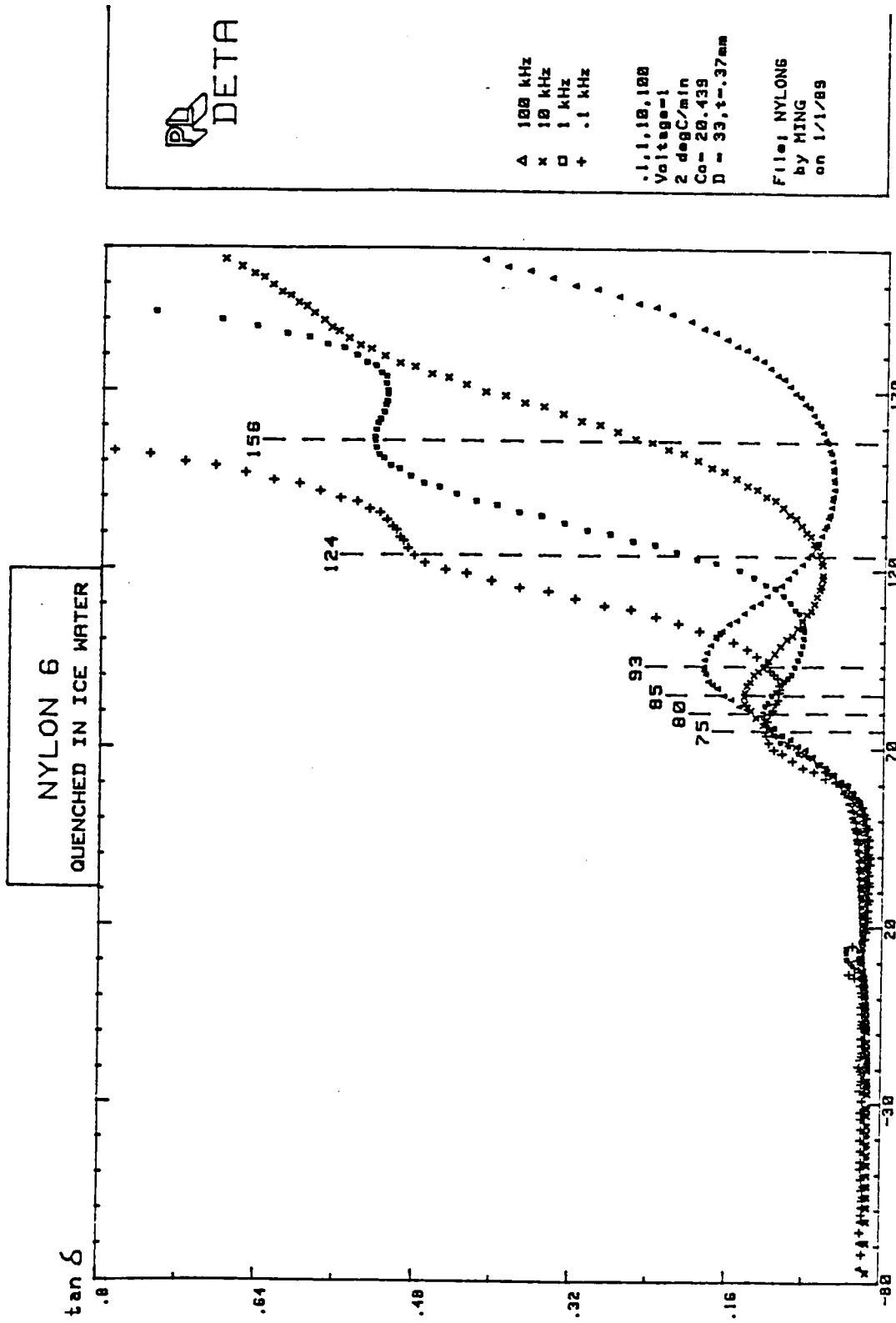

Figure 5.4 Temperature dependence of the loss tangent of nylon 6 at various frequencies.

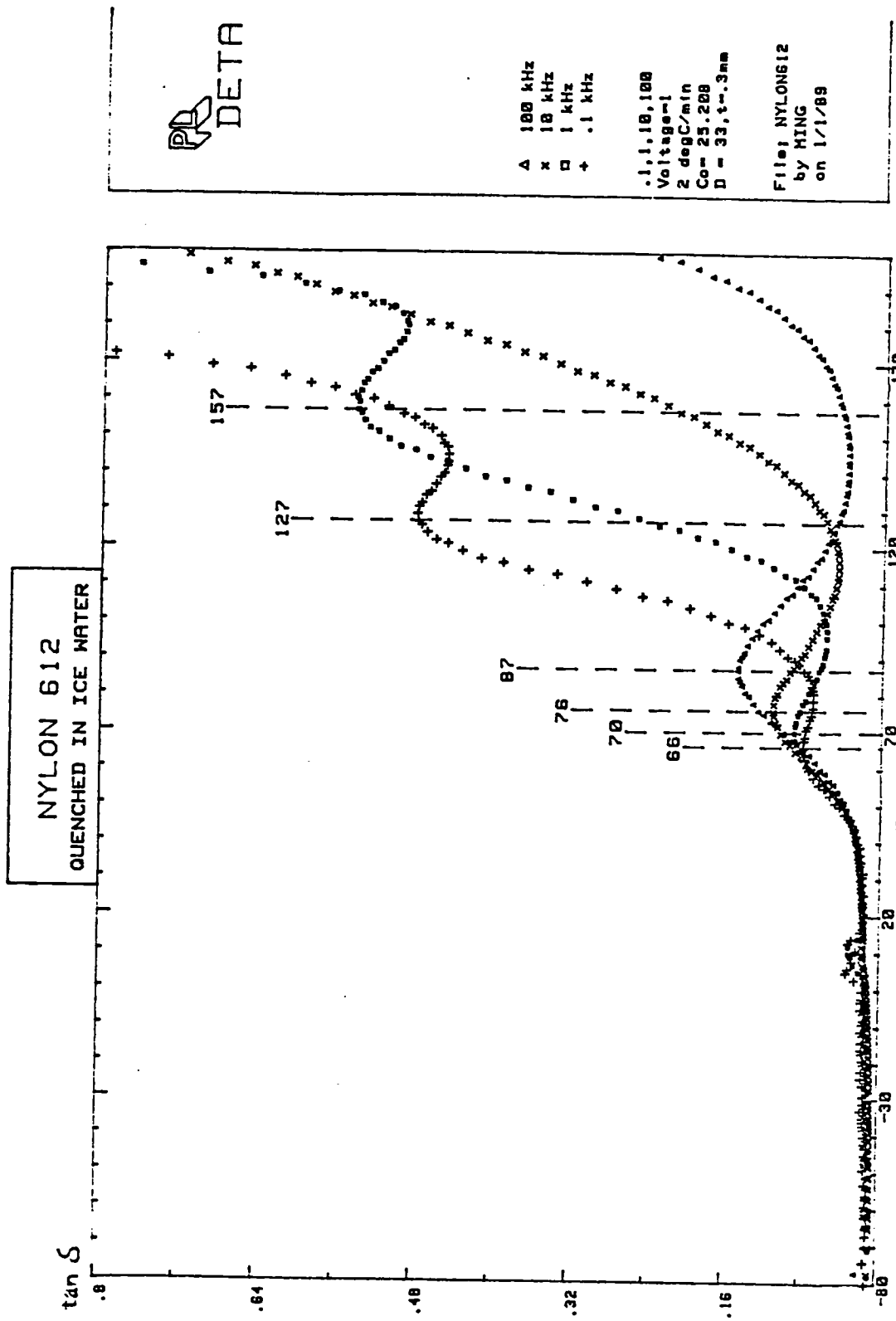

Figure 5.5 Temperature dependence of the loss tangent of nylon 612 at various frequencies.

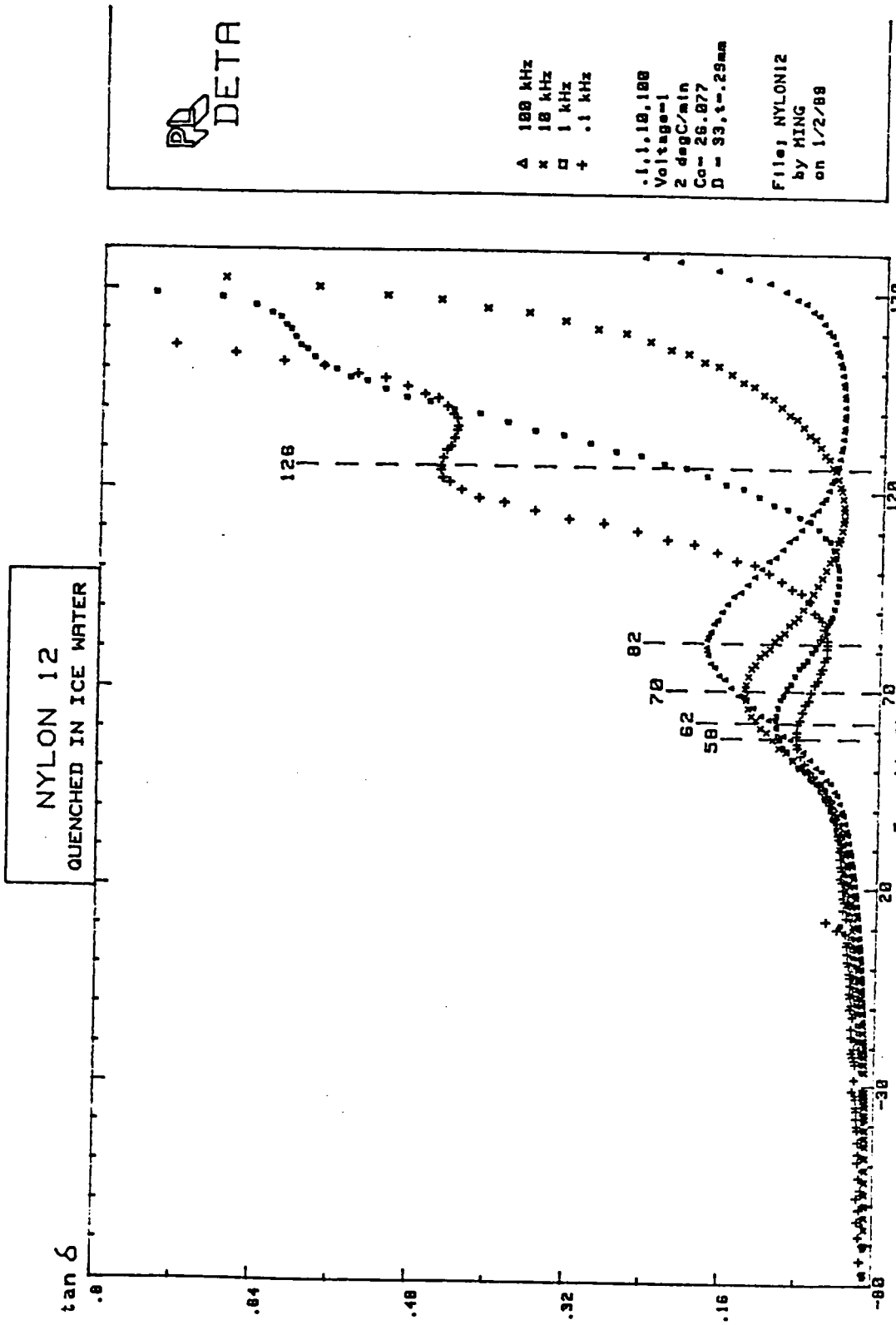

Figure 5.6 Temperature dependence of the loss tangent of nylon 12 at various frequencies.

Table 5.2 T_g, T_m and the activation energies in the kHz region of polymers

Polymer	T_g (°C)	T_m (°C)	ΔE_a* (kJ/mole)	ΔE_a# (kJ/mole)	Remark
PEEK	150	334	790	810	Q in ice water
			550		Cooled in DETA
Nylon6	63	229	370	410	Q in ice water
			350	380	Q in press
Nylon612	46		270	320	Q in ice water
Nylon12	37	178	230	270	Q in ice water
PET	81	260	420	420	Q in ice water
			350	340	Q in press

* Activation energy calculated from the peak temp. of 1,10 & 100 kHz

Activation energy calculated from the peak temp. of .1,1,10 & 100 kHz

Q: quenched

Figure 5.7 represents the temperature dependence of dielectric constant and loss tangent of the silicone flexible mold at 100 kHz. A transition around -90°C was identified as the glass transition temperature of the silicone rubber. A broad transition between -20°C and 80°C was attributed to the filler. The maximum value of tanδ was 0.016. Thus, the silicone mold was a relatively low dielectric loss material in the microwave field.

Figure 5.8 is the DMTA spectra of amorphous PEEK at 1 Hz. The thickness of the specimen was 3 mm. Samples were tested in a dual cantilever mode with a peak displacement amplitude of 20 microns to monitor the viscoelastic properties. The logarithm of storage modulus (in Pascals) drops from 9.6 at 140°C to 6.3 around 155°C indicating the typical 3 decade decay in modulus for the glass to rubber transition. The sudden rise in modulus just above 155°C is due to the rapid crystallization of PEEK. This crystallization phenomena for PEEK can be seen at other frequencies as well. Figure 5.9 clearly shows the crystallization when tested in the Dielectric Thermal Analyzer at 100 kHz. At the beginning of the transition, the dielectric constant, ε', and the dielectric loss factor, ε", increased with increasing temperature which indicated increased mobility of polar groups along the main chain. The rapid crystallization of PEEK into the crystalline phase resulted in immobilization of the dipoles such that the alternating electric field had little effect in orienting the dipoles on the polymer. Once beyond the crystallization region, ε' increased again to a maximum value as the crystallites melted. At higher temperature, the electric field once again could not couple with the sample as the material transformed to the melt state so that ε' decreased slowly with increasing temperature.

The molecular relaxation process in polymers which gives rise to dielectric relaxation also, in general, gives rise to mechanical relaxation. In correspondence to

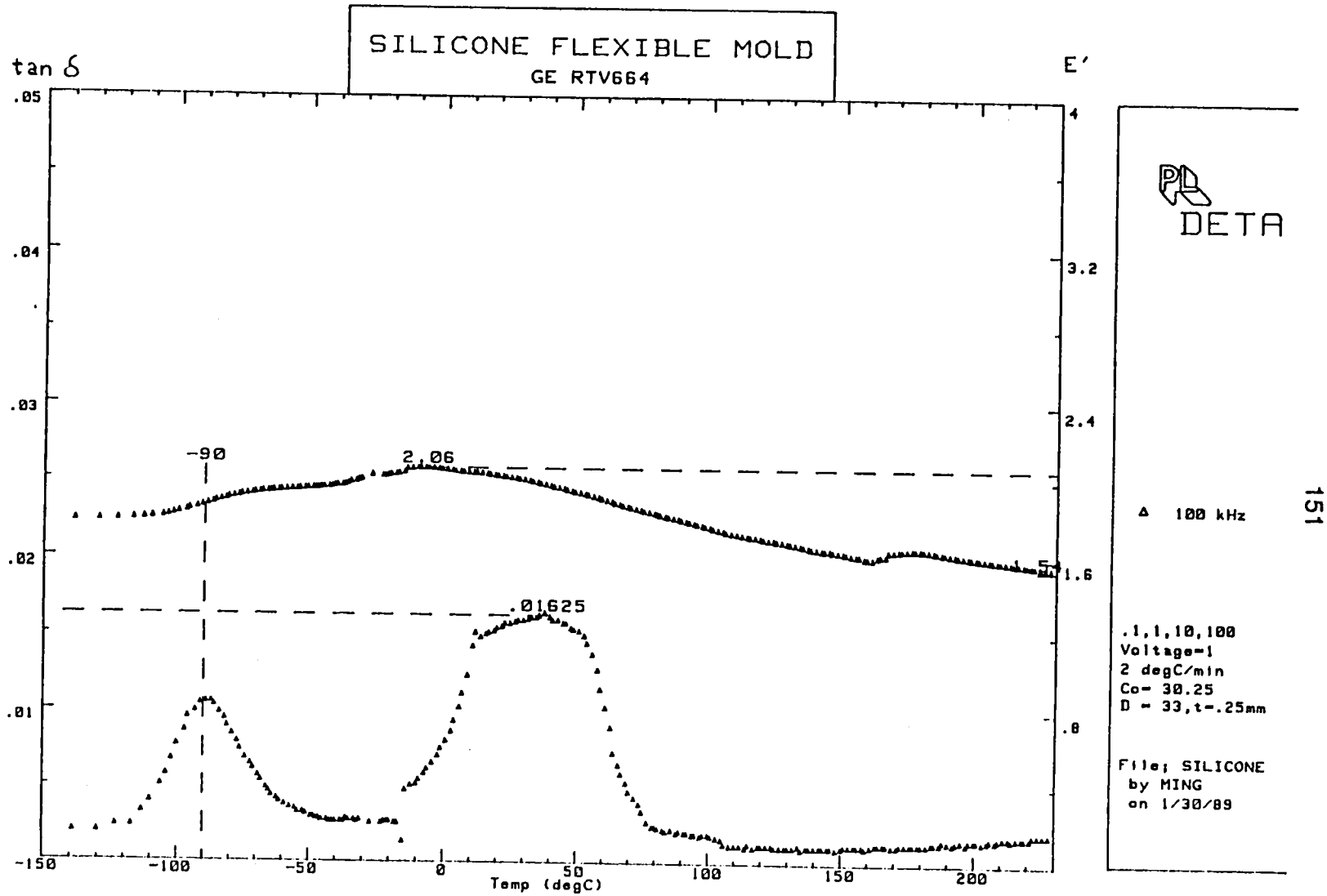

Figure 5.7 Temperature dependence of the dielectric constant and the loss tangent of silicone flexible mold at 100 kHz.

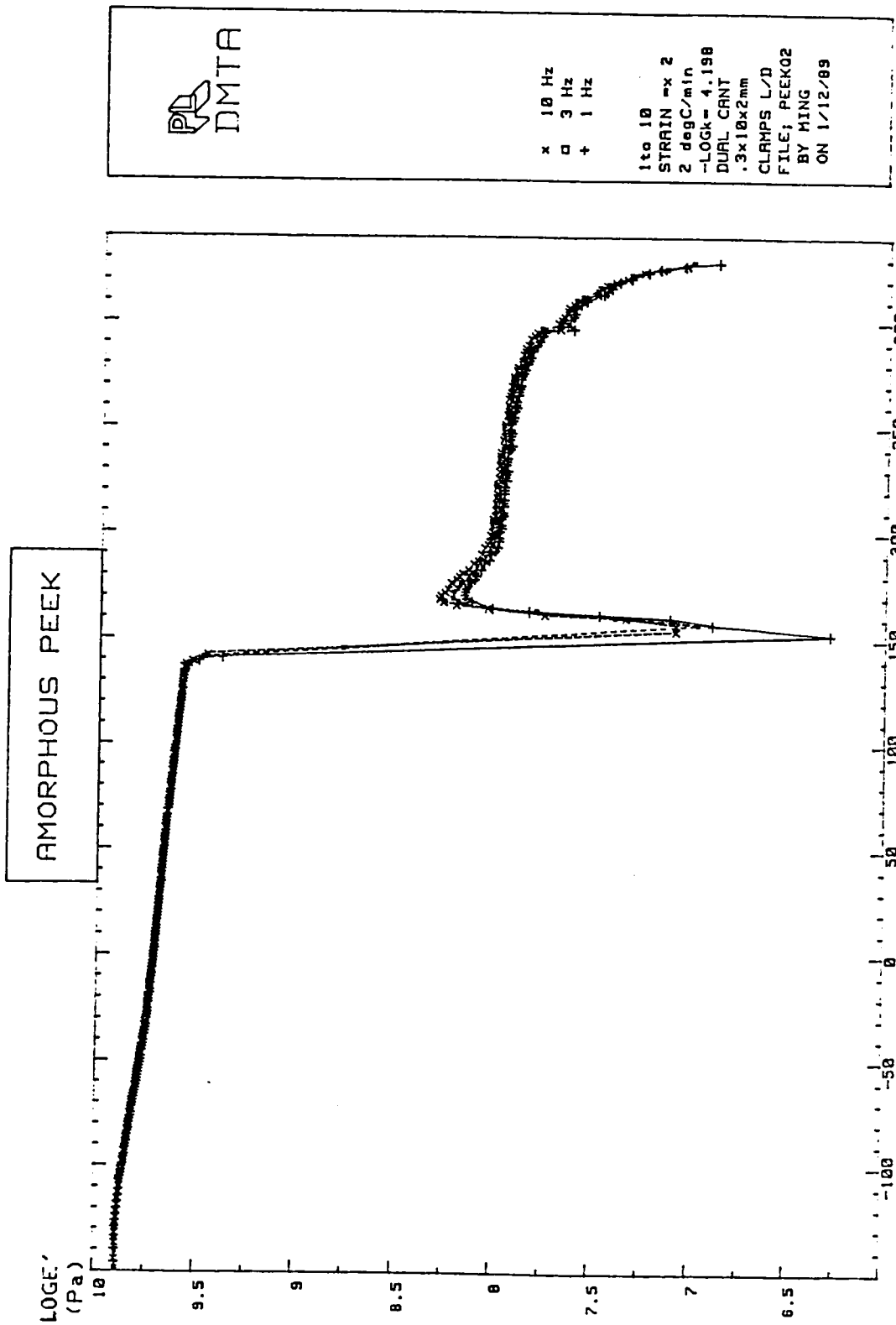

Figure 5.8 Temperature dependence of the storage modulus of amorphous PEEK at various frequencies.

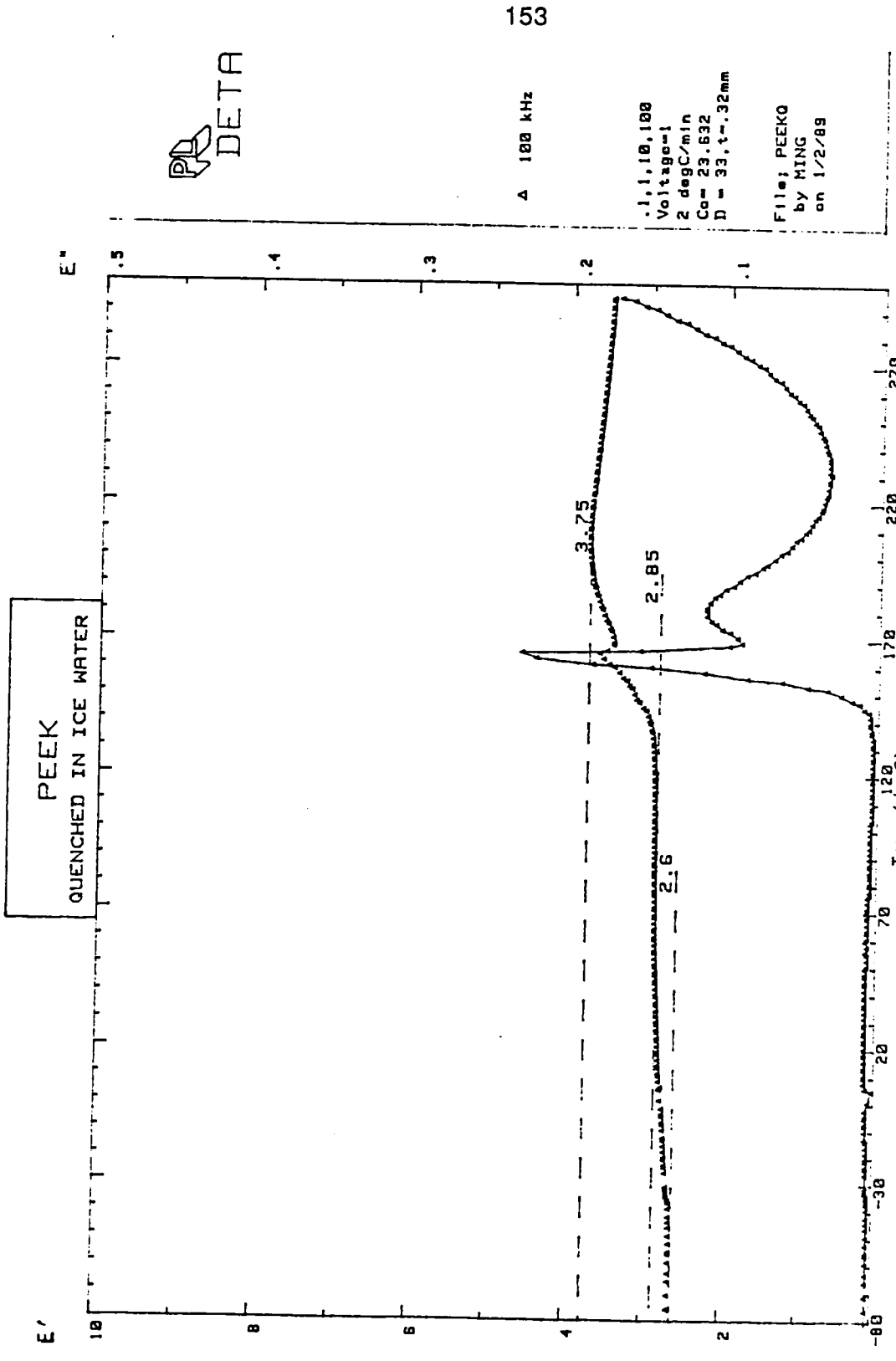

Figure 5.9 Temperature dependence of the dielectric constant and the dielectric loss factor of amorphous PEEK at 100 kHz.

the β relaxation of DMTA spectra, the dielectric constant change in this region is smaller than that of the α relaxation in the DETA spectra. The enormously high activation energy of amorphous PEEK, as shown in Table 5.2, reveals the similarity of heating rates in comparing amorphous PEEK and semicrystalline PEEK.

Figure 5.10 presents the DETA spectra of semicrystalline PEEK. ε' and ε" increased continuously in the glass transition region. The temperature at maximum ε" for semicrystalline PEEK was almost the same as that for amorphous PEEK, as shown in Figures 5.9 and 5.10 indicating amorphous phase involvement. In the DMTA spectra for semicrystalline PEEK, the logarithm of the storage modulus only drops by 0.6 in the glass transition region.

Figures 5.11 and 5.12 illustrate the DETA spectra of the amorphous PET. Figure 5.11 shows that the dielectric constant increased in the glass transition region from 70°C to 110°C. Above 110°C, ε' decreased as crystallinity increased. Between 120°C and 200°C, ε' decreased slowly. Beyond 200°C, ionic conductivity became significant so that tanδ became very large. Figure 5.12 shows the logarithm of tanδ versus temperature. The crystallization phenomena was detected from the shape of the higher temperature side of the transition region. By increasing the crystallinity, the dielectric α peak decreased.

All the DETA spectra described above have their ε' increment closer to T_g rather than to T_m. The activation energies of most of these semicrystalline polymers, as shown in Table 5.2, were much higher than those of the amorphous polymers mentioned in the preceding chapter. In general, the stiffer the polymer, the higher the T_g, and the higher the activation energy. Therefore the shift in the dipolar relaxation spectra caused by frequency rise will be smaller. In other words, the window between T_c and T_g would be

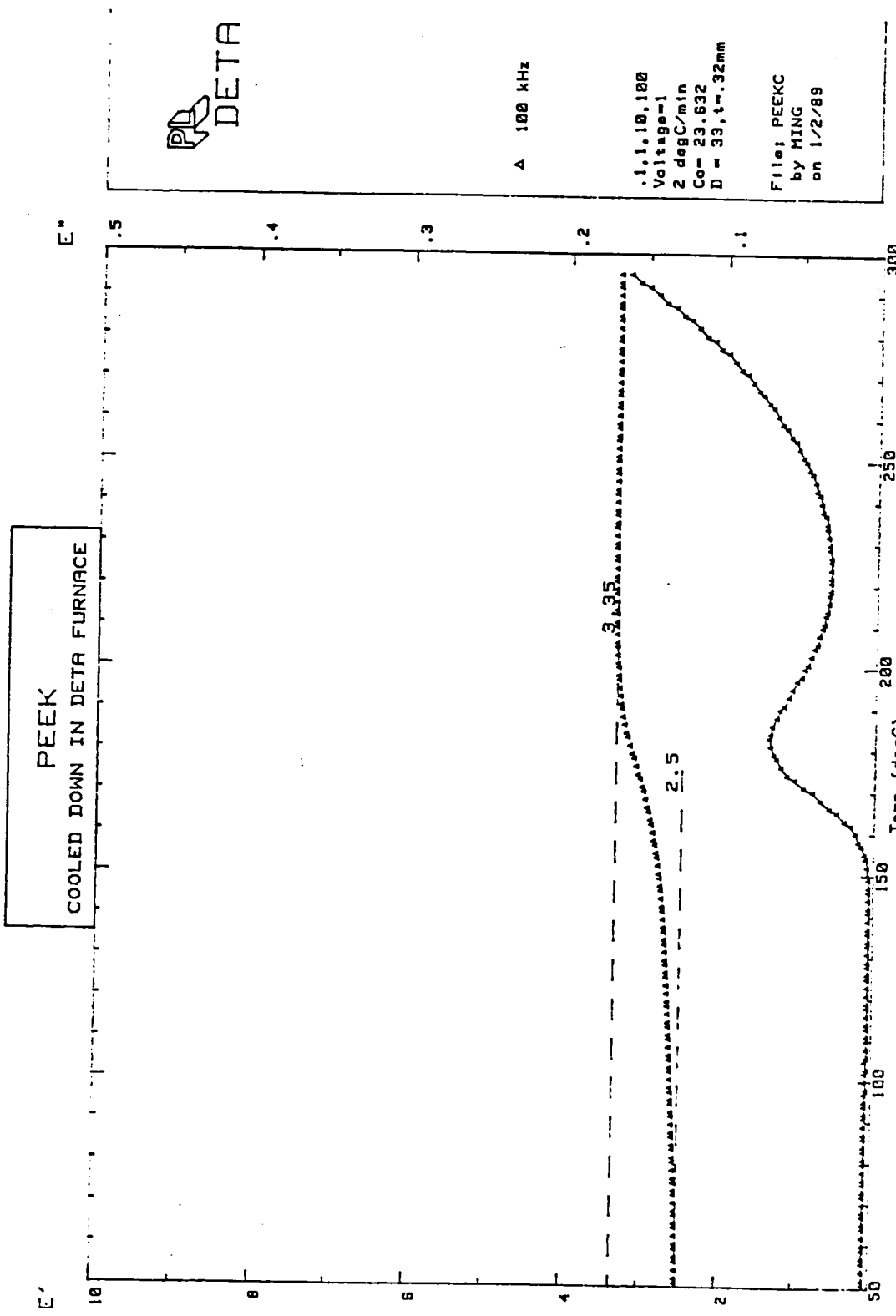

Figure 5.10 Temperature dependence of the dielectric constant and the dielectric loss factor of semicrystalline PEEK at 100 kHz.

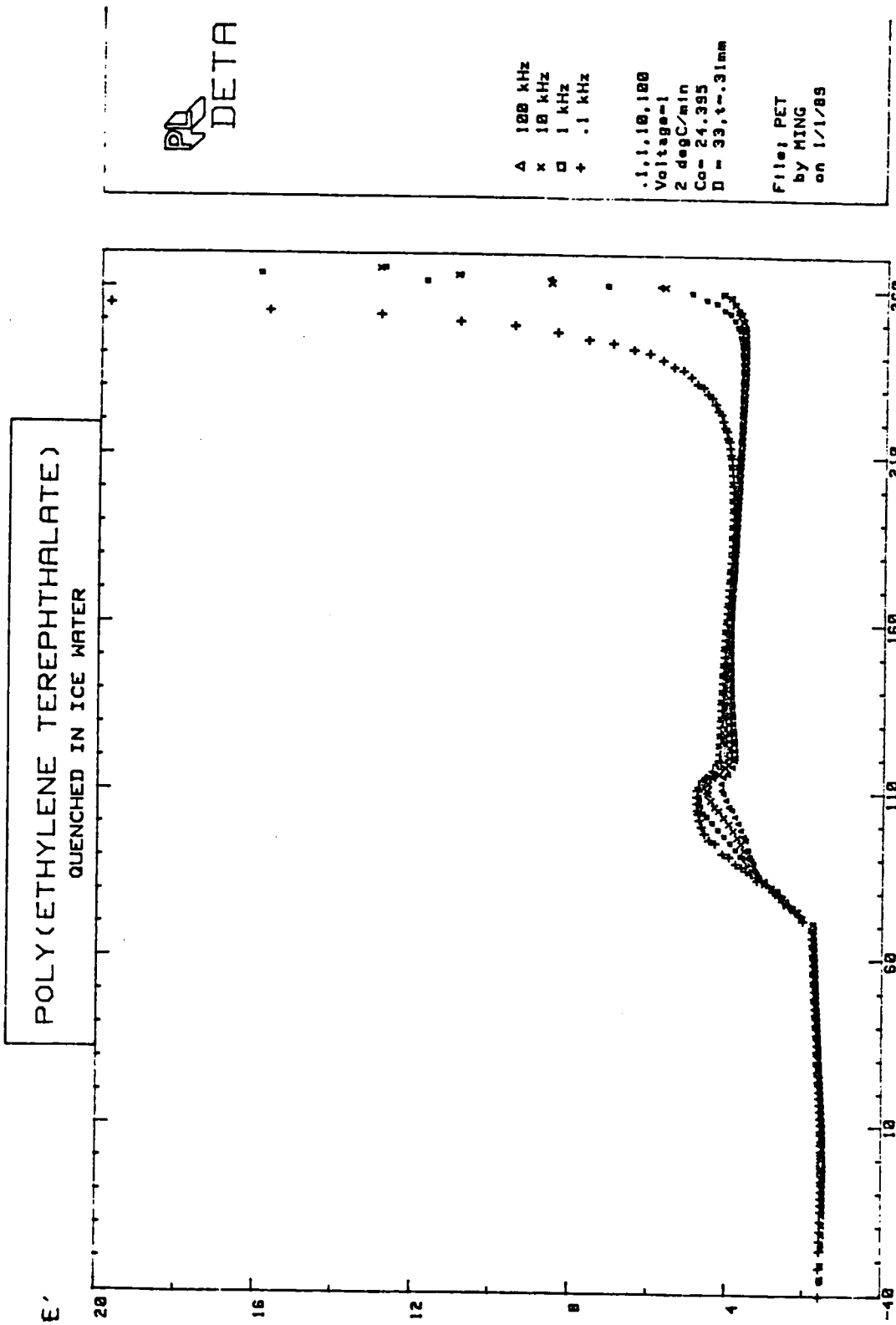

Figure 5.11 Temperature dependence of the dielectric constant of PET at various frequencies.

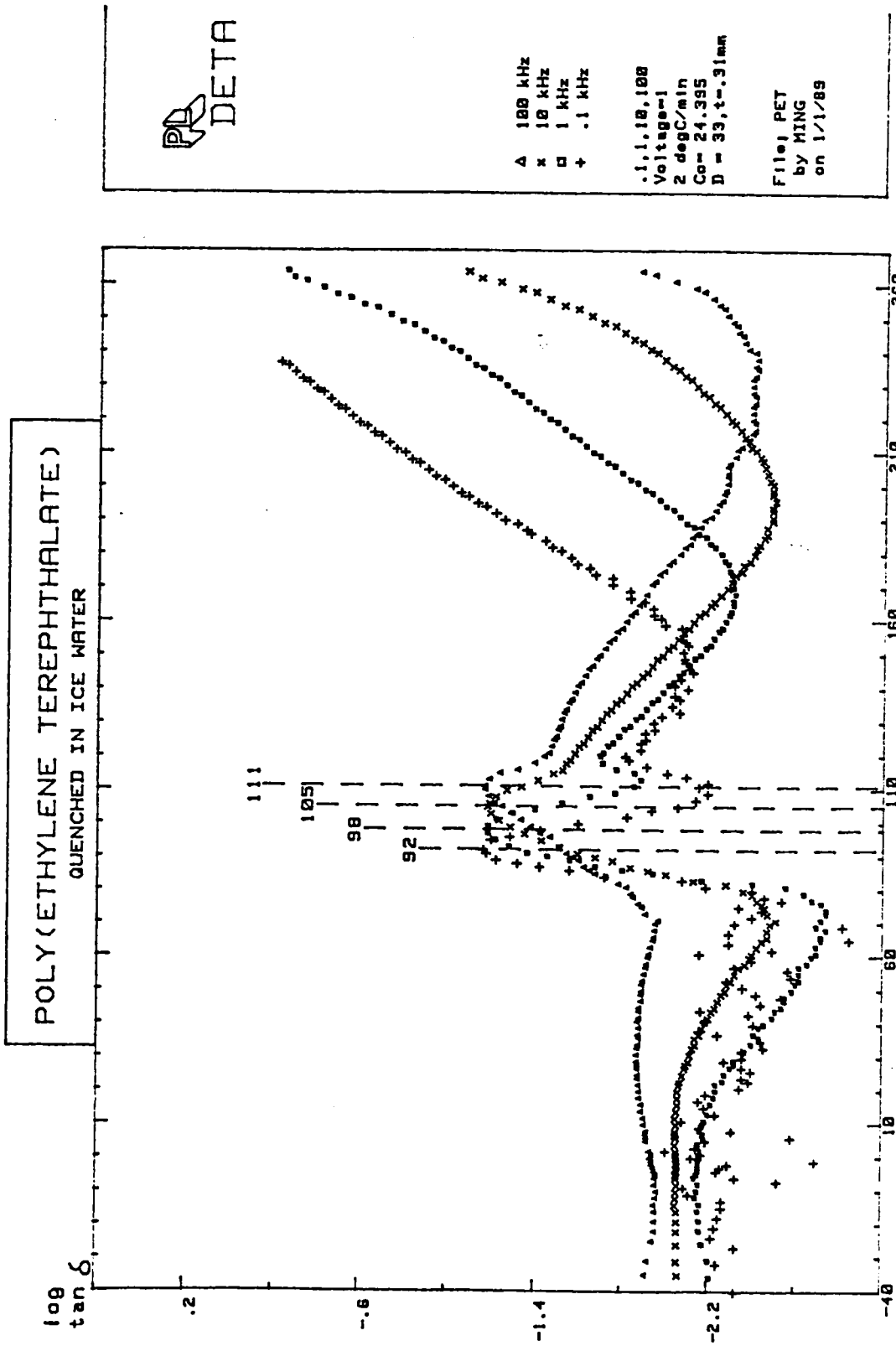

Figure 5.12 Temperature dependence of the logarithm loss tangent of PET at various frequencies.

smaller for semicrystalline polymers. For a polymer with a wide window between T_g and T_m, T_c would be closer to T_g rather than to T_m.

5.3.2 Microwave Experimental Results

Figure 5.13 represents the temperature variation of nylon6, nylon612, nylon12 and the silicone flexible mold with time. The input power was 20 watts. In the first two minutes, the temperature rise was almost the same for all polymers. After 2 minutes, the temperature of nylon6 rose rapidly, probably due to the higher concentration of polar amide group (or hydrogen bond). Around five minutes, the temperature of nylon612 started to rise faster than that of nylon12. The reason the final temperature of nylon612 was lower than that of nylon12 may be due to a difference in sample mass and variation in temperature probe placement.

The variations of input power, reflected power and temperature vs. time for nylon6, nylon612, nylon12 and the silicone mold are shown in Figures 5.14-5.17. For microwave heating of the silicone mold, the intrinsically low loss of the silicone rubber was improved by introducing fillers. The high electric field strength in the center of TE_{111} mode developed adequate coupling with the low loss silicone mold to cause heating. The silicone mold had a broad, low dielectric loss spectra as shown in Figure 5.7. This broad loss spectra allowed the mold to be heated easily over a wide temperature range. The silicone mold was heated slowly from room temperature to 95°C in 15 min. for only 20 watts of input power. At room temperature, below the T_g of nylons, the dielectric loss factors of dried nylons were small. It is important to note that the purpose of the silicone mold was to have the mold absorb the microwave energy to heat itself and then transfer that heat to the semicrystalline polymers until their T_c's were encountered. Above the T_c of nylons, nylons absorbed microwave energy by themselves because the dielectric loss factors of nylons were higher than that of the

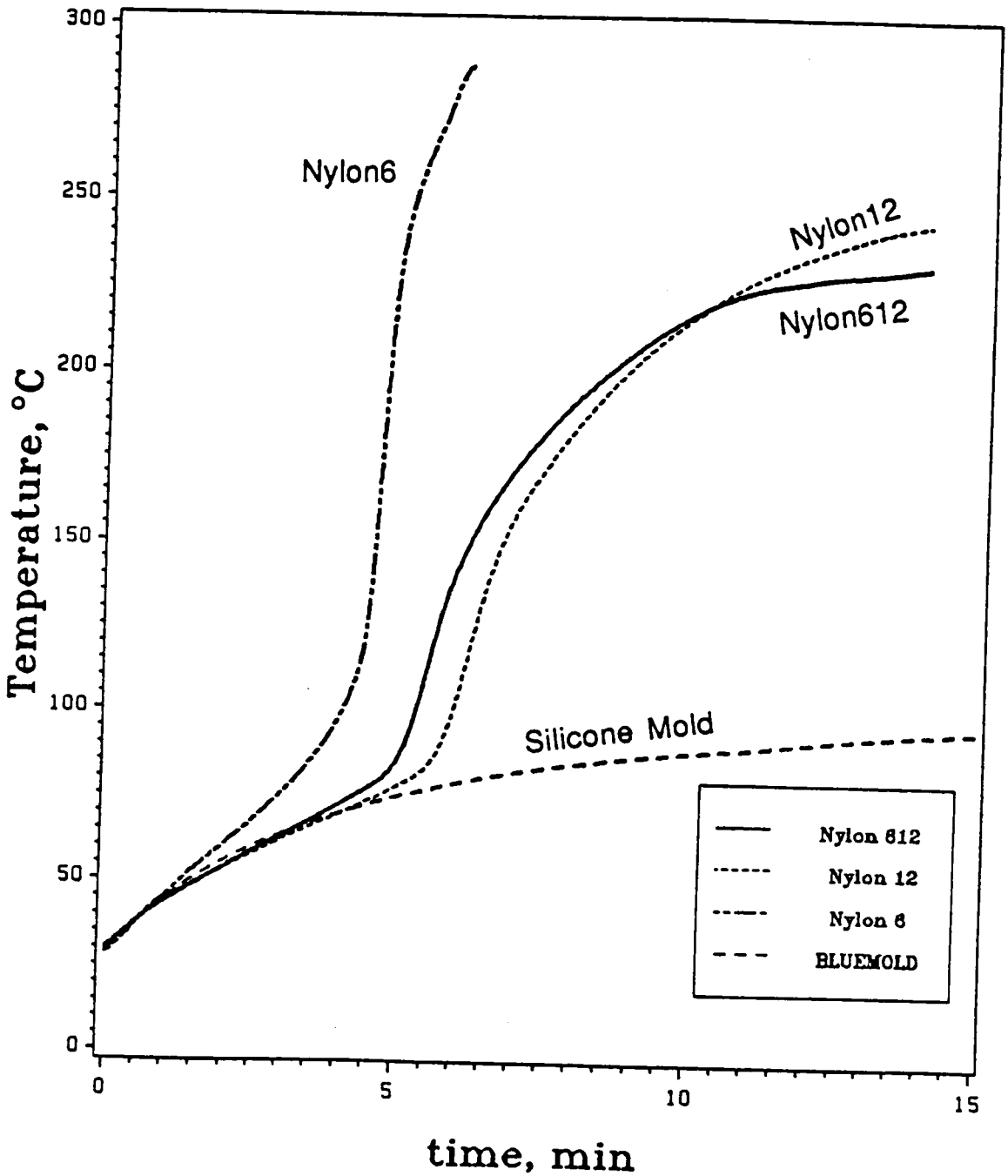

Figure 5.13 Variation of the temperature of nylons and silicone mold with time in the center of TE_{111} mode of a cylindrical cavity applicator. Input power was 20 watts.

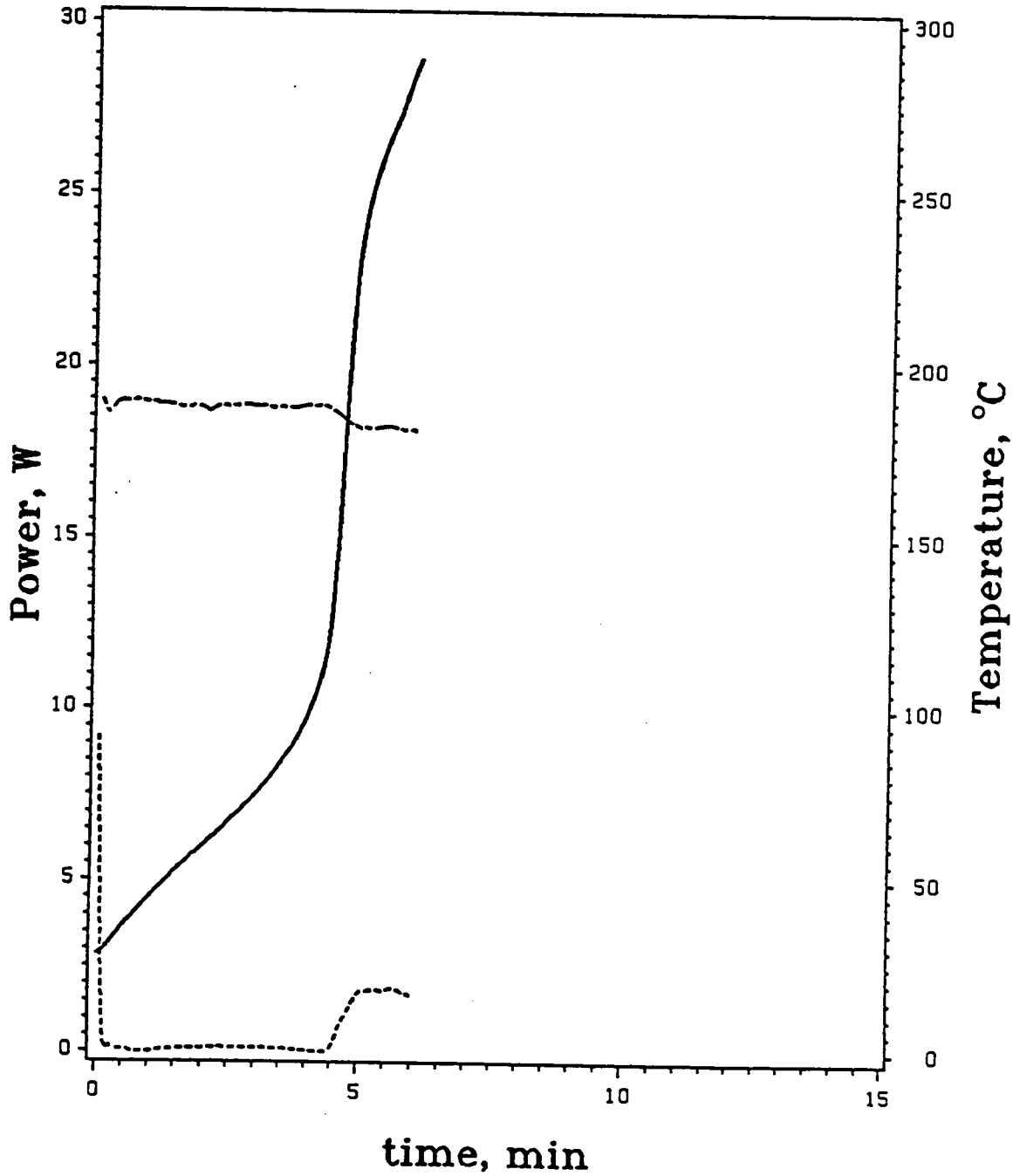

TOP :INPUT POWER
BOTTOM :REFLECTED POWER
SOLID LINE :TEMPERATURE

Figure 5.14 Variation of the temperature, input power and reflected power with time for nylon 6 in the center of TE_{111} mode of a cylindrical cavity applicator.

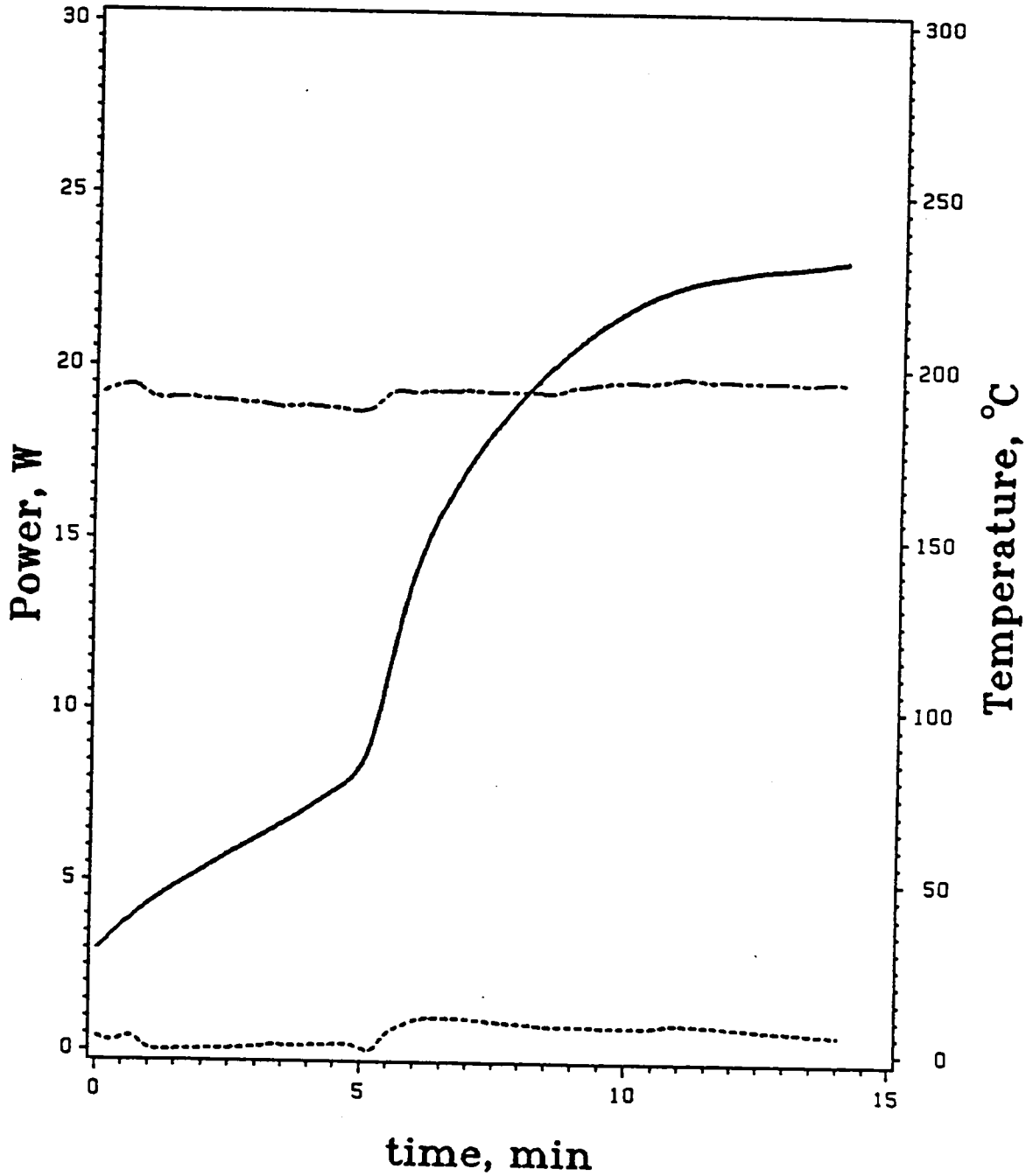

TOP :INPUT POWER
BOTTOM :REFLECTED POWER
SOLID LINE :TEMPERATURE

Figure 5.15 Variation of the temperature, input power and reflected power with time for nylon 612 in the center of TE_{111} mode of a cylindrical cavity applicator.

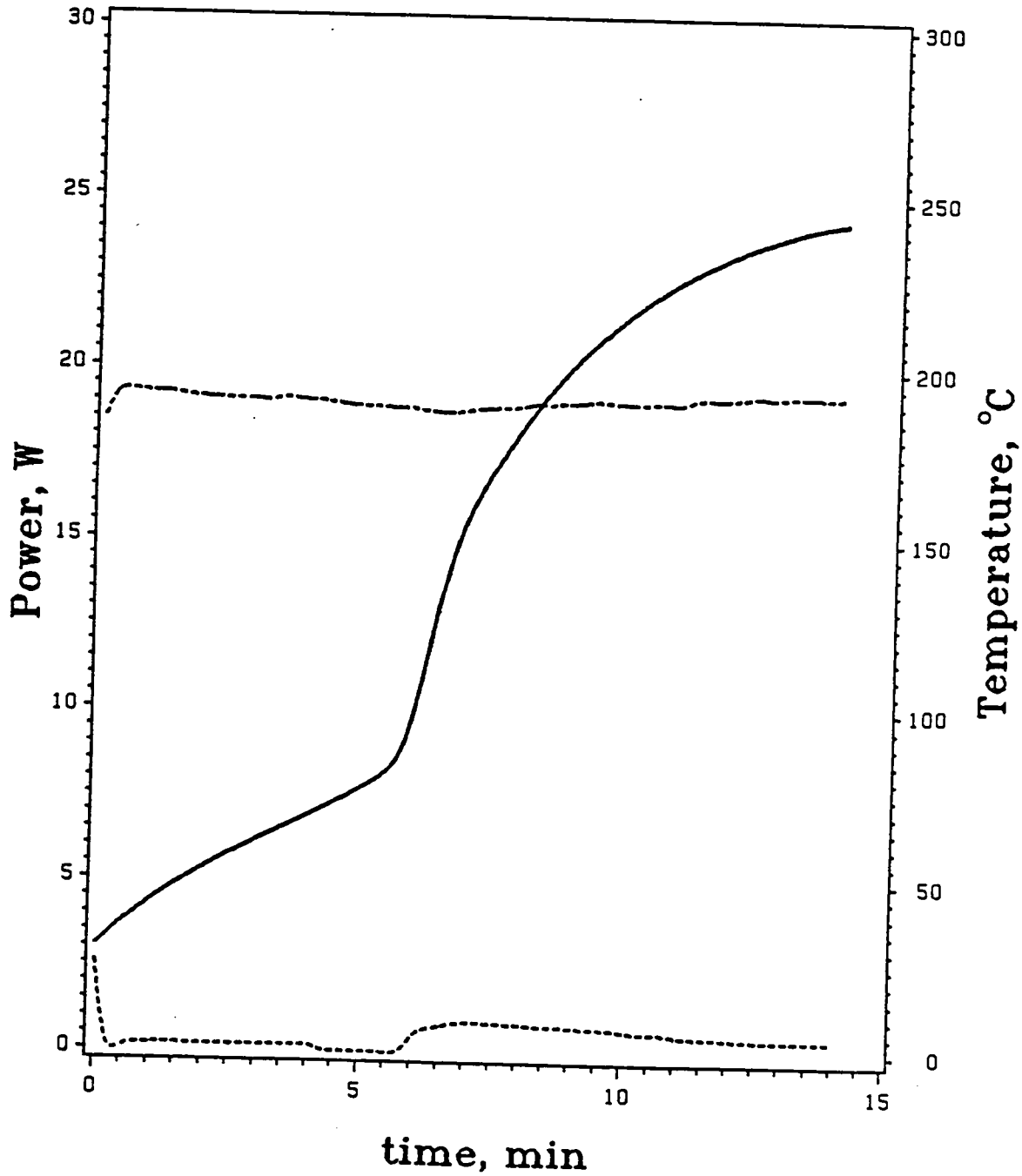

Figure 5.16 Variation of the temperature, input power and reflected power with time for nylon 12 in the center of TE_{111} mode of a cylindrical cavity applicator.

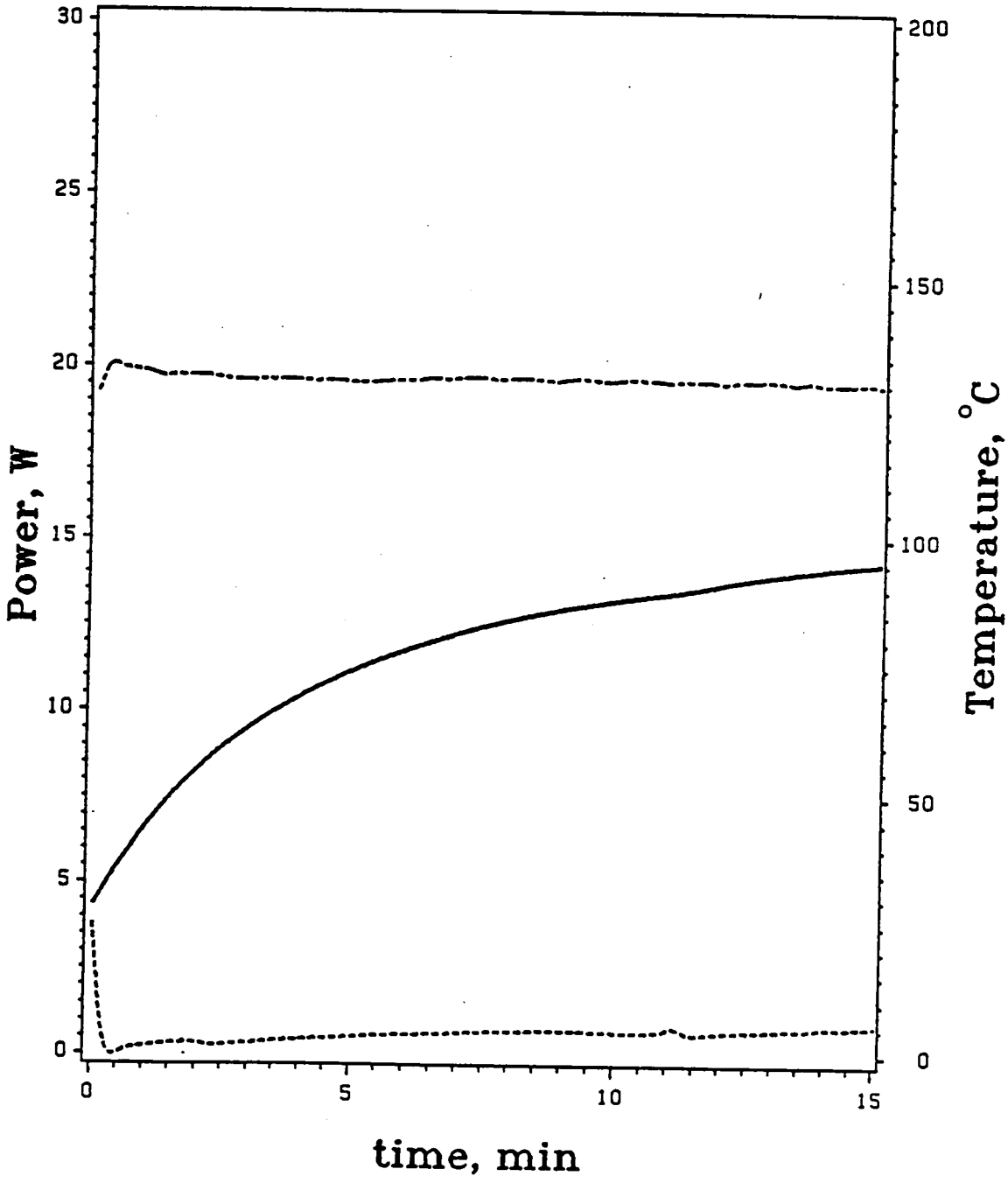

TOP :INPUT POWER
BOTTOM :REFLECTED POWER
SOLID LINE :TEMPERATURE

Figure 5.17 Variation of the temperature, input power and reflected power with time for silicone mold in the center of TE_{111} mode of a cylindrical cavity applicator.

silicone mold. The positive slope, $d\varepsilon''/dT$, from the ε'' vs. temperature plot resulted in an uncontrolled rise in temperature in the case of nylon6. This was termed the "runaway effect". The function of the silicone mold was similar to the function of the strip heater in the preceding chapters. The microwave energy absorption of nylons was thereby improved by the action of the silicone mold. Figure 5.18 is a plot of heating rate vs. temperature for nylon6 under these conditions. The critical temperatures for all of the semicrystalline polymers described in this chapter were not evaluated because the silicone mold contributed to the heating rate of the polymers which skewed their intrinsic T_c's. The maximum heating rate was about 360°C/min which is much faster than expected for thermal conductivity in conventional thermal heating.

Figure 5.19 presents the variation of powers and temperature with time for amorphous PEEK. The input power was 43 watts which was about twice that used for the nylons. The nominal T_g of PEEK obtained by DSC was greater than 140°C and was dependent on the percentage of crystallinity. Thus, the silicone mold was heated first when starting at room temperature. The heat flowed from silicone mold to the PEEK specimen via thermal conduction at temperatures below the T_c of PEEK. After 7.5 min., the temperature of PEEK was at approximately 170°C and the rate of temperature rise was increasing. Due to the high activation energy and fast crystallization rate, T_c of amorphous PEEK was expected to be very close to its T_g. The high content of phenyl and ether groups in PEEK lowered the dipolar contribution of the polar ketone group. Thus, the temperature rise was under control for the low loss PEEK. After 11 min., the sample temperature tended to level off.

Figure 5.20 shows the variation of powers and temperature with time for semicrystalline PEEK. At around 9 min., the temperature rose significantly. The heating rate of the semicrystalline PEEK was a little slower than that of amorphous

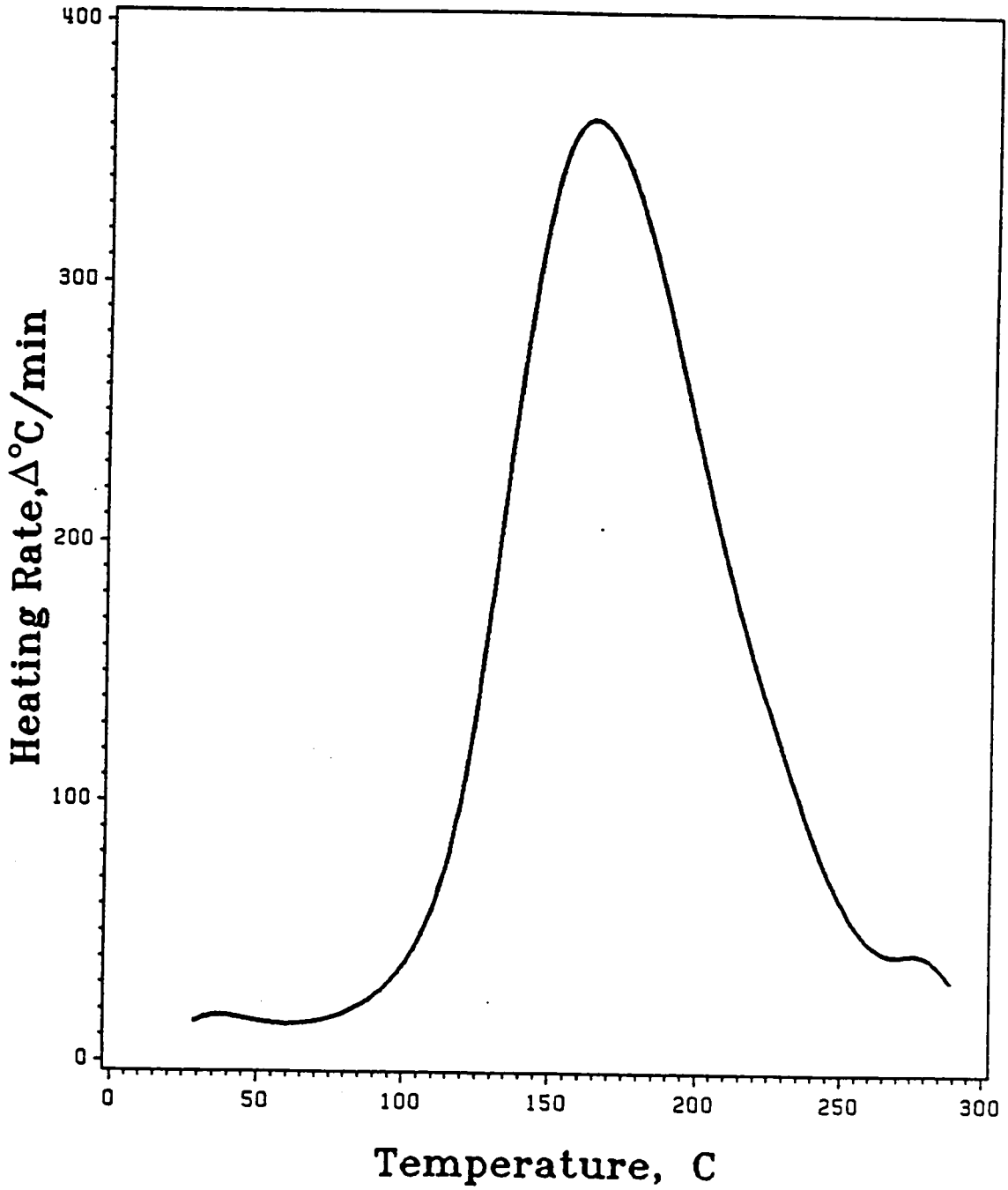

Figure 5.18 Heating rate of nylon 6 versus temperature in the center of TE_{111} mode of a cylindrical cavity applicator.

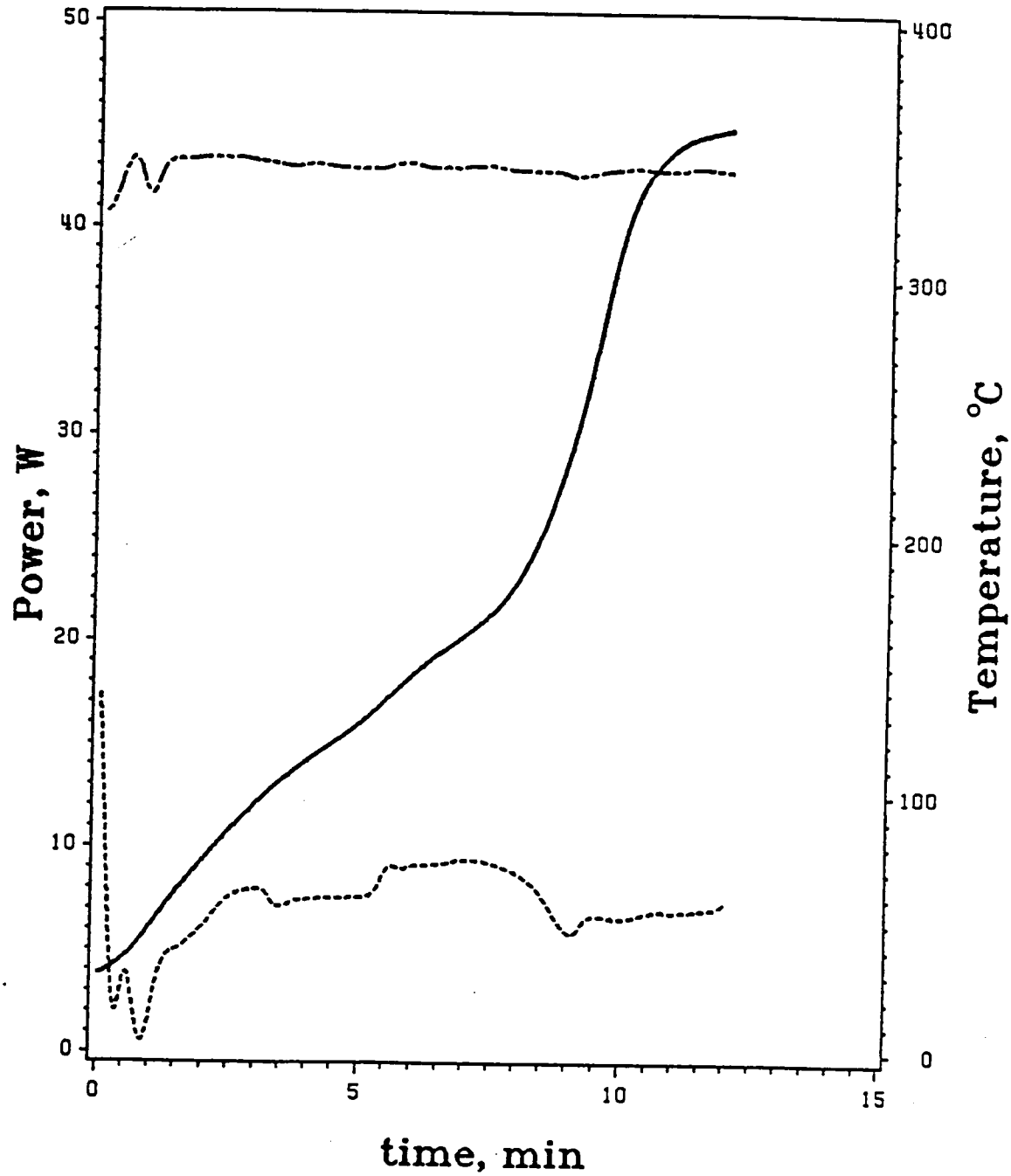

TOP :INPUT POWER
BOTTOM :REFLECTED POWER
SOLID LINE :TEMPERATURE

Figure 5.19 Variation of the temperature, input power and reflected power with time for amorphous PEEK in the center of TE_{111} mode of a cylindrical cavity applicator.

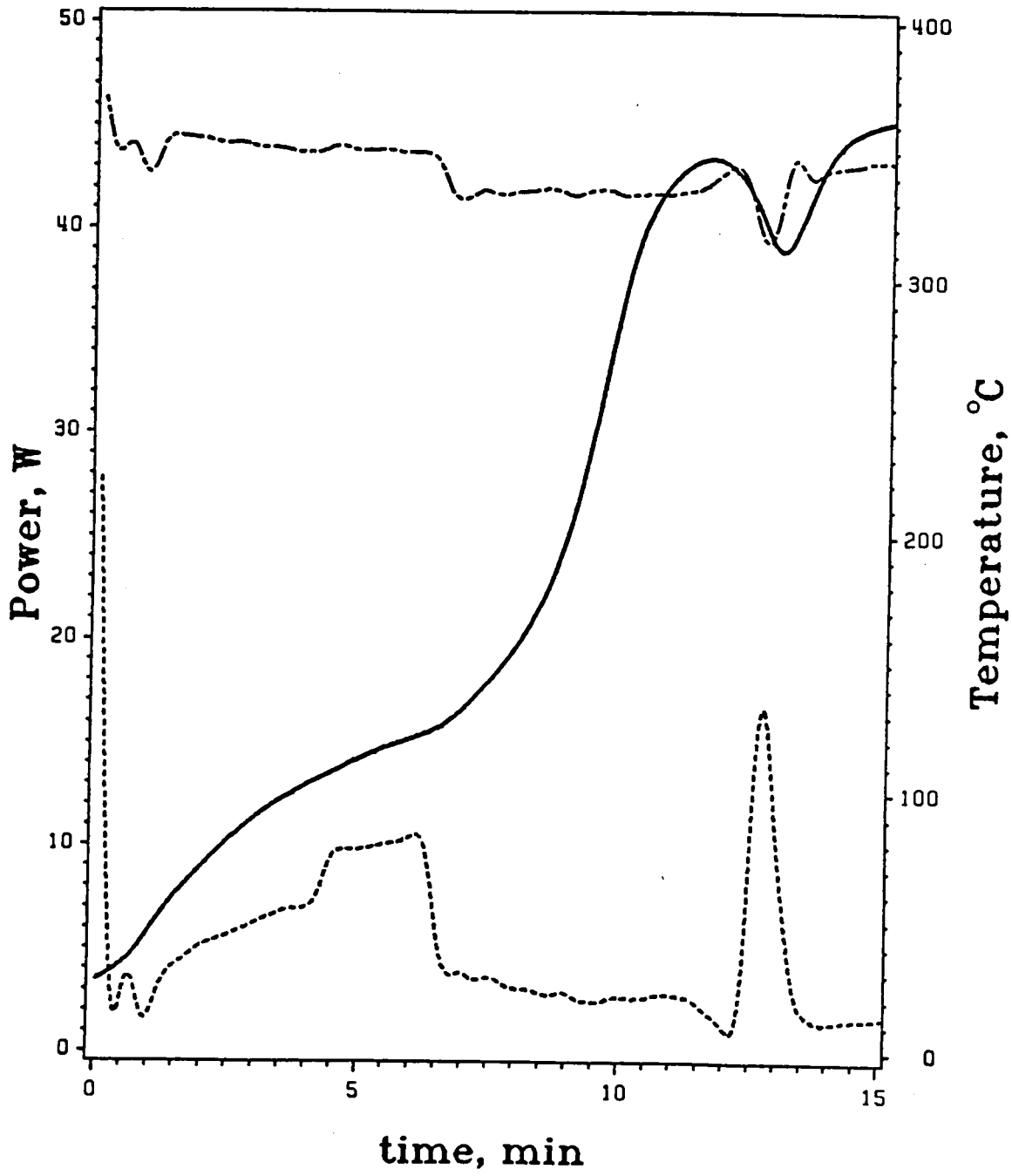

TOP :INPUT POWER
BOTTOM :REFLECTED POWER
SOLID LINE :TEMPERATURE

Figure 5.20 Variation of the temperature, input power and reflected power with time for semicrystalline PEEK in the center of TE_{111} mode of a cylindrical cavity applicator.

PEEK. The similarity of heating rates may be due to two reasons. (1) Rapid crystallization occurs at temperatures just above T_g. (2) The heat capacity of the crystalline polymer is lower than the amorphous version. In Figure 5.20, there was an endothermic peak between 12 and 14 minutes. The temperature dropped at around 350°C which was close to the T_m of PEEK similar to DSC endothermy. This illustrates one reason why this experimental method is termed "microwave calorimetry."

Figure 5.21 represents the variation of powers and temperature with time for PET in a rectangular standing wave applicator shown in Figure 3.4. The input power was around 20 watts. The temperature increased slowly in the first 2.5 minutes. After 100°C, which may already be in the positive $d\varepsilon''/dT$ region, the temperature rose rapidly. The reflected power increased continuously after 3.5 minutes. PET was heated to its T_m in 5 min. by microwave processing. Interestingly, this rapid heating rate may cause different kinetic phenomena as compared to conventional thermal heating when the temperature passes through the crystallization zone. In the case for both PET and nylon6, the heating phenomena showed the thermal runaway effect. Either decreasing the microwave energy or processing by pulsed control is necessary to avoid this runaway.

5.4 CONCLUSION

The silicone flexible mold or other possible energy "receivers" was very helpful in improving the energy absorption of nylons and PEEK at temperatures below their T_c. Above T_c, nylons and PEEK absorbed the microwave energy internally to rapidly heat above their respective melting points. Nylons, PEEK and PET, with a wide window

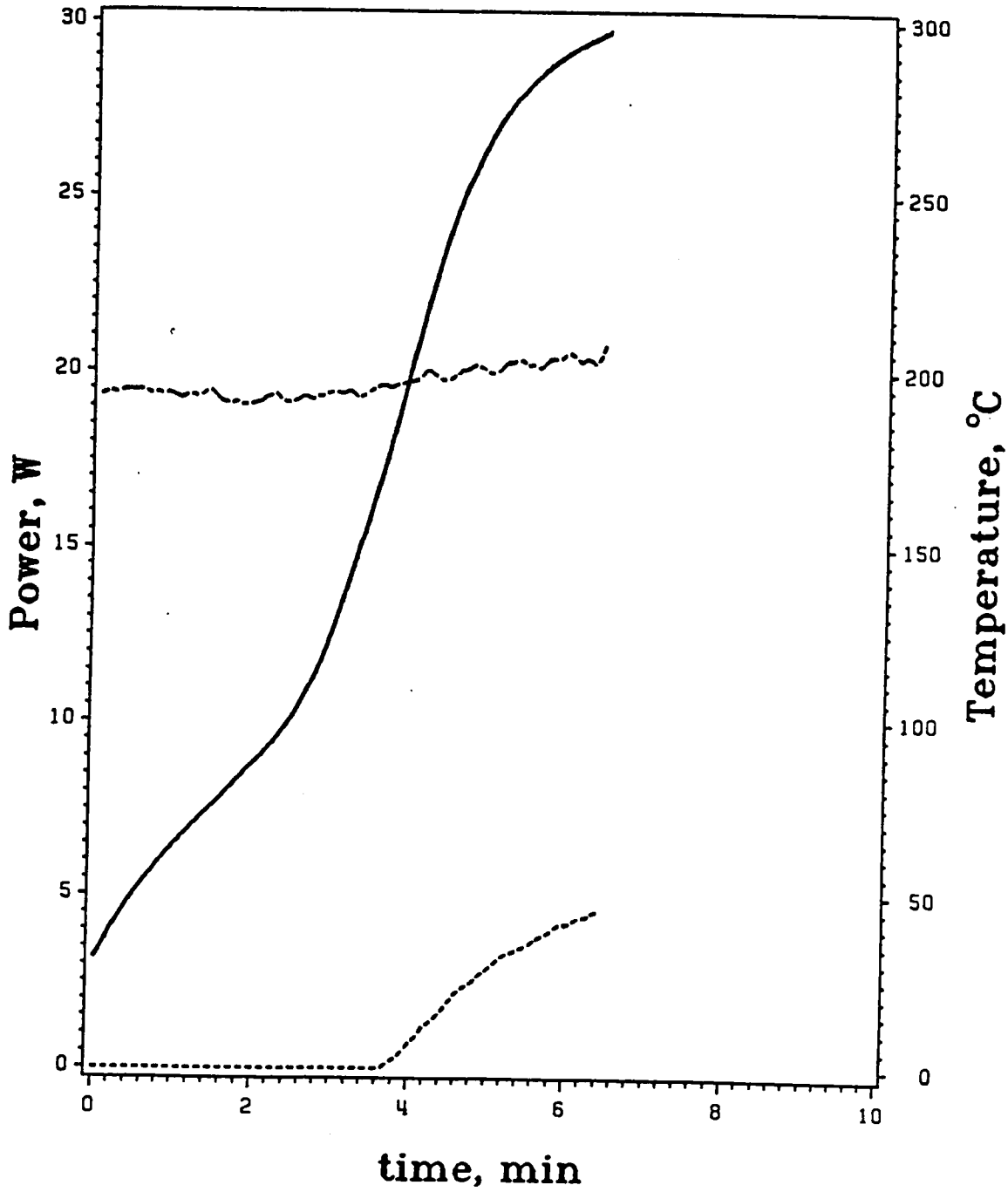

TOP :INPUT POWER
BOTTOM :REFLECTED POWER
SOLID LINE :TEMPERATURE

Figure 5.21 Variation of the temperature, input power and reflected power with time for PET in the standing wave applicator with a stub tuner.

between T_g and T_m, were processed easily by microwave energy because of the rapid heating rates at temperatures just above their T_g's. Thus, their processing times and costs can be reduced. This fast heating rate can overcome the problem of low thermal conductivity of polymers, but computer monitoring of the signal would be needed to control the temperature by turning on/off power pulsing. Since microwave processing can heat semicrystalline polymers above their melting points rapidly, another possible application would be to use the low cost microwaves to maintain samples above their T_m while they are further processed, eg., molded.

DETA spectra in the kHz region and DMTA spectra in the Hz region were used to explain the similar heating rates of amorphous and semicrystalline PEEK at 2.45 GHz. Amorphous PEEK rapidly decreased in modulus at temperatures just around the T_g, but regained parts of the drop as a result of the fast crystallization which occurred just above T_g in temperature. Therefore, both materials became semicrystalline during microwave processing, at least with a processing power of 43 watts. When a material is heated between its T_g and T_m, its rate of crystallization determines the amount of crystallinity which can develop. It may be possible in microwave processing at very high electric field strength, however, to outrun the rate of crystallization so that it is even easier to heat the material above its melting point producing fewer crystallites.

The heating rate of nylons depended on the percentage of amide group (or hydrogen bonding) in the main chain. The crystallinity not only decreased the values of ε'', but also moved the maximum of the α- and β-relaxations to higher temperatures (or lower frequencies). The change in crystallinity affected the α-relaxation processes more than the β relaxation processes. In terms of microwave processing, it is important to consider the effect of crystallinity on the position of the dielectric loss peaks as well as their loss peak amplitudes.

5.5 REFERENCES

1. A. C. Metaxas and R. J. Meredith, ***Industrial Microwave Heating,*** Peter Peregrinus, London, 1983.

2. D. A. Copson, ***Microwave Heating,*** 2nd ed., The Avi Publishing Co., Connecticut, 1975.

3. E. C. Okress, ***Microwave Power Engineering,*** Vol. 2: Applications, Academic Press, New York, 1968.

4. P. Fellows, ***Food Processing Technology: Principles and Practice,*** E. Horwood Ltd., New York, 1988.

5. M. Le Maguer and P. Jelen, ***Food Engineering and Process Applications,*** **Vol. 1: Transport Phenomena,** Elsevier Applied Science Publishers, New York, 1986.

6. H. F. Mark, N. M. Bikales, C. G. Overberger and G. Menges, ***Encyclopedia of Polymer Science and Engineering,*** **Vol. 5**: Dielectric Heating to Embedding, 2nd ed., John Wiley & Sons, New York, 1986.

7. J. Jow, M. C. Hawley, M. C. Finzel and J. Asmussen, *J. Microwave Power EE*, **24**, (1989).

8. J. Jow, J. D. Delong and M. C. Hawley, *SAMPE Quarterly*, **20(2)**, 46 (1989).

9. J. Jow, M. C. Hawley and M. Finzel, *Rev. Sci. Instrum.*, **60**, 96 (1989).

10. J. Jow, M. C. Hawley, M. Finzel and T. Kern, *Polym. Eng. Sci.*, **28**, 1450 (1988).

11. J. Jow, M. C. Hawley, M. Finzel, J. Asmussen, Jr., H. H. Lin and B. Manring, *IEEE Trans. Microwave Theory Tech.*, **MTT-35**, 1435 (1987).

12. J. Asmussen, H. H. Lin, B. Manring and R. Fritz, *Rev. Sci. Instrum.*, **58**, 1477 (1987).

13. B. Manring, Master, Michigan State University, East Lansing, MI, 1988.

14. H. F. Huang, *J. Microwave Power*, **11**, 305 (1976).

15. M. Amano and K. Nakagawa, *Polym. Commun.*, **28**, 119 (1987).

16. M. Amano and K. Nakagawa, *Polymer*, **28**, 263 (1987).

17. K. Nakagawa and T. Konaka, *Polymer*, **27**, 1553 (1986).

18. Y. Takeuchi, K. Nakagawa and F. Yamamoto, *Polymer*, **26**, 1929 (1985).

19. K. Nakagawa, T. Konaka and S. Yamakawa, *Polymer*, **26**, 84 (1985).

20. Y. Takeuchi, F. Yamamoto, K. Nakagawa and S. Yamakawa, *J. Polym. Sci. Polym. Phys. Ed.*, **23**, 1193 (1985).

21. K. Nakagawa, O. Maeda and S. Yamakawa, *J. Polym. Sci. Polym. Lett. Ed.*, **21**, 933 (1983).

22. A. E. Zachariades and R. S. Porter, ***High Modulus Polymers: Approaches to Design and Development***, Marcel Dekker, Inc., New York, 1988.

23. V. K. Varadan, V. V. Varadan, Y. Ma and W. F. Hall, *IEEE Trans. Microwave Theory Tech.*, **MTT-34**, 251 (1986).

24. T. K. Ishii, ***Microwave Engineering***, The Ronald Press Co., New York, 1966.

25. Y. F. Chen and Charles Y. C. Lee, *Polym. Mater. Sci. Eng.*, **60**, 680 (1989).

CHAPTER 6

MICROWAVE PROCESSING OF TWO PHASE SYSTEMS: COMPOSITES AND POLYMER BLENDS

6.1 INTRODUCTION

In the preceding chapters, several methods were examined to predict the absorption of microwave energy by polymers. For copolymers of acrylonitrile and butadiene (nitrile rubber) discussed in chapter 2, the power absorption, P_a, increased with increasing acrylonitrile content. The polar acrylonitrile group absorbed energy by interacting with the microwave field which subsequently heated the entire sample. As a result of the increasing temperature, the dicumyl peroxide incorporated in the copolymer during solvent casting decomposed to serve as a source of radicals for crosslinking. Glassy thermoplastics required different processing conditions due to their low dielectric losses at room temperature in the microwave region. By externally heating the thermoplastics, their dielectric relaxation spectra were shifted into the microwave region which resulted in more efficient coupling of microwave energy. By use of a silicone mold, having a broad loss spectrum, the samples were found to heat easily to their T_c's via heat flow from the silicone mold to the specimen. Above their T_c,'s, specimens intrinsically absorbed the microwave energy.

In the rubber industry, the heatability of low polarity polymers is commonly enhanced by adding various fillers including carbon black, diethylene glycol or triethanolamine. Carbon black is one of the most effective fillers for raising the dielectric constants of elastomers for processing via microwave energy. It adds to the relaxation spectrum. In all of the cases discussed in the preceding chapters, the

movement of the dielectric relaxation spectra into the microwave region by directly or indirectly increasing the temperature of the sample was of key importance, as in the carbon black case.

Thus, in this chapter, a schematic model is proposed to investigate the behavior of two phase materials upon subjecting to microwave heating. Such materials include graphite composites and polymer blends, and could include filled materials. Several potential applications of microwave processing to composite materials are also suggested. Many articles have recently appeared in the literature on the microwave processing of composites based on graphite fibers (1-3), glass fibers (4), carbon black (5) and metal powders (6-9). In general, researchers found that microwave processing of composites was quite effective. Other researchers have worked with the microwave drawing behavior of polymer blends (10). This chapter emphasizes how microwave calorimetry can be used to better understand the processing of two phase systems in general.

6.2 MODEL

In chapter 2, the importance of the variation of the dielectric constant, ε', and the dielectric loss factor, ε'', with frequency and temperature was discussed. The shift toward higher frequency for high activation energy α relaxations was faster than that for the lower activation energy β relaxations as frequency was increased. This principle can be applied to two phase materials. The ε' and ε'' of two phase material at various temperatures are schematically depicted in Figure 6.1. In this example, the first phase is assumed to have dispersions at a higher frequency which have a lower activation energy relative to the β relaxation. The second phase dispersion is centered at a lower

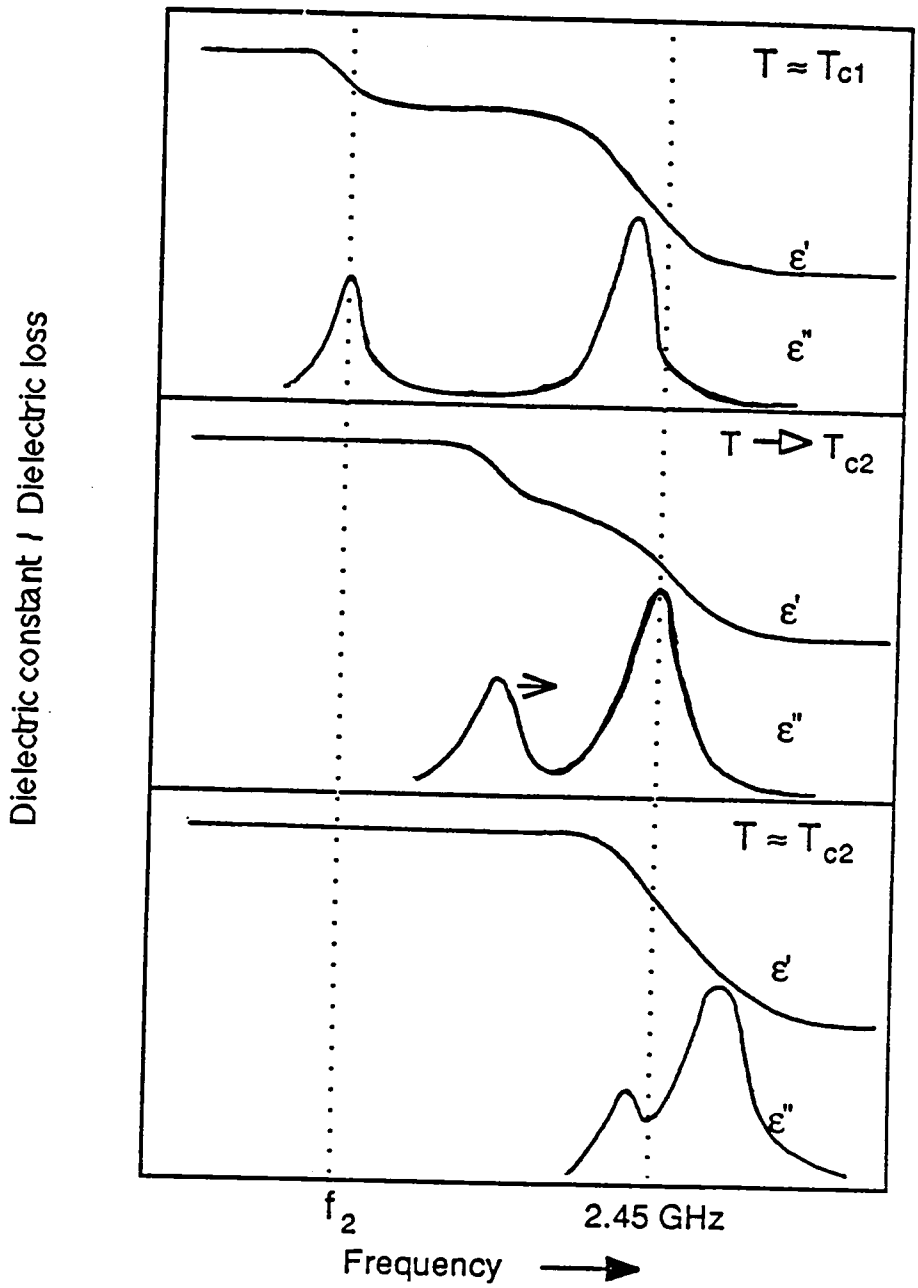

Figure 6.1 Schematic representation of the dielectric behavior of two phase material at various temperatures.

frequency and has a higher activation energy compared to the α relaxation. At the critical temperature, T_{c1}, of dielectric loss in phase 1, the dielectric loss dispersion for phase 2 is still that of background loss. Upon reaching T_{c1}, phase 1 begins to heat causing phase 2 to heat by thermal conduction. When the temperature approaches T_{c2}, the two relaxation spectra come closer together. In the ideal case, both dispersions merge at temperatures below T_{c2}. Upon further heating, phase 2 begins to couple with the microwave energy so that the entire sample becomes microwave active. In ideal cases such as this, the change in dielectric constant from high frequency to low frequency, $(\varepsilon_s - \varepsilon_\infty)$, will be smooth. It is also important to know the magnitude of the two dielectric relaxation losses in order to control the heating rate and temperature. In some cases, if the applied microwave power is not high enough, there is probably a gap between these two dielectric relaxation spectra. Because power absorption is proportional to the square of the electric field strength and the rapid heating rate begins when the 'cool side' of the dielectric relaxation spectra reaches the microwave region, it may be possible to shift the dielectric relaxation of phase 2 into the microwave frequency region. Therefore, a continuous temperature increment may be observed on microwave processing of two phase materials.

6.3 EXPERIMENTAL

6.3.1 Materials

For the composite processing experiment, Hercules As4 Graphite/Epoxy prepregs were cut to the dimension of 2.5 cm x 1 cm and were laid up into cross plies of $(0/90)_3$.

For the physical blend study, poly(methyl methacrylate), with a number average molecular weight of 1.39×10^5 g/mole and a polydispersity of 2.30 (see chapter 4), was

obtained from Inland Leidy company in powder form. Poly(vinylidene fluoride), PVDF, in powder form, was purchased from Scientific Polymer Products (catalog number 102). The T_g and T_m of PVDF were -38°C and 171°C, respectively, as stated in the catalog. Both PMMA and PVDF were used without further purification. A Bel-Art Products' micro-mill was used to blend these two polymers. PMMA and PVDF having a 50/50 weight ratio were physically blended for 10 min. in the micro-mill. This blend was then pressed into a half-filled 3.3 cm high by 1.27 cm inside diameter cylindrical teflon sample holder at 10^4 psi by using a platten press (Pasadena Hydraulics, Inc. Model number P210C-X3-5-7-20).

6.3.2 Microwave Instrumentation

Two different rectangular waveguide applicators were used to process the Graphite/Epoxy laminate. The first cavity was a standing wave applicator (see chapter 4). The second was a travelling wave applicator with a stub tuner mounted between the adapter and the waveguide, as shown in Figure 6.2. The details of the experimental instrumentation were described in the preceding chapters. Two $(0/90)_3$ laminates were separated by a teflon sheet (0.005 in. thick) and placed into a teflon sample holder. The sample holder was put at the midpoint across the wider face of the rectangular waveguide. A fiber-optic temperature probe was mounted inside the lid of the teflon sample holder. The tip of the fiber-optic probe was very close to the laminate but was kept from physically contacting the sample by carefully machining the teflon lid to leave a thin layer of teflon between the sample and the probe.

The PMMA/PVDF blend was processed in a cylindrical cavity applicator (see chapter 5). The PMMA/PVDF blend filled only half of the teflon sample holder. The fiber-optic temperature probe was passed through a hole in the teflon lid of the sample holder in order to come in physical contact with the top surface of the blend. A silicone

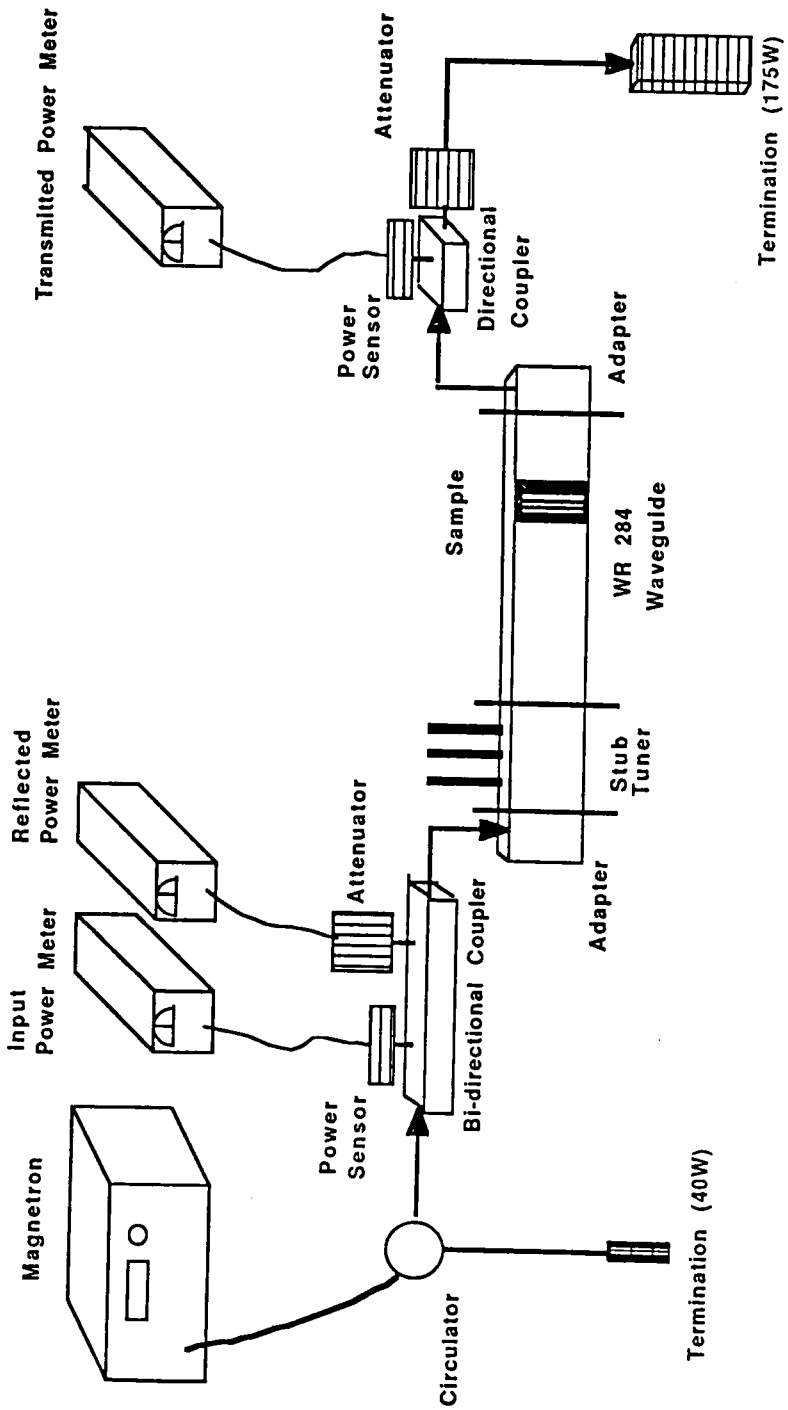

Figure 6.2 Schematic of the experimental set-up for the travelling wave applicator with a stub tuner.

mold (2 cm x 2 cm x 1.7 cm) was used to support the teflon sample holder and to raise the top surface of the blend to the center of the TE_{111} mode in the cavity.

6.4 RESULTS AND DISCUSSION

6.4.1 Microwave processing of composites

Figure 6.3 illustrates the variations in input power, reflected power and approximate sample temperature as a function of time for two $(0/90)_3$ Graphite/Epoxy laminates. Graphite fibers are highly conductive materials, as shown in Figure 6.4 (11). The conductive properties of graphite fibers made the laminates behave like a metal wall and thus to act as a good reflector. Thus, the reflected power, as shown in Figure 6.3, was very high without the adjustment of the stub tuner. The difference between the input power and the reflected power was only 5 watts initially. The approximate temperature increased slowly with time. By adjusting the stub tuner between 6 min. and 9 min. after power was applied, the reflected power was decreased to 2 watts, and the input power was increased about 1 watt. The difference between the input power and the reflected power increased four to five-fold. Because the power absorbed by the material increased with the square of the electric field strength, the heating rate was accelerated by the increased field strength as evidenced by the rapid rise in temperature. This experiment demonstrated that the efficiency of the conversion of microwave energy to heat was increased by using the stub tuner. After 9 min., the temperature increment became slower. These were due to several reasons. Below 8 min., the viscosity of epoxy was high, the relaxation spectra of the epoxy was outside 2.45 GHz region. Thus, before that time, only the graphite fibers were coupled with the microwave energy. After the electric field strength was increased by adjusting the stub

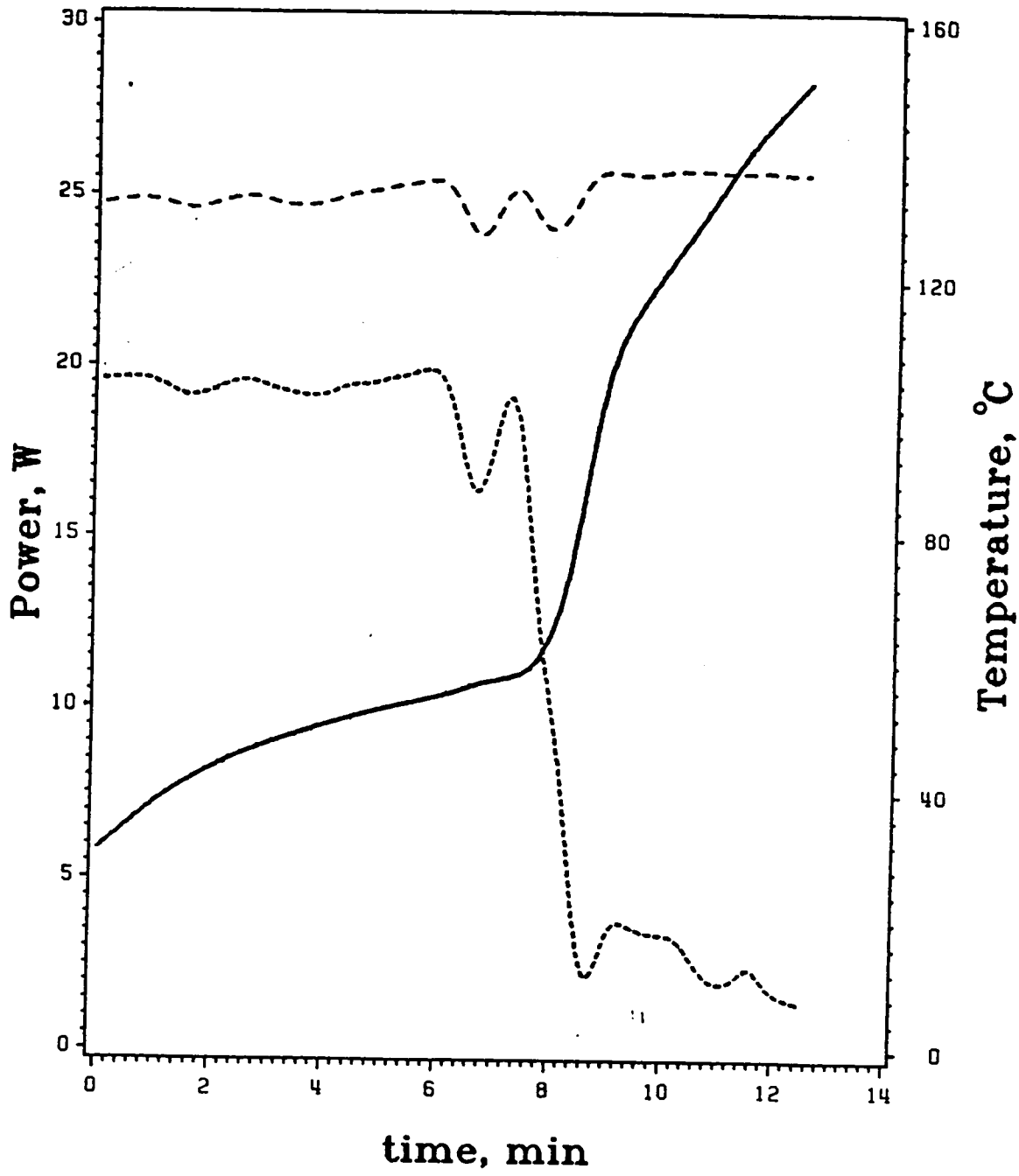

Figure 6.3 Variation of the approximate sample temperature, input power and reflected power with time for two $(0/90)_3$ Graphite/Epoxy laminates in the standing wave applicator with a stub tuner.

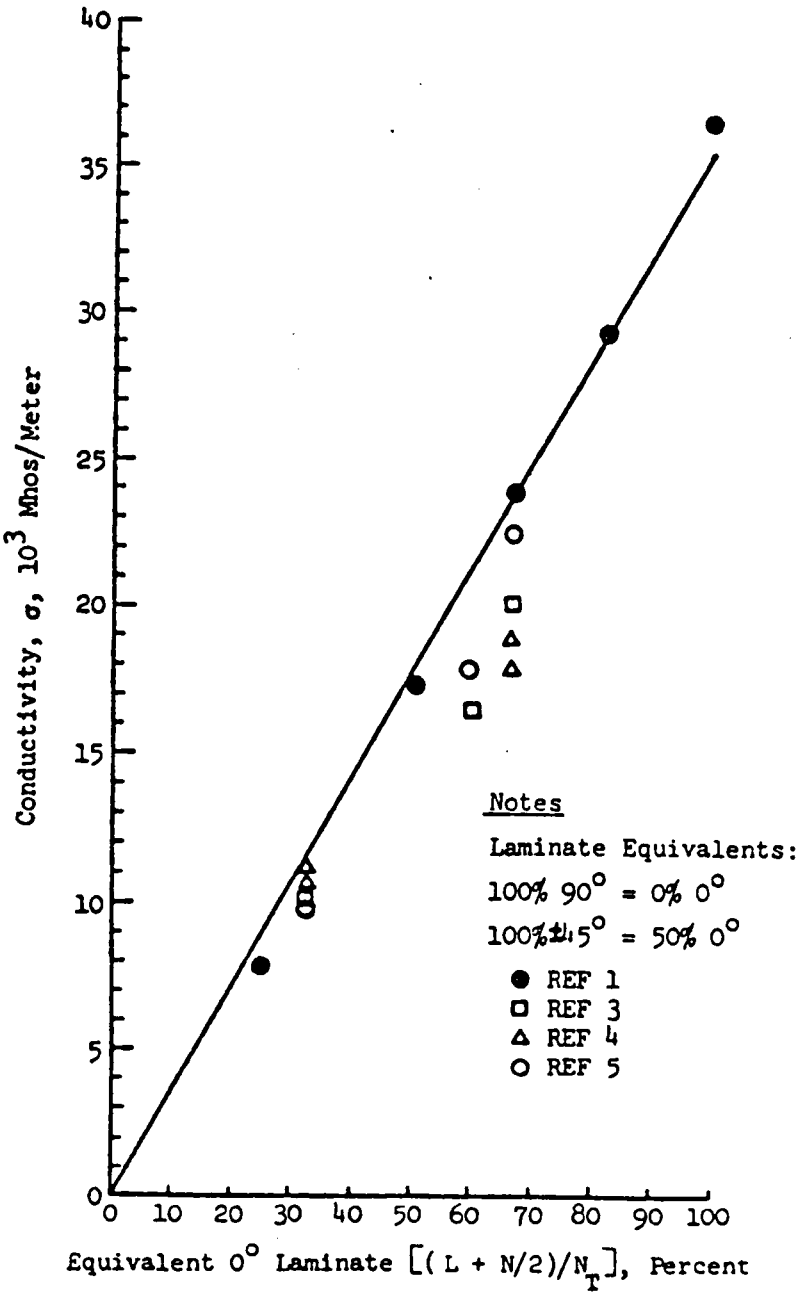

Figure 6.4 Electrical conductivity of AS3501/5A Graphite/Epoxy laminates at room temperature. (11)

tuner, the rapid heating resulted in a large temperature increase. This temperature rise was sufficient to reduce the viscosity of the epoxy, and to move the dielectric relaxation spectrum of the epoxy resin into the 2.45 GHz frequency region. Therefore, the epoxy resin started to absorb the microwave energy. In addition, the curing reaction of an epoxy resin is exothermic. These three factors - increasing electric field strength, direct absorption of microwave energy by the epoxy resin and the release of energy by the exothermic curing reaction - resulted in the rapid heating rate between 8 and 9 minutes. Curing of the epoxy resulted in a decreased concentration of polar groups and decreased segmental mobility. As the temperature difference between the composites and the environment increased, the energy loss due to the thermal convection became larger. Thus the heating rate after 9 min. became slower. In this experiment the top edge rather the center part of the Graphite/Epoxy composite was charred. This may be due to the disturbance of the electric field by the presence of conductive graphite fibers (3). This effect together with the temperature gradient inside the conductive composite undergoing microwave processing needs further study.

In Figure 6.5, three power levels and the approximate temperature are plotted vs. time for Graphite/Epoxy laminates in the travelling wave applicator. Input power was kept at 77 watts. Reflected power was adjusted to zero at the onset of the experiment by using the stub tuner. The transmitted power, P_t, was 53 watts initially. The difference between P_i and P_t, 24 watts, however, was relatively large compared to the experiments on nitrile rubbers, as described in chapter 3. These laminates were such high loss materials that the approximate temperature rose rapidly for the first 6 minutes. The transmitted power, P_t, decreased slowly only until the sample began to heat rapidly at 2 min. after the power was applied. Then P_t decreased rapidly by 7 watts, and leveled off. The reflected power, P_r, was near zero during the processing. These

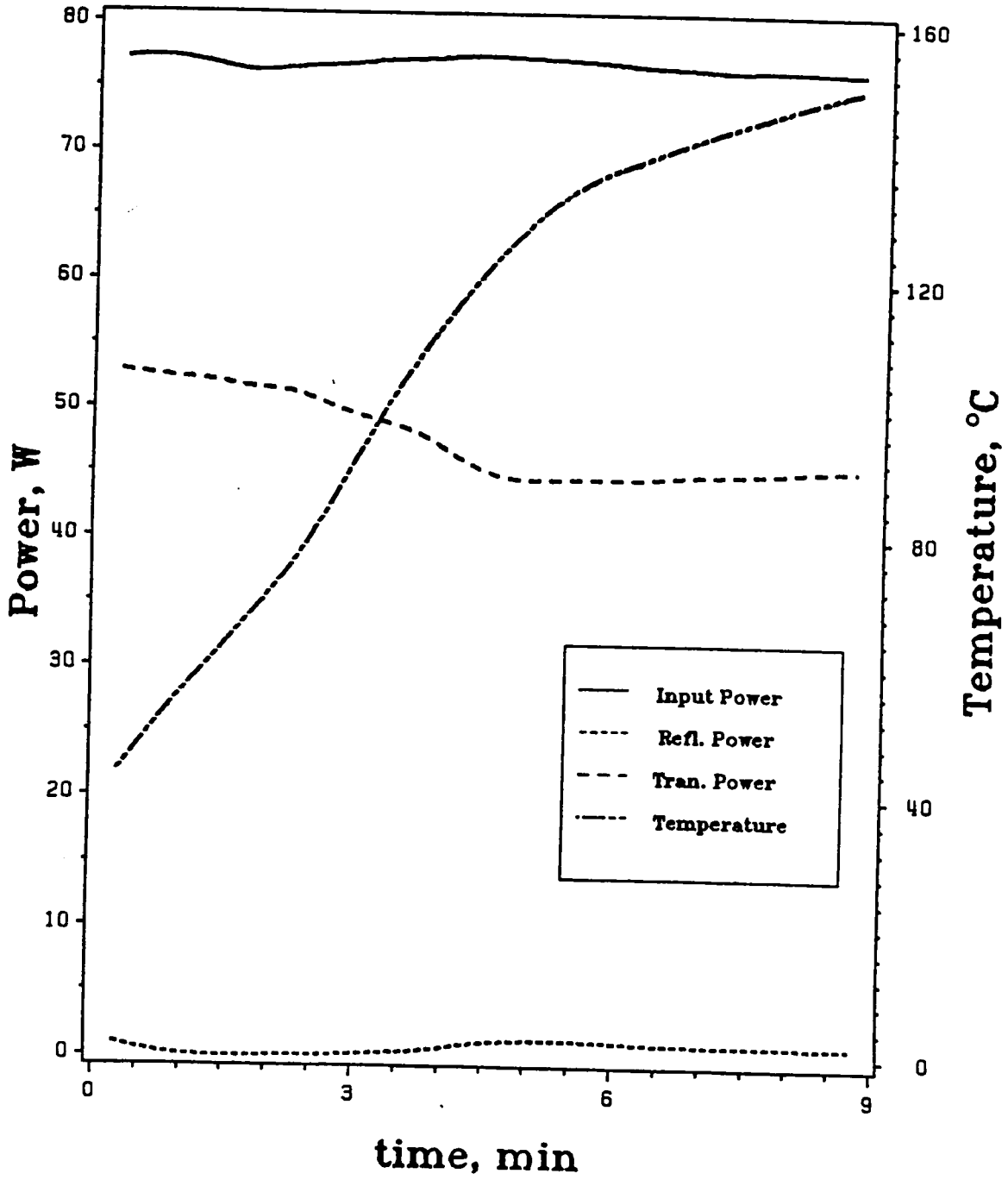

Figure 6.5 Variation of the approximate sample temperature, input power, transmitted power and reflected power with time for two $(0/90)_3$ Graphite/Epoxy laminates in the travelling wave applicator with a stub tuner.

results indicated that the energy absorbed by the laminates increased with temperature in this 9 min. experiment. A similar phenomenon was found in comparing the standing and the travelling wave experiments. The microwave energy coupled first with the graphite fibers and was subsequently conducted to the epoxy resin matrix at temperatures below the T_c of the resins. Above this T_c, the epoxy resins absorbed microwave energy without any aid. Thus, the heating rate increased at about 2.5 min. Curing and thermal convection of heat from composites to the room temperature environment caused the temperature to rise slowly.

One of the objectives of this research was to investigate the potential for field repair of a composite structure by microwave processing. Curing of composites in an autoclave is currently a high cost operation, especially for large and thick parts. Residual stress develops due to the uneven dimension and uneven heating. From the advantages of microwave processing described in chapter 5, the deep penetration of microwaves offers a possibility of uniform curing regardless of the geometry of the parts. However, in resonant cavities, to stay in tune, the frequency as well as the electric field strength decreases as the size of the rectangular or circular waveguide increases. In the microwave frequency region, only the travelling wave applicator may be practically utilized for field repair. The reduction of the high reflectance of Graphite/Epoxy laminates by using the stub tuner was clearly demonstrated above. This effect caused a higher electric field strength to built up inside the laminates. In both the standing and the travelling wave applicators, the temperature rose rapidly within 10 minutes. A portable microwave unit can therefore be used for rapid patching and to fix damage to a composite structure. To avoid possible exposure to excessive microwave energy, robotic systems are suggested to execute the field repair task.

6.4.2 Microwave processing of polymer blends

Before discussing the microwave processing of PMMA/PVDF polymer blends, one needs to investigate the dielectric behavior of PMMA and PVDF over a wide frequency range. The dielectric properties of PMMA were already discussed in chapter 4. Since PMMA possesses a large β dielectric loss relaxation, there was an induction heating period below 150°C in the microwave processing experiment. The T_c of PMMA was 185°C (which was 80°C above its T_g measured by DSC) at 2.45 GHz. In contrast to PMMA, PVDF has highly polar carbon-fluorine bonds and a low T_g, -38°C. The dielectric constant and loss tangent of PVDF are shown in Figure 6.6 (12). The dielectric relaxation spectra at room temperature is seen to be in the 2.45 GHz region from the bottom curve. In the top curve, the dielectric constant increased with decreasing frequency (increasing temperature). Thus, the dielectric loss factor at 2.45 GHz and room temperature was already on the "cool side" of the dielectric relaxation spectrum. The T_c of PVDF was below room temperature. From the preceding discussion, one can predict that PVDF can be heated easily from room temperature at 2.45 GHz.

Polymer "blends" may be simple mechanical mixtures of different polymers without formation of chemical bonds or true solution. The dielectric relaxations associated with such mixtures are not expected to be much different from those of the corresponding pure polymers, when added. However, the influence of the effective dipole moments in the case of soluble polymer components need further study. In this chapter, only the microwave heating phenomena will be discussed for such a case of "true" solution, PMMA plus PVDF, recognizing that the PVDF may partially crystallize out of as a second phase.

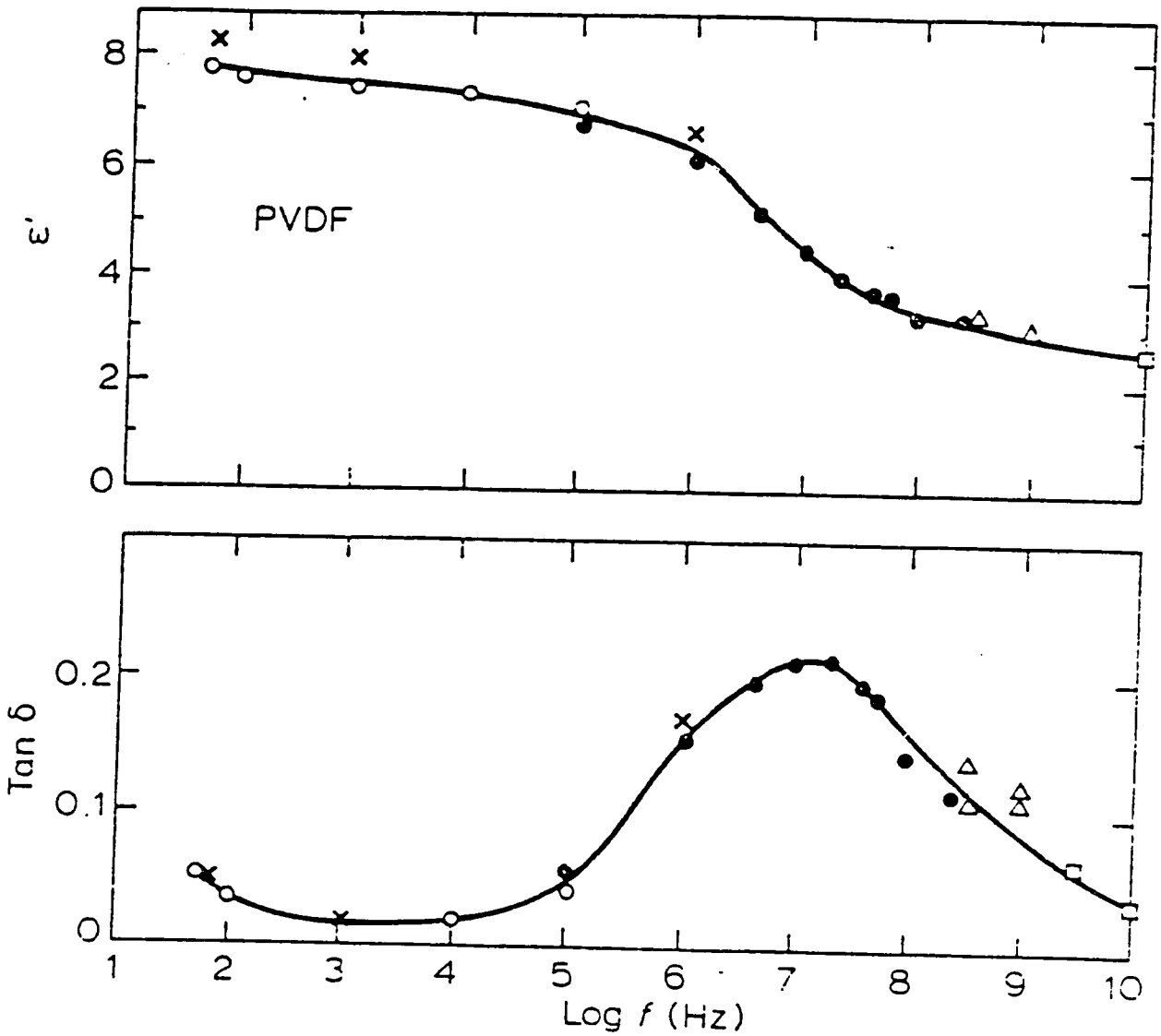

Figure 6.6 Frequency dependence of the dielectric constant and the loss tangent of poly(vinylidene fluoride) at room temperature. (12)

Figures 6.7-6.9 represent the variation of input power, reflected power and sample temperature with time for polymer blends of PMMA and PVDF. All these results were obtained for the same sample in the cylindrical cavity applicator. In Figure 6.7, the variation in powers and temperature while adjustment of the coupling probe was being conducted was recorded. Due to the relatively low loss teflon sample holder, compared to the silicone mold, there was 9 watts power reflected back to the power source. This reflected power, almost half of the input power, was very high. The temperature rose rapidly while the reflected power was adjusted to 2 watts. The increase in input power indicated that the impedance between the source and the workload became more matched, thus more power was coupled to the workload. The maximum temperature, 115°C, occurred at 1.5 min. with only 20 watts of input power. Then the temperature decreased slowly even though the input power and the reflected power were kept constant. A possible reason for this was that there was crystallization of PVDF, its T_m is 171°C. This crystallinity would not only decrease the value of ε'', but also move the maximum of the dielectric relaxations to higher temperatures.

Figure 6.8 shows the results of a second microwave heating after the blend had cooled down to room temperature. In the first-half minute, the reflected power was adjusted to be as small as possible, but it was still about 3 watts. Comparing Figures 6.7 and 6.8, in the first 3 min, both the input power and the reflected power in the second heating were higher than those in the first heating, but the heating rate and the maximum temperature were lower in the second heating. The input power was increased from 22 watts to 28 watts at 3.5 min. The coupling probe was continuously adjusted to match the impedance by trial and error. At 6 min., both input power and reflected were decreased due to the impedance matching between the microwave source and the workload. The temperature rose rapidly from 80 °C to 260 °C within 2

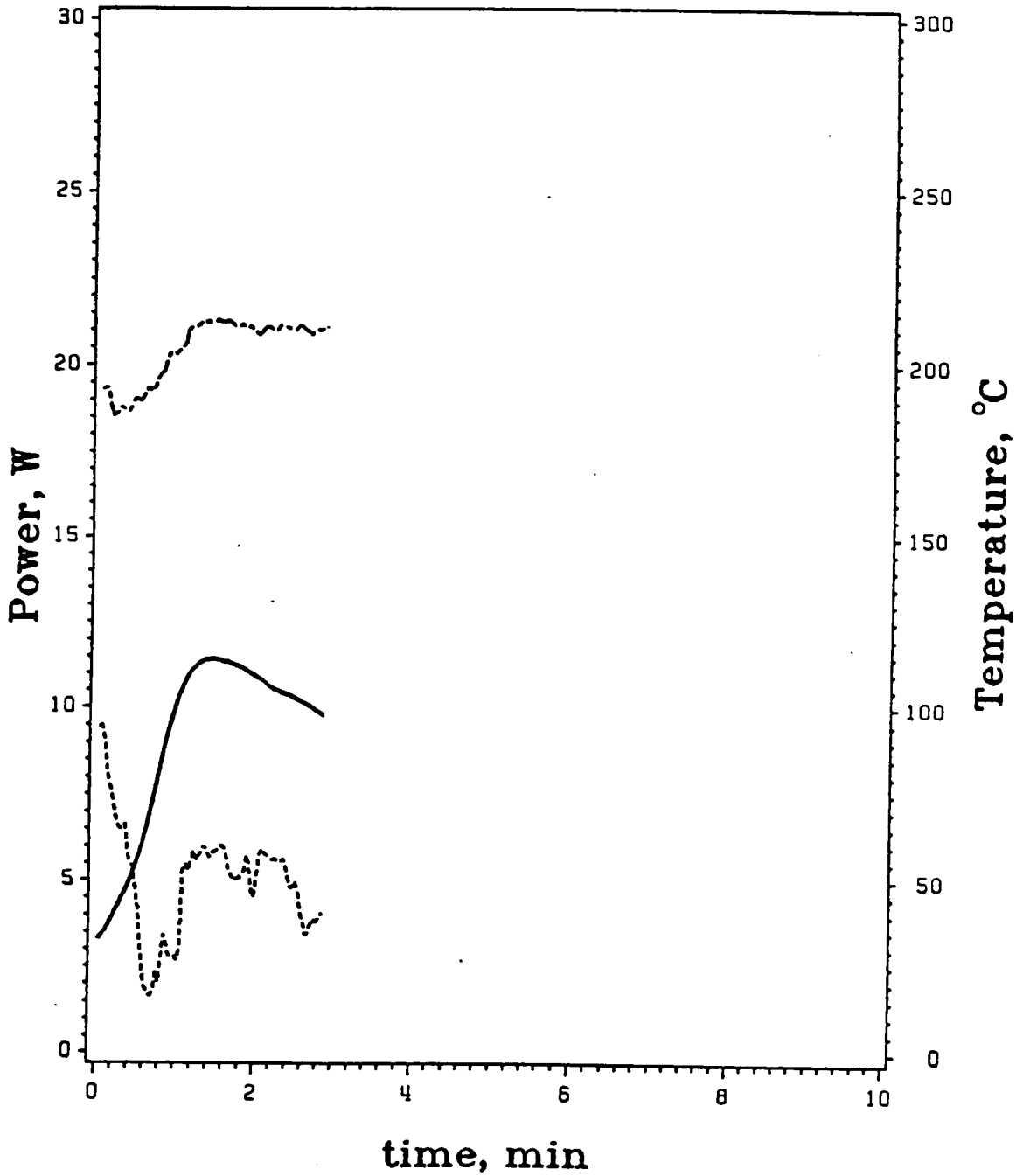

TOP :INPUT POWER
BOTTOM :REFLECTED POWER
SOLID LINE :TEMPERATURE

Figure 6.7 Variation of the temperature, input power and reflected power with time for polymer blends of PMMA and PVDF (50/50 w/w) in the center of TE_{111} mode of a cylindrical cavity applicator, first heating.

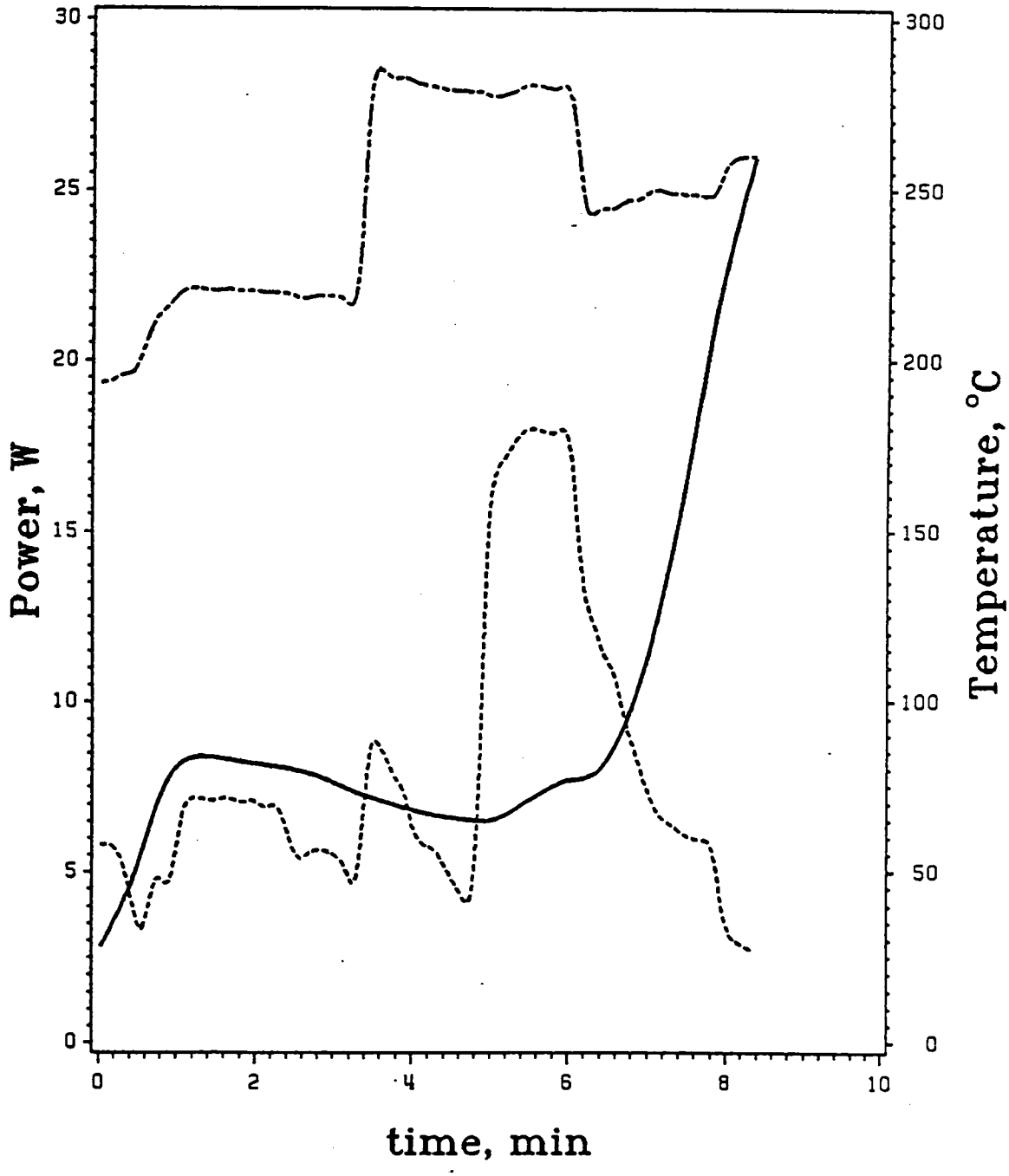

TOP :INPUT POWER
BOTTOM :REFLECTED POWER
SOLID LINE :TEMPERATURE

Figure 6.8 Variation of the temperature, input power and reflected power with time for polymer blends of PMMA and PVDF (50/50 w/w) in the center of TE_{111} mode of a cylindrical cavity applicator, second heating.

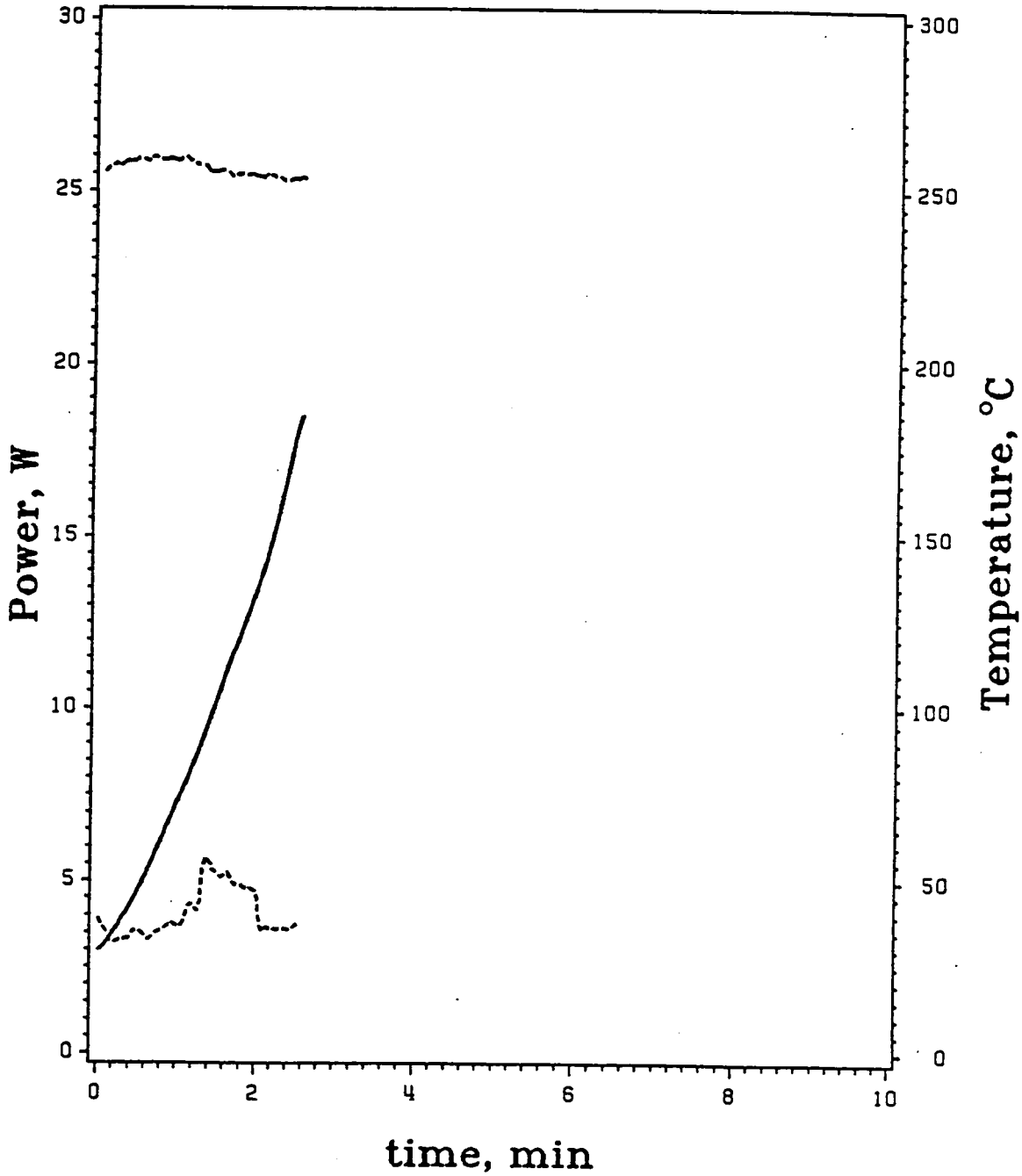

TOP :INPUT POWER
BOTTOM :REFLECTED POWER
SOLID LINE :TEMPERATURE

Figure 6.9 Variation of the temperature, input power and reflected power with time for polymer blends of PMMA and PVDF (50/50 w/w) in the center of TE_{111} mode of a cylindrical cavity applicator, third heating.

minutes. This sample was cooled down to room temperature. The input power and the adjustable coupling probe were kept at the same condition as at the end of the second heating. The third heating was rapid as shown in Figure 6.9. The slow heating rate at the beginning of the second microwave processing and the temperature decrease of first microwave processing were due to the high crystallinity of PVDF, therefore a lower dielectric loss factor was available for coupling with the microwave radiation energy. In the first two microwave heating cycles, the electric field strengths (or input powers) were not high enough to melt PVDF and raise the temperature enough to reach the T_c of PMMA (185°C as discussed in chapter 4). Application of a higher power and matching of the impedance caused the electric field strength to be strong enough to kinetically pass the low ε'' gap between the dielectric relaxation spectra of PVDF and PMMA. Upon reaching T_c of PMMA, PMMA began to couple with the microwave energy in a cascading manner. Power was turned off to avoid the thermal runaway effect.

6.5 CONCLUSION

From the preceding chapters' results, a schematic model is proposed to explain the behavior of two phase materials subjecting to microwave heating. Such materials include graphite composites and polymer blends. Combining the heatability, $(\varepsilon_s - \varepsilon_\infty)$, as discussed in chapter 2 with the dielectric relaxation spectra will be helpful in changing the formulation of two phase materials, such as adding polar fillers, blends, or block and graft copolymers. A detailed knowledge of the materials' properties at numerous stages in the process is required to evaluate the applicability of microwave power processing.

The reduction of the high reflectance of Graphite/Epoxy laminates by using the stub tuner caused a high electric field strength to build up inside the laminates. The travelling wave applicator with a stub tuner may be practically utilized for field repair. To avoid possible exposure to excessive microwave energy, robotic systems are suggested to execute the field repair task.

6.6 REFERENCES

1. W. I. Lee and G. S. Springer, *J. Compos. Mater.*, **18**, 357 (1984).
2. W. I. Lee and G. S. Springer, *J. Compos. Mater.*, **18**, 387 (1984).
3. Y. F. Chen and Charles Y. C. Lee, *Polym. Mater. Sci. Eng.*, **60**, 680 (1989).
4. A. Gourdenne, Q. Le Van, *Polym. Prepr.*, **22(2)**, 125 (1981).
5. A. Bouazizi and A. Gourdenne, *Eur. Polym. J.*, **24**, 889 (1988).
6. Y. Baziard and A. Gourdenne, *Eur. Polym. J.*, **24**, 881 (1988).
7. Y. Baziard and A. Gourdenne, *Eur. Polym. J.*, **24**, 873 (1988).
8. R. G. Raj, *Polym. Mater. Sci. Eng.*, **57**, 537 (1987).
9. R. G. Raj, *Polym. Mater. Sci. Eng.*, **55**, 49 (1986).
10. M. Amano and K. Nakagawa, *Polymer*, **28**, 263 (1987).
11. V. Volpe, *J. Compos. Mater.*, **14**, 189 (1980).
12. T. Wentink, *J. Appl. Phys.*, **32**, 1063 (1961).

CHAPTER 7

SUMMARY AND SUGGESTIONS

7.1 SUMMARY

In this work, the research was focused on the dielectric properties and high frequency electromagnetic radiation (EMR) absorption of energy of polymers. The interconnections of the research findings are summarized in Figure 7.1 and listed as follows:

Structure-Property Relationships

a) Since the electrical properties of polymers are closely associated with the mechanical properties of polymers, low frequency dynamic mechanical and dielectric frequency-temperature spectra were obtained on the materials and combined to conveniently extrapolate structure-property relationships into the GHz region. A correlation was found between the dielectric properties of various polymers and the dipole moments of small molecule analogues.

b) The area beneath the dielectric loss factor-frequency plot was proportional to $(\varepsilon_S - \varepsilon_\infty)$, and remained unchanged during the merging of the α and β relaxations. Evaluating heatability was most accurately found to be determined by the magnitude of $(\varepsilon_S - \varepsilon_\infty)$, the oscillator strength. The value of $(\varepsilon_S - \varepsilon_\infty)$ should be used together with the distribution of relaxation times and the activation energies of dipolar dispersion to predict heatability for microwave processing.

c) In order to relate structure-property relationships to the values of $(\varepsilon_S - \varepsilon_\infty)$ and chemical and morphological structures, it was necessary to examine the

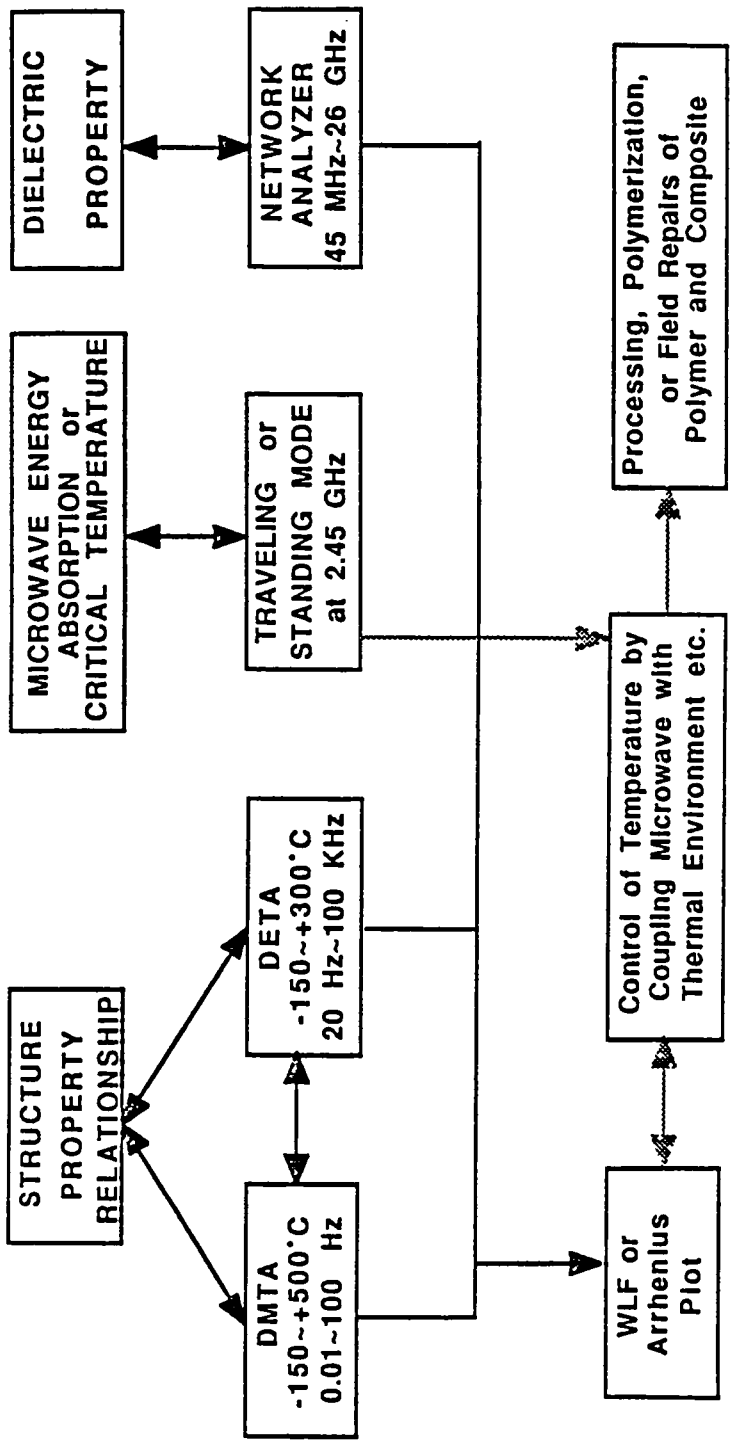

Figure 7.1 The summary of the selective coupling potential of polymers for microwave processing.

relationship between the dielectric constants of polymers and the effective dipole moments. In considering effective dipole moments it was useful to use group moments instead of bond moments. The polarity follows the sequence of group dipole moment as

$$SO_2 > CONH > CN > C{=}O > Cl > CO_2R > O > CO_3 > C\text{-}C.$$

d) A correlation was found between the dielectric properties of various polymers and the dipole moments of their small molecule counterparts. In summary, it was found that the value of $(\varepsilon_s - \varepsilon_\infty)$ depended on several factors: (A) group dipole moments, (B) mole percentage of polar groups, (C) hydrogen bonding, (D) chemical structure, (E) steric effects, (F) percentage of crystallinity, (G) crosslinking density, and (H) physical state.

Nitrile Rubbers

a) A travelling wave applicator was used to examine the microwave energy absorption of nitrile rubbers. The energy absorbed by the nitrile rubber increased with the input power and the acrylonitrile content. In addition, the maximum rate of power absorption, or rate of heating, was shifted to shorter times as nitrile content increased.

b) The critical temperatures, T_c, of dielectric loss were obtained from the intercepts of positive slope tangents of heating rate versus temperature plots at 2.45 GHz for nitrile rubbers. Microwave processing was rapid above the critical temperature where the maximum dielectric loss fell in the 2.45 GHz frequency domain for efficient coupling of energy to the polymers.

c) The critical temperature, T_c, of dielectric loss for a 30% acrylonitrile nitrile rubber was determined to be between 40 and 45°C. From experiments at three different starting temperatures it was concluded that the dielectric loss factor had increased

with increasing temperature into the dielectric loss region between room temperature and 51°C. Nitrile rubbers can, therefore, be easily heated up from a starting temperature of room temperature.

d) Glass transition temperatures at 2.45 GHz were obtained from heating rate, (dT/dt) or (dε"/dt), versus temperature curves. WLF plots revealed the temperature of maximum heating rate at 2.45 GHz. It was important to take advantage of the rapid heating on the positive slope side of dε"/dT and to avoid thermal runaway.

e) The polar nitrile group in nitrile rubbers absorbed energy by interacting with the microwave field which then heated the mass. As a result of increasing temperature, an added peroxide decomposed thereby generating crosslinks. A unique advantage of microwave curing was that the microwaves penetrated the entire mass instantaneously so that thermal peroxide decomposition started in every point of the polymer simultaneously, avoiding thermal gradients from conduction.

Thermoplastics

a) For thermoplastics at room temperature, the dielectric loss at microwave frequencies consists of only background loss because the dielectric loss spectrum at 2.45 GHz is concentrated at well above room temperature. Increased temperature was thus necessary to shift the dielectric relaxation spectra of glassy thermoplastics into the microwave region. By a combination of microwave and conventional thermal heating, improved absorption of microwave energy by these polymers was obtained.

b) Tuned cavity systems most efficiently use the microwave energy because the radiation from the feed system is continuously reflected from the walls of the cavity, passing through the material many times. The peaks (voltage maxima) of the standing wave readily couple power to the specimen because the electric field

strength is very high at the maximum. Indeed, this is sometimes the only way to develop adequate coupling to low loss materials.

c) Arrhenius plots of log(frequency) versus the inverse absolute temperature maximum from DETA spectra showed how sensitive the dielectric loss spectra were to changes in temperature. The higher the value of the activation energy, ΔE_a, the less the shift of the relaxation maxima in temperature with frequency, and the closer the window between T_c and T_g.

d) The dielectric behavior at 2.45 GHz for PMMA and PVAc was different, since PMMA possesses a large β dielectric loss relaxation. The merging of the α and β relaxations in PMMA at a frequency of about 10 kHz was clearly seen from the DETA spectra and the WLF plot.

e) The silicone flexible mold was very helpful in improving the energy absorption of nylons and PEEK at temperatures below their T_c. Above T_c, nylons and PEEK absorbed the microwave energy internally and rapidly heated to their respective melting points.

f) DETA spectra in the kHz region and DMTA spectra in the Hz region were used to explain the similar heating rates of amorphous and semicrystalline PEEK at 2.45 GHz. Amorphous PEEK rapidly decreased in modulus at temperatures just around the T_g, but regained parts of that loss as a result of a fast crystallization which occurred just above T_g. Therefore, both materials became semicrystalline during microwave processing, at least with a processing power of 43 watts.

<u>Heterogeneous Materials</u>

a) The reduction of the high reflectance of Graphite/Epoxy laminates by using a stub tuner caused a high electric field strength to build up inside the laminates. The

travelling wave applicator with the stub tuner may be practically utilized for field repair.

b) A schematic model was proposed to explain the behavior of two-phase materials subjected to microwave heating. Such materials include graphite composites and polymer blends. Combining the heatability, (ε_s - ε_∞), and the dielectric relaxation spectral response was found to be helpful in evaluating formulations of two-phase materials for electromagnetic radiation processing at high frequencies. Examples of improved heatability would include adding polar fillers, blends, and block and graft copolymers.

In summary, microwave energy absorption offers the following advantages over conventional heating methods: (A) rapid volumetric heating, (B) no overheating at the surface, (C) addressable heating, (D) energy saving and low operating costs, (E) increased throughput, (F) no direct degradation, (G) potential for field repair applications.

7.2 SUGGESTIONS

Besides the above findings, there are still many areas which need to be investigated, such as: a) direct measurement of dielectric properties at 2.45 GHz as function of temperature, b) dielectric properties as a function of crosslinking density for thermoset polymers, c) relaxation time distributions as function of temperature, d) electrical conductivity, e) skin depths, f) magnetic properties, g) thermal conductivities, h) heat capacities, i) heat transfer, j) electromagnetic field patterns, k) smoothing the electromagnetic heating pattern, l) frequency selection, m) temperature control by feedback, n) power control to avoid thermal runaway, o) chemical formulation for

optimum microwave coupling, p) the size and the shape of the processed materials. The chemist, physicist, chemical engineer, electrical engineer, material engineer, and mechanical engineer, need to combine their talents in a team effort in order to develop successful efficient microwave processing systems.

APPENDIX A

REFERENCES

A.1 France

1. A. Bouazizi and A. Gourdenne, *Eur. Polym. J.*, **24**, 889 (1988).
2. Y. Baziard and A. Gourdenne, *Eur. Polym. J.*, **24**, 881 (1988).
3. Y. Baziard and A. Gourdenne, *Eur. Polym. J.*, **24**, 873 (1988).
4. Y. Baziard S. Breton, S. Toutain and A. Gourdenne, *Eur. Polym. J.*, **24**, 633 (1988).
5. Y. Baziard S. Breton, S. Toutain and A. Gourdenne, *Eur. Polym. J.*, **24**, 521 (1988).
6. N. Beldjoudi and A. Gourdenne, *Eur. Polym. J.*, **24**, 265 (1988).
7. N. Beldjoudi and A. Gourdenne, *Eur. Polym. J.*, **24**, 53 (1988).
8. N. Beldjoudi, A. Bouazizi, D. Douibi and A. Gourdenne, *Eur. Polym. J.*, **24**, 49 (1988).
9. Q. Le Van and A. Gourdenne, *Eur. Polym. J.*, **23**, 777 (1987).
10. B. Silinski, C. Kuzmycz and A. Gourdenne, *Eur. Polym. J.*, **23**, 273 (1987).
11. F. Legros, A. Fourrier-Lamer, D. Le Pen and A. Gourdenne, *Eur. Polym. J.*, **22**, 335 (1986).
12. F. Legros, A. Fourrier-Lamer, D. Le Pen and A. Gourdenne, *Eur. Polym. J.*, **22**, 331 (1986).
13. A. Gourdenne, D. Le Pen and D. Douibi, *Polym. Prepr.*, **27(2)**, 401 (1986).
14. R. G. Raj, Y. Baziard and A. Gourdenne, Preprint of the third international conference on reactive processing of polymers, France, Sep. 5-7 (1984).
15. F. Legros, A. Fourrier-Lamer, D. Le Pen and A. Gourdenne, *Eur. Polym. J.*, **20**, 1057 (1984).
16. M. Teffal and A. Gourdenne, *Eur. Polym. J.*, **19**, 543 (1983).
17. A. Gourdenne, *Proc. Int. Conf. React. Process Polym.* 2nd, 23-30 (1982).
18. P. Heintz and A. Gourdenne, IUPAC Macromol. Symp., 28th, 486 (1982).
19. A. Gourdenne, Q. Le Van, *Polym. Prepr.*, **22(2)**, 125 (1981).
20. A. Gourdenne, A-H Maassarani, P. Monchaux, S. Aussudre and L. Thourel, *Polym. Prepr.*, **20(2)**, 471 (1979).
21. R. G. Raj, *Polym. Mater. Sci. Eng.*, **57**, 537 (1987).
22. R. G. Raj, *Polym. Mater. Sci. Eng.*, **55**, 49 (1986).
23. F. M. Thuillier, H. Jullien and M-F Grenier-Loustalot, *Polym. Commun.*, **27**, 206 (1986).
24. H. Jullien and H. Valot, *Polymer*, **26**, 506 (1985).
25. H. Jullien and H. Valot, *Polymer*, **24**, 810 (1983).
26. E. Karmazsin, P. Satre and J. F. Rochas, *Thermochim. Acta.*, **93**, 305 (1985).

A.2 Microwave Drawing

1. A. E. Zachariades and R. S. Porter, *High Modulus Polymers: Approaches to Design and Development*, Marcel Dekker, Inc., New York, 1988.
2. M. Amano and K. Nakagawa, *Polym. Commun.*, **28**, 119 (1987).
3. M. Amano and K. Nakagawa, *Polymer*, **28**, 263 (1987).
4. K. Nakagawa and T. Konaka, *Polymer*, **27**, 1553 (1986).
5. K. Nakagawa and T. Konaka, *Polymer*, **27**, 1030 (1986).
6. Y. Takeuchi, K. Nakagawa and F. Yamamoto, *Polymer*, **26**, 1929 (1985).

7. T. Konaka, K. Nakagawa and S. Yamakawa, *Polymer*, **26**, 462 (1985).
8. K. Nakagawa, T. Konaka and S. Yamakawa, *Polymer*, **26**, 84 (1985).
9. Y. Takeuchi, F. Yamamoto, K. Nakagawa and S. Yamakawa, *J. Polym. Sci. Polym. Phys. Ed.*, **23**, 1193 (1985).
10. K. Nakagawa, O. Maeda and S. Yamakawa, *J. Polym. Sci. Polym. Lett. Ed.*, **21**, 933 (1983).
11. H. F. Huang, *J. Microwave Power*, **11**, 305 (1976).

A.3 Michigan State University

1. J. Jow, J. D. Delong and M. C. Hawley, *SAMPE Quarterly*, **20(2)**, 46 (1989).
2. J. Jow, M. C. Hawley and M. Finzel, *Rev. Sci. Instrum.*, **60**, 96 (1989).
3. J. Jow, Ph.D. Michigan State University, East Lansing, MI, 1988.
4. B. Manring, Master, Michigan State University, East Lansing, MI, 1988.
5. J. Jow, M. C. Hawley, M. Finzel and T. Kern, *Polym. Eng. Sci.*, **28**, 1450 (1988).
6. J. Jow, M. C. Hawley, M. Finzel, J. Asmussen, Jr., H. H. Lin and B. Manring, *IEEE Trans. Microwave Theory Tech.*, **MTT-35**, 1435 (1987).
7. J. Asmussen, H. H. Lin, B. Manring and R. Fritz, *Rev. Sci. Instrum.*, **58**, 1477 (1987).
8. S. M. Singer, J. Jow, J. D. DeLong and M. C. Hawley, *Polym. Mater. Sci. Eng.*, **60**, 869 (1989).

A.4 Virginia Polytechnic Institute & State University

1. Y. F. Chen and Charles Y. C. Lee, *Polym. Mater. Sci. Eng.*, **60**, 680 (1989).
2. M. Chen, J. E. McGrath and T. C. Ward, *Polym. Mater. Sci. Eng.*, **60**, 443 (1989).
3. J. C. Hedrick, D. A. Lewis, G. D. Lyle, S. D. Wu, T. C. Ward and J. E. McGrath, *Polym. Mater. Sci. Eng.*, **60**, 438 (1989).
4. J. C. Hedrick, D. A. Lewis, T. C. Ward and J. E. McGrath, *Polym. Prepr.*, **29(1)**, 363 (1988).
5. Y. P. Chen, J. F. Pollard, J. D. Graybeal and T. C. Ward, *Polym. Prepr.*, **29(1)**, 207 (1988).
6. D. A. Lewis, T. C. Ward, J. D. Summers and J. E. McGrath, *Polym. Prepr.*, **29(1)**, 174 (1988).
7. D. A. Lewis, J. C. Hedrick, G. D. Lyle, T. C. Ward and J. E. McGrath, Proceedings of the Materials Research Society, Reno, Nevada, 245 (1988).
8. D. A. Lewis, J. C. Hedrick, J. E. McGrath and T. C. Ward, *Polym. Prepr.*, **28(2)**, 330 (1987).

A.5 Food Processing

1. A. C. Metaxas and R. J. Meredith, *Industrial Microwave Heating*, Peter Peregrinus, London, 1983.
2. D. A. Copson, *Microwave Heating*, 2nd ed., The Avi Publishing Co., Connecticut, 1975.
3. E. C. Okress, *Microwave Power Engineering*, Vol. 2: Applications, Academic Press, New York, 1968.
4. R. V. Decareau, *Microwaves in the Food Processing Industry*, Academic Press, Florida, 1985.

5. P. Fellows, *Food Processing Technology: Principles and Practice*, E. Horwood Ltd., New York, 1988.
6. M. Le Maguer and P. Jelen, *Food Engineering and Process Applications*, Vol. 1: Transport Phenomena, Elsevier Applied Science Publishers, New York, 1986.

A.6 Dielectric

1. N. G. McCrum, B. E. Read and G. Williams, *Anelastic and Dielectric Effects in Polymeric Solids*, John Wiley & Sons, New York, 1967.
2. P. Hedvig, *Dielectric Spectroscopy of Polymers*, John Wiley & Sons, New York, 1977.
3. Chen C. Ku and R. Liepins, *Electrical Properties of Polymers: Chemical Principles*, Hanser Publishers, New York, 1987.
4. A. Tager, *Physical Chemistry of Polymers*, 2nd ed., English translation, Mir Publishers, Moscow, 1978.
5. P. Robert, *Electrical and Magnetic Properties of Materials*, Artech House, Massachusetts, 1988.
6. J. I. Kroschwitz, *Electrical and Electronic Properties of Polymers: A State-of-the-Art Compendium*, John Wiley & Sons, New York, 1988.
7. R. Bartnikas and R. M. Eichhorn, *Engineering Dielectrics Volume IIA Electrical Properties of Solid Insulating Materials: Molecular Structure and Electrical Behavior*, ASTM Special Technical Publication 783, Pennsylvania, 1983.
8. A. R. Von Hippel, *Dielectric Materials and Applications*, The Technology Press of M.I.T. and John Wiley & Sons, New York, 1954.
9. A. K. Jonscher, *Dielectric Relaxation in Solids*, Chelsea Dielectrics Press, London, 1983.
10. R. A. Fava, *Polymers, Part C: Physical Properties*, Academic Press, New York, 1980. (L. Marton and C. Marton, Methods of Experimental Physics, Vol. 16)
11. A. R. Blythe, *Electrical Properties of Polymers*, Cambridge University Press, Cambridge, 1979.
12. A. D. Jenkins, *Polymer Science: A materials science handbook, Vol. 2*, North-Holland Publishing Co., London, 1972.
13. A. Weissberger and B. W. Rossiter, *Physical Methods of Chemistry, Part IV: Determination of Mass, Transport, and Electrical-Magnetic Properties*, John Wiley & Sons, New York, 1972. (A. Weissberger, Techniques of Chemistry, Vol. I)
14. J. B. Birks and J. H. Schulman, *Progress in Dielectrics, Vol. 2*, John Wiley & Sons, New York, 1960.
15. P. Hedvig and G. Zentai, *Microwave Study of Chemical Structures and Reactions*, The Chemical Rubber Co., Ohio, 1969.
16. V. I. Minkin, O. A. Osipov and Y. A. Zhdanov, *Dipole Moments in Organic Chemistry*, Plenum Press, New York, 1970.
17. C. P. Smyth, *Dielectric Behavior and Structure*, Dielectric Constant and Loss, Dipole Moment and Molecular Structure, McGraw-Hill Book Co., New York, 1955.
18. A. L. McClellan, *Tables of Experimental Dipole Moments*, W. H. Freeman and Co., San Francisco, 1963.

A.7 Microwave Technique

1. T. K. Ishii, *Microwave Engineering*, The Ronald Press Co., New York, 1966.

2. P. Lorrain, D. R. Corson and F. Lorrain, *Electromagnetic Fields and Waves*, W. H. Freeman and Co., New York, 1988.
3. F. L. Warner, *Microwave Attenuation Measurement*, Peter Peregrinus, England, 1977.
4. N. Marcuvitz, *Waveguide Handbook*, Peter Peregrinus, London, 1986.
5. R. L. Liboff and G. C. Dalman, *Transmission Lines, Waveguides, and Smith Charts*, Macmillan Publishing Co., New York, 1985.
6. Erich and Pehl, *Microwave Technology*, Artech House, Massachusetts, 1985.
7. D. C. Livingston, *The Physics of Microwave Propagation*, Prentice-Hall, New Jersey, 1970.
8. W. S. Cheung and F. H. Levien, *Microwave Made Simple: Principles and Applications*, Artech House, Massachusetts, 1985.
9. N. P. Cook, *Microwave Principles and Systems*, Prentice-Hall, New Jersey, 1986.
10. T. S. Laverghetta, *Microwave Materials and Fabrication Techniques*, Artech House, Massachusetts, 1984.
11. S F. Adam, *Microwave Theory and Applications*, Prentice-Hall, New Jersey, 1969.
12. T. S. Laverghetta, *Microwave Measurements and Techniques*, Artech House, Massachusetts, 1976.
13. K. C. Gupta, *Microwaves*, Wiley Eastern, New York, 1979.
14. P. A. Matthews and I. M. Stephenson, *Microwave Components*, Butler & Tanner, London, 1968.
15. T. S. Laverghetta, *Handbook of Microwave Testing*, Artech House, Massachusetts, 1981.
16. H. E. Thomas, *Handbook of Microwave Techniques and Equipment*, Artech House, Massachusetts, 1972.
17. R. F. Harrington, *Time-Harmonic Electromagnetic Fields*, McGraw-Hill, New York, 1961.
18. T. S. Saad, Microwave Engineers' Handbook, Vol. I, Artech House, Massachusetts, 1971.
19. S. Y. Liao, *Microwave Solid-State Devices*, Prentice-Hall, New Jersey, 1984.
20. R. Chatterjee, *Elements of Microwave Engineering*, Ellis Horwood Ltd., Chichester, England, 1986.
21. L. C. Shen and J. A. Kong, *Applied Electromagnetism*, PWS Publishers, Massachusetts, 1987.
22. D. Roddy, *Microwave Technology*, Prentice-Hall, New Jersey, 1986.
23. O. P. Gandhi, *Microwave Engineering and Applications*, Pergamon Press, New York, 1981.
24. V. F. Veley, *Modern Microwave Technology*, Prentice-Hall, New Jersey, 1987.
25. T. S. Laverghetta, *Practical Microwaves*, Howard W. Sams & Co., Indiana, 1984.
26. C. T. A. Johnk, *Engineering Electromagnetic Fields and Waves*, John Wiley & Sons, New York, 1988.
27. D. K. Cheng, *Field and Wave Electromagnetics*, Addison-Wesley Publishing Co., Pennsylvania, 1983.
28. S. Y. Liao, *Microwave Devices and Circuits*, 2nd ed., Prentice-Hall, New Jersey, 1980.

A.8 Others

1. V. Frosini and E. Butta, *J. Appl. Polym. Sci.*, **11**, 527 (1967).
2. R. W.-C. Chan and B. B. Krieger, *J. Appl. Polym. Sci.*, **26**, 1533 (1981).

3. G. G. Allan, B. B. Krieger and D. W. Work, *J. Appl. Polym. Sci.*, **25**, 1839 (1980).
4. G. Masszi and J. Orkenyi, *Acta Biochim. et. Biophys. Acad. Sci. Hung.*, **2**, 69 (1967).
5. J. Ippen, *Rubber Chem. Technol.*, **44**, 294 (1971).
6. N. S. Strand, *Modern Plastics*, **57(10)**, 64 (1980).
7. C. L. Lee, in *ACS Symp. Ser.*, **107**, T. L. Vigo and L. J. Nowack (eds), American Chemical Society, Washington D. C., 1979, p. 45.
8. H. F. Schwarz, R. G. Bosisio, M. R. Wertheimer and D. Couderc, *Rubber Age*, **107(11)**, 27 (1975).
9. H. F. Schwarz, R. G. Bosisio, M. R. Wertheimer and D. Couderc, *J. Microwave Power*, **8**, 303 (1973).
10. E. W. Stephansen, *J. Microwave Power*, **7**, 241 (1972).
11. N. S. Strand, 35th Annual Technical Conference, 1980, Reinforced Plastics/ Composites Institute, The Society of the Plastics Industry, Inc. Section 24-C, 1.
12. N. S. Strand, Technical Paper, EM79-368 (1979).
13. K. Beiss and G. Menges, *Proc. - Eur. Reg. Tech. Conf.: Plast. Process., 2nd*, 19-1-19-9. Edited by: C. Klason and H. R. Skov, Soc. Plast. Eng. Scand. Sect.: Copenhagen, Den. (1980).
14. William A. Smith, *Org. Coat. Plast. Chem.*, **39**, 324 (1978).
15. C. H. J. Avons and H. Roebuck, *SGF Publ.*, **46, XII**, 19pp. (1975).
16. R. Rajan, *J. Cell. Plast.*, **4**, 304 (1968).
17. K. K. S. Jamwal and Atula Dhar, *Rev. Sci. Instrum.*, **52**, 767 (1981).
18. I. J. Chabinsky, *Kautsch. Gummi, Kunstst.* **39**, 424 (1986).
19. W. I. Lee and G. S. Springer, *J. Compos. Mater.*, **18**, 357 (1984).
20. W. I. Lee and G. S. Springer, *J. Compos. Mater.*, **18**, 387 (1984).
21. N. Probst and J. Iker, *Kautsch. Gummi, Kunstst.* **37**, 385 (1984).
22. W. I. Lee, Ph.D. The University of Michigan, Ann Arbor, MI, 1983, 167pp
23. M. Martinelli, P. A. Rolla and E. Tombari, *IEEE Trans. Instrum. Meas.*, **IM-34**, 417 (1985).
24. C. Carlini, M. Martinelli, P. A. Rolla and E. Tombari, *J. Polym. Sci. Polym. Lett. Ed.*, **23**, 5 (1985).
25. A. J. Bur, *Polymer*, **26**, 963 (1985).
26. P. C. Bandyopadhyay and T. K. Chaki, *Proc. IUPAC, I. U. P. A. C., Macromol. Symp.*, **28th**, 421. Int. Union Pure Appl. Chem.: Oxford, UK (1982).
27. S. A. Wald and C. C. Winding, *Polym. Eng. Sci.*, **11**, 64 (1971).
28. S. Osaki, *J. Appl. Phys.*, **64**, 4181 (1988).
29. C. Carlini, F. Ciardelli, P. A. Rolla and E. Tombari, *J. Polym. Sci. Polym. Phys. Ed.*, **25**, 1253 (1987).
30. S. L. Inkpen and J. R. Melcher, *Polym. Eng. Sci.*, **25**, 289 (1985).
31. H. F. Mark, N. M. Bikales, C. G. Overberger and G. Menges, *Encyclopedia of Polymer Science and Engineering*, Vol. 5: Dielectric Heating to Embedding, 2nd ed., John Wiley & Sons, New York, 1986.
32. G. B. Taggart, *Electromagnetic Processing of Materials*, The BDM Corporation, Virginia, Technical Report, 1984.
33. H. M. Kingston and L. B. Jassie, *Introduction to Microwave Sample Preparation*: Theory and Practice, American Chemical Society, Washington, DC 1988.
34. J. V. Dawkins, *Developments in Polymer Characterization-3*, Applied Science Publishers, London, 1982.
35. C. M. Srivastava and C. Srinivasan, *Science of Engineering Materials*, Wiley Eastern, New York, 1987.
36. A. Benatar and T. G. Gutowski, *SAMPE Quarterly*, **18(1)**, 35 (1986).
37. G. K. N. Rashmi and P. K. C. Pillai, *J. Macromol. Sci.-Phys.*, **B26**, 185 (1987).

38. K. W. Watkins, *J. Chem. Educ.*, **60**, 1043 (1983).
39. D. C. Bassett, R. H. Olley and I. A. M. Al Raheil, *Polymer*, **29**, 1745 (1988).
40. H. F. Mark etc., *Encyclopedia of Polymer Science and Technology, Vol. 15*, John Wiley & Sons, New York, 1971.
41. Y. Ishida, *J. Polym. Sci., A-2*, **7**, 1835 (1969).
42. I. J. Chabinsky, *Rubber World*, **188**, 34, April (1983).
43. I. J. Chabinsky, *Elastomerics*, **115**, 17, January (1983).
44. R. Bakule and A. Havranek, *Rubber Chem. Technol.*, **51**, 72 (1978).
45. E. Hecht, *Optics*, 2nd ed., Addison-Wesley Pub. Co., Pennsylvania, 1987.
46. V. Volpe, *J. Compos. Mater.*, **14**, 189 (1980).
47. C. S. Lee, S. W. Lee and S. L. Chuang, *IEEE Trans. Microwave Theory Tech.*, **MTT-33**, 271 (1985).
48. C. L. Hu, J. G. Smith and J. F. Lindsey, *Int. SAMPE Symp. Exhib.*, **31**, 1413 (1986).
49. V. K. Varadan, V. V. Varadan, Y. Ma and W. F. Hall, *IEEE Trans. Microwave Theory Tech.*, **MTT-34**, 251 (1986).
50. G. Roussy, A. Mercier, J. M. Thiebaut and J. P. Vaubourg, *J. Microwave Power*, **20**, 47 (1985).
51. H. J. Gohlisch, *Rubber Age*, **103(4)**, 49 (1971).
52. M. A. Wheelans, *NR Technol.*, **6(1)**, 13 (1975).

APPENDIX B

COMPONENTS OF MICROWAVE INSTRUMENTATION

Component	Company	Model
Magnetron, 0-120 watts	Raytheon	PGM-10X1
Coaxial Cable, modified	Raytheon	57111G2E
Circulator	Ferrite Control	2620
Coaxial Cable (RG-214)	Coax Connection	CC2547-36
Termination, 175 watts	NARDA	369BNF
Termination, 40 watts	NARDA	376BNF
Directional Coupler, dual (20dB)	NDADA	3022
Directional Coupler (20dB)	NARDA	3003
Adapter	NARDA	614A
Adapter	Hewlett Packard	S281A
Waveguide tubing	Microwave Development	WR284
Attenuators (20dB)	Weinschel	49-20-43
Power Sensors	Hewlett Packard	8481B
Power Meter	Hewlett Packard	435B
Frequency Meter	Hewlett Packard	536A
Flange, Butt, Round, 8 holes	American Radar	UG-584/2
Side Grip Work Holder	Mckinnby	SG3/4x1
Sliding Short	Microlab/FXR	S630C
Stub Tuner	Maury Microwave	S351C
Coaxial Cable	Maury Microwave	8913C-36

* Components in 50 ohm and/or coaxial form.

The vita has been removed from the scanned document